

**The Catalytic Role of a Single Water on Keto-Enol Tautomerization Explored by
Fourier Transform Microwave Spectroscopy and Ab Initio Calculations**

by

Jiao Gao

A thesis submitted in partial fulfillment of the requirements for the degree of

Doctor of Philosophy

Department of Chemistry
University of Alberta

© Jiao Gao, 2019

Abstract

Keto-enol tautomerization plays important roles in biochemistry, atmospheric chemistry, and crystallography. It has attracted much attention for a long time. Solvation (hydration) is found to play essential roles in controlling this tautomerization process. Here, the effects of a single water molecule on the keto-enol tautomerization process were explored using chirped-pulse and cavity-based Fourier transform microwave spectroscopy with the aid of high-level ab initio calculations. Systematic studies on selected neutral molecular complexes involving keto-enol tautomerization provide new insights into understanding how hydration is responsible for making changes in distribution among tautomers.

I first explored how water affects the keto-enol tautomerization of acetone using microwave spectroscopy. I assigned the quantum numbers to observed rotational transitions of the most stable keto form of the acetone-water complex and experimentally determined the internal rotation barriers of the two methyl groups in acetone, which are inequivalent due to the hydrogen-bonded water unit.

Next, I investigated the keto-enol tautomeric and conformational changes of the cyclohexanone monomer and its monohydrate by Fourier-transform microwave spectroscopy and ab initio calculations. Ten isotopologues, including all six single ^{13}C substitutions observed in natural abundance and four different isotopic species of water (H_2O , D_2O , DOH , and HOD) were measured for the most stable structure of the chair conformer of the keto tautomer-water complex. The experimental structure of cyclohexanone-water complex was determined directly using this isotopic information.

Finally, I explored the keto-enol tautomerization of two β -diketones, i.e., acetylacetone and benzoylacetone. I only observed the enol form of acetylacetone-water complex, and the internal rotation barrier of the methyl group involved in hydrogen bonding in the complex was determined experimentally. For the benzoylacetone monomer, the experimental and theoretical results suggest that the experimental structure is an average

of the two most stable enol tautomers, i.e., the proton is near the middle position between the two carbonyl groups. The study also shows that the proton transfer between the two carbonyl groups in the benzoylacetone monomer is coupled with the internal rotation of the methyl group. Apart from that, two isomers out of six of the benzoylacetone-water complexes also were detected using the chirped-pulse Fourier-transform microwave spectrometer. The study shows that both isomers of the enol tautomer exist in its water complexes, which further confirms that two enol tautomers should coexist in its monomer.

Overall, these studies are important contributions to understanding how a single water molecule catalyzes the keto-enol tautomerization and changes relative energies. This work establishes a solid foundation for future work on larger ketone-(water)_N clusters.

Preface

This thesis is based on the research I have done at the University of Alberta between September 2013 and August 2018. The nature and extent of my contributions to the research included in this thesis are briefly summarized below.

Chapter 3 of the thesis has been published as J. Gao, N. A. Seifert, J. Thomas, Y. Xu, and W. Jäger. “Structure and internal rotation dynamics of the acetone-neon complex studied by microwave spectroscopy”, *J. Mol. Spectrosc.* **2016**, *330*, 228-235. I was responsible for the calculations, measurements, data analysis, and preparation of the manuscript. Dr. N. A. Seifert assisted in theoretical calculations and manuscript edits. Dr. J. Thomas assisted in experiments. Professor Y. Xu assisted in data analysis. Professor W. Jäger was the supervisory author and was involved in the concept formation, data analysis, and manuscript composition.

Chapter 4 of the thesis is in the preparation of submission. I was responsible for the calculations, measurements, data analysis, and preparation of the manuscript. Dr. J. Thomas and Professor Y. Xu assisted in data analysis. Professor W. Jäger was the supervisory author and was involved in the concept formation and manuscript composition.

Chapter 5 of the thesis is submitted. I was responsible for the calculations, measurements, data analysis, and preparation of the manuscript. Dr. N. A. Seifert assisted in theoretical calculations, data analysis and manuscript edits. Professor W. Jäger was the supervisory author and was involved in the concept formation and manuscript composition.

Chapter 6 of the thesis is in the preparation of submission. I was responsible for the calculations, measurements, data analysis, and preparation of the manuscript. Professor W. Jäger was the supervisory author and was involved in the concept formation and manuscript composition.

Chapter 7 of the thesis is in the preparation of submission. I was responsible for the calculations, measurements, data analysis, and preparation of the manuscript. Dr. N. A. Seifert assisted in experiment and data analysis. Professor Y. Xu assisted in data analysis.

Professor W. Jäger was the supervisory author and was involved in the concept formation and manuscript composition.

Acknowledgements

I would like first to express my thanks to my supervisor Wolfgang Jäger for his support, encouragement and guidance over the past 6 years. Without his supervision and support, my research works may not have been completed. I am so grateful for him giving me opportunities to learn and grow in this research area. His constructive suggestions on my research always opens my vision and helps me a lot in completing my research projects smoothly. His rigorous attitude towards teaching and research wins my full respect. I would like to also thank Prof. Yunjie Xu for her invaluable advice and help during the course of my research, and her shared experience in her career is very useful when I am thinking of my future career.

I also would like to thank my supervisor committee, Prof. Alex Brown and Prof. Jonathan Veinot, for their help and support during my entire Ph.D. program. I am grateful to my external examiner Prof. Melanie Schnell from Christian-Albrechts-Universität zu Kiel and Deutsches Elektronen-Synchrotron (DESY). I also would like to thank Prof. Gabriel Hanna and Prof. Roderick E. Wasylshen for agreeing readily to be my exam committee member and non-examining chair.

I would like to thank the technical staff in the department, especially Kim Do, Andrew Hillier, Dieter Starke, Vincent Bizon, and Dirk Kelm. A special note of many thanks goes to Dr. Anna Jordon for editing my thesis, and her support as my teaching assistant coordinator. I am also grateful to the support of my other teaching assistant coordinators, Dr. Norman Gee and Dr. Yoram Apelblat.

I thank past and current members of the Jäger and Xu groups for many useful discussions. I express my special thanks to Dr. Elijah G. Schnitzler and Dr. Nathan A. Seifert for their helpful suggestions and discussions. I thank Dr. Javix Thomas and Supriya Ghosh for much help and guidance in the initial days of my research work. I am also thankful to all my great colleges and friends- Reza, Zahra, Fahim, Chrissy, Prasanta, Angelo, Amin, Wenyuan, Dan, Leo, Joseph, and Fan for their friendship and support. Outside the group members, I am

grateful to my friends Di Fan, Yuping Zhou, Lu Sun, and Zhe Lv, for their selfless help to take care of my daughter when I had trouble myself.

I would like to present my sincere thankfulness to my Mum, who died during my Ph.D. program, for her great support when I was pregnant and her great role in my life.

Finally, I would like to express my deepest gratitude to my husband, Jiwen, for his comfort and soothe when I felt so sad in those days, and his encouragement both in life and my academic studies. Thank my little cute daughter, Eve, for being good kids, not creating lots of trouble for me when I take care of her by myself. Additionally, I want to thank my mother- and father- in- law for supporting me to finish the work during my program.

Table of Contents

Chapter 1. Introduction	1
1.1 Tautomerisim	1
1.2 Intermolecular Interactions	2
1.3 Microwave Spectroscopy and Ab-Initio Calculations	3
1.4 Objectives and Structure of the Thesis	4
References	8
Chapter 2. Experimental Set-Up and Theoretical Calculations	10
2.1 Overview of Rotational Spectroscopy	10
2.1.1 Time-Independent Schrödinger Equation	10
2.1.2 Solution of the Time-Dependent Schrödinger Equation.....	14
2.2 Cavity-Based Fourier Transform Microwave Spectrometer (FTMW).....	18
2.2.1 Microwave Cavity.....	19
2.2.2 Supersonic Jet Expansion	20
2.2.3 Generation of Microwave Excitation Pulse and Detection of Molecular Emission Signal	21
2.2.4 Timing of Pulse Sequences.....	22
2.3 Chirped-Pulse Fourier Transform Microwave Spectrometer	23
2.3.1 Generation of the Chirped Microwave Pulse.....	24
2.3.2 Sample Cell- the Interaction Region of Microwave Excitation Pulse and Molecular Beam.....	25
2.3.3 Detection of the Molecular Emission Signal	25
2.3.4 Timing of Chirped Pulse Sequences	26
2.4 Theoretical Calculations	27
2.4.1 Ab Initio Calculations.....	28

2.4.2	Density Functional Theory (DFT) Calculations	28
2.4.3	Basis Sets	30
2.4.4	Analysis of the Rotational Spectra.....	30
	References	32
Chapter 3. Structure and Internal Rotation Dynamics of the Acetone-neon Complex		
Studied by Microwave Spectroscopy		34
3.1	Introduction.....	34
3.2	Experimental Details.....	35
3.3	Theoretical Methods	36
3.4	Results and Discussion	37
3.4.1	Primary photodissociation products.....	37
3.4.2	Van der Waals interaction.....	41
3.4.3	Internal Rotation Dynamics	42
3.4.4	Structure	46
3.5	Conclusions.....	50
	References	51
Chapter 4. Non-Equivalent Methyl Internal Rotations in Acetone-Water Complex		
Studied by Microwave Spectroscopy and Ab Initio Calculations		54
4.1	Introduction.....	54
4.2	Experimental Section.....	55
4.3	Results and Discussion	56
4.3.1	Spectral Search and Assignment.....	56
4.3.2	Structure and Hydrogen Bonding	58
4.3.3	Internal Rotation Dynamics	61
4.3.4	Enol Form of Acetone.....	72
4.4	Conclusions.....	72

References	74
Chapter 5. A Microwave Spectroscopic and Ab Initio Study of Keto-Enol	
Tautomerism and Isomerism in the Cyclohexanone-Water Complex.....	76
5.1 Introduction.....	76
5.2 Experiments and Calculations.....	78
5.3 Results and Discussion	79
5.3.1 Ab-Initio Calculations of Keto-Enol Tautomeric and Conformational Changes of the Cyclohexanone Monomer and Its Monohydrate.....	79
5.3.2 Spectroscopic Assignments of the Cyclohexanone-Water Complex.....	82
5.3.3 Molecular Structure of the Cyclohexanone-Water Complex.....	84
5.3.4 Intermolecular Interaction Analyses of Cyclohexanone-Water and Other Typical Ketone-Water Complexes.....	87
5.3.5 Enol Form of Cyclohexanone-Water Complex	89
5.4 Conclusion	92
References	94
Chapter 6. Keto-Enol Tautomeric and Internal Rotation Dynamics Study of the Acetylacetone-Water Complex Investigated by Microwave Spectroscopy and Ab Initio Calculations.....	
6.1 Introduction.....	97
6.2 Experimental and Computational Details	98
6.3 Results and Discussion	99
6.3.1 Ab Initio Calculations of Keto-Enol Tautomeric and Conformational Changes of the Acetylacetone Monomer and the Monohydrated Complex	99
6.3.2 Spectral Assignment of the Enol Tautomer Acetylacetone-Water Complex	103

6.3.3	Structure and Hydrogen Bonding	104
6.3.4	Internal Rotation Dynamics	108
6.4	Conclusions.....	111
	References	112
Chapter 7. Rotational Spectra of Benzoylacetone Monomer and Its Complex with		
Water		114
7.1	Introduction.....	114
7.2	Experimental and Computational Details	115
7.3	Results and Discussion	116
7.3.1	Spectral Search and Assignment of the Benzoylacetone Monomer	116
7.3.2	Spectral Search and Assignment of the Benzoylacetone-Water Complexes	123
7.3.3	Hydrogen Bonding and Non-covalent Interaction Analysis.....	126
7.4	Conclusions.....	128
	References	129
Chapter 8. Further Molecular Systems I Have Explored		
8.1	Theoretical Calculations of the Acetone-Formic Acid Complex	131
8.2	¹⁴ N Nuclear Quadrupole Coupling in the 4-Hydroxypyrimidine Monomer and Its Water Complex	133
8.3	Theoretical Calculations of the Dibenzoylmethane Monomer	136
8.4	Theoretical Calculations of the Ethyl Benzoylacetone Monomer	138
8.5	Theoretical Calculations of the 2-Acetylcyclohexanone Monomer	139
8.6	Theoretical Calculations of the 1,3-Cyclohexanedione-Water Complex	140
	References	144
Chapter 9. Conclusions.....		
		145
Bibliography		
		149

Appendix I. Supplementary Material for Chapter 3.....	158
Appendix II. Supplementary Material for Chapter 4.....	163
Appendix III. Supplementary Material for Chapter 5.....	166
Appendix IV. Supplementary Material for Chapter 6.....	186
Appendix V. Supplementary Material for Chapter 7.....	188

List of Tables

Table 3.1. Predicted rotational constants and dipole moment components of the acetone-Ne complex from a variety of theoretical methods.....	37
Table 3.2. Experimental spectroscopic parameters for the acetone-Ne complex.....	40
Table 3.3 Differences in bond lengths (Δr), local bond critical point (BCP) densities ($\Delta\rho$), and atomic energies (ΔE) among acetone-Ne complex and acetone monomer upon internal rotation at the MP2/6-311 ++ G (2d, p) level of theory.....	45
Table 3.4 Calculated and experimental structural parameters for acetone-Ne.....	49
Table 3.5 Comparison of fitted structural parameters, including angles from the methyl rotor direction cosines, of acetone-Ne and acetone-Ar complexes.....	49
Table 4.1. Predicted rotational constants and transition dipole moments of the acetone-water complex using DFT and MP2 methods with the 6-311 ++ G (2d, p) basis set.....	55
Table 4.2. Experimental spectroscopic parameters for the acetone-water complex and its D ₂ O isotopologues.....	57
Table 4.3. Calculated bond lengths, bond angles, and complexation energies of the acetone-water complex using DFT and MP2 methods with the 6-311 ++ G (2d, p) basis set.....	58
Table 4.4. Experimental spectroscopic parameters for the acetone-water complex and acetone-D ₂ O complex.....	63
Table 4.5.1. Differences in bond lengths(Δr) and integrated electronic populations ($\Delta\rho$), atomic energies (ΔE) among the acetone-water complex and acetone monomer with internal rotational of “free” methyl groups using B3LYP-D3 method with the aug-cc-pVTZ basis set.....	67
Table 4.5.2. Differences in bond lengths(Δr), integrated electronic populations ($\Delta\rho$), and atomic energies (ΔE) between the acetone-water complex and the acetone monomer with	

internal rotational of the methyl group hydrogen bonded to water using B3LYP-D3 method with the aug-cc-pVTZ basis set.....	69
Table 5.1. Calculated spectroscopic constants and relative energies of five tautomeric/conformational species of the cyclohexanone monomer and its eight most relevant monohydrates at the B3LYP-D3/aug-cc-pVTZ level of theory.....	79
Table 5.1. (continued).....	80
Table 5.2. Calculated rotational constants and dipole moment components of cyclohexanone-water using DFT and MP2 methods with the 6-311++G (2d, p) basis set; the aug-cc-pVTZ basis set was employed for the B3LYP/D3 method.....	82
Table 5.3. Experimental rotational and centrifugal distortion constants of the cyclohexanone-water complex.....	83
Table 5.4. Predicted and experimental structural parameters for the cyclohexanone ring as determined using the cyclohexanone-water microwave data from this study, with comparison to previous electron diffraction (ED) and FTMW data for the monomer.....	84
Table 5.5. Relevant hydrogen bonding structural parameters for selected ketone-water complexes. Geometries used are the same as in Table 5.6. Values in square brackets are derived.....	86
Table 5.6. Results of SAPT(0)/jun-cc-pVDZ non-covalent interaction energy analyses for several ketone-water complexes.....	88
Table 6.1. Calculated rotational constants, dipole moment components, and relative energies of four tautomeric/conformational species of the acetylacetone monomer at the MP2/6-311++G(2d, p) level of theory.....	99
Table 6.2. Calculated rotational constants, dipole moment components, and relative energies of five acetylacetone monohydrates at the MP2/6-311++G(2d, p) level of theory.....	100
Table 6.3. Experimental spectroscopic parameters for the acetylacetone-water complex.....	103

Table 6.4. Calculated bond lengths, bond angles, and complexation energies of acetylacetonewater complex using the MP2 method with the 6-311 ++ G (2d, p) basis set.....	104
Table 7.1. Calculated rotational constants, dipole moment components, and relative energies of four tautomeric/conformational species of the benzoylacetone monomer at the B3LYP-D3BJ/aug-cc-pVTZ and MP2/cc-pVTZ levels of theory.....	117
Table 7.2. Experimental spectroscopic parameters for the benzoylacetone monomer.....	118
Table 7.3. Experimental spectroscopic parameters for the deuterated benzoylacetone monomer (the central hydrogen atoms is replaced by deuterium).....	122
Table 7.4. Calculated spectroscopic constants and the relative energies of four tautomeric/conformational species of six benzoylacetone monohydrated complexes at the levels of B3LYP-D3BJ/aug-cc-pVTZ theory.....	123
Table 7.5. Experimental spectroscopic parameters for the two isomers of the benzoylacetone-water complexes.....	124
Table 8.1. Calculated rotational constants, dipole moment components, and relative energies of four tautomeric/conformational species of the acetone-formic acid (FM) complex at the MP2/cc-pVDZ level of theory.....	131
Table 8.2. Experimental spectroscopic parameters for the keto and enol tautomers of 4-hydroxypyrimidine.....	133
Table 8.3. Calculated rotational constants, dipole moment components, and relative energies of four tautomeric/conformational species of the 4-hydroxypyrimidine monohydrated complexes at the B3LYP/6-31G(d,p), MP2/6-311++G (2d, p), and B3LYP-D3BJ/aug-cc-pVDZ levels of theory.....	134
Table 8.4. Calculated rotational constants, dipole moment components, and relative energies of three tautomeric/conformational species and one special enol form (Enol 1) of the dibenzoylmethane (DBM) monomer at the MP2/cc-pVDZ level of theory.....	136

Table 8.5. Calculated rotational constants, dipole moment components, and relative energies of three tautomeric/conformational species of the ethyl benzoylacetone monomer at the B3LYP-D3BJ/aug-cc-pVDZ level of theory.....	137
Table 8.6. Calculated rotational constants, dipole moment components, and relative energies of three tautomeric/conformational species of the 2-acetylcyclohexaneone monomer at the B3LYP-D3BJ/aug-cc-pVDZ level of theory.....	139
Table 8.7. Calculated rotational constants, dipole moment components, and the relative energies of seven tautomeric/conformational species of the 1, 3-cyclohexanedione monohydrated complexes at the MP2/6-311++G(2d,p) and B3LYP-D3BJ/aug-cc-pVDZ levels of theory.....	141

List of Figures

Figure 1.1. Tautomerization in DNA bases.....	2
Figure 1.2. The keto-enol tautomerization of the prototype molecules that I studied.....	5
Figure 2.1. The two-level system with the microwave excitation.....	14
Figure 2.2. A schematic diagram of the components of the cavity-based FTMW spectrometer.....	19
Figure 2.3. Time sequence of an experimental measurement cycle with the cavity-based FTMW spectrometer.....	22
Figure 2.4. A schematic diagram of components of the chirped-pulse broadband FTMW spectrometer.....	24
Figure 2.5. Time sequence of a measurement cycle with the chirped-pulse broadband FTMW spectrometer.....	27
Figure 3.1. Schematic rotational energy level diagram of the acetone-Ne complex. Closed frequency loops, which were used to confirm the initial assignments, are shown with different colors.....	38
Figure 3.2. NCI isosurface for acetone-Ne with reduced density gradient $s=0.7$ a.u., colored by the values of $\text{sign}(\lambda_2)\rho$ $[-0.04, 0.02]$ at each point in space, with colorations specified by the legend in the up right (red color denotes positive value, and blue color denotes negative value). The blue ball is the Ne atom.....	41
Figure 3.3. Calculated potential energies (red dots) and interpolated curve (blue dashes) for a single methyl internal rotation in acetone-Ne, holding the other fixed at its minimum position. The red curve is a standard torsional potential of a single uncoupled methyl internal rotor, $\Delta E(\theta) = 1 - V_3 \cos(3\theta)$	42
Figure 3.4. Comparison of the contour map of the 2D potential energy surface of both methyl internal rotation torsional angles in the acetone-Ne complex (Coupled, left figure), calculated	

at the MP2/6-311++G(d,p) level of theory, and a schematic surface where both the internal rotation of both methyl groups are uncoupled (Uncoupled, right figure).....43

Figure 3.5. Electrostatic potential (ESP) map of the acetone monomer in its minimum structure (a) and transition state (b) and of the acetone-Ne complex in its minimum structure (c) and transition state (d).....43

Figure 3.6. Schematic of structure parameterization used to characterize the non-covalent interaction in acetone-Ne. The axes shown are parallel to the principal inertial axes of the acetone monomer and originate at the position of the carbonyl carbon atom.....47

Figure 3.7. Contour maps of the three possible two-dimensional slices of the 3D potential energy surface for the non-covalent interaction potential for acetone-Ne, calculated at the B3LYP-D3/aug-cc-pVTZ level of theory. The third parameter is held at its minimum position in each slice.....47

Figure 3.8. 1D cross sections of the 3D interaction potential, holding the other two parameters fixed at their equilibrium positions, calculated at both the CCSD(T)/aug-cc-pVTZ (top half) and B3LYP-D3/aug-cc-pVTZ (bottom half) levels of theory. Calculated ground state wavefunctions (green curves) presented were calculated using the Numerov-Cooley numerical procedure. For the “stretch” potentials (left third), the dissociation energies of the neon at equilibrium (D_e) were estimated by the asymptotic behavior of the potentials.....48

Figure 4.1. Assigned broadband spectrum of the acetone-water complex. The black lines denote experimental spectra, and the blue, red, magenta, and olive colors represent the assigned spectra for the acetone-water, acetone-Ne²⁰, acetone-Ne²² complexes, and the acetone monomer, respectively.....56

Figure 4.2. Rotational spectrum of the $3_{03} \leftarrow 2_{02}$ transition for the acetone-water complex, which was measured using a 0.5 mW excitation pulse with a duration of 0.25 μ s and averaged over 10 cycles.....56

Figure 4.3. The structure of the acetone-water complex with hydrogen-bond parameters....59

Figure 4.4. Bond critical points (BCPs) and the corresponding bond path of the acetone-water complex.....	59
Figure 4.5. Potential curves of internal rotation of two methyl groups in the acetone-water complex.....	61
Figure 4.6. Two-dimensional methyl internal rotation scans of the acetone monomer (a), the acetone-Ne (b) and the acetone-water (c) complexes, calculated at the MP2/6-311 ++ G (2d, p) level of theory.....	62
Figure 4.7. ESP map of the acetone monomer in its minimum state (a) and transition state (b); the acetone-water complex in its minimum state (c), transition state 1 (d) rotating the methyl group far away from water, and transition state 2 (e) rotating the methyl group close to water.....	65
Figure 5.1. B3LYP-D3/aVTZ calculated structures of five tautomeric/conformational species of the cyclohexanone monomer and its eight most relevant monohydrates.....	81
Figure 5.2. Side (top) and birds-eye (bottom) views of the B3LYP-D3/aVTZ structure (ball and stick model) overlaying the $r_m^{(1)}$ experimental geometry (colored spheres) of the <i>keto</i> -cyclohexanone-H ₂ O complex.....	85
Figure 5.3. Results from QTAIM and NCI analyses for the five compared ketone-water complexes. The hydrogen bonding interactions are identified by the bond paths (orange splines) and corresponding bond critical points (yellow spheres). Also shown are the NCI isosurfaces at a fixed reduced density gradient, $s = 0.5$ a.u, colored by the values of $\text{sign}(\lambda_2)\rho$ [-0.04, 0.02] at each point in space, with colorations specified by the legend in the bottom right (red color denotes positive value, and blue color denotes negative value).....	87
Figure 5.4. B3LYP-D3/aVTZ reaction coordinates of keto-enol tautomerization of the cyclohexanone monomer (red) and its most stable monohydrate (black).....	89

Figure 5.5. A difference map of electron density in the cyclohexanone-water complex after complexation. Blue regions specify relative depletion of electron density upon complexation, and red regions correspond to regions where electron density has increased.....	90
Figure 6.1. Structures of four tautomeric/conformational species of the acetylacetone monomer calculated at the MP2/6-311++G(2d, p) level of theory.....	99
Figure 6.2. Structures of five acetylacetone monohydrates calculated at the MP2/6-311++G(2d, p) level of theory.....	100
Figure 6.3. Spectrum of the $3_{21} \leftarrow 2_{12}$ transition for acetylacetone-water measured by the chirped-pulse FTMW spectrometer.....	102
Figure 6.4. A plot resulting from a NCI analysis, including BCPs and the corresponding bond paths of the enol acetylacetone-water complex. The orange lines are the bond paths for the weak bonds, and the yellow balls correspond to BCPs.....	105
Figure 6.5. Calculated potential energies for two methyl internal rotations in the acetylacetone-water complex. The left bottom graph is for the internal rotation of methyl group hydrogen bonded with the water molecule, the right bottom graph is for the internal rotation of the methyl group far away from water.....	107
Figure 6.6. Calculated potential energies for two methyl internal rotations in the acetylacetone monomer with C_{2v} symmetry.....	108
Figure 6.7. Calculated potential energies for two methyl internal rotations in the acetylacetone monomer with C_s symmetry.....	109
Figure 7.1. Structures of four tautomeric/conformational species of the benzoylacetone monomer at the B3LYP-D3BJ/aug-cc-pvtz level of theory.....	117
Figure 7.2. An example for internal rotation splitting of rotational transitions of the benzoylacetone monomer, measured with a chirped-pulse FTMW spectrometer (2–6 GHz).....	119
Figure 7.3. The proton transfer reaction path in the benzoylacetone monomer.....	120

Figure 7.4. An example for internal rotation splitting in transitions of the deuterated benzoylacetone monomer (the centered hydrogen is replaced by deuterium) measured using a chirped-pulse FTMW spectrometer (2–6 GHz).....	121
Figure 7.5. Structures of six benzoylacetone monohydrated complexes at the B3LYP-D3BJ/aug-cc-pvtz level of theory.....	123
Figure 7.6. Results from NCI analyses of the benzoylacetone monomer; the isomer on the left side is Enol 1, and the isomer on the right side is Enol 2. Also shown are the NCI isosurfaces at a fixed reduced density gradient, $s = 0.54$ a.u., colored by the values of $\text{sign}(\lambda_2)\rho$ [-0.04, 0.02] at each point in space, with colorations specified by the legend in the bottom right (red color denotes positive value, and blue color denotes negative value).....	125
Figure 7.7. NCI analysis of the benzoylacetone-water complexes, (a) Enol 2-H ₂ O I complex (0 kJ/mol); (b) Enol 1-H ₂ O I complex (1.3 kJ/mol); (c) Enol 1-H ₂ O II complex (4.5 kJ/mol); (d) Enol 2-H ₂ O II complex (7.5 kJ/mol). Also shown are the NCI isosurfaces at a fixed reduced density gradient, $s = 0.54$ a.u., colored by the values of $\text{sign}(\lambda_2)\rho$ [-0.04, 0.02] at each point in space, with colorations specified by the legend in the bottom right (red color denotes positive value, and blue color denotes negative value).....	126
Figure 8.1. Structures of the acetone-formic acid complex.....	131
Figure 8.2. Structures of the 4-hydroxypyrimidine-water complex.....	132
Figure 8.3. Structures of the dibenzoylmethane (DBM) monomer, (a) Enol 1; (b) Enol 2; (c) Keto 1; (d) Keto 2.....	135
Figure 8.4. Structures of the ethyl benzoylacetone monomer.....	138
Figure 8.5. Structures of the 2-acetylcyclohexanone monomer.....	139
Figure 8.6. Structures of the 1,3-cyclohexanedione monomer.....	140
Figure 8.7. Structures of the 1,3-cyclohexanedione–water complexes: (a) Diketo 1; (b) Diketo 2; (c) <i>Cis</i> -ketoenol 1; (d) <i>Cis</i> -ketoenol 2; (e) <i>Trans</i> -ketoenol 1; (f) <i>Trans</i> -ketoenol 2; (g) <i>Trans</i> -ketoenol 3.....	142

List of Symbols

J	Rotational quantum number
$K_{a, c}$	Quantum number in the prolate or oblate symmetric top
I	Moments of inertia
A, B, C	Rotational constants
h	Planck's constant
μ_a, μ_b, μ_c	Electric dipole moment components
V_3	Three-fold barrier of the methyl group
\hat{H}_0	Time-independent Hamiltonian
$\hat{H}(t)$	Time-dependent Hamiltonian
ω	Microwave radiation with angular frequency
ρ_{12}, ρ_{21}	Time dependent density matrix elements
$w(t), s(t)$	Population difference and sum terms of the two energy levels
$u(t), v(t)$	Coherence terms, the real and imaginary part of the macroscopic polarization, respectively
ω_0	Rotational transition frequency
x	Rabi frequency
$P(t)$	Macroscopic polarization
σ	Standard deviation
$D_J, D_{JK}, D_K, d_1, d_2$	Quartic distortion constants for Watson's S- reduction
$\Delta_J, \Delta_{JK}, \Delta_K, \delta_j, \delta_k$	Quartic distortion constants for Watson's A-reduction
P	Related to the ratio of the molecular rotational constants and the internal rotor rotational constant
F_{12}	Top-top coupling term

F_0	Internal rotor rotational constant of a methyl group
$\Phi_{JK}, \Phi_{KJ}, \Phi_K$	Sixth-order centrifugal distortion constants for Watson's A-reduction
D_{pi2J}, D_{pi2K}	Fourth order distortion terms describing coupling between overall rotation and internal rotation
ε	Angle between the projection of the internal rotation axis onto the bc-plane and the b-principal inertial axis of the complex
δ	Angle between internal rotation axis and a-axis of the complex
β, γ	Euler angles
χ	Nuclear quadrupole coupling constant

List of Abbreviations

FTMW	Fourier transform microwave
RF	Radio frequency
TTL	Transistor-transistor logic
A/D	Analog-to-digital
PDRO	Phase-locked dielectric resonator oscillator
AWG	Arbitrary wave generator
DFT	Density functional theory
HF	Hartree-Fock
CCSD(T)	Coupled cluster singles and doubles with perturbative estimates of triples
MP2	Second order Møller-Plesset perturbation
ESP	Electrostatic potential
QTAIM	Quantum Theory of Atoms in Molecules
BCP	Bond critical point
DNA	Deoxyribonucleic acids
VUV	Vacuum ultraviolet
BSSE	Basis set superposition error
SOA	Secondary organic aerosol
NCI	Non-covalent interaction
SAPT	Symmetry adapted perturbation theory
PCM	Polarizable continuum model
ED	Electron diffraction
RDG	Reduced density gradient
AcAc	Acetylacetone

NMR	Nuclear magnetic resonance
FM	Formic acid
DBM	Dibenzoylmethane
FTIR	Fourier transform infrared spectroscopy
IR	Infrared

Chapter 1

Introduction

1.1 Tautomerism

In chemistry, different molecular formulas usually represent molecules that have different physical or chemical properties. In some cases, even molecules with the same chemical formula have very contrasting properties. For example, butane and isobutane have the same formula (C_4H_{10}) but very different properties. Butane is a hydrocarbon with four carbon atoms connected in a straight chain, its boiling point is $-0.5\text{ }^\circ\text{C}$, and its freezing point is $-138.3\text{ }^\circ\text{C}$; isobutane has a branched-chain, and its boiling and freezing points are -11.7 and $-159.6\text{ }^\circ\text{C}$, respectively. More importantly, the branched-chain hydrocarbons are better motor fuels than the straight chain hydrocarbons. The conversion of straight chain hydrocarbons into their corresponding branched-chain hydrocarbons plays vital roles in industry.¹ Such an interconversion process within molecules is called isomerization. Isomerization is a chemical process involving interconversion of molecules, while maintaining the same molecular formula but changing the atom arrangement and bond connectivity. In chemistry, there are several kinds of isomerization, for example, cis-trans isomerization,² keto-enol tautomerization, etc. The process of tautomerization involves the migration of a proton from one tautomer to another, with an accompanying shift of π electrons in the participating double bonds.³ Tautomerism is an equilibrium process, where the equilibrium constant (K) of the reaction depends on the Gibbs free energy difference (ΔG°) of the two tautomers at a constant temperature and pressure, as shown in Eq. 1.1 (R is the gas constant):

$$\Delta G^\circ = -RT \ln K \quad (1.1)$$

Tautomerism is of great importance in chemistry. It is involved in the biochemical activity of amino acids, sugars, and nucleic acids.^{4, 5} One important group of nucleic acids is DNA. Some DNA bases can undergo keto-enol tautomerism.⁶ For example, in the keto form of thymine, the hydrogen atom shifts to the carbonyl oxygen atom, and the carbonyl double bond shifts to the $C=N$ double bond in the six-membered ring to form the enol form of thymine. The reaction is shown in Figure 1.1 (a). A similar reaction also occurs in guanine (see Figure 1.1

(b)). In the normal case, the keto tautomer of thymine (T) will pair with adenine (A). However, if the keto form of thymine converts into the enol form, then the enol tautomer of thymine (T) will pair with guanine (G), shown in Figure 1.1 (c) and (d), respectively. Such keto-enol tautomerization in DNA may give rise to the occurrence of gene mutations.⁷ Understanding gene mutations is essential as it is useful in explaining, predicting, and eliminating diseases.⁸ The significance of tautomerism extends also to the crystal growth of compounds that can undergo proton migration.⁹⁻¹² The isocytosine crystal, for example, was found to be co-crystallized from two tautomers.⁹ Moreover, different tautomers in the protein crystal structure^{13, 14} will have different hydrogen-bond donor and acceptor sites. Thus, their precise structures in drugs with those tautomerise systems may exert potential influence on pharmaceutical functions when those drugs are applied into biological systems. The recognition of those different functionalities in different tautomers could help to promote the development of drug discovery¹⁵ and computer-aided drug design.¹⁶⁻¹⁸

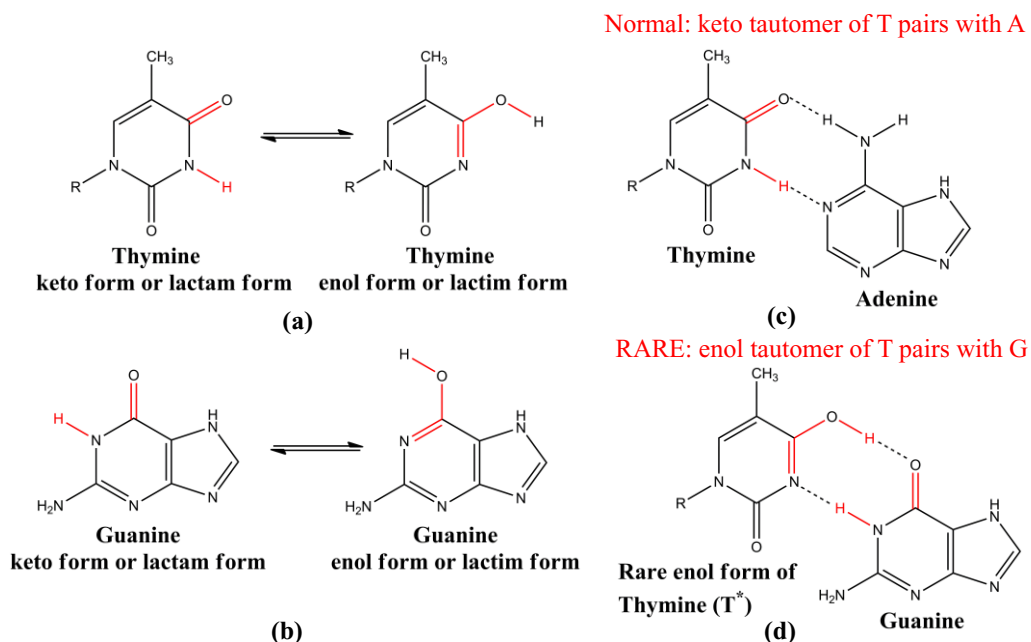


Figure 1.1. Tautomerization in DNA bases.

1.2 Intermolecular Interactions

Because of its significance, tautomerism has been studied for a long time (since 1884), but specific questions remain open. One challenge is that the equilibrium of tautomerization can

be tuned significantly by temperature and other environmental factors. Among a number of physical and chemical factors, such as excitation, chemical modification, metal stabilization, electron attachment, irradiation, etc.,¹⁹ solvation (hydration) occupies one of the most important roles. The solvent can control the dynamics of a proton transfer by solute/solvent interactions. A limited number of solvent molecules often can have dominant effects on the tautomerization process. The process also depends on the properties of the solvent.

Water, as the most important solvent molecule, can act both as a proton donor and as a proton acceptor and thus mediates the intramolecular proton transfer that leads to the formation of tautomers, supplying a bridge for proton relay. A recent experimental study reported the effect of the aqueous environment on tautomeric transformations, i.e., the enol-amide tautomer piroxicam in ethanol and DMSO will shift to the zwitterionic tautomer when water is involved.²⁰ In the above cases, intermolecular interactions play also vital roles in determining the structures of tautomers.

There are several kinds of intermolecular interactions, including dipole-dipole and similar interactions (ion-induced dipole and ion-dipole interactions), hydrogen bonding, and van der Waals interactions. In this thesis, I mainly focus on hydrogen bonding and van der Waals interactions (acetone-Ne complex in Chapter 3). The hydrogen bond determines the structures and functions of biomolecules; for example, it affects the structure and folding of proteins and is very important in determining the secondary structures of proteins, such as α -helices, β -sheets, and π -helices.^{21, 22} Water is an essential solvent in nature and is involved in many physical and chemical processes in chemistry, biology, and geochemistry.^{23, 24} For example, the hydration process has a remarkable effect on the stabilities of products in aqueous chemical reactions.²⁵ Over the past decades, theoretical studies of hydration effects on tautomeric equilibria have received considerable interest.²⁶⁻²⁹ For instance, Alagona et al. calculated the keto-enol tautomerism of pyruvate and acetylacetone in the presence of one or two water molecules.²⁷

1.3 Microwave Spectroscopy and Ab-Initio Calculations

The experimental investigation of water catalyzed keto-enol tautomerization in the gas phase faces unprecedented challenges as it requires measuring the microsolvation effects

stepwise. For one solvent molecule, applying IR spectroscopy plus the supersonic expansion of molecules, Matsuda et al. have measured the catalytic role of a single H₂O molecule in proton transfer in the acetone ion successfully.²⁵ Up to now, there has been only one reported experimental method, namely Fourier transform microwave (FTMW) spectroscopy, which has been used to elucidate the role of an H₂O molecule on the proton transfer in neutral tautomers.³⁰ FTMW spectroscopy is an extremely sensitive tool that has been used for measuring fine structural details of neutral molecules and clusters.³¹ It can be used to determine the structures of different tautomers precisely and even differentiate minor structural changes in molecules, as in the two different enol tautomers of benzoylacetone, discussed in Chapter 7. Moreover, FTMW spectroscopy has also been used to determine the barrier of the internal rotation of methyl groups accurately as described in this thesis for the acetone-Ne, acetone-water, acetylacetone-water, and benzoylacetone-water complexes in Chapters 3–4, and 6–7.

Ab initio calculations are very useful theoretical tools for predicting structures of different conformational isomers. They can also be used to calculate reaction barriers, such as the interconversion barrier in keto-enol tautomerism. Ab initio calculations also are used to predict the methyl internal rotation barrier, such as those in the acetone-Ne, acetone-water, acetylacetone-water, and benzoylacetone-water complexes. Thus, in the work for this thesis, I used microwave spectroscopy, aided by ab initio calculations, to explore the role of H₂O molecules on tautomerism of neutral molecules.

1.4 Objectives and Structure of the Thesis

The prototype molecules I have studied are selected from the ketone family of compounds, namely acetone (C₃H₆O), cyclohexanone ((CH₂)₅CO), acetylacetone (C₅H₈O₂), and benzoylacetone (C₁₀H₁₂O); their keto-enol tautomerizations are shown in Figure 1.2. Acetone is the simplest and smallest molecule in the ketone family. Its enol tautomer has been studied only using a titration method in solution.³² In the gas phase, to obtain the enol form, the ionic form of acetone has been studied;²⁵ there is no study on the keto-enol tautomerization in neutral acetone. Theoretical calculations suggest that water can lower the barrier of the keto-enol tautomerization in acetone, which might enable the detection of

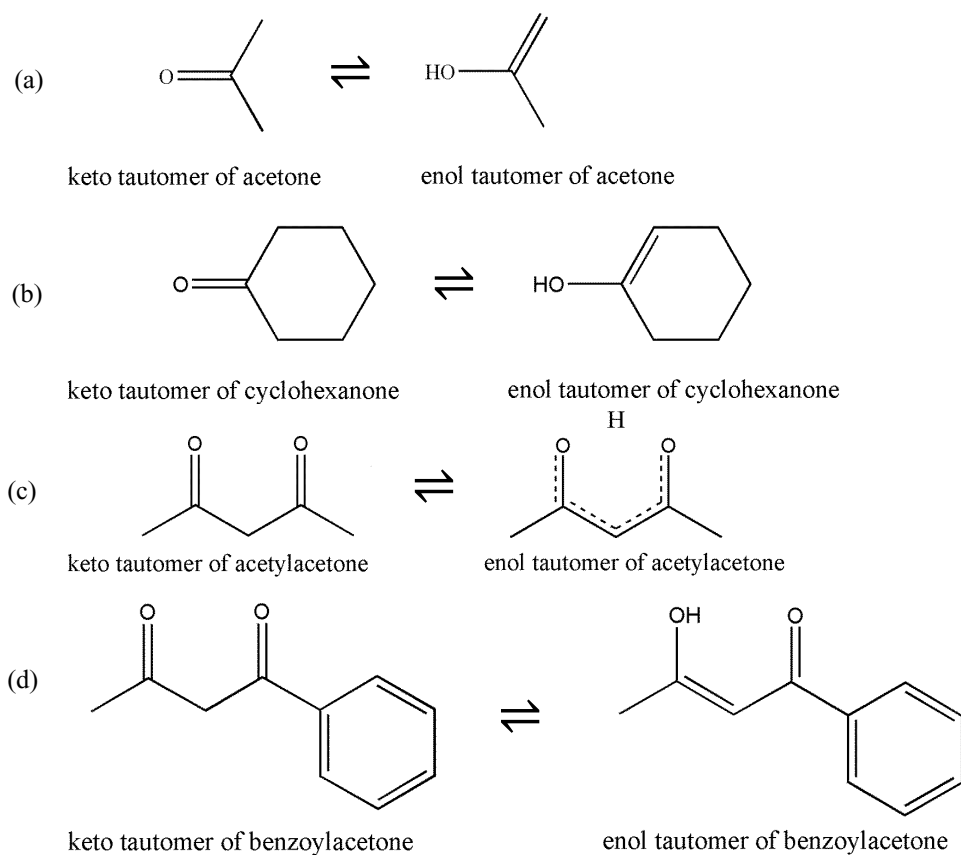


Figure 1.2. The keto-enol tautomerization of the prototype molecules that I studied.

the enol form of acetone in the acetone-water complex (Chapter 4). In the experimental study of the acetone-water complex, I used Ne as backing gas. The resulting spectrum is quite dense and I decided to study the acetone-Ne complex (Chapter 3) to reduce the number of unknown lines in the spectrum. Next, I studied cyclohexanone. In contrast to acetone, cyclohexanone has no methyl groups, and no internal rotation splittings would be expected, leading to less complicated spectra, which can be assigned more straightforwardly (Chapter 5). Lastly, I investigated two diketones, acetylacetone and benzoylacetone, which contain two carbonyl groups. The two carbonyl groups allow molecules more possibilities for interconversion between the keto and enol tautomers. Acetylacetone, a prototype molecule of β -diketones ($R_1-C=O-CH_2-O=C-R_2$, $R_1 = R_2 = CH_3$) with keto-enol tautomerization, attracts considerable interest.³³⁻⁴³ The enol form is the dominant tautomer, but the keto to enol tautomer ratio is in dispute; in the monomer study, only the enol tautomer was detected.⁴¹ My aim was to detect both the keto and enol tautomers in its complex with water (Chapter 6). Benzoylacetone,

another prototype molecule of β -diketones ($R_1 = C_6H_5$, $R_2 = CH_3$), with only one methyl group in the molecule, simplifies the spectra compared to the two methyl groups containing acetylacetone (Chapter 7). No studies of the monomer and water complexes had been carried out before.

The following is a summary of the contents of each chapter:

- Chapter 2 gives an introduction to the theoretical basis of rotational spectroscopy and a detailed description of the cavity-based FTMW and broadband chirped-pulse FTMW spectrometers. Apart from that, the theoretical calculations on the molecular systems I studied, together with some software I have used in my research, also are described.
- In Chapter 3, the microwave spectra of the van der Waals complexes acetone- ^{20}Ne and acetone- ^{22}Ne , which were measured using a cavity-based supersonic jet FTMW spectrometer, are described. The spectral assignments were achieved with the aid of constructing closed frequency loops. Experimental data allowed me to determine the position of the Ne atom.
- In Chapter 4, I report the rotational spectra of the acetone-water complex, combined with ab initio calculations, to investigate the effect of hydrogen bonding upon the internal rotation of the two methyl groups. Theoretical calculations were also performed to predict the possibility of detecting the enol tautomer of acetone when water is involved.
- I discuss the rotational spectrum of cyclohexanone-water complex in Chapter 5. The water assisted keto-enol tautomerism was investigated, and the most stable conformer of the cyclohexanone-water complex was assigned. Several isotopologues were found and analyzed to derive an experimental, r_0 , structure of the cyclohexanone-water complex.
- In Chapter 6, I report the microwave spectroscopic study of the acetylacetone-water complex which is supplemented by high-level theoretical calculations. Thus far, I have observed only the enol form of the acetylacetone-water complex.
- Chapter 7 describes the microwave spectra of the benzoylacetone monomer and its monohydrate. The assignment of the acetylacetone monomer shows that the methyl

internal rotation is coupled with the proton transfer between two carbonyl groups. The determined methyl internal rotation barrier in the benzoylacetone monomer helped me to identify the experimental structure as an average of these two enol tautomers. To confirm the position of the hydrogen atom between the two carbonyl groups, the spectrum of the deuterium of the benzoylacetone monomer is collected and assigned, and only the assignment of the deuterium of the most stable enol tautomer is obtained. Apart from that, two conformers of the benzoylacetone-water complex were also detected.

- The molecules I have studied and described in the previous chapters are either in their keto form or their enol form. None of the studies have captured both keto and enol tautomers simultaneously. In an effort to detect both keto- and enol-tautomers of the same molecule, exploratory work on several additional projects is described in Chapter 8.
- Chapter 9 presents the general conclusions of this thesis and provides suggestions of possible work that could be carried out in the future.

References

1. I. Lukovits, J. Fodor, Á. Gömöry, K. István, G. Keresztury and L. Kótai, *SAR QSAR Environ. Res.*, 2006, **17**, 323-335.
2. C. Dugave and L. Demange, *Chem. Rev.*, 2003, **103**, 2475-2532.
3. C. S. Cucinotta, A. Ruini, A. Catellani and A. Stirling, *ChemPhysChem*, 2006, **7**, 1229-1234.
4. E. P. Kündig, A. Enríquez García, T. Lomberget and G. Bernardinelli, *Angew. Chem. Int. Ed.*, 2006, **45**, 98-101.
5. W. Wang, H. W. Hellenga and L. S. Beese, *Proc. Natl. Acad. Sci.*, 2011, **108**, 17644-17648.
6. O. K. Abou-Zied, R. Jimenez and F. E. Romesberg, *J. Am. Chem. Soc.*, 2001, **123**, 4613-4614.
7. J. D. Watson and F. H. Crick, *Nature*, 1953, **171**, 964-967.
8. H. Grebneva, *J. Mol. Struct.*, 2003, **645**, 133-143.
9. J. McConnell, B. Sharma and R. Marsh, *Nature*, 1964, **203**, 399.
10. T. Steiner and G. Koellner, *Chem. Commun.*, 1997, **13**, 1207-1208.
11. M. Kubicki, *Acta Crystallogr., Sect. B: Struct. Sci.*, 2004, **60**, 191-196.
12. Z. H. Wu, J. P. Ma, X. W. Wu, R. Q. Huang and Y. B. Dong, *Acta Crystallogr., Sect. C: Cryst. Struct. Commun.*, 2009, **65**, 0128-0130.
13. H. Brandstetter, F. Grams, D. Glitz, A. Lang, R. Huber, W. Bode, H.-W. Krell and R. A. Engh, *J. Biol. Chem.*, 2001, **276**, 17405-17412.
14. K. Senthilkumar and P. Kolandaivel, *J. Comput. Aided Mol. Des.*, 2002, **16**, 263-272.
15. A. R. Katritzky, C. D. Hall, B. E.-D. M. El-Gendy and B. Draghici, *J. Comput. Aided Mol. Des.*, 2010, **24**, 475-484.
16. Y. C. Martin, *J. Comput. Aided Mol. Des.*, 2009, **23**, 693.
17. P. Pospisil, P. Ballmer, L. Scapozza and G. Folkers, *J. Recept. Signal Transduct.*, 2003, **23**, 361-371.
18. X. Yan, P. Day, T. Hollis, A. F. Monzingo, E. Schelp, J. D. Robertus, G. Milne and S. Wang, *Proteins: Struct., Funct., Bioinf.*, 1998, **31**, 33-41.
19. L. Gorb and J. Leszczynski, *J. Am. Chem. Soc.*, 1998, **120**, 5024-5032.
20. D. Ivanova, V. Deneva, D. Nedeltcheva, F. S. Kamounah, G. Gergov, P. E. Hansen, S. Kawauchi and L. Antonov, *RSC Adv.*, 2015, **5**, 31852-31860.
21. J. Šponer, J. Leszczynski and P. Hobza, *J. Phys. Chem.*, 1996, **100**, 1965-1974.
22. A. L. Lehninger, D. L. Nelson, M. M. Cox, *Lehninger Principles of Biochemistry*, Worth Publishers, New York, 2000.
23. W. Stumm, J. J. Morgan, *Aquatic Chemistry, Chemical Equilibria and Rates in Natural Waters*, 3rd ed. Wiley, New York, 1996.
24. P. M. Wiggins, *Microbiol. Rev.*, 1990, **54**, 432-449.
25. Y. Matsuda, A. Yamada, K. i. Hanaue, N. Mikami and A. Fujii, *Angew. Chem.*, 2010, **122**, 5018-5021.
26. M. W. Wong, K. B. Wiberg and M. J. Frisch, *J. Am. Chem. Soc.*, 1992, **114**, 1645-1652.
27. G. Alagona, C. Ghio and P. I. Nagy, *Phys. Chem. Chem. Phys.*, 2010, **12**, 10173-10188.

28. M. Kabeláč, and P. Hobza, *Phys. Chem. Chem. Phys.*, 2007, **9**, 903–917.
29. P. I. Nagy, *Biochem. Pharmacol.*, 2013, **S4**, 2167-0501.
30. S. Mata, V. Cortijo, W. Caminati, J. L. Alonso, M. E. Sanz, J. C. López and S. Blanco, *J. Phys. Chem. A*, 2010, **114**, 11393-11398.
31. G. B. Park and R. W. Field, *J. Chem. Phys.*, 2016, **144**, 200901.
32. Y. Chiang, A. Kresge and N. Schepp, *J. Am. Chem. Soc.*, 1989, **111**, 3977-3980.
33. J. L. Burdett and M. T. Rogers, *J. Am. Chem. Soc.*, 1964, **86**, 2105-2109.
34. T. J. Zielinski and A. Grushow, *J. Chem. Educ.*, 2002, **79**, 707.
35. J. W. Bunting, J. P. Kanter, R. Nelander and Z. Wu, *Can. J. Chem.*, 1995, **73**, 1305-1311.
36. A. Andreassen and S. Bauer, *J. Mol. Struct.*, 1972, **12**, 381-403.
37. K. Iijima, A. Ohnogi and S. Shibata, *J. Mol. Struct.*, 1987, **156**, 111-118.
38. S. A. Broadbent, L. A. Burns, C. Chatterjee and P. H. Vaccaro, *Chem. Phys. Lett.*, 2007, **434**, 31-37.
39. M. A. Rios and J. Rodríguez, *J. Mol. Struct. THEOCHEM*, 1990, **204**, 137-144.
40. J. Dannenberg and R. Rios, *J. Phys. Chem.*, 1994, **98**, 6714-6718.
41. W. Caminati and J.-U. Grabow, *J. Am. Chem. Soc.*, 2006, **128**, 854-857.
42. N. V. Belova, H. Oberhammer, N. H. Trang and G. V. Girichev, *J. Org. Chem.*, 2014, **79**, 5412-5419.
43. V. Feyer, K. C. Prince, M. Coreno, S. Melandri, A. Maris, L. Evangelisti, W. Caminati, B. M. Giuliano, H. G. Kjaergaard and V. Carravetta, *J. Phys. Chem. Lett.*, 2018, **9**, 521-526.

Chapter 2

Experimental Set-Up and Theoretical Calculations

The rotational spectra of all the molecular systems that I studied have been recorded using a cavity-based molecular beam Fourier transform microwave (FTMW) spectrometer and a broadband chirped-pulse FTMW spectrometer. This Chapter consists of an introduction to the theoretical basis of rotational spectroscopy, a detailed description of the cavity-based FTMW spectrometer, the principle and design of the broadband chirped-pulse FTMW spectrometer, an introduction to the theoretical calculations used to determine properties of the molecular systems I studied, and a brief description of software used for analyses of spectra and theoretical results.

2.1 Overview of Rotational Spectroscopy

Rotational spectroscopy is a powerful tool to determine structures of gas phase molecules. High-resolution and high-sensitivity spectroscopic techniques exist that can be used to measure rotational transitions of molecules with permanent dipole moments. The rotational transitions for many molecules occur upon microwave excitation in a wavelength range of 0.3 mm to 30 cm; therefore, rotational spectroscopy also is called microwave spectroscopy.

2.1.1 Solution of Time-Independent Schrödinger Equation

The time-independent rotational Schrödinger equation can be expressed using the rigid rotor approximation, and the Hamiltonian can be written as follows: ¹

$$\hat{H}_{\text{rot}} = \frac{\hat{J}_a^2}{2I_A} + \frac{\hat{J}_b^2}{2I_B} + \frac{\hat{J}_c^2}{2I_C} \quad (2.1)$$

where \hat{J}_a , \hat{J}_b , \hat{J}_c are the angular momentum operators in different principal inertial axes (a , b , c axis, respectively), and I_A , I_B , and I_C are moments of inertia. First, we need to determine the principal inertial axes, which are chosen in the following steps. The moment of inertia I_{xx} , in the x axis, for example, is defined as follows:

$$I_{xx} = \sum_{\alpha} m_{\alpha} r_{x,\alpha,\perp}^2 \quad (2.2)$$

where m_{α} is the mass of atom α and $r_{x,\alpha,\perp}$ is the perpendicular distance of atom α to the x axis; similarly, one calculates I_{xy} or I_{yy} , etc (for example, $I_{xy} = -\sum_{\alpha} m_{\alpha} x_{\alpha} y_{\alpha}$). Then, the moment of inertia tensor \mathbf{I} is processed by diagonalization. After that, the tensor \mathbf{I} can be calculated from the nonzero diagonal elements by:

$$\mathbf{I} = \begin{pmatrix} I_{xx} & 0 & 0 \\ 0 & I_{yy} & 0 \\ 0 & 0 & I_{zz} \end{pmatrix} \quad (2.3)$$

The axes are chosen based on the relative magnitudes of the principal moments of inertia, and the a -, b -, c -axes are labelled according to the following relations (for example, if the I_{xx} is the largest, the original x -axis will be labeled as the a -axis in the principal axis system, then if I_{yy} is the second largest, the original y -axis will be labeled as the b -axis, lastly, if I_{zz} is the smallest, the original z -axis will be labeled as the c -axis):

$$I_A \leq I_B \leq I_C \quad (2.4)$$

The rotational constants are defined as:

$$A = \frac{h^2}{8\pi I_A}; B = \frac{h^2}{8\pi I_B}; C = \frac{h^2}{8\pi I_C} \quad (2.5)$$

Molecules can be classified into five categories based on the different values of the three moments of inertia. Most molecules have three different moments of inertia ($I_A < I_B < I_C$); they are classified as asymmetric tops. When the three moments of inertia are the same, the molecules are classified as spherical tops. Linear molecules have one moment of inertia equal to zero and the other two moments of inertia are the same, i.e., ($I_A = 0, I_B = I_C$); if all moments of inertia are non-zero and two are equal, the molecules are classified as either prolate symmetric tops ($I_A < I_B = I_C$) or oblate symmetric tops ($I_A = I_B < I_C$).

The rotational energy levels, E_J , of linear molecules and spherical tops are given by the following equation:

$$E_J = BJ(J+1) = \frac{h^2}{8\pi I} J(J+1) \quad (2.6)$$

Here, J is the rotational angular momentum quantum number, I is the moment of inertia, h is Planck's constant. When deriving an expression for the rotational energy levels of symmetric tops, another quantum number, K , needs to be introduced; it is defined as the projection of the rotational quantum number J onto the molecular z axis. The energy levels of prolate, E_p , and oblate, E_o , symmetric tops can be expressed as follows:

$$E_p = BJ(J + 1) + (A - B)K_p^2; E_o = BJ(J + 1) + (C - B)K_o^2 \quad (2.7)$$

Note that A , B , C are rotational constants, and the energy levels of the asymmetric tops are labelled as $J_{K_a K_c}$ (here K_a (K_c) correlates to K_p (K_o) in the limit of the prolate (oblate) top), where J is a good quantum number and K is only a good quantum number when it is a symmetric top. In asymmetric tops, K is not a good quantum number anymore because there is no quantum number to describe the projection component of the angular momentum J along a certain fixed molecular axis. In addition, there is no way to solve the Schrödinger equation analytically in quantum mechanics for asymmetric tops. Instead, the Hamiltonian of the asymmetric tops should have matrix elements from the solution of symmetric tops. The wavefunction would be the superposition of the symmetric tops' wavefunctions.

Some selection rules need to be obeyed if a rotational transition happens when microwave excitation is applied to molecules. The first is that molecules must have permanent dipole moments. A molecule in general will have three dipole moment components, μ_a , μ_b , μ_c , along the principal inertial axes. If $\mu_a \neq 0$, a -type transitions can occur, which are characterized by the specific selection rules $\Delta K_a = \text{even}$ and $\Delta K_c = \text{odd}$, as in the case of the $J_{K_a, K_c} = 1_{01}-0_{00}$, transition, for example. Similarly, if $\mu_b \neq 0$, and $\Delta K_a = \text{even}$ and $\Delta K_c = \text{even}$, a b -type transition occurs ($J_{K_a, K_c} = 1_{11}-0_{00}$, for example), and if $\mu_c \neq 0$, $\Delta K_a = \text{even}$ and $\Delta K_c = \text{odd}$, and the observed transition, $J_{K_a, K_c} = 1_{10}-0_{00}$, for example, is a c -type transition.

The chemical bond in a certain molecule or complex is usually not rigid, especially when the molecule or complex rotates and experiences centrifugal forces that elongate the bond; then, the moments of inertia will be increased. To account for such an effect, fourth or sixth order centrifugal distortion constants are used to correct the energy level expression.

Sometimes, the Hamiltonian needs to be corrected when the rotor experiences a hindered motion, such as a methyl internal rotation, which is discussed in Chapters 3, 4, 6, and 7. For example, if we had one methyl groups in one molecule, the internal rotation of one methyl

group relative to the other part of the molecule can be described by the torsional angle a , and the potential energy, $V(a)$, can be expressed as follows²:

$$V(a) = \frac{V_3}{2}(1 - \cos 3a) \quad (2.8)$$

where V_3 is the three-fold barrier of the methyl group, since the methyl group has three equivalent hydrogen atoms. The wavefunction for the internal rotation with respect to a , $U(a)$, is as follows:

$$-F \frac{d^2 U(a)}{da^2} + \left[\frac{V_3}{2}(1 - \cos 3a) - E \right] U(a) = 0 \quad (2.9)$$

where $F = \hbar^2/2I_r$, I_r is the reduced moment of inertia for two methyl groups. To solve the equation, we need to consider these conditions, two of which are extreme.

a) The first condition is when V_3 is very small, i.e., tends to be zero, the methyl rotor can be assumed to be a free rotor. Eq. 2.9 will be simplified and can be solved by using the boundary condition $U(a) = U(a+2\pi)$; the solution of the eigen wavefunction $U(a)$ and the torsional eigenvalue are as follows:

$$U(a) = \sqrt{\frac{1}{2}} \pi e^{ima} = \sqrt{\frac{1}{2}} \pi (\cos ma + i \sin ma) \quad (2.10)$$

$$E = Fm^2 \quad (2.11)$$

where $m = 0, \pm 1, \pm 2, \dots$, which is the torsional state of the free rotor. According to Eq. (2.11), the quantum number m is doubly degenerate, except for $m = 0$.

b) The second extreme condition is when V_3 is very large, i.e. tends to be ∞ , and the internal rotation will be restricted in the potential well. The solution of the eigen energy can be expressed through expansion of $\cos 3a$ with respect to small values of a and using the harmonic oscillator approximation by introducing new quantum number ν as follows:

$$E = 3\sqrt{V_3 F} \left(\nu + \frac{1}{2} \right) \quad (2.12)$$

$$f = \frac{3}{2\pi} \left(\frac{V_3}{2I_r} \right) \quad (2.13)$$

where $\nu = 0, 1, 2, \dots$, which is the torsional energy level quantum number, and f is the torsional oscillation frequency, which determines the internal rotation barrier in microwave study.

c) For the normal case, when $0 < V_3 < \infty$, if $E < V_3$, classically there is no internal rotation because the barrier is too high. However, in quantum mechanics, the molecule could pass through the barrier by tunneling just as the wave function could penetrate through the classically forbidden area. The internal rotation occurs in such a case, and the triply degenerate torsional level ν will split into two sublevels: one sublevel is nondegenerate, labeled the A level, and the other sublevel is degenerate, labeled the E level. Then, the total wavefunction will be the linear combination of the three wavefunctions in the potential well; this is the case for the one methyl rotor, which is discussed in Chapters 6 and 7. In the case of two methyl groups, if the two methyl groups are equivalent, then the A and E levels will split further into AA, AE, EA, and EE levels; this is discussed for the acetone-Ne complex in Chapter 3. The EE levels will split further into $E_i E$ and $E E_j$ if the two methyl groups are not equivalent, i.e., one rotational transition will split into five components; this is discussed for the acetone-water complex in Chapter 4.

2.1.2 Solution of the Time-Dependent Schrödinger Equation

The previous Section provides the solution of the time-independent Schrödinger equation, which supplies information about the rotational transition energy levels and frequencies. The intensity of a rotation transition also is crucial, and it is directly related to the macroscopic polarization. To understand this, we need to solve the time-dependent Schrödinger equation.

The Bloch equations³⁻⁵ can be used for a theoretical description of microwave spectroscopy. The equations describe the interaction between the electric dipole moments of the molecular ensemble and the coherent pulsed microwave radiation, and the molecular ensemble is considered as N two-level systems. In a two-level system, as shown in Figure 2.1, ω_0 is the angular transition frequency.

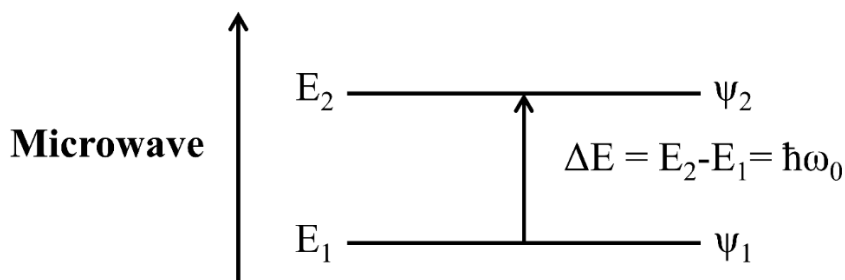


Figure 2.1. The two-level system with the microwave excitation.

The overall Hamiltonian \hat{H} for the molecule under the effect of electromagnetic radiation is given by:

$$\hat{H} = \hat{H}_0 + \hat{H}(t) \quad (2.14)$$

where \hat{H}_0 is the time-independent Hamiltonian and $\hat{H}(t)$ is the interaction between the electric dipole moment $\hat{\mu}$ of the molecules and the microwave radiation with angular frequency ω , and is given by:

$$\hat{H}(t) = -\hat{\mu} \varepsilon_0 \cos(\omega t) \quad (2.15)$$

The wavefunction of each two-level system can be written as follows:

$$\Psi(t) = a_1(t)\Psi_1 + a_2(t)\Psi_2 \quad (2.16)$$

where Ψ_1 and Ψ_2 are the stationary wavefunctions of the two states, respectively, and $a_1(t)$ and $a_2(t)$ are time dependent coefficients.

The electric dipole moment of the molecular ensemble average $\langle \bar{\mu} \rangle$ can be written in the density matrix formalism as follows:

$$\langle \bar{\mu} \rangle = \frac{1}{N} \sum_{m=1}^N \langle \bar{\mu} \rangle_m = \text{tr} \{ \bar{\rho} \cdot \bar{\mu} \} \quad (2.17)$$

where the superscript “=” is the density matrix notation and $\bar{\rho}(t)$ is the 2×2 matrix that contains all the time dependent matrix elements,⁶ defined as follows:

$$\bar{\rho}(t) = \begin{pmatrix} \rho_{11}(t) & \rho_{12}(t) \\ \rho_{21}(t) & \rho_{22}(t) \end{pmatrix} = \frac{1}{N} \begin{pmatrix} \sum_{m=1}^N a_{1,m}(t)a_{2,m}(t)^* & \sum_{m=1}^N a_{1,m}(t)a_{2,m}(t)^* \\ \sum_{m=1}^N a_{1,m}(t)a_{1,m}(t)^* & \sum_{m=1}^N a_{2,m}(t)a_{2,m}(t)^* \end{pmatrix} \quad (2.18)$$

Here $a_{1,m}(t)$ and $a_{2,m}(t)$ are time dependent coefficients. The diagonal elements of the density matrix are the population probabilities of Ψ_1 and Ψ_2 , and the off-diagonal terms are the coherence that correlates the phase relations between two energy levels. In Eq. 2.17, the term $\bar{\mu}$ is a 2×2 matrix of the transition dipole moment, in this matrix, $\bar{\mu}$, the diagonal matrix elements are zero and $\mu_{21} = \mu_{12}$, which is written as follows:

$$\bar{\mu} = \begin{pmatrix} 0 & \mu_{12} \\ \mu_{21} & 0 \end{pmatrix} \quad (2.19)$$

The macroscopic polarization $P(t)$, which is directly related to the experimental signal, is defined as follows:

$$P(t) = N \langle \bar{\mu} \rangle = N \cdot \mu_{12}(\rho_{12} + \rho_{21}) \quad (2.20)$$

To understand how the macroscopic polarization is generated better, we first need to find the solution to the time dependent density matrix elements ρ_{12} and ρ_{21} . The density matrix $\bar{\rho}$ evolving with time (t) could be expressed by the von Neumann equation,⁷ which is based on the time-dependent Schrödinger equation and is given by:

$$i\hbar \frac{\partial \bar{\rho}}{\partial t} = [\bar{H}, \bar{\rho}] = \bar{H}\bar{\rho} - \bar{\rho}\bar{H} \quad (2.21)$$

where both $\bar{\rho}$ and \bar{H} are in their matrix form, and \bar{H} is the Hamiltonian. After expanding Eq. 2.21, we will obtain a set of differential equations for elements of density matrix $\bar{\rho}$ evolving with time (t). To simplify the differential equation, the density matrix $\bar{\rho}$ is transformed from a laboratory frame into a rotating reference frame, which rotates with a frequency ω under the microwave excitation by utilizing the rotating wave approximation (RWA), which omits the high frequency term.⁸ To solve the time-dependent equation of $\bar{\rho}$, the Bloch variables $u(t)$, $v(t)$, $w(t)$ and $s(t)$ are introduced:^{9, 10}

$$\begin{aligned} w(t) &= \rho_{11}(t) - \rho_{22}(t); s(t) = \rho_{11}(t) + \rho_{22}(t); \\ u(t) &= \rho_{12}(t)e^{-i\omega t} + \rho_{21}(t)e^{i\omega t}; v(t) = i [\rho_{12}(t)e^{-i\omega t} + \rho_{21}(t)e^{i\omega t}] \end{aligned} \quad (2.22)$$

where $w(t)$ and $s(t)$ are the population difference and sum terms of the two energy levels, respectively, and $u(t)$ and $v(t)$ are coherence terms, which are the real and imaginary part of the macroscopic polarization. Then, the sum of the off-diagonal terms ($\rho_{12} + \rho_{21}$) in the density matrix can be written as follows:

$$\rho_{12} + \rho_{21} = u(t) \cos(\omega t) - v(t) \sin(\omega t) \quad (2.23)$$

The Bloch equations are formed by these four new Bloch variables:¹⁰

$$\begin{cases} \dot{u}(t) = -\Delta\omega(t) \cdot v(t); \\ \dot{v}(t) = \Delta\omega(t) \cdot u(t) - x \cdot w(t); \\ \dot{w}(t) = x \cdot v(t); \\ \dot{s}(t) = 0. \end{cases} \quad (2.24)$$

where $\Delta\omega(t) = \omega_0 - \omega$ is an off-resonance term (ω_0 is the rotational transition frequency, ω is the frequency of microwave excitation) and $x = \mu_{12}\epsilon/\hbar$ is the Rabi frequency. The latter represents the coupling strength between the microwave radiation and the molecules and measures the population fluctuations between Ψ_1 and Ψ_2 . In the derivation of the Bloch equations, phenomenological relaxation terms, which accounts for the decay of the molecular emission signal, could be added.

To solve Eq. 2.24, two conditions need to be considered to better understand how molecular signals are generated. One condition is that when $x \geq \Delta\omega(t)$, i.e., the microwave excitation power is assumed to be high, the term $\Delta\omega(t)$ could be omitted. Then, Eq. 2.24 will be simplified, i.e., $\dot{u}(t) = 0$, $\dot{v}(t) = -x \cdot w(t)$, and the solution will be as follows when applying the initial condition that $u(0) = v(0) = 0$, $w(0) = w_0$:

$$\begin{cases} u(t) = 0; \\ v(t) = -w_0 \sin(x \cdot t); \\ w(t) = w_0 \cos(x \cdot t). \end{cases} \quad (2.25)$$

According to Eq. 2.25, if we want to achieve the maximum coherence, where $\sin(x \cdot t) = 1$, then $x \cdot t = \pi/2 + 2n\pi$, $n = 0, 1, 2, \dots$ etc. This case is called the $\pi/2$ pulse, and $v(\pi(4n + 1)/2x) = -w_0$, $w(\pi(4n + 1)/2x) = 0$. Then, the macroscopic polarization $P(t)$ in Eq. 2.7 combined with Eq. 2.17, which is directly related to the experimental signal, can be expressed as follows:

$$P(t) = N \cdot \mu_{12}(\rho_{12} + \rho_{21}) = N \cdot \mu_{12} [u(t) \cos(\omega t) - v(t) \sin(\omega t)] \quad (2.26)$$

When $\sin(x \cdot t) = 0$, $x \cdot t = \pi + 2n\pi$, $n = 0, 1, 2, \dots$ etc, such a case is called a π pulse, and $v(\pi(2n + 1)/x) = 0$, $w(\pi(4n + 1)/2x) = w_0$. Then, the population is inversed, and the molecules will return to the ground state; thus, there is no coherence under such conditions. After the macroscopic polarization, i.e., when the microwave excitation is gone, $x = 0$ and

$\Delta\omega(t) \neq 0$. In such cases, it is off-resonance, then $w(t) = 0$, so the Bloch equation can be solved as follows:

$$\begin{cases} u(t) = w_0 \sin(\Delta\omega \cdot t); \\ v(t) = -w_0 \cos(\Delta\omega \cdot t); \\ w(t) = 0. \end{cases} \quad (2.27)$$

when Eq. 2.27 is substituted into Eq. 2.26, then:

$$P(t) = N \cdot \mu_{12} [w_0 \sin(\Delta\omega \cdot t) \cos(\omega t) + w_0 \cos(\Delta\omega \cdot t) \sin(\omega t)] \quad (2.28)$$

Under such conditions, the molecular emission signal is still oscillating with the rotational transition frequency ω_0 , and Eq. 2.28 can be simplified as follows:

$$P(t) = N \cdot \mu_{12} w_0 \sin(\omega_0 t) \quad (2.29)$$

2.2 Cavity-Based Fourier Transform Microwave Spectrometer (FTMW)

Most of the rotational spectra of the molecules and complexes described in this thesis were recorded using the cavity-based molecular beam FTMW spectrometer. In early studies of microwave spectroscopy, the waveguide Stark spectrometer was used^{11, 12} to study important topics in molecular structure, including separating conformers with a low barrier and methyl group internal rotation tunneling.¹³ The cavity-based FTMW spectrometer was designed by Balle and Flygare in 1979;¹⁴⁻¹⁶ it provides higher sensitivity and greater resolution.¹⁷⁻²³ The spectrometer I used is based on the Balle and Flygare design. The detailed design is shown in Figure 2.2 and the components of the spectrometer are listed as follows: (1) Hewlett Packard MW synthesizer, (2) pulse generator, (3) power divider, (4) isolator, (5) MW PIN diode switch, (6) 20 MHz double balanced mixer, (7) MW power amplifier, (8) MW PIN switch, (9) circulator, (10) antenna, (11) nozzle, (12) MW PIN switch, (13) MW power amplifier, (14) image rejection mixer, (15) isolator, (16) radio frequency (RF) amplifier, (17) RF mixer, (18) band pass filter, (19) RF amplifier, (20) transient recorder, (21) personal computer, (22) diffusion pump, (23) mechanical pump, (24) detector, (25) oscilloscope, (26) antenna.

stored in the cavity to the power dissipation. In our instrument, the Q factor is on the order of 10^4 . At a frequency of 10 GHz, the bandwidth of the cavity is ~ 1 MHz.

2.2.2 Supersonic Jet Expansion

For molecules in the size regime of those described in this thesis, a broad distribution of rotational energy levels is populated at room temperature. As a result, the intensities of rotational transitions are low, because they depend on population differences; this can make the measurement of rotational spectra and their assignment quite difficult. The application of a supersonic jet expansion to cool down the molecules leads to a narrower distribution of populated energy levels and therefore to more intense lines and simplified spectra. The technique of a supersonic expansion beam has expanded the range of accessible molecular systems greatly and significantly improved the sensitivity and frequency resolution in rotational spectroscopy²⁴⁻²⁶. In a supersonic jet expansion, the molecules of interest are mixed with noble gases (usually He, Ne, or Ar) at a high pressure (1–5 bar) and expanded adiabatically through a, in our case pulsed, nozzle orifice into a vacuum chamber (10^{-6} Torr). The nozzle orifice should be selected carefully so that the diameter of the orifice is much larger than the mean free path of the molecules. Once the nozzle is opened, many collisions occur near the orifice in the nozzle, most of which will be between the carrier gas atoms (He, Ne were usually used). Through the expansion, the volume is increases, and a very low translational temperature can be obtained (<1 K) because part of the thermal energy of molecules will convert into kinetic energy (directed). After passing the orifice, the flow velocity rapidly approaches a limiting value in one direction and becomes almost constant for the rest of the expansion resulting in a collision free environment. The cluster formation in the expanding gas occurs through a three-body collision, where the noble gas carries off the excess kinetic energy so that the cluster is stabilized during this process. The molecules are cooled down to rotational temperatures of ~ 1 –4 K because of the efficiency of the energy exchange between the translational and rotational degrees of freedom. A result is greatly simplified rotational spectra at these low temperatures, as compared to room temperature.

In my experiments, the nozzle, with an orifice diameter of 0.5 mm, is mounted near the center of the fixed mirror, just below one antenna (10). The sample is prepared at room temperature by mixing the molecules of interest with a noble gas as a carrier in a gas cylinder,

and then they are introduced with a pulsed supersonic jet expansion into the microwave cavity through the pulsed nozzle (11). The coaxially oriented design between the molecular beam and cavity results in a occurrence of a Doppler doublet in each transition; the transition frequency is taken as the average of the two Doppler components. The coaxial setup of the nozzle and resonator also gives us very high spectral resolution, about five kHz, compared with the perpendicular design.²⁴

2.2.3 Generation of Microwave Excitation Pulse and Detection of Molecular Emission Signal

The microwave excitation frequency (ν_0) is generated by a continuous-wave Hewlett Packard microwave generator (1). A power divider (2) is used to divide the excitation frequency into two arms, an excitation arm and a detection arm. In the excitation arm, the microwave signal passes through an isolator (4), then goes to a first PIN diode switch (5), and then is mixed with a 20 MHz reference frequency via a double balanced mixer (6) to generate two sidebands ($\nu_0 \pm 20$ MHz). The output signal then goes into a power amplifier (7) and passes through a second PIN diode switch (8) to a circulator (9). Next, the microwave pulse is coupled into the cavity through the wire-hook antenna. The molecules that have been introduced into the cavity will interact with this microwave excitation pulse, their dipole moments align, and a macroscopic polarization will be generated. Due to the weakness of the molecular emission signal,⁵ a double superheterodyne mixing scheme is used in the detection. The frequency of the molecular emission signal is $\nu_0 - 20$ MHz + ν_d , where ν_d is the difference between ν_0 and the molecular transition frequency ν_l . This emission signal is picked up by the same antenna, enters the circulator (9), and an additional PIN diode (12) is used to protect the detection arm from the high-power microwave excitation pulse. The molecular emission signal then is amplified and down-converted to 20 MHz + ν_d by mixing it with the excitation frequency (ν_0) from the second arm (detection arm) of the synthesizer (1) in an image rejection mixer (14). Then, the radio frequency (RF) signal, is amplified by a RF amplifier (16), and further mixed with a 35 MHz reference frequency using an RF mixer (17), so that the frequency is down-converted to 15 MHz + ν_d . This signal passes through a 15 MHz band pass filter (18) and is amplified one last time. The final signal is coupled into a transient recorder (20) for analog-to-digital(A/D) conversion (8 bit A/D converter, 50MHz sampling interval, 32 k on-board memory). In my

experiment, 8 k data points are collected at intervals of 60 or 120 ns in high resolution measurement, while the sampling interval of 20 ns is employed when performing an automated scans to obtain broader frequency ranges.²⁷ Finally, the time domain signal is fed into the personal computer (21) and Fourier transformed to yield the frequency spectrum.

2.2.4 Timing of Pulse Sequences

The timing of MW excitation pulses, data acquisition trigger, and A/D-converter clock in the cavity-based microwave spectrometer is crucial because it needs to guarantee phase coherence when collecting successive molecular emission signals. The time sequence of one experiment is shown in Figure 2.3. In carrying out microwave experiments, the transistor-transistor logic (TTL) pulse sequences are used to control microwave pulse generation and molecular emission signal detection. First, I tune the cavity into resonance. Then, the prepared sample mixture is introduced into the cavity through a supersonic jet expansion, i.e., the first molecular pulse is generated, and its period is 400–900 μs ; Next, the microwave excitation pulse ($\sim 1 \mu\text{s}$) is applied to excite the molecules with a $\pi/2$ pulse, and a PIN diode switch is used simultaneously to protect the detection arm from the high power microwave excitation pulse. Lastly, after a trigger delay (8–26 μs) until the microwave excitation signal has dissipated, the transition recorder begins to process the molecular emission signal.

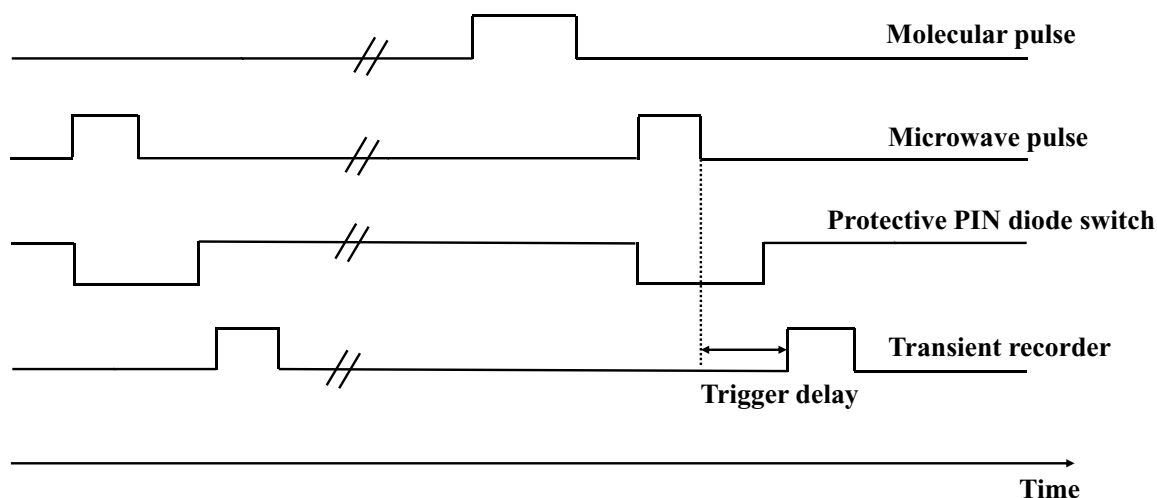


Figure 2.3. Time sequence of an experimental measurement cycle with the cavity-based FTMW spectrometer.

2.3 Chirped-Pulse Fourier Transform Microwave Spectrometer

The cavity-based FTMW spectrometer has two advantages over the chirped pulse FTMW spectrometer: one is that it requires relatively low power for the microwave excitation pulse (a few mW); the other is that it enhances the amplitude of the molecular emission signal. However, it is a narrowband spectrometer as its measurement bandwidth is just 1 MHz; this makes it laborious to obtain a wide frequency spectrum. For example, it takes approximately overnight (~12h) to acquire a spectrum over a 250 MHz range using 50 signal averages with 0.2 MHz frequency steps, and most of the time is spent on measuring spectral ranges without detectable lines. Therefore, the invention of the broadband chirped-pulse FTMW spectrometer brings us great convenience in acquiring molecular emission data. With the advanced development in arbitrary waveform generators and broadband signal digitizers, the first chirped-pulse Fourier transform microwave spectrometer was built in 2006 in Brooks Pate's group at the University of Virginia.²⁸ Our chirped pulse FTMW spectrometer was reported previously, and its resolution is ~25 kHz.²⁹ A schematic diagram of the instrument is shown in Figure 2.4. The components of the above diagram are the following: (1) 10 MHz rubidium (Rb) frequency standard, (2) 3.96 GHz phase-locked dielectric resonator oscillator (PDRO), (3) arbitrary waveform generator, (4) microwave synthesizer, (5) double balanced mixer, (6) solid state amplifier (power 20 W), (7) horn antennas, (8) nozzle, (9) nozzle driver, (10) digital delay generator 1, (11) digital delay generator 2, (12) oscilloscope, (13) personal computer, (14) amplifier, (15) power limiter, (16) PIN diode switch, (17) amplifier, (18) double balanced mixer, (19) microwave synthesizer, (20)-(21) low pass filter, (22) diffusion pump, (23) mechanical pump.

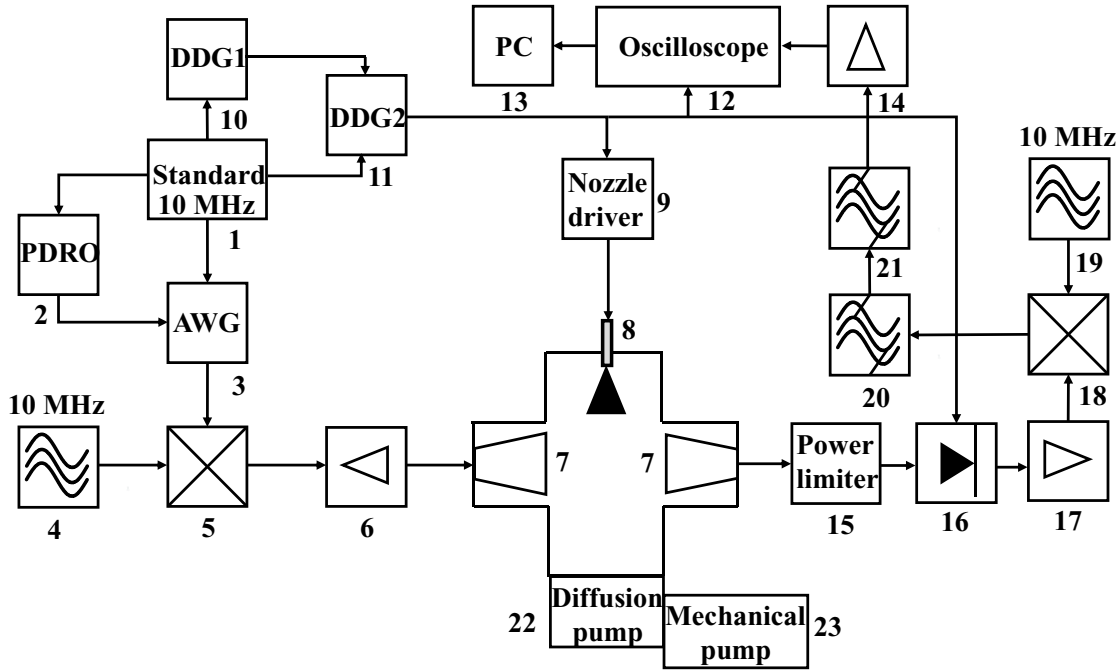


Figure 2.4. A schematic diagram of components of the chirped-pulse broadband FTMW spectrometer.

2.3.1 Generation of the Chirped Microwave Pulse

To perform a broadband FTMW experiment, we need a chirped microwave pulse as the microwave source. The chirped pulse is a phase-reproducible linear frequency sweep within a short period ($\sim 4 \mu\text{s}$) so that the sample can be polarized faster than the pure dephasing of the molecular emission. It can be generated by an arbitrary wave generator (AWG, sample rate is 4.2 GS/s; Tektronix, AWG710B; (3)). The AWG is referenced to an external 3.96 GHz signal, which is produced by a phase-locked dielectric resonator oscillator (PDRO, (2)). In the experiment, the AWG generates a $4 \mu\text{s}$ chirped pulse (v_{cp}) with a frequency range of 0–1 GHz. To ensure high phase stability when averaging the molecular emission signal, both AWG and PDRO are phase locked to a Rb-disciplined crystal oscillator at a standard frequency of 10 MHz (Stanford Research Systems, FS725; (1)). Then, the generated chirped pulse from AWG is mixed with a fixed microwave frequency ν_0 (produced by a microwave synthesizer (Agilent Technologies, E8257D; (4))) via a double balanced mixer (Microwave Power, L0818-43; (5)). The purpose of this mixing is to up-convert the chirped-pulse range of 0–1 GHz from the AWG to a microwave frequency range. The resulting chirped pulse has then a 2 GHz bandwidth, $\nu_0 \pm v_{\text{cp}}$, with the center frequency at ν_0 . The measurement range of the broadband chirped-pulse

microwave spectrometer is 8–18 GHz; therefore the desired frequency range can be obtained by setting a proper center frequency. To excite molecules in a wide frequency range, it is necessary to have a high-power pulse because there is no cavity to accumulate the energy, as in the cavity-based microwave spectrometer. Therefore, the up-converted output from the mixer is amplified by a 20 W solid-state amplifier (6). After that, the signal is broadcasted into the vacuum chamber via a horn antenna (7).

2.3.2 Sample Cell- the Interaction Region of Microwave Excitation Pulse and Molecular Beam

A six-way cross aluminium vacuum chamber forms the sample cell of the chirped pulse FTMW spectrometer. The vacuum in the sample cell is maintained by a diffusion pump (Edwards, Diffstak 160; (22)) with a speed of 1300 L/s, supported by a rotary-vane mechanical pump (Edwards, E2M30; (23)). Molecules are introduced into the vacuum chamber through a supersonic jet expansion via a pulsed nozzle (8), which is driven by a nozzle driver (9). A pair of high gain horn antennae (7) is mounted inside of the vacuum chamber, and the function of one horn antenna is to broadcast the amplified microwave chirped pulse to excite the molecules, while that of the other horn antenna is to collect the molecular emission signal. The two horn antennae are parallel to each other in the horizontal direction, and the separation is ~30 cm, while the nozzle is perpendicular to the position of two horn antennae; as a result, no Doppler splitting is observed in the spectra. Due to this perpendicular design of the molecular beam and the microwave chirped excitation pulse, the interaction time (the pulse duration is ~500 μ s) between molecules and the microwave excitation is less than that in the cavity-based FTMW spectrometer. Microwave absorbing foam covers the interior surfaces of the vacuum chamber to avoid reflections of the microwave radiation, which would contaminate the molecular emission signal.

2.3.3 Detection of the Molecular Emission Signal

Once the molecular sample is polarized by the high-power chirped microwave excitation pulse, the molecular emission signal is collected by one of the high gain horn antennae. Then, the signal passes through a power limiter (15), and a PIN diode switch, which is used to protect the low noise signal amplifier (17) from the high-power microwave chirped pulse. After going

through the low noise amplifier (17), the signal is mixed by a double balanced mixer (18) with a microwave frequency (from microwave synthesizer 2, (19)), which is 1.5 GHz higher than the center frequency of the chirped pulse ($\nu_0 + 1.5$ GHz) to prevent folding of the rotational spectrum about the center frequency. The mixed signal is filtered by two 4.4 GHz low pass filters ((20), (21)) to delete any high frequency artifacts. Then, the filtered signal is amplified again by another low noise amplifier (14). Next, the amplified signal is digitized with a fast-digital oscilloscope (12) at a rate of 40 GS/s. This oscilloscope also is phase-locked to the 10 MHz reference from the Rb-disciplined master clock to ensure phase coherence during the averaging of the molecular emission signal. Finally, the time domain signal from the oscilloscope is transferred to a personal computer (13), averaged, and Fourier transformed to generate the frequency domain spectrum. The resolution of the chirped pulse FTMW spectrometer is ~ 25 kHz.

2.3.4 Timing of Chirped Pulse Sequences

To ensure phase coherence of successive time domain signals in the broadband FTMW measurement, a phase stabilized time sequence is essential. Figure 2.5 shows the time sequence during the experiment. First, molecules of interest are introduced into the sample cell through a supersonic jet expansion (usually 400–900 μs molecular pulse); second, a microwave chirped-pulse is applied to excite the molecules, and usually is repeated four to six times after certain delay cycles in order to acquire high quality signals; third, the PIN diode switch is used always to protect the low noise amplifier from the high-power microwave chirped-pulse signal; finally, a trigger delay pulse is used to start recording of the molecular emission signal. To achieve the high phase stability, all frequency sources are phase locked to a Rb-disciplined crystal oscillator at a frequency of the 10 MHz standard (1). A digital delay generator (10) generates the TTL pulse sequence, and it controls one experiment cycle. For timing between successive experiment cycles, the other digital delay generator (11) also is used to avoid signal overlapping.

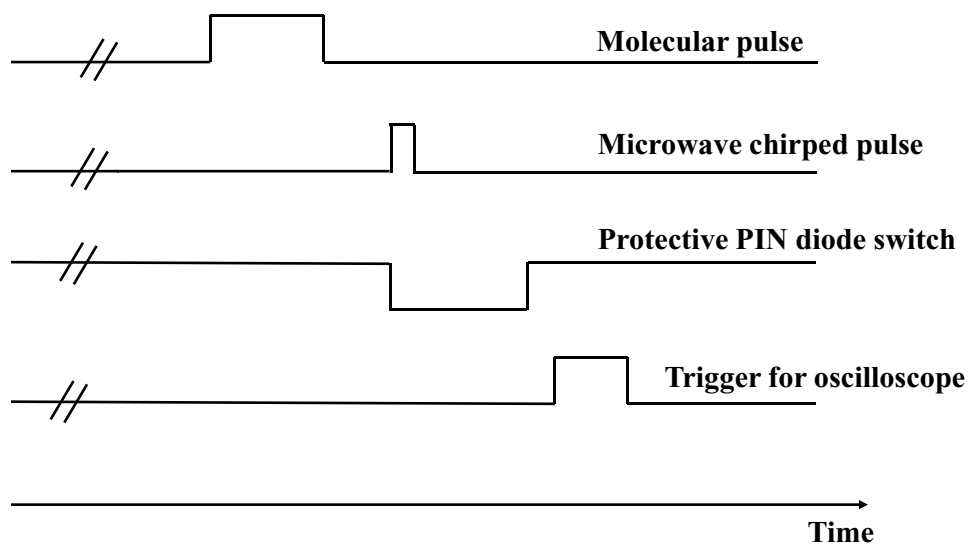


Figure 2.5. Time sequence of a measurement cycle with the chirped-pulse broadband FTMW spectrometer.

2.4 Theoretical Calculations

Based on Section 2.1, it is crucial to obtain the molecular structure using theoretical calculations. From the calculated molecular structure, we can get rotational constants and dipole moments of molecules of interest. The basis of all the theoretical calculations is quantum mechanics, which is the most accurate model to describe the behavior of molecules. According to this model, the basic equation for describing the structure of molecules is the time-independent Schrödinger equation:

$$\hat{H} \Psi = E \Psi \quad (2.30)$$

Solving Eq.2.30, we can obtain the energy of a molecule, and some other properties (such as electron density, dipole moments, etc.) can be derived from its solution. Because we cannot solve the Schrödinger equation exactly, only approximate solutions are possible. There are two categories of approximation approaches to solve the Schrödinger equation: one is to solve the wave function directly, usually called wave function based ab initio calculation; the other is to solve the electron density instead, called the density functional theory (DFT) calculation (also can be called density functional based ab initio calculation). I will summarize the properties of these two methods briefly.

2.4.1 Ab Initio Calculations

The first approximation is the Born-Oppenheimer approximation; it presumes that the nuclei do not move relative to the electrons because light electrons move much faster than the heavy nuclei. Next, the Hartree-Fock (HF) approximation³⁰ is introduced and assumes that electrons move independently of each other. Specifically, the repulsion between single pairs of electrons is replaced by the repulsion between a given electron and an average charge cloud from all other electrons. This approximation overestimates the electron-electron correlation (repulsion); as a result, the HF energy is higher than the true energy, not only due to the variational principle but also because of the overestimation of interactions when more than one electron is treated simultaneously. Therefore, this approximation has problems when calculating systems where dispersive forces are the dominant interactions, such as weakly-bound complexes. There are many methods that include electron correlation in a molecular orbital calculation. With the development of the HF method, the Møller-Plesset (MP) perturbation theory³¹ (MP2, MP4, etc.) first takes the electron correlation as the “perturbation” to the HF solution when HF is a good starting point. MP2, which includes the double excitations, usually is the most common method to obtain highly accurate results because it is sufficient and less expensive compared with other high order perturbation theories (MP4, etc.). In Chapters 3 to 6 and 8, MP2 (second-order perturbation theory) is used. The calculated energy in MP2 usually is lower than the true energy because it is not a variational method compared with HF. The coupled cluster (CC) method³² is another category that includes electron correlation. It takes the HF molecular orbital method as the basis and uses the exponential cluster operator to operate on multi-electron wavefunctions to take the electron correlation into account. The CCSD(T) (coupled cluster singles and doubles with perturbative estimates of triples)³³ is thought of as the “gold standard” computational method because it covers not only the dominant two electron interactions but also the simultaneous interactions of three or more electrons when all possible excitations are included. However, the calculation is very expensive, so it is only used for the acetone-Ne system in Chapter 3.

2.4.2 Density Functional Theory (DFT) Calculations

Ab initio calculations, such as HF or MP2 methods, aim to obtain the solutions for the wavefunction, which itself is an approximation for electron density. DFT calculations compute electron density directly through constructing proper functions, and the energy can be calculated from the electron density using the Kohn–Sham equations³⁴:

$$E[\rho] = T_e[\rho] + E_{ne}[\rho] + E_{ee}[\rho] + E_{xc}[\rho] \quad (2.30)$$

where ρ is the electron density function, $T_e[\rho]$ is the kinetic energy of the electrons, $E_{ne}[\rho]$ is the electron-nuclei interaction energy, $E_{ee}[\rho]$ is the Hartree (or Coulomb) energy or electron-electron repulsion energy, and $E_{xc}[\rho]$ is the exchange-correlation energy. The first three terms can be calculated exactly, but the fourth term needs an approximation because there is no exact solution for this term.

Most of the DFT theorists focused on getting a better definition and solution for the exchange-correlation energy. Axel Becke³⁵ in 1993 first applied hybrid functionals, which combines part of the exact exchange from HF with the rest of the ab initio or empirical parameters into the fourth term. The most popular exchange-correlation functional is B3LYP (Becke, three-parameter, Lee-Yang-Parr)^{36, 37}, which improves many molecular properties, such as bond length and vibrational frequencies³⁸ that are not well described in simple ab initio calculations. However, the B3LYP functional has one limitation in that it completely neglects the long-range interactions, such as dispersion forces and π - π interactions. M06-2X was introduced³⁹ in 2006 to describe dispersion interactions better as it captures the medium range electron correlation by constructing E_{xc} with empirical fitting of their parameters; it is used for the acetone-Ne system in chapter 2. However, the long-range electron correlation that is omitted by these functionals also can be crucial.

In 2010, the density functional dispersion correction (DFT-D)⁴⁰ was introduced, especially the DFT-D3BJ correction⁴¹, which is crucial to calculate the rotational constants accurately. There are two versions in DFT-D3 that differ in the format of their damping functions. Damping functions are utilized to adjust the short- and mid-range of the dispersion correction to avoid the double-counting effects because, although the traditional DFT functionals can describe the short-range interaction properly, if the correction is too large in short distances, then repetition will occur. One version of DFT-D3 uses a zero-damping function, and the other uses the Becke-Johnson (BJ) damping function, which not only has a more sophisticated empirical fitting procedure but also contains more physical ingredients and makes the

calculated results closer to the experimental values. In Chapters 5 and 8, the DFT-D3BJ correction is used, and the calculated rotational constants are very close to the experimental results. The advantage of using DFT-D3BJ is that it can achieve CCSD(T) accuracy of optimizing structures with low cost.

2.4.3 Basis Sets

A basis set is a set of functions that is used to describe the atomic orbitals, which enable one to approximate the actual wave functions. Gaussian functions usually are utilized to mimic Slater-Type Orbitals (STO) because of the simplicity in mathematical calculations. The selection of a proper basis set is crucial because it will save significant time for a given calculation method. For example, one of Pople's split-valence basis sets⁴², 6-311++G(2d,p), is used always with the MP2 method in this thesis. A split-valence basis uses only one basis function for each core atomic orbital (AO) and a larger basis function for the valence AOs. Here, "6" denotes the core atomic orbitals, and one basis function is made of six Gaussian functions; "-" is the split valence symbol; "311" is the valence triple zeta, which means that the valence AOs are described by three orbitals, where the first orbital is made of three Gaussian functions, and the second and the third orbital are made of one Gaussian function. The polarization functions are denoted by * or (d, p), and the diffuse functions are marked by +. Dunning's correlation-consistent basis set also is used in the thesis, for example, the aug-cc-pVTZ basis set, where "aug" denotes the diffuse function, "cc" means correlation consistent, and "pVTZ" is polarized valence triple zeta functions.

2.4.4 Analysis of the Rotational Spectra

Once I have optimized the molecular structure using different theoretical calculations in GAUSSIAN 09⁵², I could get rotational constants of molecules from calculation. Using the coordinates of the optimized structure, I calculated the rotational constants of isotopologues using the PMIFST program⁴³ in Chapters 3–5. From the calculated rotational constants, I put them into the PGOPHER program⁴⁴ to predict the rotational spectrum. Based on the predicted spectrum, I do the experiment to measure the candidate lines. After measuring the experimental spectrum, I also use this program to do the fitting. After fitting, I will obtain the experimental rotational constants and distortion constants. If the molecular systems had methyl group(s), as

in Chapters 3–4 and 6–7, I will first calculate the internal rotation barrier(s) of the methyl group(s). Then based on the prediction of the rotational constants and internal rotation barrier(s), I will use XIAM⁴⁵ to predict internal rotation splittings in each rotational transition. Then I do the experiment to measure the candidate lines. After measuring the experimental spectrum, I will first fit the candidate A(A) components in rotational transitions using the PGOPHER program. If the fitting for the A(A) components is successful, I will put those fitted rotational constants and distortion constants from the PGOPHER program, the calculated internal rotation barrier(s), and all the measured candidate lines into the XIAM program to do the final fit. After fitting, the new experimental rotational constants, distortion constants, internal barrier(s) of methyl group(s), and the angles of the methyl group(s) relative to the principal inertial axis can be obtained. Once I had all the new experimental rotational constants including the parent and isotopologues species, I can use the STRFIT program⁴⁶ to fit the experimental structure in Chapters 3 and 5. For example, to determine the experimental position of Ne atom relative to acetone monomer in the Ne-acetone complex in Chapter 3, I first obtain the optimized structure from theoretical calculation, and then put the calculated distance, angles and the fitted rotational constants of acetone-²⁰Ne and acetone-²²Ne complexes into the STRFIT program, after fitting, the fitted distance and angles of Ne atom relative to the acetone monomer will be obtained. Analysis of the topology of the molecular electron density using the Quantum Theory of Atoms in Molecules (QTAIM)^{47, 48}, the Multiwfn⁴⁹ and Visual Molecular Dynamics (VMD, version 1.9.3)⁵⁰ programs were utilized. The programs were also used to generate graphical representations of the Non-Covalent Interactions (NCI)⁵¹ analyses.

References

1. P. F. Bernath, *Spectra of Atoms and Molecules*, New York, 1995, 159-194.
2. W. Gordy, R. L. Cook, 1984. *Microwave Molecular Spectra*, John Wiley & Sons.
3. J. C. McGurk and W. H. Flygare, *J. Chem. Phys.*, 1973, **59**, 5742-5743.
4. T. G. Schmalz, W. H. Flygare, 1978. *Laser and Coherence Spectroscopy*, (ed.; J. I. Steinfeld) Plenum, New York, pp. 125-196.
5. H. Dreizler, *Mol. Phys.*, 1986, **59**, 1-28.
6. Blum, K., 2012. *Density matrix theory and applications (Vol. 64)*. Springer Science & Business Media.
7. Von Neumann, J., 1927. Wahrscheinlichkeitstheoretischer aufbau der quantenmechanik. *Nachrichten von der Gesellschaft der Wissenschaften zu Göttingen, Mathematisch-Physikalische Klasse*, **1927**, pp.245-272.
8. Y. Wu and X. X. Yang, *Phys. Rev. Lett.*, 2007, **98**, 013601.
9. Allen, L. and Eberly, J.H., 2012. *Optical resonance and two-level atoms*. Courier Corporation.
10. Arecchi, F. and Bonifacio, R., 1965. Theory of optical maser amplifiers. *IEEE Journal of Quantum Electronics*, **1**, pp.169-178.
11. K. B. McAfee, R. H. Hughes and E. B. Wilson, *Rev. Sci. Instrum.*, 1949, **20**, 821-826.
12. R. H. Hughes and E. B. Wilson, *Phys. Rev.*, 1947, **71**, 562-563.
13. N. L. Owen, *J. Mol. Struct.*, 1970, **6**, 37-47.
14. T. J. Balle, E. J. Campbell, M. R. Keenan and W. H. Flygare, *J. Chem. Phys.*, 1979, **71**, 2723-2724.
15. T. J. Balle, E. J. Campbell, M. R. Keenan and W. H. Flygare, *J. Chem. Phys.*, 1980, **72**, 922-932.
16. T. J. Balle and W. H. Flygare, *Rev. Sci. Instrum.*, 1981, **52**, 33-45.
17. Y. Hirahara, Y. Ohshima and Y. Endo, *J. Chem. Phys.*, 1994, **101**, 7342-7349.
18. Y. Ohshima and Y. Endo, *J. Mol. Spectrosc.*, 1992, **153**, 627-634.
19. K. Seki, Y. Sumiyoshi and Y. Endo, *J. Chem. Phys.*, 2002, **117**, 9750-9757.
20. Y. Ohshima and Y. Endo, *Chem. Phys. Lett.*, 1996, **256**, 635-640.
21. M. Becucci and S. Melandri, *Chem. Rev.*, 2016, **116**, 5014-5037.
22. W. Li, L. Evangelisti, Q. Gou, W. Caminati and R. Meyer, *Angew. Chem.*, 2019, **131**, 869-875.
23. L. Spada, I. Uriarte, W. Li, L. Evangelisti, E. J. Cocinero and W. Caminati, *Phys. Chem. Chem. Phys.*, 2019.
24. J. U. Grabow and W. Stahl, *Z Naturforsch.*, 1990, **45A**, 1043-1044.
25. J. U. Grabow, W. Stahl and H. Dreizler, *Rev. Sci. Instrum.*, 1996, **67**, 4072-4084.
26. E. Arunan, S. Dev and P. K. Mandal, *Appl. Spectrosc. Rev.*, 2004, **39**, 131-181.
27. Y. Xu and W. Jäger, *J. Chem. Phys.*, 1997, **106**, 7968-7980.
28. G. G. Brown, B. C. Dian, K. O. Douglass, S. M. Geyer, S. T. Shipman and B. H. Pate, *Rev. Sci. Instrum.*, 2008, **79**, 053103.
29. S. P. Dempster, O. Sukhorukov, Q. Y. Lei and W. Jäger, *J. Chem. Phys.*, 2012, **137**, 174303.
30. J. C. Slater, *Phys. Rev.*, 1952, **87**, 807-835.

31. C. Moller and M. S. Plesset, *Phys. Rev.*, 1934, **46**, 0618-0622.
32. U. Fano, *Phys. Rev.*, 1961, **124**, 1866.
33. K. L. Bak, P. Jorgensen, J. Olsen, T. Helgaker and J. Gauss, *Chem. Phys. Lett.*, 2000, **317**, 116-122.
34. W. Kohn and L. J. Sham, *Phys. Rev.*, 1965, **140**, 1133.
35. A. D. Becke, *J. Chem. Phys.*, 1993, **98**, 5648-5652.
36. K. Kim and K. D. Jordan, *J. Phys. Chem.*, 1994, **98**, 10089-10094.
37. P. Stephens, F. Devlin, C. Chabalowski and M. J. Frisch, *J. Phys. Chem.*, 1994, **98**, 11623-11627.
38. J. P. Perdew, M. Ernzerhof and K. Burke, *J. Chem. Phys.*, 1996, **105**, 9982-9985.
39. E. G. Hohenstein, S. T. Chill and C. D. Sherrill, *J. Chem. Theory Comput.*, 2008, **4**, 1996-2000.
40. S. Grimme, J. Antony, S. Ehrlich and H. Krieg, *J. Chem. Phys.*, 2010, **132**, 154104.
41. S. Grimme, S. Ehrlich and L. Goerigk, *J. Comput. Chem.*, 2011, **32**, 1456-1465.
42. R. Krishnan, J. S. Binkley, R. Seeger and J. A. Pople, *J. Chem. Phys.*, 1980, **72**, 650-654.
43. H. B. Thompson, *J. Chem. Phys.*, 1967, **47**, 3407-3410.
44. C. M. Western, *J. Quant. Spectrosc. Radiat. Transf.*, 2017, **186**, 221-242.
45. H. Hartwig and H. Dreizler, *Z. Naturforsch.*, 1996, **51**, 923-932.
46. Z. Kisiel, *J. Mol. Spectrosc.*, 2003, **218**, 58-67.
47. R. F. Bader, *Chem. Rev.*, 1991, **91**, 893-928.
48. K. B. Wiberg and P. R. Rablen, *J. Comput. Chem.*, 1993, **14**, 1504-1518.
49. T. Lu and F. Chen, *J. Comput. Chem.*, 2012, **33**, 580-592.
50. W. Humphrey, A. Dalke and K. Schulten, *J. Mol. Graph.*, 1996, **14**, 33-38.
51. E. R. Johnson, S. Keinan, P. Mori-Sanchez, J. Contreras-Garcia, A. J. Cohen and W. Yang, *J. Am. Chem. Soc.*, 2010, **132**, 6498-6506.
52. M. J. Frisch, G. W. Trucks, H. B. Schlegel, G. E. Scuseria, M. A. Robb, J. R. Cheeseman, G. Scalmani, V. Barone, B. Mennucci, G. A. Petersson, H. Nakatsuji, M. Caricato, X. Li, H. P. Hratchian, A. F. Izmaylov, J. Bloino, G. Zheng, J. L. Sonnenberg, M. Hada, M. Ehara, K. Toyota, R. Fukuda, J. Hasegawa, M. Ishida, T. Nakajima, Y. Honda, O. Kitao, H. Nakai, T. Vreven, J. A. Montgomery, Jr., J. E. Peralta, F. Ogliaro, M. Bearpark, J. J. Heyd, E. Brothers, K. N. Kudin, V. N. Staroverov, T. Keith, R. Kobayashi, J. Normand, K. Raghavachari, A. Rendell, J. C. Burant, S. S. Iyengar, J. Tomasi, M. Cossi, N. Rega, J. M. Millam, M. Klene, J. E. Knox, J. B. Cross, V. Bakken, C. Adamo, J. Jaramillo, R. Gomperts, R. E. Stratmann, O. Yazyev, A. J. Austin, R. Cammi, C. Pomelli, J. W. Ochterski, R. L. Martin, K. Morokuma, V. G. Zakrzewski, G. A. Voth, P. Salvador, J. J. Dannenberg, S. Dapprich, A. D. Daniels, O. Farkas, J. B. Foresman, J. V. Ortiz, J. Cioslowski, and D. J. Fox, Gaussian 09, Revision D.01, Gaussian, Inc., Wallingford CT, 2013.

Chapter 3

Structure and Internal Rotation Dynamics of the Acetone-neon Complex Studied by Microwave Spectroscopy

The contents of this chapter have been copied and adapted from the following publication:

J. Gao, N. A. Seifert, J. Thomas, Y. Xu, W. Jäger. *J. Mol. Spectrosc.*, 2016, **330**, 228-235.

3.1 Introduction

Pure rotational transitions of acetone first were observed using microwave spectroscopy by Weatherly and Williams,¹ but they were not assigned. Subsequently, Swalen and Costain studied the completely deuterated isotopic species and determined the structure.² Several further studies of normal acetone^{3,4} and its isotopic forms⁵⁻⁷ have been reported since then. In 1987, Combes et al. initially identified interstellar acetone in Sgr B2,⁸ and Snyder et al. confirmed this discovery in 2002.⁹

Microwave spectroscopy of weakly bound complexes has been a powerful probe of intermolecular interactions for long and has resulted in the experimental determination of structural and dynamical parameters of countless systems.¹⁰⁻¹² Part of this research has focused on the spectroscopy of systems that are complicated by the internal rotation of a methyl group, which splits each torsional level into nondegenerate (A symmetry) and degenerate (E symmetry) sublevels, consistent with the C_{3v} point group of the methyl group. These A-E doublets may be closely or widely spaced, a sensitive indicator of the height of the potential barrier associated with the internal rotation.¹³ Because of its natural high resolution, microwave spectroscopic techniques have been employed widely to study the effect of internal rotation of the methyl group on the rotational spectra of the systems concerned.^{14,15}

Upon complexation with a rare gas atom, the internal rotation barrier of a methyl group bearing molecule can be affected. Earlier studies have indicated that the effect on the internal rotation barrier depends sensitively on the particular system.¹⁵⁻²⁰ For example, in weakly bound complexes of methanol with rare gas atoms, the internal rotation barrier of the methyl group is reduced significantly with respect to its monomeric value.¹⁶⁻¹⁸ In the case of the *p*-

fluorotoluene-Ar complex, it was found that the molecular symmetry changes upon complexation, which introduces a three-fold term in the internal rotation potential in addition to the purely six-fold potential in the monomer.¹⁹ As for the 1,1-difluoroethane-Ar and acetaldehyde-Kr complexes, the internal rotation barriers decrease in both cases due to the interaction between a rare gas atom and methyl group hydrogen atoms.^{15,20} Kang et al. studied the acetone-Ar complex and suggested that the decrease of the internal rotation barrier compared to the acetone monomer is a result of an additional V_3 term from the Ar \cdots H-H₂C interaction, which is out of phase with the original V_3 term.²¹

Here, microwave spectra of the acetone-Ne complex combined with ab initio calculations to investigate the effect of complexation upon the internal rotation of the two methyl groups are reported. By comparing the experimental data with a careful theoretical study of the Ne-acetone interaction potential and using results derived from Bader's Quantum Theory of Atoms in Molecules (QTAIM),^{22,23} the effect of complexation of neon to acetone on the methyl internal rotation barrier in terms of changes in atomic energies is described. A discussion on the change in barrier height as a function of the electrostatic potential and atomic electronic populations, based on theoretical calculations, is presented. Furthermore, with the success of the spectral assignment of the acetone-Ne complex, this study may lay the foundation for finding firm quantum number assignments for observed transitions of hydrated acetone when using neon as a carrier gas.

3.2 Experimental Details

Broadband microwave spectra of the acetone-Ne complexes were recorded using a chirped pulse Fourier transform microwave (FTMW) spectrometer for which the design has been reported previously,^{24,25} its frequency uncertainty is ~ 25 kHz. All final frequencies were measured with a resonator-based FTMW spectrometer in the region from 5 to 18 GHz, which has been described in detail elsewhere.^{26,27} A sample mixture of 0.04 % acetone in neon at a total pressure of 3–7 atm was expanded through a pulsed nozzle to generate the complexes. The acetone-²²Ne complex was studied in its natural abundance ($\sim 10\%$). The broadband spectra were obtained by applying a chirped MW pulse (2 GHz bandwidth, 0.25 GHz/s chirp rate, ~ 20 W power) to the complexes generated in the molecular expansion. The resulting coherence leads to a molecular emission signal (free-induction decay, FID) which was

averaged in the time domain. 5 FIDs per gas pulse over 40,000 gas injection cycles, corresponding to a total of 200,000 FIDs were collected at a repetition rate of 0.5 Hz. Each FID was recorded for 40 μ s at a sampling rate of 40 GS/s, and a subsequent Fourier Transformation yielded the frequency spectrum.

In the resonator-based experiments, the spectra of the complexes were obtained by applying a near $\pi/2$ microwave excitation pulse to generate a macroscopic polarization of the sample. The resulting FID was collected at a sampling rate of 100 MS/s for 80 μ s, averaged, and Fourier transformed to yield the frequency spectrum.

3.3 Theoretical Methods

To predict the rotational spectra of the acetone-²⁰Ne and acetone-²²Ne complexes, several ab initio geometry optimizations of these two complexes were carried out using the GAUSSIAN 09 package.²⁸ Second order Møller-Plesset perturbation (MP2) theory and density functional theory (DFT) with the M06-2X functional²⁹ methods with the 6-311++G(2d,p) basis set were utilized to obtain structural parameters, including rotational constants, for initial spectroscopic searches. Harmonic vibrational frequencies were calculated to make sure that the optimized structures are minimum-energy conformations, as indicated by the absence of imaginary frequencies. Calculations of the acetone-Ne interaction potential also were performed with B3LYP using Grimme's -D3 corrections³⁰ and CCSD(T), both with the aug-cc-pVTZ basis set. For the interaction potentials of acetone-Ne using the above two theoretical methods, the acetone monomer structure was optimized at the B3LYP-D3/aug-cc-pVTZ level of theory in both cases as analytic gradients are not available for CCSD(T) in GAUSSIAN 09. This procedure is justified by the high quality structural parameters from those DFT calculations³¹ and the assumption that intermolecular potentials are affected only minimally by slight changes in the monomer structure.

Transition frequencies were calculated from the ab initio rotational constants using the PGOPHER program.³² The same program was used to perform spectroscopic fits to produce experimental spectroscopic constants using the measured transition frequencies. Finally, the XIAM program was used to predict internal rotation splittings,^{33,34} and the PMIFST program was used to predict rotational constants for acetone-²²Ne.³⁵

3.4 Results and Discussion

3.4.1. Spectral Search and Assignment

In order to detect and identify rotational transitions of the complex, known transitions of the acetone monomer^{4,5} and the acetone-Ar complex²¹ were relied on. I started the search for transitions of acetone-Ne using the rotational constants and dipole moments from MP2 and M06-2X calculations, shown in Table 3.1. It is predicted that the μ_c dipole component is dominant (~ 3 D), so automated scans were performed to observe the strongest μ_c -type transitions, such as the fundamental $1_{10} \leftarrow 0_{00}$ transition, and the frequency ranges were set to reflect deviations of $\pm 5\%$ of the predicted rotational constants. Based on the results of the previous acetone-Ar study,²¹ rotational transitions were expected to be split into four to five internal rotation components, i.e. AA = (0,0), EA = (1,0), AE = (0,1), EE = (1,1), and EE' = (1,-1). Here, the A/E notation indicates the symmetry species, A has a torsional symmetry of 0, and the doubly degenerate E has torsional symmetry of ± 1 .

Table 3.1. Predicted rotational constants and dipole moment components of the acetone-Ne complex from a variety of theoretical methods.

	MP2 ^a	CCSD(T) ^{b,c}	M06-2X ^a	B3LYP-D3 ^b
<i>A</i> /MHz	5003.06 (-0.7%) ^d	4926.73 (-2.3 %)	4951.63 (-1.8%)	4928.40 (-2.2%)
<i>B</i> /MHz	2426.36 (4.9%)	2534.15 (9.0%)	2644.85 (12.8%)	2574.79 (10.4%)
<i>C</i> /MHz	2336.8 (5.9%)	2420.09 (9.1%)	2519.65 (12.7%)	2456.71 (10.5%)
$ \mu_a $ /D	0.45	0.07	0.01	0.15
$ \mu_b $ /D	0.29	0	3.16	0
$ \mu_c $ /D	3.43	2.9	0	3.05

^a The 6-311 ++ G(2d,p) basis set was used.

^b The aug-cc-pVTZ basis set was used.

^c The acetone monomer geometry was fixed to the optimized B3LYP-D3 geometry and the intermolecular coordinates alone were allowed to relax.

^d The values in parentheses are signed percent errors relative to the experimental rotational constants given in Table 3.2.

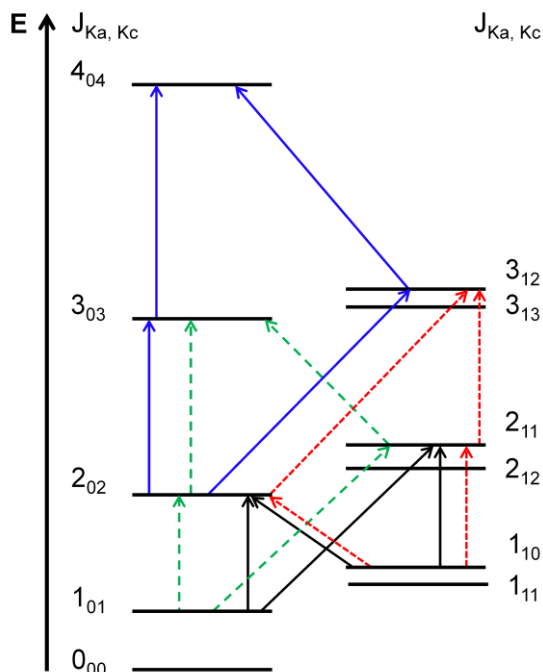


Figure 3.1. Schematic rotational energy level diagram of the acetone-Ne complex. Closed frequency loops, which were used to confirm the initial assignments, are shown with different colors.

Initially, a fit of the AA components (which can be described by a semi-rigid asymmetric top Hamiltonian and do not require an internal rotation analysis) was performed using PGOPHER. To assist the assignment, closed loops of rotational transitions were constructed, as illustrated in Figure 3.1. The first loop, as shown with black lines in Figure 3.1, was constructed with the $J = 2 \leftarrow 1$ transitions; their frequency relationship is shown in Eq. 3.1:

$$\nu(2_{02} \leftarrow 1_{01}) = \nu(2_{11} \leftarrow 1_{01}) - \nu(2_{11} \leftarrow 1_{10}) + \nu(2_{02} \leftarrow 1_{10}) \quad (3.1)$$

The four rotational transitions involved are each split into four internal rotation components, and the frequencies of all 16 components were measured in the initial spectroscopic search. Four combinations of internal rotation fine-structure components, which satisfy the relationship in Eq. 3.1, were identified and used in semi-rigid rotor fits with PGOPHER. The set of transitions which produced the lowest standard deviation was assigned to be of AA symmetry. Additional AA symmetry components were found and assigned by using further closed frequency loops (see Figure 3.1) and forward predictions, and their frequency relationship is shown in Eq. 3.2–3.4. In total, 21 fine structure components of AA symmetry were found for acetone- ^{20}Ne .

$$\nu(3_{03} \leftarrow 2_{02}) = \nu(2_{11} \leftarrow 1_{01}) + \nu(3_{03} \leftarrow 2_{11}) - \nu(2_{02} \leftarrow 1_{01}) \quad (3.2)$$

$$\nu(3_{12} \leftarrow 2_{11}) = \nu(2_{02} \leftarrow 1_{10}) + \nu(3_{12} \leftarrow 2_{02}) - \nu(2_{11} \leftarrow 1_{10}) \quad (3.3)$$

$$\nu(3_{03} \leftarrow 2_{02}) = \nu(3_{12} \leftarrow 2_{02}) + \nu(4_{04} \leftarrow 3_{12}) - \nu(4_{04} \leftarrow 3_{03}) \quad (3.4)$$

Prediction of the internal rotation splittings using the resulting rotational constants and the *ab initio* internal rotation parameters in XIAM then enabled assignment of all detectable internal rotation components in the observed spectrum. The measured transition frequencies, together with the quantum number assignments, are listed in Table S3.1 of the Appendix I, and all parameters from the XIAM internal rotation fit, including rotational and centrifugal distortion constants, are given in Table 3.2.

The PMFIST program was used to predict rotational constants for acetone-²²Ne. To assign the rotational transitions, the same strategy was used as for the acetone-²⁰Ne complex. I also established closed loops of the relevant rotational transitions of acetone-²²Ne (see Figure 3.1). The frequency relationships of the rotational transitions are the same in Eq. 3.1–3.4 and an additional Eq. 3.5, as follows:

$$\nu(3_{12} \leftarrow 2_{11}) = \nu(2_{02} \leftarrow 1_{01}) + \nu(3_{12} \leftarrow 2_{02}) - \nu(2_{11} \leftarrow 1_{01}) \quad (3.5)$$

The measured transition frequencies and quantum number assignments are listed in Table S3.2 (Appendix I), and parameters resulting from the XIAM internal rotation fit, including rotational and centrifugal distortion constants, are given in Table 3.2. An example broadband spectrum with assigned transitions of acetone-²⁰Ne and acetone-²²Ne is shown in Figure S1 of the Appendix I.

Table 3.2. Experimental spectroscopic parameters for the acetone-Ne complex.

Parameter	acetone- ²⁰ Ne	acetone- ²² Ne
A /MHz	5038.831(10)	5037.698(9)
B /MHz	2305.828(47)	2186.458(47)
C /MHz	2198.548(47)	2089.791(48)
Δ_J /kHz	38.48(23)	35.53(19)
Δ_{JK} /kHz	465(1)	421(2)
Δ_K /kHz	-490(4)	-443(2)
δ_j /kHz	1.54(12)	1.296(93)
δ_k /kHz	134(23)	133(23)
Φ_{JK} /kHz	0.31(11)	-0.18(9)
Φ_{KJ} /kHz	-0.10(36)	0.89(31)
Φ_K /kHz	-7.12(76)	-7.22(34)
	-1.206	-1.136
D_{pi2J} /MHz ^b	0.35(6)	0.38(7)
D_{pi2K} /MHz ^b	-1.13(6)	-1.15(7)
V_3 /cm ⁻¹	259(5)	256(6)
ε /° ^c	29.8 / 150.1(6)	29.8 / 150.1(6)
δ /° ^c	86.2(0)	86.3(0)
F_0 /GHz ^d	157(3)	155(3)
N	21	21
σ /kHz	24.6	20.3

^a F_{12} is a top-top coupling term, derived from other internal rotation parameters.

^b Fourth order distortion terms describing coupling between overall rotation and internal rotation.

^c ε is the angle between the projection of the internal rotation axis onto the bc-plane and the b-principal inertial axis of the complex;

δ is the angle between internal rotation axis and a-axis of the complex.

^d F_0 is the rotational constant of the methyl top ($F_0 = 505.379/I_a$ (in GHz); where I_a is the moment of inertia of the methyl top).

In comparing the fitted rotational constants with those from the ab initio calculations (Table 3.1), one finds that the MP2 method provides the smallest deviations, while the DFT methods

produce less accurate results. The CCSD(T) single point calculations also show larger errors than the other post-Hartree-Fock methods. This, however, is a result of the B3LYP-D3 optimized geometry for the acetone monomer in these calculations, rather than a poor description of the acetone-Ne interaction potential.

3.4.2. Van der Waals interaction

QTAIM is a useful method for the characterization of weak van der Waals interactions and hydrogen bonding.^{22,23} Based on Bader's theory,^{22,23} bonding interactions between the atoms in the molecule can be identified by bond critical points (BCP), in which the electron density gradient, $\nabla\rho = 0$. The MULTIWFN³⁶ program was used to generate the BCPs along with the corresponding bond paths. Compared with the acetone monomer, the C–C and C=O bond lengths decrease by about 0.0006 Å and 0.0002 Å, respectively, in the acetone-Ne complex. Furthermore, by integrating the electron populations over the volume of the atoms in the complex (Table S3.3 in the Appendix I), it is found that the Ne atom loses some electron population (-0.002 a.u.), in a “donor”-like effect, whereas acetone can be considered a weak “acceptor”, since it has gained electron population (+0.002 a.u.). The Non-Covalent Interactions (NCI) method of analyzing the electron density topology can give a more detailed representation of, in particular, weak intermolecular interactions.³⁷ The NCI method was used to generate the isosurface (the green color region) of the reduced electron density gradient representing the interaction between Ne and acetone shown in Figure 3.2.

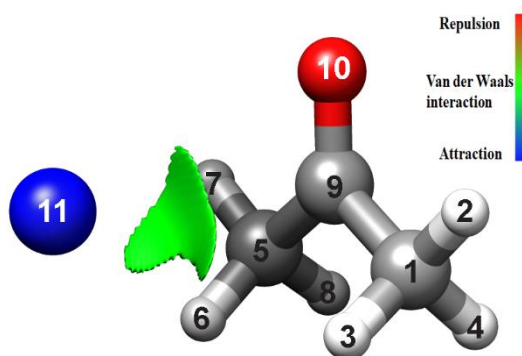


Figure 3.2. NCI isosurface for acetone-Ne with reduced density gradient $s=0.7$ a.u., colored by the values of $\text{sign}(\lambda_2)\rho$ [-0.04, 0.02] at each point in space, with colorations specified by the legend in the up right (red color denotes positive value, and blue color denotes negative value). The blue ball is the Ne atom.

3.4.3 Internal Rotation Dynamics

The barrier to internal rotation of the methyl groups was calculated by fixing one of the methyl groups to its equilibrium position and scanning the torsional angle of the other one (see Figure 3.3). The barrier, i.e., the energy difference between the equilibrium position and the methyl rotation transition state, was determined to be 2.8 kJ mol⁻¹ [234 cm⁻¹] at the MP2/6-311++g(2d,p) level of theory. The slight asymmetry in the calculated potential energy curve is a result of the definition of the torsional angle, which is the dihedral angle O-C9-C1-H2. For example, the dihedral angle at 0° for H4 will not be 120° since a structure optimization was performed.

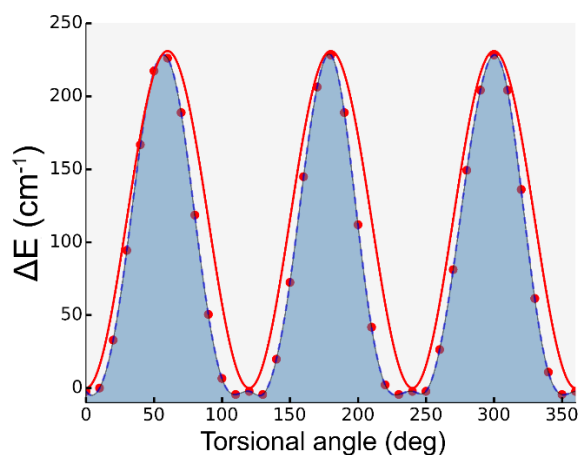


Figure 3.3. Calculated potential energies (red dots) and interpolated curve (blue dashes) for a single methyl internal rotation in acetone-Ne, holding the other fixed at its minimum position. The red curve is a standard torsional potential of a single uncoupled methyl internal rotor, $\Delta E(\theta) = 0.5 \cdot V_3 \cdot [1 - \cos(3\theta)]$.

To study the coupling between the two methyl groups, a two-dimensional scan along both methyl internal rotation angles was performed with a step size of 10°, and the result is shown in Figure 3.4. The linear elongation of the wells and troughs of the potential about their diagonals is a signature of coupling of the internal rotation of the methyl groups and is similar to what was found previously for the acetone monomer by Crighton et al.³⁸ The shapes of the wells and troughs would be hemispherical if the two motions were not coupled.

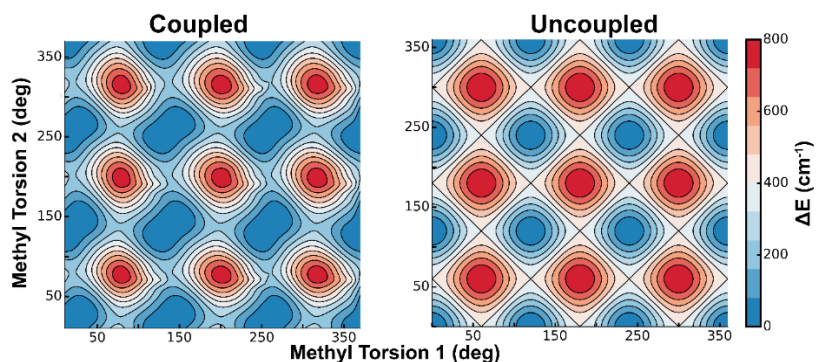


Figure 3.4. Comparison of the contour map of the 2D potential energy surface of both methyl internal rotation torsional angles in the acetone-Ne complex (Coupled, left figure), calculated at the MP2/6-311++G(d,p) level of theory, and a schematic surface where both the internal rotation of both methyl groups are uncoupled (Uncoupled, right figure).

The experimental internal rotation splittings were fitted to barrier heights of $3.10(6) \text{ kJ mol}^{-1}$ [$259(5) \text{ cm}^{-1}$] and $3.06(7) \text{ kJ mol}^{-1}$ [$256(6) \text{ cm}^{-1}$] for the acetone- ^{20}Ne and acetone- ^{22}Ne complexes, respectively. These values are comparable to that of the acetone-Ar complex ($3.110 \text{ kJ mol}^{-1}$, or 260 cm^{-1})²¹ but are slightly lower than that of the acetone monomer ($3.182 \text{ kJ mol}^{-1}$, or 266 cm^{-1}).⁴ This indicates that the weak van der Waals interaction with a neon or argon atom has some effect on the internal rotation of the methyl groups.

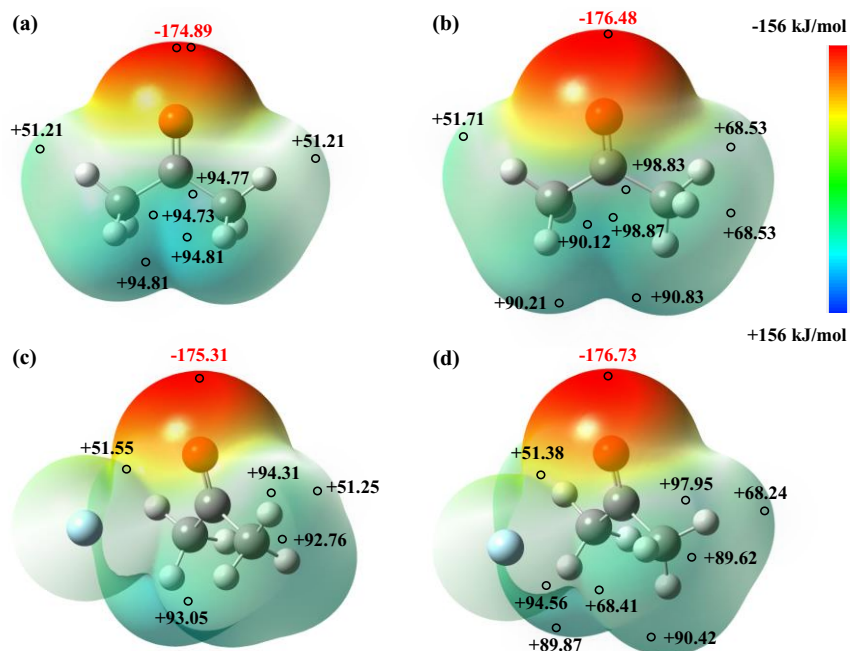


Figure 3.5. Electrostatic potential (ESP) map of the acetone monomer in its minimum structure (a) and transition state (b) and of the acetone-Ne complex in its minimum structure (c) and transition state (d) calculated at the MP2/6-311++G(d,p) level of theory.

Figure 3.5 shows electrostatic potential (ESP) maps of the acetone monomer and the acetone-Ne complex at their minimum energy and transition state structures, respectively. The colors of red, white and blue denote ESP values varying from 156 to -156 kJ mol⁻¹. The cyan and orange small spheres indicate minima and maxima, respectively, on the ESP surface. For the most stable structure of the acetone monomer, the two methyl tops are in an eclipsed position, while in its transition state structure, the two tops are in a staggered position. In moving from the minimum to the transition state, more ESP surface maxima are generated in both the acetone monomer and the acetone-Ne complex, especially in the areas close to the rotated methyl group, indicating that the electronic densities change with rotation of the methyl groups. Moreover, the value of the ESP surface minimum at the carbonyl oxygen atom increases in going from the minimum to the transition state for both the acetone-Ne and the acetone monomer. For a more quantitative characterization, variations of bond lengths and of integrated atomic energies of both monomer and complex were determined for eclipsed and staggered positions of the methyl groups using QTAIM. Numerical results can be found in Table 3.3.

Table 3.3 Differences in bond lengths (Δr), local bond critical point (BCP) densities ($\Delta\rho$), and atomic energies (ΔE) among acetone-Ne complex and acetone monomer upon internal rotation at the MP2/6-311 ++ G(2d, p) level of theory.

	Acetone ^a	Ne-acetone ^b
$V_3^{\text{MP2}}/\text{kJ/mol}$	2.731	2.661 ^c
Δr (C1-C9) /pm	0.503	0.506
Δr (C9-C5) /pm	-0.264	-0.262
Δr (C9-O) /pm	-0.053	-0.053
$\Delta\rho$ (C1-C9) /a.u.	-0.00271	-0.00273
$\Delta\rho$ (C9-C5) /a.u.	0.00130	0.00129
$\Delta\rho$ (C9-O) /a.u.	0.00082	0.00081
ΔE (C1-H ₃) /a.u.	0.00127	0.00108
ΔE (C5-H ₇) /a.u.	-0.00053	-0.00109
ΔE ((C5)H ₂) /a.u.	0.00155	0.00148
ΔE (C9=O) /a.u.	-0.00114	-0.00092
ΔE (Ne) /a.u.	N/A	-0.00010

^a The difference for acetone between the minimum and transition state.

^b The difference for the Ne-acetone complex between the minimum and transition state.

^c The energy of internal rotation barrier of the Ne-acetone complex was counterpoise corrected.

In the acetone monomer, the bond length between the carbonyl carbon atom (C9) and methyl carbon atom (C1) increases slightly ($\Delta r = 0.00503 \text{ \AA}$) as the methyl group C1H₃ rotates from the minimum to the maximum energy position. This is accompanied by a decrease of the C=O bond length ($\Delta r = -0.00053 \text{ \AA}$) and the bond between the other methyl carbon (C5) and C9 ($\Delta r = -0.00264 \text{ \AA}$). The changes occur because electron density of the C1-C9 single bond shifts to C9=O and the C5-C9 single bond, as can be seen in the changes of the corresponding electron densities (Table 3). The electron densities at the local bond critical points (BCPs) of the C9=O bond and the C5-C9 single bond increase ($\Delta\rho = +0.00212 \text{ a.u.}$) but decrease in the C1-C9 single bond by about the same extent ($\Delta\rho = -0.00271 \text{ a.u.}$). Because of this electron population transfer, both methyl groups become destabilized (total 0.00229 a.u.), while the C9=O is

stabilized (-0.00114 a.u.). The internal rotation barrier originates essentially in the destabilization of two methyl groups, i.e., C1H3 and C5H3, mainly C1-H3 (0.00127 a.u.) and C5H2 (0.00155 a.u.).

I now consider the acetone-Ne complex. Through the involvement of the Ne atom, acetone has gained some electron population, acting as an “acceptor”, the C9=O, C1-C9, and C9-C5 bond lengths in the complex are shortened, and their BCP electronic densities (ρ) increase accordingly compared to the acetone monomer. Starting from these new equilibrium positions for acetone-Ne, the changes of bond lengths and electronic densities with methyl group rotation were expected to be similar to those in the acetone monomer. In Table 3.3, very slight changes are found in bond lengths and BCP densities compared to the acetone monomer, as a result of the quite weak interaction between acetone and the Ne atom. Instead, I have analyzed the changes in atomic energies. When the methyl group C1-H₃ rotates in the Ne-acetone complex, the extent of destabilization is slightly less than in the monomer (0.00108 a.u. vs. 0.00127 a.u.). At the same time, the C9=O unit is stabilized slightly less than in the monomer (-0.000922 a.u. vs. -0.00114 a.u.) when going from the minimum to the maximum energy position. However, the stabilization of the C5-H7 unit (-0.00109 a.u.) is much greater in the Ne-acetone complex than that in the acetone monomer (-0.00053 a.u.), while the destabilization extent in the remaining two hydrogen atoms ((C5)H₂) in this methyl group is similar (0.00155 a.u. vs 0.00148 a.u.). This greater stabilization of the C5-H7 unit ultimately is reflected in the lower internal rotation barrier in acetone-Ne.

3.4.4 Structure

Since the ²²Ne-substituted species was the only minor isotopologue measured, only the experimental position of the neon atom with respect to the acetone unit could be obtained. However, because of the weakly bound nature of the complex and the apparent floppiness of the complex, several experimentally-derived and theoretical approaches were undertaken to characterize the interaction potential between neon and acetone fully.

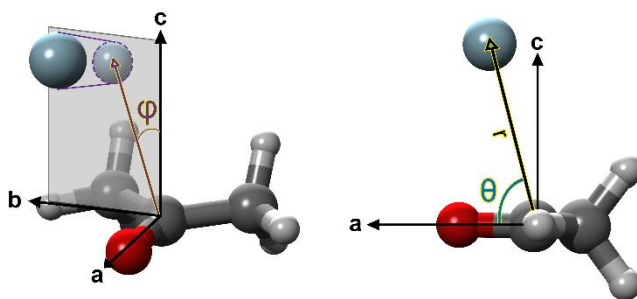


Figure 3.6. Schematic of structure parameterization used to characterize the non-covalent interaction in acetone-Ne. The axes shown are parallel to the principal inertial axes of the acetone monomer and originate at the position of the carbonyl carbon atom.

Parameterization of the neon position relative to the acetone frame can be achieved by use of three independent parameters, illustrated in Figure 3.6. The first is the radial variable r , which in this case is defined as the internuclear distance between the carbonyl carbon and neon atoms; the second is θ , defined as the angle between the line connecting the neon and carbonyl carbon atoms and the C=O axis; the third is the angle φ , which is defined as the dihedral angle between the ac -plane of the monomer and the plane that contains the carbonyl and neon atoms.

An initial 3D potential energy scan at the B3LYP-D3/aug-cc-pVTZ level of theory revealed that two equivalent minima exist at $(r, \theta, \varphi) = (3.33 \text{ \AA}, 89.8^\circ, \pm 3.0^\circ)$. However, the barrier separating the two minima along φ is only ca. 0.4 cm^{-1} at this level of theory, and the zero-point energy level lies above this barrier. 2D slices of the 3D potential can be found in Figure 3.7.

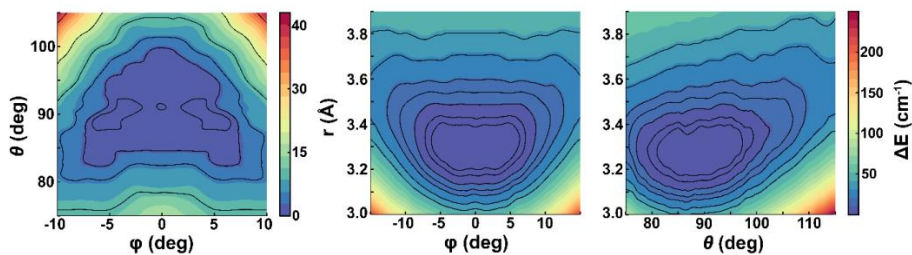


Figure 3.7. Contour maps of the three possible two-dimensional slices of the 3D potential energy surface for the non-covalent interaction potential for acetone-Ne, calculated at the B3LYP-D3/aug-cc-pVTZ level of theory. The third parameter is held at its minimum position in each slice.

Three independent 1D scans along each parameter were performed by fixing the others to their global minimum values at the B3LYP-D3 and CCSD(T) levels of theory with the aug-

cc-pVTZ basis set. The results are shown in Figure 3.8. Unlike the B3LYP-D3 surface, the double well minimum along φ is not present in the CCSD(T) surface.

Fixing the reduced masses for these motions to their respective harmonic reduced masses derived from a harmonic vibrational calculation for the r_e geometry optimized at B3LYP-D3/aug-cc-pVTZ, 1D ground state wavefunctions were calculated using the Numerov-Cooley procedure.³⁹ Using these wavefunctions, a ground-state averaged (“ r_0 ”) structure was determined. The averaged quantities were determined using the formulae

$$r_0 = \left\langle \frac{1}{r^2} \right\rangle^{-1/2} \quad (3.6a)$$

$$\cos(\omega_0) = \langle \cos^2 \omega \rangle^{1/2} \quad (3.6b)$$

where $\omega = \theta$ or φ and approximating $\langle \omega \rangle \approx \cos^{-1}[\langle \cos^2 \omega \rangle^{1/2}]$. The averaged coordinates were calculated to be $(r, \theta, \varphi)_0 = (3.27 \text{ \AA}, 87.5^\circ, \pm 2.45^\circ)$ for CCSD(T) and $(3.38 \text{ \AA}, 86.5^\circ, 1.65^\circ)$ for B3LYP-D3.

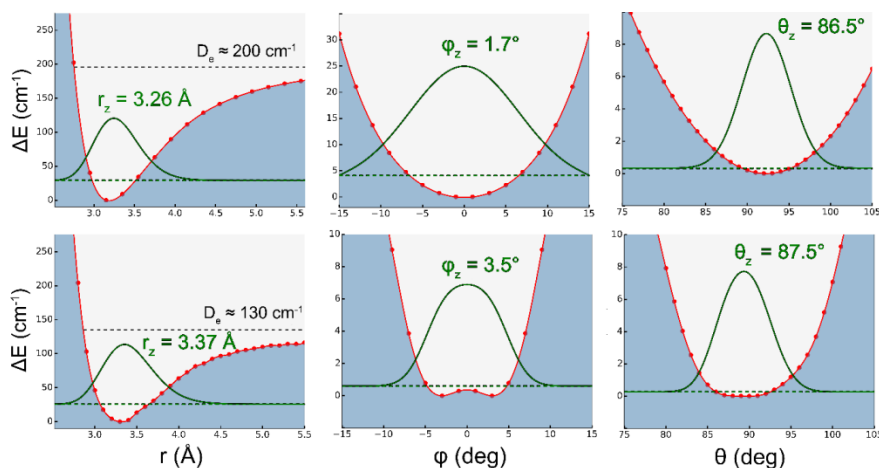


Figure 3.8. 1D cross sections of the 3D interaction potential, holding the other two parameters fixed at their equilibrium positions, calculated at both the CCSD(T)/aug-cc-pVTZ (top half) and B3LYP-D3/aug-cc-pVTZ (bottom half) levels of theory. Calculated ground state wavefunctions (green curves) presented were calculated using the Numerov-Cooley numerical procedure. For the “stretch” potentials (left third), the dissociation energies of the neon at equilibrium (D_e) were estimated by the asymptotic behavior of the potentials.

Experimental determinations of the neon position were made using several methods. Application of Kraitchman’s equations to the experimental data set determined the experimental r_s position of the neon atom to be $(r, \theta, \varphi)_s = (3.387(20) \text{ \AA}, 79.81(41)^\circ, \pm 4.88(47)^\circ)$.⁴⁰ This is similar to the r_0 determination, calculated using the STRFIT program,⁴¹

of $(r, \theta, \varphi)_0 = (3.349(1) \text{ \AA}, 80.90(24)^\circ, 2.46(49)^\circ)$. However, the fit for the r_0 determination did not converge well because of insufficient experimental information, and might not be very reliable. Experimental and theoretical values for these three parameters are summarized in Table 3.4. A comparison with structural parameters of acetone-Ar can be found in Table 3.5.

Table 3.4 Calculated and experimental structural parameters for acetone-Ne.

Method	$r / \text{\AA}$	$\varphi / ^\circ$	$\theta / ^\circ$
r_e , MP2 ^a	3.24	12.5	87.5
r_e , M06-2X ^a	3.09	-8.0	91.8
r_e , B3LYP-D3 ^b	3.14	± 3.0	93.4
r_z , B3LYP-D3	3.38	0	89.4
r_e , CCSD(T) ^b	3.18	0	92.3
r_z , CCSD(T)	3.27	0	92.3
r_0^c	3.34893(97)	2.46(49)	80.90(24)
r_s^d	3.387(20)	4.88(47)	79.81(41)
RGDFIT ^g	3.35	0	80.7 / 102.7 ^f

^a MP2 and M06-2X calculations were done with the 6-311++G(2d,p) basis set.

^b CCSD(T) and B3LYP-D3 were done with the aug-cc-pVTZ basis set.

^c Fitted parameters from STRFIT program. (Might not be reliable; see the text.)

^d Kraitchman determination with Costain's error of $0.015 \text{ \AA}/|z|$ added.

^f Two possible solutions due to sign ambiguity.

^g See Refs. ^{42, 43}

Table 3.5 Comparison of fitted structural parameters, including angles from the methyl rotor direction cosines, of acetone-Ne and acetone-Ar complexes.

	acetone-Ne		acetone-Ar ^[a]	
RG-C _{C=O} / \AA	3.387(20)		3.604	
	top1	top2	top1	top2
$\cos^{-1}\lambda_a$	86.22°	86.22°	80.48°	90.66°
$\cos^{-1}\lambda_b$	29.91°	150.09°	35.60°	151.94°
$\cos^{-1}\lambda_c$	60.38°	60.38°	56.07°	61.95°

^a Derived using the parameters from reference [21].

In general, the theoretical averaged values are in good agreement with the experimental data. There are some discrepancies regarding the angular position of the neon, but these are likely

due to a combination of factors relating to both the theoretical and experimental methodologies used. For instance, the magnitude of the centrifugal distortion constants suggests that an experimental structural analysis using merely the rigid rotor components of the rotational Hamiltonian will bias the ground state structural determination towards a specific orientation. Although some of the motional averaging along these large amplitude modes is encoded in the rigid rotor part of the overall semi-rigid Hamiltonian, a full experimental structural description requires treating the molecular structure to more than “zeroth-order” – the magnitude of the perturbation plays a significant and appreciable role in defining structure as a measurable quantity.

3.5 Conclusions

Microwave spectra of the acetone-Ne van der Waals complex were measured using a cavity-based molecular beam Fourier-transform microwave spectrometer in the region from 5 to 18 GHz. Both *c*- and weaker *a*-type rotational transitions were observed for the ^{20}Ne and ^{22}Ne isotopologues of the complex. With the help of ab initio calculations and by constructing closed frequency loops, the pure rotational spectrum, complicated by the splittings arising from the internal rotation of two high-barrier methyl rotors, was assigned fully. The two methyl groups are found to be equivalent, as evidenced by the splitting of each transition into four components. The acetone methyl group tunneling barrier height was determined experimentally to be $3.10(6) \text{ kJ mol}^{-1}$ [$259(5) \text{ cm}^{-1}$] in the acetone-Ne complex, which is lower than in the acetone monomer but comparable to the acetone-Ar complex. Analyses based on ab initio calculations and QTAIM were done to rationalize the change in internal rotation barrier in terms of changes in atomic energies. High-level [CCSD(T)] ab initio calculations suggest that the Ne atom lies directly above the plane formed by the carbonyl group and the two carbon-carbon bonds in the equilibrium configuration. Large amplitude motions in the internal coordinates lead to an average Ne-atom position that is slightly offset, similar to what was previously found in the acetone-Ar complex.

References

1. T. L. Weatherly and D. Williams, *J. Chem. Phys.*, 1952, **20**, 755-755.
2. J. Swalen and C. Costain, *J. Chem. Phys.*, 1959, **31**, 1562-1574.
3. P. Groner, S. Albert, E. Herbst, F. C. De Lucia, F. J. Lovas, B. J. Drouin and J. C. Pearson, *Astrophys. J. Suppl. Ser.*, 2002, **142**, 145-151.
4. J. M. Vacherand, B. P. Vaneijck, J. Burie and J. Demaison, *J. Mol. Spectrosc.*, 1986, **118**, 355-362.
5. R. Nelson and L. Pierce, *J. Mol. Spectrosc.*, 1965, **18**, 344-352.
6. R. Peter and H. Dreizler, *Z. Naturforsch.*, 1965, **20 A**, 301-312.
7. F. J. Lovas and P. Groner, *J. Mol. Spectrosc.*, 2006, **236**, 173-177.
8. F. Combes, M. Gerin, A. Wootten, G. Wlodarczak, F. Clausset and P. J. Encrenaz, *Astron. Astrophys.*, 1987, **180**, L13-L16.
9. L. E. Snyder, F. J. Lovas, D. M. Mehringer, N. Y. Miao, Y. J. Kuan, J. M. Hollis and P. R. Jewell, *Astrophys. J.*, 2002, **578**, 245-255.
10. S. A. Peebles, R. A. Peebles, Y. Tatamitani and Y. Kawashima, *J. Phys. Chem. A*, 2006, **110**, 7080-7085.
11. D. J. Frohman, E. S. Contreras, R. S. Firestone, S. E. Novick and W. Klemperer, *J. Chem. Phys.*, 2010, **133**, 244303-244307.
12. Q. Wen and W. Jaeger, *Phys. Chem. Chem. Phys.*, 2008, **10**, 2496-2501.
13. C. C. Lin and J. D. Swalen, *Rev. Mod. Phys.*, 1959, **31**, 841-892.
14. Y. Q. Liu and W. Jager, *J. Chem. Phys.*, 2003, **119**, 8449-8463.
15. S. Melandri, P. G. Favero, W. Caminati and B. Velino, *J. Chem. Phys.*, 2005, **122**, 134310-134317.
16. R. D. Suenram, F. J. Lovas, G. T. Fraser, J. Z. Gillies, C. W. Gillies and M. Onda, *J. Mol. Spectrosc.*, 1989, **137**, 127-137.
17. G. T. Fraser, F. J. Lovas and R. D. Suenram, *J. Mol. Spectrosc.*, 1994, **167**, 231-235.
18. X. Q. Tan, L. H. Sun and R. L. Kuczkowski, *J. Mol. Spectrosc.*, 1995, **171**, 248-264.
19. J. Rottstegge, H. Hartwig and H. Dreizler, *J. Mol. Spectrosc.*, 1999, **195**, 1-10.
20. B. Velino, S. Melandri, P. G. Favero, A. Dell'Erba and W. Caminati, *Chem. Phys. Lett.*, 2000, **316**, 75-80.
21. L. Kang, A. R. Keimowitz, M. R. Munrow and S. E. Novick, *J. Mol. Spectrosc.*, 2002, **213**, 122-129.
22. R. F. Bader, *Atoms in molecules*, Wiley Online Library, 1990.
23. R. F. W. Bader, *Chem. Rev.*, 1991, **91**, 893-928.
24. S. P. Dempster, O. Sukhorukov, Q.-Y. Lei and W. Jaeger, *J. Chem. Phys.*, 2012, **137**, 174303-174308.
25. J. Thomas, J. Yiu, J. Rebling, W. Jaeger and Y. Xu, *J. Phys. Chem. A*, 2013, **117**, 13249-13254.
26. Y. J. Xu, J. Van Wijngaarden and W. Jager, *Int. Rev. Phys. Chem.*, 2005, **24**, 301-338.
27. Y. J. Xu and W. Jager, *J. Chem. Phys.*, 1997, **106**, 7968-7980.

28. M. Frisch, G. Trucks, H. Schlegel, G. Scuseria, M. Robb, J. Cheeseman, G. Scalmani, V. Barone, B. Mennucci and G. Petersson, *Gaussian Inc., Wallingford, CT*, 2010.
29. E. R. Johnson, I. D. Mackie and G. A. DiLabio, *J. Phys. Org. Chem.*, 2009, **22**, 1127-1135.
30. L. Goerigk and S. Grimme, *J. Chem. Theory Comput.*, 2011, **7**, 291-309.
31. S. Grimme and M. Steinmetz, *Phys. Chem. Chem. Phys.*, 2013, **15**, 16031-16042.
32. C. Western, *J. Quant. Spectrosc. Radiat. Transfer*, 2016, doi:10.1016/j.jqsrt.2016.04.010 ; C. M. Western, PGOPHER version 9.1. Bristol, UK: University of Bristol Research Data Repository; <http://dx.doi.org/10.5523/bris.1nz94wvrfzdo1d67et0t4v4nc..>
33. H. Hartwig and H. Dreizler, *Z. Naturforsch.*, 1996, **51 A**, 923-932.
34. N. Hansen, H. Mäder and T. Bruhn, *Molec. Phys.*, 1999, **97**, 587-595.
35. J. O. Richardson, C. Perez, S. Lobsiger, A. A. Reid, B. Temelso, G. C. Shields, Z. Kisiel, D. J. Wales, B. H. Pate and S. C. Althorpe, *Science*, 2016, **351**, 1310-1313.
36. T. Lu and F. Chen, *J. Comput. Chem.*, 2012, **33**, 580-592.
37. E. R. Johnson, S. Keinan, P. Mori-Sanchez, J. Contreras-Garcia, A. J. Cohen and W. T. Yang, *J. Am. Chem. Soc.*, 2010, **132**, 6498-6506.
38. J. S. Crichton and S. Bell, *J. Mol. Spectrosc.*, 1986, **118**, 383-396.
39. C. E. Dykstra and D. J. Malik, *J. Chem. Phys.*, 1987, **87**, 2806-2811.
40. J. Kraitchman, *Am. J. Phys.*, 1953, **21**, 17-24.
41. Z. Kisiel, *J. Mol. Spectrosc.*, 2003, **218**, 58-67.
42. R. D. Suenram, G. T. Fraser, F. J. Lovas, C. W. Gillies and J. Zozom, *J. Chem. Phys.*, 1988, **89**, 6141-6146.
43. L. N. Hadley and D. M. Dennison, *Phys.Rev.*, 1946, **70**, 780-781.

Chapter 4

Non-Equivalent Methyl Internal Rotations in the Acetone-Water Complex Studied by Microwave Spectroscopy and Ab-Initio Calculations

4.1 Introduction

The process of keto-enol tautomerization plays important roles in many areas; its energetics and dynamics can determine, for instance, rates of chemical reactions and the biochemical activity of amino acids, sugars, and nucleic acid.^{1, 2} Watson and Crick, for example, wrongly believed that the nucleotide bases in deoxyribonucleic acids (DNA) are in the enol tautomeric form, which prevented them from solving the structure of DNA until it was corrected later by Donohue.³ Moreover, such keto-enol tautomerization processes in DNA may give rise to the occurrence of gene mutations.⁴

Acetone is a prototypical system that undergoes keto-enol tautomerization. In the gas phase, the keto tautomer of acetone is more stable, by 41 kJ/mol, than the enol form and separated by a relatively high barrier of 68 kcal/mol.⁵ In solvent assisted systems, the involvement of water molecules, for example, can effectively reduce the barrier height by about 20–30 kcal/mol.⁶ The reason is that acetone and water can form a hydrogen bonded complex, where water acts as a “bridge” that connects the carbonyl oxygen and methyl proton. Nevertheless, the resulting equilibrium is still shifted significantly to the keto form in neutral aqueous solution.⁷ Despite this, in many reactions involving acetone, such as halogenation, C–C coupling, and condensation reactions, the enol form plays very important roles.⁶ We note that there appears to be no direct spectroscopic evidence for the occurrence of the enol form of acetone (1-propen-2-ol) in either gas phase or solution.

As mentioned above, in aqueous solution water is hydrogen bonded to acetone, which effectively lowers the barrier height of keto-enol tautomerization. Recently, several groups have utilized different methods to study keto-enol tautomerization in acetone in hydrogen bonded complexes. Bundet et al. have studied the tautomerization reaction of acetone on acidic zeolites in aqueous solution,⁵ and Matsuda et al. have reported on insights into the proton

transfer in the keto-enol tautomerization of monohydrated acetone in the gas phase gained by means of the vacuum ultraviolet (VUV) photoionization method.⁸ These studies were done on acetone in an acidic environment⁵ or on the acetone cation,⁸ there are no experimental studies which have focused on the tautomerization of neutral acetone.

Microwave, rotational spectroscopy is a particularly powerful method to study weakly bound complexes, and has been used to determine structures and hydrogen bond dynamics of a number of neutral hydrogen bonded clusters (see, for example, Refs.9-17). Here I report rotational spectra of the keto form of the acetone-water complex. The spectra were analyzed and interpreted with the aid of ab initio calculations to gain insights into structural, energetic, and dynamical aspects of the hydrogen bonding. Theoretical, ab initio, calculations were also used to investigate the effect of hydrogen bonding upon the internal rotation of the two methyl groups, and I try to explain the barrier height changes due to hydrogen bonding by considering ESP, electronic populations, and atomic energies of the complex with the aid of theoretical calculations. Apart from that, I also tried to detect the enol form of acetone bound to one water molecule.

4.2 Experimental and Computational details

Microwave spectra of the acetone-water complex were recorded initially using a broadband chirped pulse FTMW spectrometer, whose design has been reported previously^{18, 19}. The measurement uncertainty of this instrument is ~25 kHz. All final frequencies were measured with a cavity based FTMW spectrometer (7–14 GHz, measurement uncertainty ~2 kHz), which is described in detail elsewhere^{20, 21}. The complexes were formed in a molecular expansion of a sample gas mixture through a pulsed nozzle. The sample gas consisted of about 0.1 % water and 1 % acetone in neon at pressures of 3–5 atm. To produce the acetone-D₂O complex, fully deuterated water was used after the gas cylinder was thoroughly conditioned with D₂O (Aldrich, 99.8% purity).

To help assign the spectra of the acetone-water complex, several ab initio calculations were performed using the Gaussian 09 package²². Second order Møller-Plesset perturbation (MP2) theory (6-311++G (2d, p) basis set²³) and density functional theory (DFT) with B3LYP²⁴, B3LYP-D3^{25, 26}, and with M06-2X functionals²⁷ (6-311++G (2d, p) basis set), were used to obtain structural parameters, rotational constants, and dipole moment components for initial

spectroscopic searches. Harmonic vibrational frequency calculations were performed to confirm that the obtained structures are minimum energy configurations by the absence of imaginary frequencies.

Transition frequencies were predicted from the calculated rotational constants using the PGOPHER program.²⁸ The same program was then used to produce an initial fit of rotational and centrifugal distortion constants. The XIAM program was used to first predict methyl internal rotation splittings and then fit internal rotation parameters.^{29,30} The PMIFST program was employed to predict rotational constants for acetone-D₂O.³¹

4.3 Results and Discussion

4.3.1 Spectral Search and Assignment

The rotational spectrum of acetone-water is complicated by the hindered internal rotations of the two methyl groups. These internal rotations lead to splittings of the rotational lines into five components, with symmetry labels AA, AE, EA, E_iE, and EE_i. The AA species are expected to produce a regular semi-rigid rotor spectrum, and were the initial target of our assignment efforts. To aid the assignment process, we first removed known lines of the acetone monomer^{30,31} and of the acetone-Ne complex³² (Chapter 3) from the dense broad-band spectra that were collected with the chirped pulse instrument (see Figure 4.1).

Table 4.1. Predicted rotational constants and transition dipole moments of the acetone-water complex using DFT and MP2 methods with the 6-311 ++ G (2d, p) basis set.

	MP2	B3LYP	M06-2X	B3LYP-D3
A /MHz	9204.9	9166.6	9312.5	9216.5
B /MHz	2201.0	2175.4	2261.4	2222.3
C /MHz	1816.9	1797.6	1861.7	1830.9
$ \mu_a $ /D	2.3	3.1	2.7	3.0
$ \mu_b $ /D	0.9	0.5	0.5	0.6
$ \mu_c $ /D	0.0	0.4	0.3	0.1

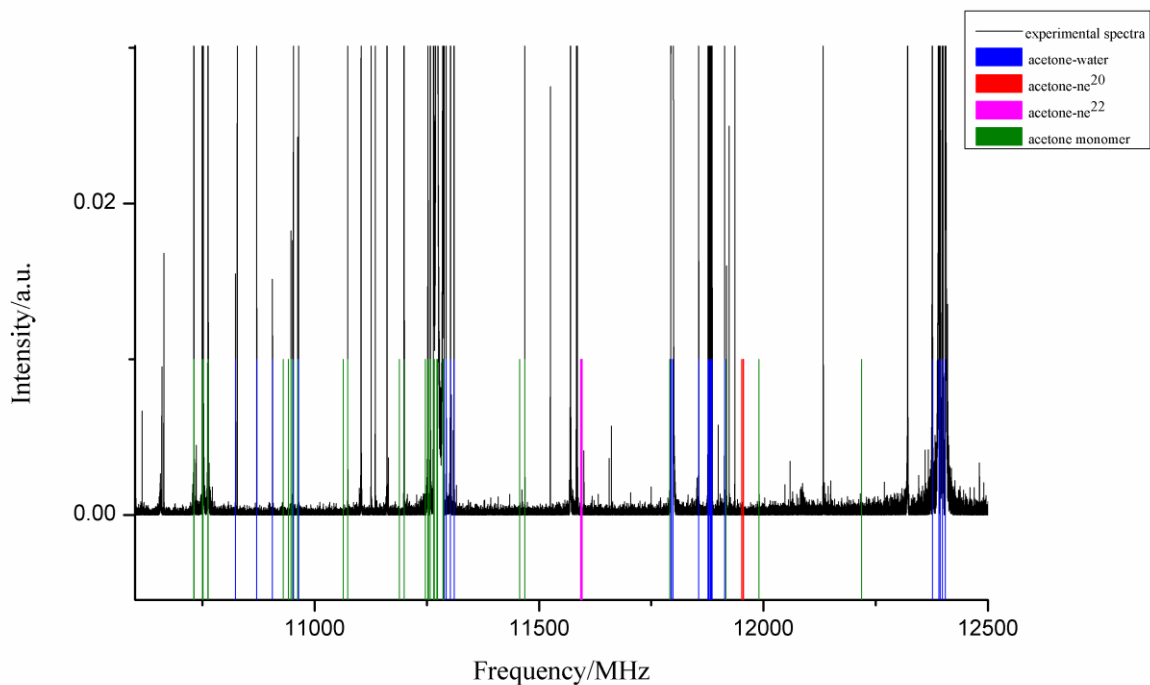


Figure 4.1. Assigned broadband spectrum of the acetone-water complex. The black lines denote experimental spectra, and the blue, red, magenta, and olive colors represent the assigned spectra for the acetone-water, acetone-Ne²⁰, acetone-Ne²² complexes, and the acetone monomer, respectively.

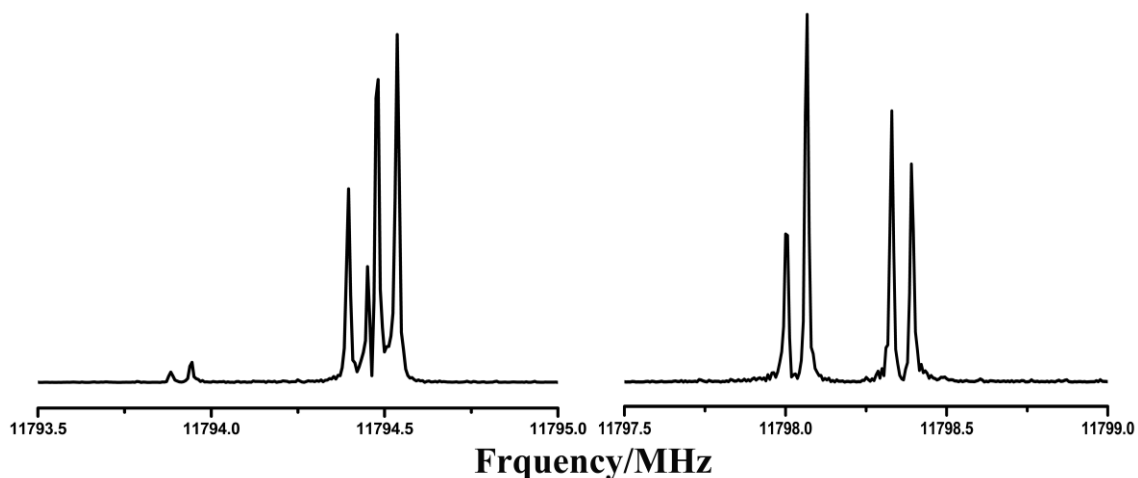


Figure 4.2. Rotational spectrum of the $3_{03}\leftarrow 2_{02}$ transition of the acetone-water complex, which was measured using a 0.5 mW excitation pulse with a duration of 0.25 μ s and averaged over 10 cycles.

I started the search for transitions of acetone-water using rotational constants and dipole moments from MP2, B3LYP, M06-2X, and B3LYP-D3 calculations, shown in Table 4.1. The μ_a dipole moment is predicted to be much larger than μ_b and μ_c , so I first looked for the stronger

a-type transitions. I could assign several *a*-type transitions, which were found to be split into five internal rotation components; as an example, the spectrum of the $J_{KaKc} = 3_{03} \leftarrow 2_{02}$ rotational transition is shown in Figure 4.2. After fitting several *a*-type transitions to refine the rotational constants, we were able to locate a number of *b*-type transitions. Similar methods were employed to search for and assign transitions of the acetone-D₂O complex. Rotational constants and centrifugal distortional constants were fitted to the transition frequencies of the AA components, and the results are listed in Table 4.2 for acetone-water and acetone-D₂O. Prediction of the internal rotation splittings using the resulting rotational constants and the ab initio internal rotation parameters (see Section 4.3.3 for details) with the XIAM code then enabled assignment of all detectable internal rotation components in the observed spectrum. The broadband spectrum of acetone-water with assigned acetone-water transitions is showed in Figure 4.1. All the observed transition frequencies of acetone-water and acetone-D₂O are listed in Table S 4.1 and S 4.2 of the supplementary information in Appendix II.

Table 4.2. Experimental spectroscopic parameters for the acetone-water complex and its D₂O isotopologue.

Parameter	acetone-water	acetone-D ₂ O
<i>A</i> /MHz	9174.37103(191)	9070.90800(286)
<i>B</i> /MHz	2162.17118(93)	2038.25807(125)
<i>C</i> /MHz	1789.88020(68)	1701.05688(82)
Δ_J /kHz	1.932(18)	1.615(21)
Δ_{JK} /kHz	13.970(94)	11.55(15)
δ_1 /kHz	0.343(12)	0.250(15)
<i>N</i>	23	18
σ /kHz	4.0	4.6

4.3.2 Structure and Hydrogen Bonding

Table 4.3 lists the bond lengths, bond angles, and complexation energies of the acetone-water complex calculated by the four levels of theory mentioned in Table 4.3. Comparing the experimental and calculated rotational constants of acetone-water with different levels of theories in Table 4.1 and 4.2, it is found that the structure calculated using the B3LYP method reproduces the experimental rotational constants much better than the other two methods. The

average deviation between experimental and calculated A, B, and C rotational constants is only ~0.4% using the B3LYP method, while it is ~1.2% for the MP2 method, ~3.4% in the M06-2X method and ~1.8% in the B3LYP-D3 method. Figure 4.3 shows the acetone-water complex in its principal inertial axis system, calculated at the B3LYP/6-311++G (2d, p) level. In this structure, the distance between the carbonyl oxygen atom and the hydrogen atom in the water molecule is 1.91 Å (Table 4.3), typical of a strong hydrogen bond with distances in the range between 1.5 and 2.2 Å.⁴⁶ The angle of the C=O⋯H(water) (see Figure 4.3) is smaller than 120°, which can be expected for a sp² lone pair.¹² The (water)O11-H13⋯O(C) angle deviates quite significantly from linearity and is found to be 165.3°. A secondary hydrogen bond is formed between (water)O11 and a hydrogen of a methyl group. The O-H bond distance is 2.56 Å, typical of secondary hydrogen bonding with distances in the range between 2.5 and 2.7 Å.¹²

Table 4.3. Calculated bond lengths, bond angles, and complexation energies of the acetone-water complex using DFT and MP2 methods with the 6-311 ++ G (2d, p) basis set.

	B3LYP	MP2	M06-2X	B3LYP-D3
$r(\text{C}=\text{O}) / \text{Å}$	1.21	1.22	1.21	1.22
$r(\text{C}=\text{O}\cdots\text{H}-\text{O}(\text{w})) / \text{Å}$	1.91	1.92	1.91	1.88
$r(\text{C}-\text{H}\cdots\text{O}-\text{H}(\text{w})) / \text{Å}$	2.56	2.48	2.36	2.49
$\angle \text{C}=\text{O}\cdots\text{H}13(\text{w}) / ^\circ$	118.4	116.5	115.5	117.4
$\angle \text{O}11-\text{H}13\cdots\text{O}(\text{C}) / ^\circ$	165.3	163.3	160.5	164.7
$\angle \text{O}11\cdots\text{H}2-\text{C} / ^\circ$	136.7	137.0	139.0	136.8
$\angle \text{O}11-\text{H}13\cdots\text{O}=\text{C} / ^\circ$	1.96	1.96	-1.20	-0.86
^a $\Delta E / \text{kcal mol}^{-1}$	-5.90	-5.86	-7.13	N/A

^a Basis set superposition error (BSSE) corrected complexation energy.

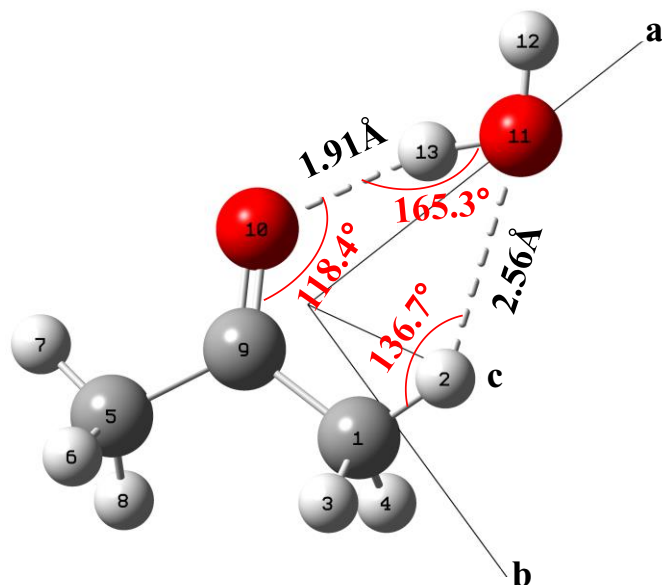


Figure 4.3. The structure of the acetone-water complex with hydrogen-bond parameters.

I also have employed Bader's QTAIM theory^{33, 34} to examine the intermolecular interactions, and the results are shown in Figure 4.4. It displays BCPs (yellow dots) along the corresponding bond paths (the orange lines). The analysis was done, and the plot generated, using the Multiwfn³⁵ program. The analysis indicates both canonical hydrogen bond and secondary hydrogen bond exist in acetone-water complex as two BCPs are generated along $C=O\cdots H(\text{water})$ and $(\text{water})O\cdots H-C$.

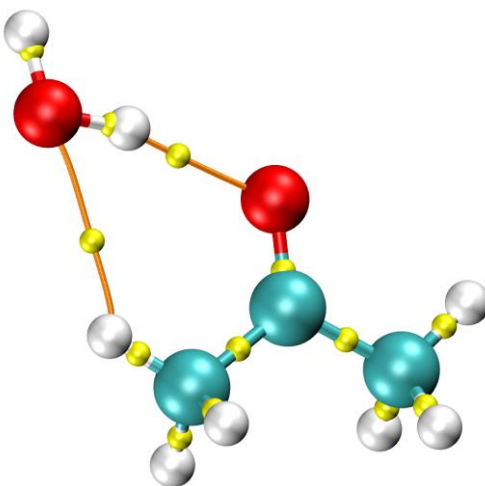


Figure 4.4. Bond critical points (BCPs) and the corresponding bond paths in the acetone-water complex.

The hydrogen bond energy can be estimated by the equation $E_{HB} = -0.5a_0^3V(r)$; here, a_0 is the Bohr radius.^{36,37} The energy for the regular hydrogen bond, i.e., C=O...H(water), is 25.3 kJ/mol, whereas it is 5.8 kJ/mol for the secondary hydrogen bond, (water)O...H-C. However, a previous study by our group has shown that the hydrogen bonding energy can be overestimated by using such a method.³⁸ So we also calculated the hydrogen bond energy using the empirical relationship $E_{HB} = 1.38(\Delta\nu_{OH} - 40)^{1/2}$, where $\Delta\nu_{OH}$ is the redshift wavenumber of the OH stretching vibration.³⁹ For the C=O...H(water) hydrogen bond, Zhang et al. have observed a redshift of -140 cm^{-1} of the OH stretching vibration of the water molecule within the acetone-water complex using FTIR in solid argon matrices.⁴⁰ Based on this, we can estimate the corresponding hydrogen bond energy to be 3.3 kcal/mol, i.e. 13.8 kJ/mol, indicating that the above hydrogen bond energy estimation based on $V(r)$ indeed is overestimated. Lastly, I applied a semi-empirical formula relating hydrogen bond energy and electron density (ρ_{BCP}) at the BCP, $E_{OH...O}$ (kcal/mol) = $-3.09+239\rho_{BCP}$.⁴¹ From the QTAIM analysis, the electron density(ρ_{BCP}) of C=O...H(water) is 0.024 a.u., and the estimated hydrogen bond energy is 2.6 kcal/mol, i.e. 11.1 kJ/mol, which is very close to the above value derived from the band shift of the OH stretch vibration.

I could not observe splittings of the rotational lines due to the internal motions of the water moiety in the acetone-water complex. The reason is probably a too high or too low barrier height of the internal rotation of water.¹²

4.3.3 Internal Rotation Dynamics

To estimate the height of the internal rotation barrier of the methyl groups, the MP2 level of theory with the 6-311++G (2d, p) basis set was used, and a potential energy curve was generated by scanning the dihedral angles $\angle 1(\text{H3, C1, C9, O10})$ and $\angle 2(\text{H6, C5, C9, O10})$ in steps of 10° ; the results are shown in Figure 4.5. The barrier was determined to be about 2.37 kJ/mol (hydrogen bonded methyl group) and 2.67 kJ/mol (“free” methyl group) after basis set superposition error (BSSE) corrections. The calculated barrier for the acetone monomer at the same level of theory is approximately 2.73 kJ/mol.

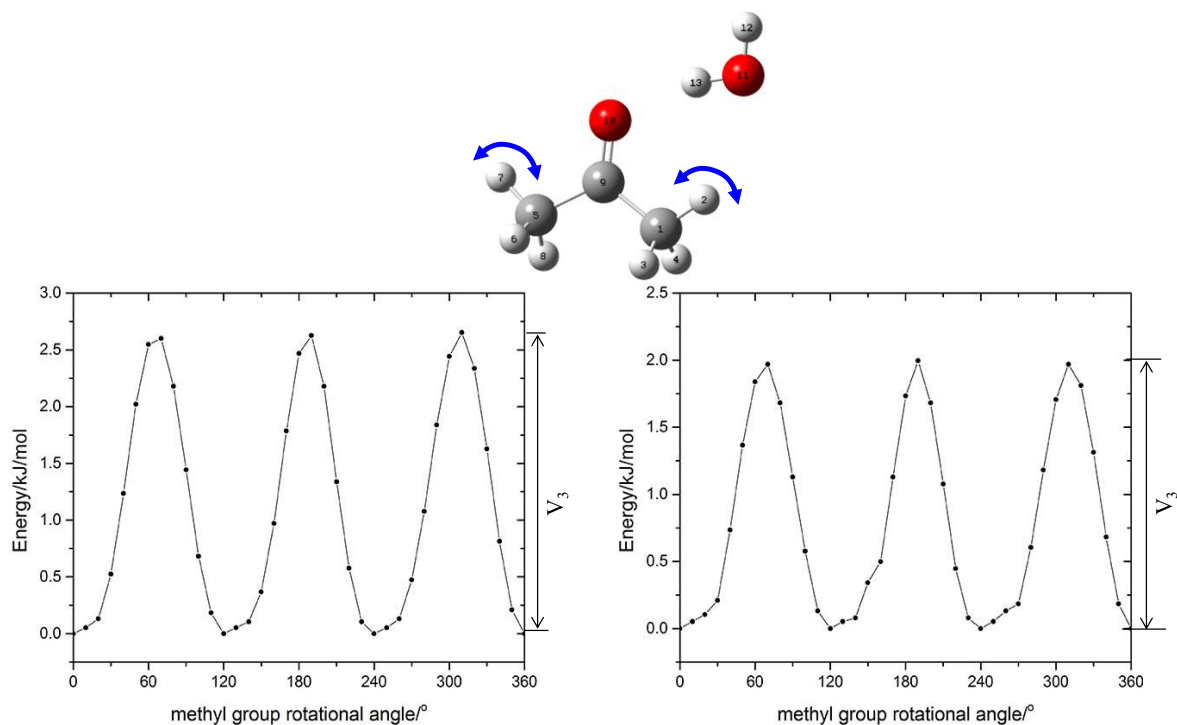


Figure 4.5. Potential curves of internal rotation of two methyl groups in the acetone-water complex.

To study the coupling between the two methyl groups in the acetone-water complex, I have performed a two-dimensional scan, in which the two dihedral angles $\angle 1(\text{H3, C1, C9, O10})$ and $\angle 2(\text{O10, C9, C5, H6})$ were varied in steps of 10° ; the result is shown in Figure 4.6 (c). I could observe the two-tops coupling in the acetone-water complex, similar to case of the acetone monomer, which has been investigated by J. S. Crighton et al.⁴² If the two tops are not coupled, the shapes of the wells and troughs would be hemispherical (See Figure 3.4 in Chapter 3). However, here in acetone-water complex, both the blue wells and rainbow wells are broadened in Figure 4.6(c), suggesting there is some coupling between the two methyl groups in the acetone-water complex. However, the two-methyl coupling in the acetone-water complex is not as strong as that in the acetone monomer (Figure 4.6 (a)) since the maxima energy (8.125 kJ/mol) in the water complex is smaller than that in the acetone monomer (8.828 kJ/mol). For the acetone-Ne complex (see Figure 4.6 (b)), it seems that the van der Waals interaction between acetone and Ne is so weak that it does not affect the coupling of these two methyl groups (the maxima energy only differs by 0.1 kJ/mol). It should be noticed that the

energy maximum in the acetone-Ne complex seems shifts several degrees compared with the acetone monomer and the acetone-water complex.

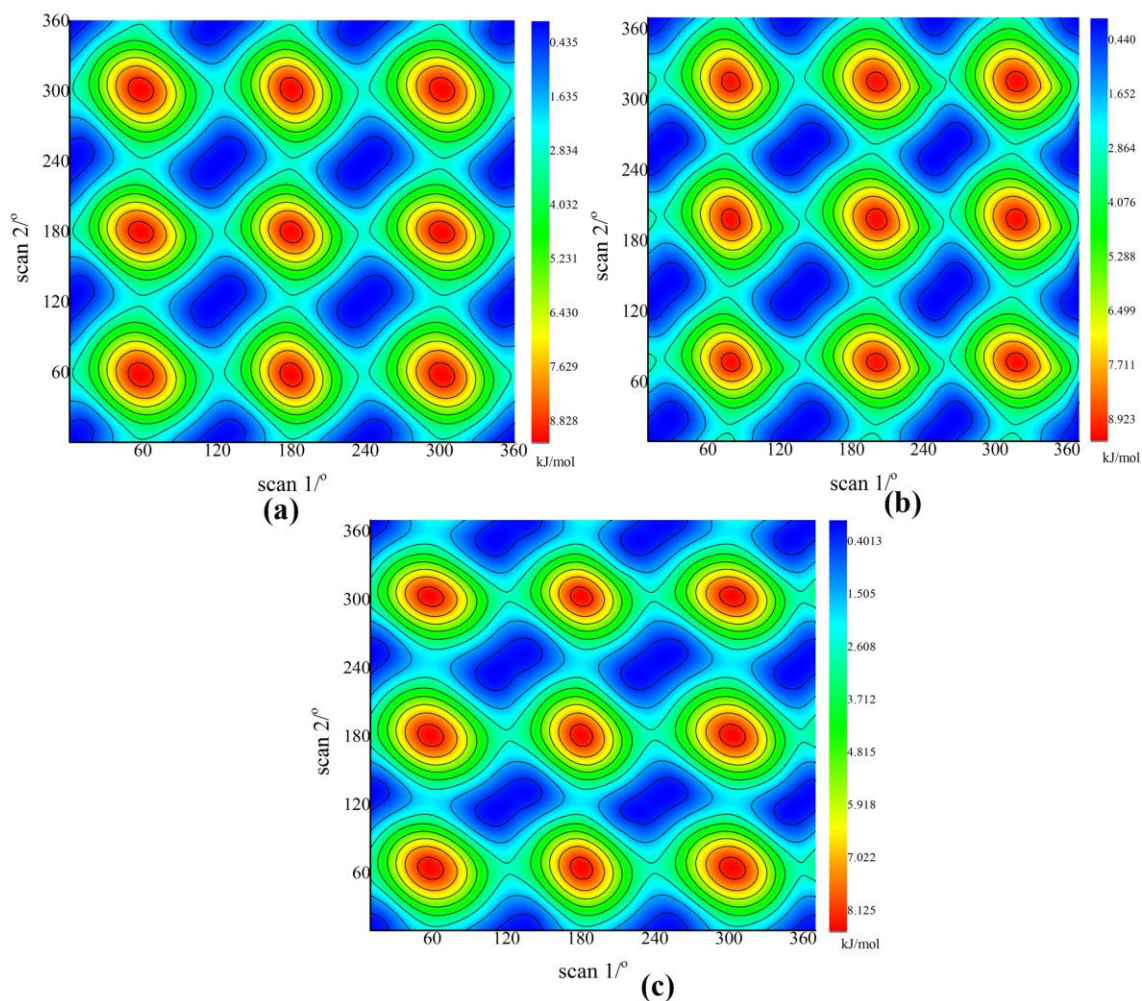


Figure 4.6. Two-dimensional methyl internal rotation scans of the acetone monomer (a), the acetone-Ne (b) and the acetone-water (c) complexes, calculated at the MP2/6-311 ++ G (2d, p) level of theory.

The internal rotation barrier heights of the methyl groups are fitted experimentally to be 2.770(11) and 3.061(2) kJ/mol in the acetone-water complex, as shown in Table 4.4. These two values are underestimated in theoretical calculations with the MP2 method, but the trend is consistent with the experimentally fitted values for the acetone monomer and the acetone-water complex. The first value corresponds to the rotation of the methyl group far away from the water molecule, whereas the latter one denotes the rotation of the methyl group close to the water molecule. Both internal rotation barrier heights are lowered in the acetone-water complex compared with the acetone monomer and other acetone complexes (for example,

acetone-Ne and acetone-Ar complexes). The barrier in the acetone-²⁰Ne and acetone-²²Ne complexes is 3.10(6) and 3.06(7) kJ/mol, respectively, in the acetone-Ar complex it is 3.110 kJ/mol,⁴³ and in the acetone monomer it is 3.182 kJ/mol.⁴⁴

Table 4.4. Experimental spectroscopic parameters for the acetone-water and acetone-D₂O complexes.

Parameter	acetone-water		acetone-D ₂ O	
<i>A</i> /MHz	9160.707(17)		9057.686(21)	
<i>B</i> /MHz	2161.482(3)		2037.600(3)	
<i>C</i> /MHz	1789.805(2)		1700.985(4)	
ΔJ /kHz	1.822(60)		1.474(51)	
ΔJK /kHz	13.26(37)		11.04(42)	
δ_j /kHz	0.306(37)		0.196(39)	
Top	Methyl group 1	Methyl group 2	Methyl group 1	Methyl group 2
D_{pi2J} /MHz ^a	-0.333(16)	-0.030(8)	-0.312(18)	-0.020(8)
D_{pi2K} /MHz ^a	-0.569(1)	0.000	-0.373(79)	0.000
V_3 /kJ/mol	2.772(7)	3.061(2)	2.702(26)	3.058(2)
ρ^b	0.0222(1)	0.05651(3)	0.02135(29)	0.05564(3)
β /rad ^c	0.6469(23)	3.0899(6)	0.6457(32)	3.0882(5)
γ /rad ^c	3.142(193)	0.027 ^d	3.218(26)	0.027 ^d
F_0 /GHz ^e	153.58	158.56	151.71	158.58
<i>N</i>	23/111		22/99	
σ /kHz	32.924		31.363	

^a Fourth order distortion terms describing the coupling between overall rotation and internal rotation.

^b ρ is dimensionless, related to the ratio of the molecular rotational constants and the internal rotor rotational constant F_0 .

^c β and γ are two Euler angles to transform each methyl top from their own internal axes to the principal axes.

^d fixed.

^e Derived parameters; the rotational constant of the methyl top ($F_0 = 505.379/I_a$ (in GHz), where I_a is the moment of inertia of the methyl top).

From our recent study of the acetone monomer,³² the barrier to methyl internal rotation is due mainly to the delocalized electrons shifting from (methyl carbon) C1-C9 (carbonyl oxygen) or (methyl carbon) C5-C9 bond to the C9=O10 bond when the methyl group C1H₃ rotates from the minimum to the transition state. This electron redistribution coincides with a bond length increase of C1-C9 and shrinkage of the C=O and C5-C9 bonds. Because of this electron population transfer, both methyl groups become destabilized, while the C9=O10 bond is stabilized. The destabilization of the two methyl groups makes the total energy of the transition state of acetone higher than the minimum state, thus generating the barrier of the methyl rotation. In the acetone-Ne complex, the extent of destabilization of the methyl group C1-H₃ is slightly less than in the acetone monomer when it rotates from the minimum to the maximum energy position. Simultaneously, the C9=O10 unit is less stabilized than in the monomer. However, the stabilization of the C5-H7 unit is much greater in the acetone-Ne complex than in the monomer, while the destabilization extent in the remaining two hydrogen atoms ((C5)H₂) in this methyl group is similar. This greater stabilization of the C5-H7 unit ultimately is reflected in the lower internal rotation barrier in the acetone-Ne complex. Both of the above cases involve rotation of two symmetric tops. In the acetone-water complex, the two methyl groups are inequivalent because each rotational transition is split into five components (as shown in Figure 4.2), and water is hydrogen bonded with one carbonyl group and one methyl hydrogen atom of acetone, which breaks the symmetry of the two methyl groups in acetone monomer. Then the question is how to analyze the barrier change with two asymmetric tops, in particular, when water is involved in hydrogen bonding.

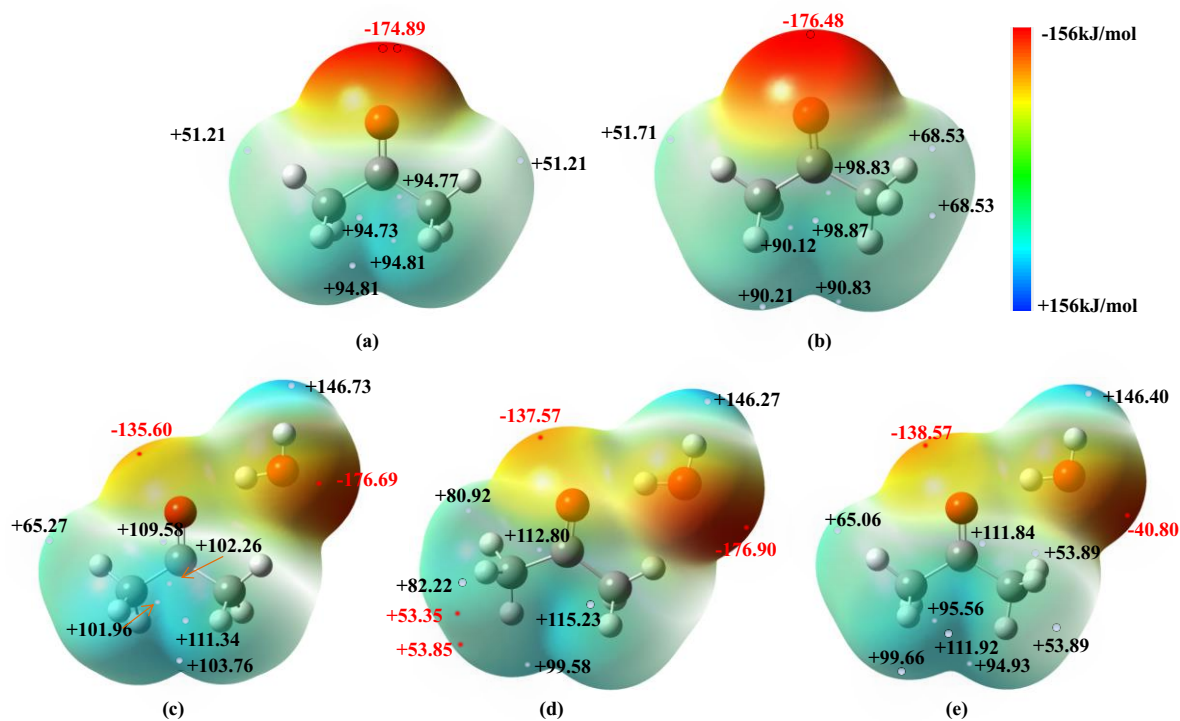


Figure 4.7. ESP map (unit: kJ/mol) of the acetone monomer in its minimum state (a) and transition state (b); the acetone-water complex in its minimum state (c) and transition state 1 (d), rotating the methyl group far away from water, and transition state 2 (e) rotating the methyl group close to water, calculated at the MP2/6-311 ++ G (2d, p) level of theory.

Figure 4.7 exhibits an electrostatic potential (ESP) map of the acetone monomer and the acetone-water complex with their minimum energy and transition state structures. The colors red, green, and blue denote that ESP values vary from 156 to -156 kJ mol^{-1} , and the white and orange small balls correspond to the surface maxima and minima, respectively. For the most stable structure of the acetone monomer, the two methyl tops are in an eclipsed position, while in its transition structure, the two tops are in a staggered position (we rotate the methyl top on the right side). From the minimum energy state to the transition state, more ESP surface maxima are generated in both the acetone monomer and in the acetone-water complex, especially in areas close to the rotated methyl group, indicating that the electronic densities change with the rotation of methyl groups. When comparing Figure 4.7 (b) and (d), that is, by rotating the methyl group far away from water, it is observed that the values of ESP surface maxima close to the hydrogen atoms of the rotated methyl group become larger than the transition state of the acetone monomer. Simultaneously, two new ESP surface minima (still a positive value, $\sim 54 \text{ kJ/mol}$) appear (Figure 4.7 (d)). On rotating the methyl group hydrogen

bonded to the water molecule in Figure 4.7 (e), compared with (b), the values of ESP surface maxima close to the hydrogen atoms in the rotated methyl group become smaller, which may be an indication that electrons from the acetone shifted to the water molecule. For a more quantitative characterization, variations in bond lengths and the integrated electronic densities and energies in atoms between the acetone monomer and the acetone-water complex were determined when going from the eclipsed to the staggered position of the two methyl groups, using QTAIM. Numerical results can be found in Table 4.5.1 and Table 4.5.2.

First, let us consider the case of the rotating the methyl group (C1H_3) far away from water (“free” methyl rotation) in the acetone-water complex. The internal rotation barrier is a little lower than in the acetone monomer based on the experimental fitting results from the microwave spectra. Similarly, we notice that the length of the (carbonyl carbon) C9-C1 (methyl carbon) bond increases, accompanied by a decrease in the bond lengths C9=O10 and (methyl) C5-C9 (carbonyl carbon) when going from the minimum to the transition state (Table 4.5.1). However, all these bond length changes and the corresponding BCP electronic densities are almost the same in the acetone monomer and its water complex. Therefore, we calculated the integrated atomic energies (Table 4.5.1) in these two systems, using Multiwfn³⁵ with the B3LYP-D3⁴⁵ method with the aug-cc-pvtz basis set based on QTAIM theory,^{33, 34} and tried to find the relative stabilities of atoms or groups in order to explain the lower barrier in the complex than in the monomer.

Table 4.5.1. Differences in bond lengths (Δr), integrated electronic populations ($\Delta\rho$), and atomic energies (ΔE) between the acetone-water complex and the acetone monomer with internal rotational of the “free” methyl groups using the B3LYP-D3 method with the aug-cc-pvtz basis set.

	^a Acetone	^b Acetone-water
$V_3^{\text{B3LYP-D3}}/\text{kJ/mol}$	2.636	2.394
$\Delta r(\text{C1-C9})/\text{pm}$	0.480	0.463
$\Delta r(\text{C9-O10})/\text{pm}$	-0.016	-0.005
$\Delta r(\text{C9-C5})/\text{pm}$	-0.296	-0.289
$\Delta\rho(\text{C1-C9})/\text{a.u.}$	-0.0027	-0.0026
$\Delta\rho(\text{C9-C5})/\text{a.u.}$	0.0015	0.0015
$\Delta\rho(\text{C9-O10})/\text{a.u.}$	0.0004	0.0003
$\Delta E(\text{C1-H}_2)/\text{a.u.}$	0.01177	0.01342
$\Delta E(\text{H3})/\text{a.u.}$	-0.01072	-0.01281
$\Delta E(\text{C5-H}_3)/\text{a.u.}$	0.00122	0.00168
$\Delta E(\text{C9=O10})/\text{a.u.}$	-0.00131	-0.00236
$\Delta E(\text{O11-H13})/\text{a.u.}$	N/A	0.00209
$\Delta E(\text{H12})/\text{a.u.}$	N/A	-0.00110
$\Delta N(\text{C1-H}_2)/\text{a.u.}$	0.01521	0.01822
$\Delta N(\text{H3})/\text{a.u.}$	-0.01694	-0.02015
$\Delta N(\text{C5-H}_3)/\text{a.u.}$	0.00343	0.00446
$\Delta N(\text{C9=O10})/\text{a.u.}$	-0.00168	-0.00249
$\Delta N(\text{O11-H13})/\text{a.u.}$	N/A	0.00042
$\Delta N(\text{H12})/\text{a.u.}$	N/A	-0.00046

^a Differences in acetone when going from the minimum to the transition state.

^b Difference between the acetone-water complex and the acetone monomer, both in their minimum state.

In going from the eclipsed to the staggered position in the acetone monomer, the C1-H₂ methyl group obtains electronic population from the hydrogen atom (H3); consequently, the C1-H₂ is highly destabilized (0.01177 a.u.). Simultaneously, the hydrogen atom (H3) is stabilized to about 0.01072 a.u., which destabilizes the C1H₃ unit by about 0.00105 a.u. In the acetone-water cluster, the extent of destabilization of the C1H₂ methylene group is a little

larger than the extent of stabilization of the H3 atom, so that the entire C1H3 group is destabilized by 0.00061 a.u.; this is less than the destabilization in the acetone monomer in going from the minimum to the transition state. However, the destabilization trend is not similar in the other methyl group, C5H3, between the monomer and the complex. In the acetone monomer, the C5H3 group gains electronic population (0.00343 a.u.) from the adjacent C9=O10 and C1H3 bonds; as a result it is destabilized (0.00122 a.u.). In the acetone-water complex, the C5H3 group gains much more electronic population (0.00446 a.u.) than in the acetone monomer, so that it is destabilized more (0.00168 a.u.) than in the monomer. In fact, the total destabilization extent of these two methyl groups is the same in the acetone monomer and in the acetone-water complex when rotating the C5H3 methyl group. However, the C9=O10 group in the acetone-water complex loses more electronic population (-0.00249 a.u. vs -0.00168 a.u.) than that in the monomer, so the stabilization extent is much larger in the acetone-water complex (-0.00236 a.u. vs -0.00131 a.u.). Although the water unit is destabilized (0.00099 a. u.), which may lift the total energy a little bit in the cluster, it is still not enough to offset the larger stabilization part that the C9=O10 group makes in the complex. Overall, the internal rotation barrier of the “free” methyl group in the acetone-water complex is a little lower than that in the acetone monomer. In other words, the stabilization of the C9=O10 carbonyl group in acetone-water mainly makes the barrier lower than the acetone monomer when rotating the “free” methyl group (C1H3).

When the other methyl group (i.e., C5H3) close to the water molecule rotates in the acetone water cluster (Table 4.5.2), things become more complicated because such a methyl rotation acts as a “perturbation” that affects not only the hydrogen bonding strength between acetone and water but also influences the stability of almost every part in the system. First, a little stretch of the C9=O10 bond (0.040 pm) appears instead of shrinking when going from the minimum to the transition state in the acetone-water cluster. Note that in the previous methyl rotation case, the C9=O10 shrinkage (-0.005 pm) from the minimum to the transition state in acetone-water had a more negative contribution (-0.00236 a.u.) to the rotation barrier compared with the acetone monomer, but now there is even more negative contribution (-0.00251 a.u.) to the rotation barrier in the acetone-water complex. Such a change in the C9=O10 bond contributes a large part to lowering the rotation barrier.

Table 4.5.2. Differences in bond lengths (Δr), integrated electronic populations ($\Delta\rho$), and atomic energies (ΔE) between the acetone-water complex and the acetone monomer with internal rotation of the methyl group hydrogen bonded to water using the B3LYP-D3 method with the aug-cc-pvtz basis set.

	^a acetone	^b acetone-water
$V_3^{\text{B3LYP-D3}}/\text{kJ/mol}$	2.636	2.187
$\Delta r(\text{C9-O10})/\text{pm}$	-0.017	0.040
$\Delta r(\text{C1-C9})/\text{pm}$	-0.296	-0.328
$\Delta r(\text{C9-C5})/\text{pm}$	0.481	0.333
$\Delta\rho(\text{C9-O10})/\text{a.u.}$	0.0004	0.0003
$\Delta\rho(\text{C1-C9})/\text{a.u.}$	0.0015	0.0015
$\Delta\rho(\text{C9-C5})/\text{a.u.}$	-0.0027	-0.0026
$\Delta E(\text{C1-H}_3)/\text{a.u.}$	0.00123	0.00189
$\Delta E(\text{C5-H}_3)/\text{a.u.}$	0.00107	-0.00056
$\Delta E(\text{C9})/\text{a.u.}$	0.00123	-0.00416
$\Delta E(\text{O10})/\text{a.u.}$	-0.00255	0.00165
$\Delta E(\text{O11}(\text{water}))/\text{a.u.}$		0.00219
$\Delta E(\text{H12}(\text{water}))/\text{a.u.}$		-0.00011
$\Delta E(\text{H13}(\text{water}))/\text{a.u.}$		-0.00013
$\Delta N(\text{C9})/\text{a.u.}$	0.00182	-0.00256
$\Delta N(\text{C5-H}_3)/\text{a.u.}$	-0.00168	-0.00137
$\Delta N(\text{C1-H}_3)/\text{a.u.}$	0.00336	0.00481
$\Delta N(\text{C9=O10})/\text{a.u.}$	-0.00167	-0.00298
$\Delta N(\text{H}_2\text{O})/\text{a.u.}$		-0.00046

^a The difference of acetone from the minimum to the transition state.

^b The difference between the acetone-water complex and the acetone monomer both in their minimum state.

I also noticed that the oxygen atom (O11) in water is destabilized significantly (0.00219 a.u.), even if two other hydrogen atoms in water are stabilized (-0.00024 a.u.) but still not

enough to compensate for the destabilization of the oxygen atom in water. Such a destabilization of the oxygen atom also could be partly compensated by the stabilization of the C9=O10 bond. In total, the C9=O10 bond and the water unit still are stabilized (-0.00056 a.u.) due to the larger stabilization of C9=O10 in the acetone-water complex. Correspondingly, the extent of losing electronic population in C9=O10 in the acetone-water complex also is much larger than that in the acetone monomer (-0.00298 a.u. vs -0.00167 a.u.).

Moreover, when the methyl group C5H₃ rotates, the adjacent C9 atom gains electronic population (0.00182 a.u.) from the C5H₃ group in the acetone monomer, while it loses electronic population in the acetone-water complex (-0.00256 a.u.), i.e., the C5H₃ group loses less electronic population in the complex in going from the minimum to the transition state; as a result, it is stabilized (-0.00056 a.u.) instead of destabilized (+0.00107 a.u.) in the acetone monomer. Also, it is noticed that the C9-C5 bond elongates less (0.333 pm) when going from the minimum to the transition state than the acetone monomer (0.481 pm) with water involvement, and the electronic density at the BCP of C9-C5 does not decrease to the same extent as that in the acetone monomer. Lastly, the methyl group C1H₃ on the other side (i.e. far away from water molecule, “free methyl”) is destabilized more (0.00189 a.u. vs 0.00123 a.u.) in the complex than that in the monomer, and the C1H₃ group gained more electronic population from C9=O10. It is also found that the C1-C9 bond length shrinks more (0.328 pm) in the acetone-water complex than in the acetone monomer (0.296 pm), and the electronic density at the BCP of C1-C9 correspondingly increases a little. Overall, the rotation barrier of the methyl group close to water is much lower than that in the acetone monomer. One may ask why the rotation barrier is lower when the rotating methyl group is close to water than when the rotating methyl group is far away from the water. This may be due to the larger stabilization of the methyl group C5H₃ (hydrogen bonded methyl) and C9=O10 in the acetone molecule when rotating the C5H₃ near the water molecule, rather than the stabilization of only the C9=O10 group when the “free” methyl group is rotating.

Although we only captured the keto form of acetone water using rotational spectra, it still gives us rich information about the hydrogen bonding of the ketone and water interaction, as well as the methyl rotation tunneling motion while hydrogen bonding is involved.

4.3.4. Enol Form of Acetone

It is known that the keto form of acetone is thermodynamically more stable than its enol form; the energy difference of these two forms is ~ 10 kcal/mol in the gas phase,⁵ and the barrier for the keto form converting into the enol form is rather high, ~ 68 kcal/mol. However, when water is added into the system, the water acts as a catalyst that lowers the barrier to 40 kcal/mol, as calculated at the M06-2X/ 6-311+G(2df,2p) level of theory.⁵ When two water molecules are added to the system, the energy difference between keto-(water)₂ and enol-(water)₂ is ~ 8 kcal/mol, and the barrier of the interconversion between these two forms is lowered further, to ~ 33 kcal/mol.⁵ Assuming a Boltzmann distribution, we can expect approximately 0.0003% of the enol form, enol-(water)₂, at room temperature (25 °C). However, the signal to noise ratio in one of the strongest transitions ($J_{KaKc} = 202-101$) of the acetone-water cluster that we can observe in the cavity-based microwave spectrometer is ~ 62500 within 10 averaging cycles, which means that it is impossible for us to detect the enol form of acetone-water complex in its neutral form.

4.4 Conclusions

Microwave spectra of the acetone-water complex were measured using both chirp-pulsed and cavity-based molecular beam Fourier-transform microwave spectrometers in the region from 5 to 18 GHz. Both *a*- and weaker *b*- type rotational transitions were observed for the acetone-water complex and the acetone-D₂O complex. The assignment of these rotational transitions was completed with the help of ab initio calculations. Moreover, we have focused on why the methyl internal rotation barrier is lower than in the acetone monomer when water is involved in forming hydrogen bonding. It is found that more stabilization of the carbonyl group makes the internal barrier lower when forming the acetone-water complex compared with an acetone monomer when rotating the “free” methyl group (i.e., not the hydrogen bonded methyl group). The electronic populations shifts much more from the C9=O10 bond in the acetone-water complex than that in the acetone monomer when the methyl group rotates, thus a lower barrier height results in the acetone-water complex. But why does the rotation barrier become even lower when the other methyl group (close to the water molecule) is rotating in the same acetone-water complex? The reason is that with the help of a water molecule, the C9=O10 bond is stabilized much more, the rotating methyl group (C5H₃) is stabilized compared with

the acetone monomer, and it even cancels some by the destabilization of the water molecule. Overall, the larger stabilization of both the C=O and the rotating methyl group makes the rotational barrier even lower compared with rotating the “free methyl”. Unfortunately, I failed in finding the enol form of acetone in its hydrated form because its amount is so low that we could not detect it.

References

1. E. P. Kundig, A. E. Garcia, T. Lomberget and G. Bernardinelli, *Angew. Chem., Int. Ed.*, 2006, **45**, 98-101.
2. W. N. Wang, H. W. Hellinga and L. S. Beese, *Proc. Natl. Acad. Sci.*, 2011, **108**, 17644-17648.
3. H. F. Judson, *The Eighth Day of Creation*, Simon & Schuster, New York, 1979.
4. M. D. Topal and J. R. Fresco, *Nature*, 1976, **263**, 285-289
5. B. Boekfa, P. Pantu, M. Probst and J. Limtrakul, *J. Phys. Chem. C*, 2010, **114**, 15061-15067.
6. C. S. Cucinotta, A. Ruini, A. Catellani and A. Stirling, *Chemphyschem*, 2006, **7**, 1229-1234.
7. E. Tapuhi and W. P. Jencks, *J. Am. Chem. Soc.*, 1982, **104**, 5758-5765.
8. Y. Matsuda, A. Yamada, K. Hanaue, N. Mikami and A. Fujii, *Angew. Chem., Int. Ed.*, 2010, **49**, 4898-4901.
9. M. Juanes, W. Li, L. Spada, L. Evangelisti, A. Lesarri and W. Caminati, *Phys. Chem. Chem. Phys.*, 2019, **21**, 3676-3682.
10. F. J. Lovas and C. Lugez, *J. Mol. Spectrosc.*, 1996, **179**, 320-323.
11. T. Lu, J. Zhang, J. Chen, Q. Gou, Z. Xia and G. Feng, *J. Chem. Phys.*, 2019, **150**, 064305.
12. S. Melandri, A. Maris, B. M. Giuliano and W. Caminati, *J. Chem. Phys.*, 2005, **123**, 164304.
13. N. A. Seifert, J. Thomas, W. Jäger and Y. Xu, *Phys. Chem. Chem. Phys.*, 2018, **20**, 27630-27637.
14. P. A. Stockman, G. A. Blake, F. J. Lovas and R. D. Suenram, *J. Chem. Phys.*, 1997, **107**, 3782-3790.
15. J. Thomas and Y. Xu, *J. Chem. Phys.*, 2014, **140**, 234307/1-5.
16. E. G. Schnitzler and W. Jäger, *Phys. Chem. Chem. Phys.*, 2014, **16**, 2305-2314.
17. S. Ghosh, J. Thomas, W. Huang, Y. Xu and W. Jäger, *J. Phys. Chem. Lett.*, 2015, **6**, 3126-3131.
18. S. P. Dempster, O. Sukhorukov, Q. Y. Lei and W. Jäger, *J. Chem. Phys.*, 2012, **137**, 174303.
19. J. Thomas, J. S. Yiu, J. Rebling, W. Jäger and Y. J. Xu, *J. Phys. Chem. A*, 2013, **117**, 13249-13254.
20. Y. J. Xu, J. Van Wijngaarden and W. Jäger, *Int. Rev. Phys. Chem.*, 2005, **24**, 301-338.
21. Y. J. Xu and W. Jäger, *J. Chem. Phys.*, 1997, **106**, 7968-7980.
22. M. J. Frisch, G. W. Trucks, H. B. Schlegel, G. E. Scuseria, M. A. Robb, J. R. Cheeseman, G. Scalmani, V. Barone, B. Mennucci, G. A. Petersson, H. Nakatsuji, M. Caricato, X. Li, H. P. Hratchian, A. F. Izmaylov, J. Bloino, G. Zheng, J. L. Sonnenberg, M. Hada, M. Ehara, K. Toyota, R. Fukuda, J. Hasegawa, M. Ishida, T. Nakajima, Y. Honda, O. Kitao, H. Nakai, T. Vreven, J. A. Montgomery, Jr., J. E. Peralta, F. Ogliaro, M. Bearpark, J. J. Heyd, E. Brothers, K. N. Kudin, V. N. Staroverov, T. Keith, R. Kobayashi, J. Normand, K. Raghavachari, A. Rendell, J. C. Burant, S. S. Iyengar, J. Tomasi, M. Cossi, N. Rega, J. M. Millam, M. Klene, J. E. Knox, J. B. Cross, V. Bakken, C. Adamo, J. Jaramillo, R. Gomperts, R. E. Stratmann, O. Yazyev, A. J. Austin, R. Cammi, C. Pomelli, J. W. Ochterski, R. L. Martin, K. Morokuma, V. G. Zakrzewski, G. A. Voth, P. Salvador, J. J. Dannenberg, S. Dapprich, A. D. Daniels, O. Farkas, J. B. Foresman, J. V. Ortiz, J. Cioslowski, and D. J. Fox, *Gaussian 09, Revision D.01*, Gaussian, Inc., Wallingford CT, 2013.
23. J. E. Del Bene, *J. Comput. Chem.*, 1985, **6**, 296-301.

24. T. Yanai, D. P. Tew and N. C. Handy, *Chem. Phys. Lett.*, 2004, **393**, 51-57.
25. S. Grimme, J. Antony, S. Ehrlich and H. Krieg, *J. Chem. Phys.*, 2010, **132**, 154104.
26. S. Grimme, S. Ehrlich and L. Goerigk, *J. Comput. Chem.*, 2011, **32**, 1456-1465.
27. E. R. Johnson, I. D. Mackie and G. A. DiLabio, *J. Phys. Org. Chem.*, 2009, **22**, 1127-1135.
28. C. M. Western, *J. Quant. Spectrosc. Radiat. Transf.*, 2017, **186**, 221-242.
29. H. Hartwig and H. Dreizler, *Z. Naturforsch.*, 1996, **51a**, 923-932.
30. N. Hansen, H. Mäder and T. Bruhn, *Molec. Phys.*, 1999, **97**, 587-595.
31. H. B. Thompson, *J. Chem. Phys.*, 1967, **47**, 3407-3410.
32. J. Gao, N. A. Seifert, J. Thomas, Y. J. Xu and W. Jäger, *J. Mol. Spectrosc.*, 2016, **330**, 228-235.
33. R. F. W. Bader, *Atoms in Molecules: A Quantum Theory*, Oxford University Press, New York, 1990.
34. R. F. W. Bader, *Chem. Rev.*, 1991, **91**, 893-928.
35. T. Lu and F. W. Chen, *J. Comput. Chem.*, 2012, **33**, 580-592.
36. E. Espinosa, E. Molins and C. Lecomte, *Chem. Phys. Lett.*, 1998, **285**, 170-173.
37. I. Mata, I. Alkorta, E. Espinosa and E. Molins, *Chem. Phys. Lett.*, 2011, **507**, 185-189.
38. E. G. Schnitzler, M. R. Poopari, Y. J. Xu and W. Jäger, *Phys. Chem. Chem. Phys.*, 2015, **17**, 21942-21949.
39. A. V. Iogansen, *Spectrochim. Acta*, 1999, **55A**, 1585-1612.
40. X. K. Zhang, E. G. Lewars, R. E. March and J. M. Parnis, *J. Phys. Chem.*, 1993, **97**, 4320-4325.
41. T. Y. Nikolaienko, L. A. Bulavin and D. M. Hovorun, *Phys. Chem. Chem. Phys.*, 2012, **14**, 7441-7447.
42. J. S. Crighton and S. Bell, *J. Mol. Spectrosc.*, 1986, **118**, 383-396.
43. L. Kang, A. R. Keimowitz, M. R. Munrow and S. E. Novick, *J. Mol. Spectrosc.*, 2002, **213**, 122-129.
44. J. M. Vacherand, B. P. Vaneijck, J. Burie and J. Demaison, *J. Mol. Spectrosc.*, 1986, **118**, 355-362.
45. L. Goerigk and S. Grimme, *J. Chem. Theory Comput.*, 2011, **7**, 291-309.
46. G.R. Desiraju and T. Steiner, *The weak hydrogen bond: in structural chemistry and biology*, Oxford University Press Inc., New York, 2001.

Chapter 5

A Microwave Spectroscopic and Ab Initio Study of Keto-Enol Tautomerism and Isomerism in the Cyclohexanone-Water Complex

The contents of this chapter have been copied and/or adapted from the following publication:
J. Gao, N. A. Seifert, W. Jäger, *Phys. Chem. Chem. Phys.* 2019, **21**, 12872-12880.

5.1 Introduction

Intermolecular interactions between oxygenated organic compounds and water are of great interest in a wide range of areas, including atmospheric, aqueous, and biological chemistry. In atmospheric chemistry, for example, oxidation of volatile organic compounds leads to highly oxygenated substances with low vapor pressures, which can partition from the gas into the condensed phase to form a secondary organic aerosol. The initial steps of SOA particle formation are thought to involve molecular clusters consisting of sulfuric acid, water, and oxidized organic compounds, such as organic acids.^{1,2} Cyclohexanone is a partially oxidized compound that has been detected in secondary organic aerosols produced in photo-reaction chamber experiments³ and in the ambient atmosphere in concentrations similar to those of acetone, the most abundant atmospheric ketone.⁴⁻⁸ Cyclohexanone can be emitted into the atmosphere directly from industrial plants, as well as vehicle and cooking exhaust.⁴ It also is produced by the atmospheric oxidation of cyclohexane, a compound used for the production of adipic acid, which is a precursor for nylon, and an industrial solvent. Cyclohexanone itself undergoes chemical transformations in the troposphere and it can be removed from the atmosphere by reaction with Cl,⁹⁻¹¹ oxidation by OH radical,¹² and photochemical processes.^{13, 14}

Hydrogen bonding in general and interactions with water specifically have significant effects on atmospheric reactions involving ketones such as cyclohexanone, giving impetus for the present study of the structure and dynamics of the cyclohexanone-water complex. In fact, atmospheric reaction pathways involving ketones cannot be described properly without

considering the reactivity of the enol tautomer. For instance, side-reactions of OH with enols provide statistically significant increases in carboxylic acid concentrations compared to atmospheric models that consider only the keto form.¹⁵ Enolic and enol-derived products also have been observed in atmospherically relevant combustion reactions.^{16, 17} It is also necessary to consider these enols when studying the existing detailed kinetic mechanisms.¹⁸ Since water is an important species in these contexts, it is essential to understand the role hydration plays in both kinetically and thermodynamically stabilizing reactions involving species exhibiting keto-enol tautomerism.

Cyclohexanone exists in several isomeric and conformeric forms, and how hydration affects their relative stabilities gives further motivation for this study. The cyclohexanone monomer has been studied previously by IR,¹⁹ gas-phase electron diffraction,²⁰ and microwave spectroscopy.²⁰⁻²² These studies show that the keto tautomer of cyclohexanone can exist in three possible conformations: the chair form, the boat form, and the skew-boat form.²² Only the chair form exists in significant abundance in the gas phase. Additionally, cyclohexanone can undergo keto-enol tautomerization, and its keto form is the more stable one, by 45 kJ/mol.²³ In the gas phase, only the keto form has been detected, and in the aqueous phase, the abundance determination of the enol form varies over several orders of magnitude. The earliest quantitation is that of G. Schwarzenbach et al., who found an enol abundance of 0.02 % using a bromine titration technique.²⁴ However, a later study by Bell and Smith found significant issues with the experimental protocol of the study by Schwarzenbach et al. and determined a revised enol abundance of $\sim 4.1 \times 10^{-4}$.²⁵ More recent studies using different methodologies find abundances even lower than that of Bell and Smith; for instance, J. Dubois et al. found the abundance to be $\sim 2.3 \times 10^{-5}$,²⁶ and A. Kresge et al. reported that the enol content is $\sim 4.1 \times 10^{-7}$ %.²⁷ Ab initio calculations may help us understand how water is responsible for changes in distribution among conformers and isomers of cyclohexanone during the transition from the gas to the aqueous phase.

My aim is to quantify and observe the effects of hydration with a single water molecule on cyclohexanone isomerism. Changes in conformer and isomer distributions can, for example, be a result of canonical C=O \cdots O-H(water) hydrogen bonding and weaker, secondary interactions.^{28, 29} Such secondary hydrogen bonds have been detected previously in other model systems. For example, in a microwave study of formaldehyde-water, Lovas et al. found

a C-H...O-H bond length of 2.68 Å, short enough to be considered a secondary hydrogen bond.³⁰ Our recent rotational spectroscopic study of acetone-water suggests that there is also a secondary hydrogen bond, with a C-H ... O-H bond length of 2.56 Å.³¹ On the other hand, Melandri et al. have investigated the hydrogen bonded cyclobutanone-water complex using Fourier-transform microwave spectroscopy,³² and their results indicate a C-H...O-H distance of about 3.01 Å, too long to be considered a secondary hydrogen bonding interaction.

In this report, I describe a microwave spectroscopic study of the cyclohexanone-water complex, supplemented by ab initio calculations. Spectra of numerous isotopologues of the chair-*keto* form were assigned and used to derive an experimental, least-squares fit structure, which exhibits both canonical and secondary hydrogen bonding. I also discuss the characteristics of these hydrogen bonding interactions in several atmospherically relevant monohydrated ketones, including cyclohexanone, using QTAIM and symmetry adapted perturbation theory (SAPT) analyses.

5.2 Experimental and Computational Details

Spectral information from Fourier transform microwave (FTMW) spectroscopy in combination with the molecular beam technique has proven to be quite sensitive to fine structural differences between conformers of molecular species, such as complexes and clusters.³³⁻³⁶ Rotational spectra of the cyclohexanone-water complex initially were recorded between 8 and 14 GHz using a broadband chirped pulse Fourier transform microwave spectrometer. This instrument has a frequency resolution of ~25 kHz and has been described in detail previously.^{37,38} All final measurements were performed using a cavity based Fourier transform microwave spectrometer between 7 and 14 GHz. This instrument has a higher resolution of ~2 kHz and has been described in detail elsewhere and in Chapter 2.^{39,40}

The samples were introduced into the spectrometer as a pulsed supersonic molecular expansion. The pulsed expansion leads to the formation of molecular complexes and clusters such as the cyclohexanone-water complex. The rotational temperatures are typically 1 to 2 K, and the conformational temperature can be between about 60 K and room temperature, depending on the thermodynamics of the specific system. The sample mixtures consisted of about 0.1% cyclohexanone (99.8% purity, Fisher Scientific) and 0.2% water in helium or neon for the broadband and cavity instruments, respectively, at backing pressures of 2–5 atm.

Spectra of the ^{13}C mono-substituted isotopologues were measured in their natural abundances ($\sim 1\%$). The spectra of HDO isotopologues were recorded using a mixture of 0.1% cyclohexanone and 0.2% of a 1:1 mixture of $\text{H}_2\text{O} / \text{D}_2\text{O}$.

To help search for and assign the rotational transitions of the cyclohexanone-water cluster, high level ab initio calculations were performed using GAUSSIAN 09.⁴¹ MP2/6-311++G(2d,p), B3LYP/6-311++G(2d,p), and B3LYP-D3/aug-cc-pVTZ (aVTZ)⁴² levels of theory were used to perform geometry optimizations and vibrational frequency calculations. The symmetry adapted perturbation theory [SAPT(0)] calculations⁴⁶ were done with the Psi4 quantum chemistry suite⁴⁷ using the jun-cc-pVDZ basis set, and quantum theory of atoms in molecules (QTAIM)^{43, 44} analyses were performed using the Multiwfn software suite.⁴⁵

Rotational transition frequencies were predicted from the calculated rotational constants using the PGOPHER program⁴⁸, and the measured transition frequencies were analyzed in a fitting procedure to give spectroscopic parameters with the same program. The PMIFST program⁴⁹ was employed to predict rotational constants for mono-substituted ^{13}C , HDO, and D_2O isotopologues.

5.3 Results and Discussion

5.3.1 Ab Initio Calculations of Keto-Enol Tautomeric and Conformational Changes of the Cyclohexanone Monomer and Its Monohydrate

There are three possible conformers for the keto form of cyclohexanone, which have different ring conformations (chair, boat, and skew-boat), and two conformers for the enol form, with different O-H group orientations. The existence of these five tautomeric/conformational species of the cyclohexanone monomer was confirmed at the B3LYP-D3/aVTZ level of theory. The obtained structures are shown in Figure 5.1, along with their relative energies and the corresponding spectroscopic constants (shown in Table 5.1). The chair form of the cyclohexanone monomer is found to have the lowest energy, lower by $\sim 15 \text{ kJ mol}^{-1}$ than the boat and skew conformers. The two enol conformers have higher energies, by about 40–50 kJ mol^{-1} , than the keto forms. Assuming a Boltzmann distribution^{50, 51} at room temperature, the relative abundances of the higher energy species (i.e., the enol forms) are calculated to be $\sim 10^{-6}$ – $10^{-5}\%$, and the relative abundance of the ring isomers (i.e., skew-boat isomers) is 0.1%.

This infers that detection of the low abundance enol forms would require highly sensitive experimental techniques.

I also performed a computational search for tautomers and isomers of the cyclohexanone-water complex. Four *keto* tautomer-water clusters (including one chair and one boat conformer of cyclohexanone and the skew conformer with two different water binding sites) and four *enol* tautomer-water clusters were found at the B3LYP-D3/aVTZ level of theory. The obtained structures are shown in Figure 5.1, along with their relative energies and spectroscopic constants (shown in Table 5.1). The chair conformer of the keto tautomer hydrate is found to be far more stable than the other seven cyclohexanone-water isomers. The keto form is 45–55 kJ mol⁻¹ lower in energy than the enol form, which means that the keto form will have the highest abundance.

Table 5.1. Calculated spectroscopic constants and relative energies of five tautomeric/conformational species of the cyclohexanone monomer and its eight most relevant monohydrates at the B3LYP-D3/aVTZ level of theory.

^b monomer	<i>keto</i> chair	<i>keto</i> boat	<i>keto</i> skew	Cis-Enol	Trans-Enol
<i>A</i> /MHz	4220.5	4465.9	4126.6	4581.7	4579.6
<i>B</i> /MHz	2503.7	2391.4	2506.3	2348.1	2343.5
<i>C</i> /MHz	1754.9	1728.8	1795.2	1655.5	1653.5
$ \mu_a /D$	3.3	3.4	3.2	0.6	0.8
$ \mu_b /D$	0.0	0.0	0.2	0.7	1.8
$ \mu_c /D$	1.0	0.0	1.0	0.0	0.0
^a $\Delta E/kJ mol^{-1}$	0	14.0	15.8	40.9	46.0

Table 5.1. (continued)

^b Complex	<i>keto chair</i> H ₂ O	<i>keto boat</i> H ₂ O	<i>keto skew</i> H ₂ O I	<i>keto skew</i> H ₂ O II
<i>A</i> /MHz	3334.1	3534.1	3187.1	3333.7
<i>B</i> /MHz	1141.1	1098.0	1153.5	1150.0
<i>C</i> /MHz	916.3	889.0	946.5	925.4
$ \mu_a /D$	3.4	3.4	3.3	3.4
$ \mu_b /D$	0.2	0.2	0.1	0.2
$ \mu_c /D$	0.4	0.4	0.4	0.4
^a $\Delta E/kJ mol^{-1}$	0	13.6	15.0	15.2
^b Complex	<i>cis-enol</i> H ₂ O I	<i>cis-enol</i> H ₂ O II	<i>trans-enol</i> H ₂ O I	<i>trans-enol</i> H ₂ O II
<i>A</i> /MHz	3197.1	3693.8	3636.4	3728.8
<i>B</i> /MHz	1064.8	1001.6	998.1	1012.6
<i>C</i> /MHz	904.7	816.8	811.3	825.8
$ \mu_a /D$	1.5	2.8	3.1	3.0
$ \mu_b /D$	1.0	0.6	2.2	1.6
$ \mu_c /D$	1.5	0.1	1.3	0.2
^a $\Delta E/kJ mol^{-1}$	48.2	45.1	53.1	49.7

^a Harmonic zero-point vibrational energy corrections included.

^b Cartesian coordinates for all the predicted structures are listed in Tables S5.1-S5.13 of the Appendix III.

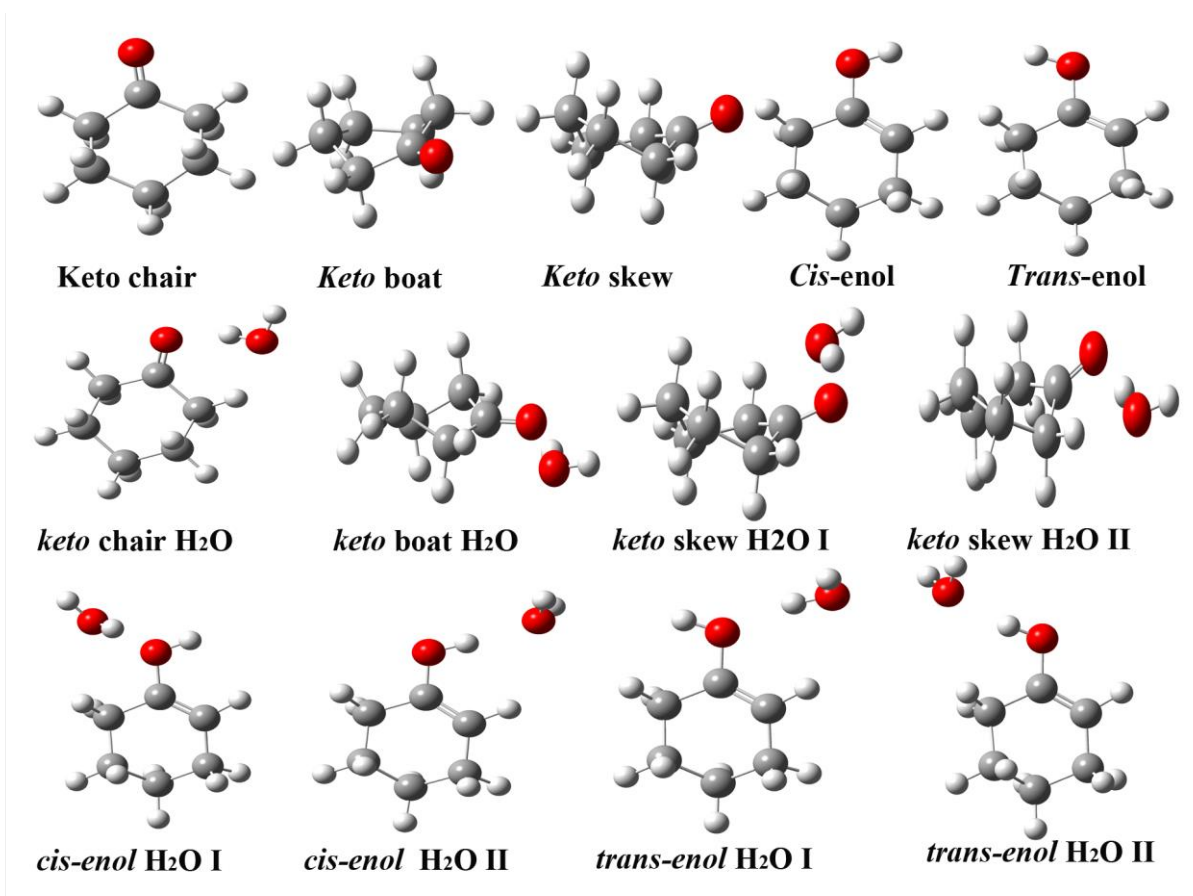


Figure 5.1. B3LYP-D3/aVTZ calculated structures of five tautomeric/conformational species of the cyclohexanone monomer and its eight most relevant monohydrates.

5.3.2 Spectroscopic Assignments of the Cyclohexanone-Water Complex

Initially, I decided to focus on the most stable conformer, the chair conformer of the keto tautomer of cyclohexanone-water. The rotational constants and dipole moment components in Table 5.2 were used to predict rotational transition frequencies and line strengths. In all cases, a dominant μ_a dipole component of 3 D is predicted and several μ_a -type transitions were identified readily in the experimental spectra.

Table 5.2. Calculated rotational constants and dipole moment components of cyclohexanone-water using DFT and MP2 methods with the 6-311++G (2d, p) basis set; the aug-cc-pVTZ basis set was employed for the B3LYP/D3 method.

	MP2	B3LYP	B3LYP/D3
A/MHz	3122.3	3375.9	3334.1
B/MHz	1202.1	1102.3	1141.1
C/MHz	963.4	889.5	916.3
$ \mu_a /\text{D}$	3.2	3.5	3.4
$ \mu_b /\text{D}$	0.0	0.3	0.2
$ \mu_c /\text{D}$	0.7	0.3	0.4

After an initial spectroscopic fitting, additional weaker μ_c -type transitions were identified. In the initial search scan performed with a chirped-pulse FTMW spectrometer, only the parent species was detected. All isotopically substituted species, including six ^{13}C mono-substituted and three deuterium substituted isotopologues (DOH, D_2O and HOD) were detected using our cavity FTMW spectrometer. The six ^{13}C mono-substituted species were observed in natural abundance. A listing of all measured transition frequencies can be found in Tables S5.14 and S5.15 in the Appendix III. Experimental rotational and centrifugal distortion constants were determined in a fitting procedure, and they are listed in Table 5.3 for the parent species (the Watson's A reduction is used in the fit).⁵² The spectroscopic constants for the minor isotopologues are listed in Table S5.16 in the Appendix III. The standard deviations of the fits are around 2 kHz, on the order of the measurement uncertainty.

The theoretical rotational constants from the B3LYP-D3/aVTZ calculations (Table 5.2) deviate by only $\sim 1\%$ from the experimental ones (Table 3). The other two theoretical methods result in larger differences; for example, the deviation between the experimental and theoretical rotational constants is $\sim 6\%$ in the MP2 and $\sim 2\%$ in the B3LYP calculations. The results indicate DFT method is a better method in accurately calculating the rotational constants, especially when adding empirical dispersion terms (D3).

Table 5.3. Experimental rotational and centrifugal distortion constants of the cyclohexanone-water complex.

Rotational constant	Parent species
A / MHz	3296.3801(50)
B / MHz	1123.55603(68)
C / MHz	905.93629(45)
Δ_K / kHz	24.5(10)
Δ_{JK} / kHz	-7.60(3)
Δ_J / kHz	1.0512(45)
δ_j / kHz	0.1695(42)
N	25
σ / kHz	2.7

5.3.3 Molecular Structure of the Cyclohexanone-Water Complex

With the large isotopic data set available for the chair conformer of the keto form of cyclohexanone-water, an experimental structure determination is possible. Through a least-squares fitting method, all heavy-atom structural parameters of the cyclohexanone ring can be determined, as well as the hydrogen bonding orientation of the water molecule. To reduce the number of independent structural parameters, it is assumed that there is an inversion plane in the cyclohexanone ring. In addition, all aliphatic hydrogens were fixed to their ab initio positions, and the water molecule was constrained to its ab initio geometry.

In order to model the structure as carefully as possible, Watson's $r_m^{(1)}$ scheme was used, where the experimental ground state moments of inertia were fitted with three additional, axis-dependent terms, which are proportional to the square root of the corresponding components of the moment of inertia tensor, $\mathbf{I}^{1/2}$. These terms correct for vibrational contributions to a rigid molecular frame across the structure that a standard rigid, r_0 , fit ignores or treats as a constant,

averaged quantity in a traditional determination with Kraitchman's equations.⁵³ These three correction terms (c_{aa} , c_{bb} , and c_{cc}), one for each inertial axis, are listed in Table 5.4.

Table 5.4. Predicted and experimental structural parameters for the cyclohexanone ring as determined using the cyclohexanone-water microwave data from this study, with comparison to previous electron diffraction (ED) and FTMW data for the monomer.

	B3LYP-D3/aVTZ	$r_m^{(1)}$	FTMW + ED ²⁰
^aBond Lengths / Å			
C1-C2	1.511	1.496(18)	1.503(4)
C2-C3	1.538	1.565(21)	1.542(2)
C3-C4	1.528	1.522(20)	[1.545]
C=O	1.217	1.329(11)	1.229(3)
Bond Angles / °			
C1-C2-C3	111.3	110.16(155)	111.5(1)
C2-C3-C4	111.5	110.12(89)	110.8(2)
C3-C4-C5	111.1	110.97(103)	110.8(2)
C2-C1-C6	115.5	116.55(236)	115.3(3)
Dihedral Angles / °			
O-C1-C2-C3	128.8	127.9(21)	[128.3] [*]
C1-C2-C3-C4	52.2	53.6(17)	[51.7]
C2-C3-C4-C5	56.1	59.2(11)	[56.3]
$r_m^{(1)}$ Parameters/ $u^{1/2}$ Å			
c_{aa}	--	0.04(20)	--
c_{bb}	--	-0.71(54)	--
c_{cc}	--	-0.62(46)	--
δ_H [O..HOH]	--	0.0049(67)	--
δ_H [O..HOH]	--	-0.44(1)	--

^a Carbon labeling begins at the carbonyl carbon (C1) and runs clockwise. Parameters equivalent by symmetry are not listed.

* Parameters in brackets are derived.

Moreover, coordinates derived from deuterium substitution (such as those in water) can generate anomalies in the fitting of the molecular structure because of the large fractional change in the reduced mass of the associated vibrational modes, inducing observationally significant changes in the ground state geometry.⁵⁴ To correct for this, two additional Laurie-type corrections terms, δ_H , were fitted to compensate for the distortion of the hydrogen bonding geometry due to deuteration (cf. the Ubbelohde effect).⁵⁵ The fitted δ_H parameters are shown in the last two rows of Table 5.4. The C-C and C=O bond lengths and bond angles (including dihedral angles) of predicted and experimental structures for the cyclohexanone ring in the cyclohexanone-water complex are given in Table 5.4, together with the previous electron diffraction and FTMW data for the cyclohexanone monomer.²⁰ The Cartesian coordinates for the fitted experimental structure of the cyclohexanone-water complex are listed in Table S5.17 of Appendix III. Figure 5.2 displays the B3LYP-D3/aVTZ structure overlaying the $r_m^{(1)}$ experimental geometry.

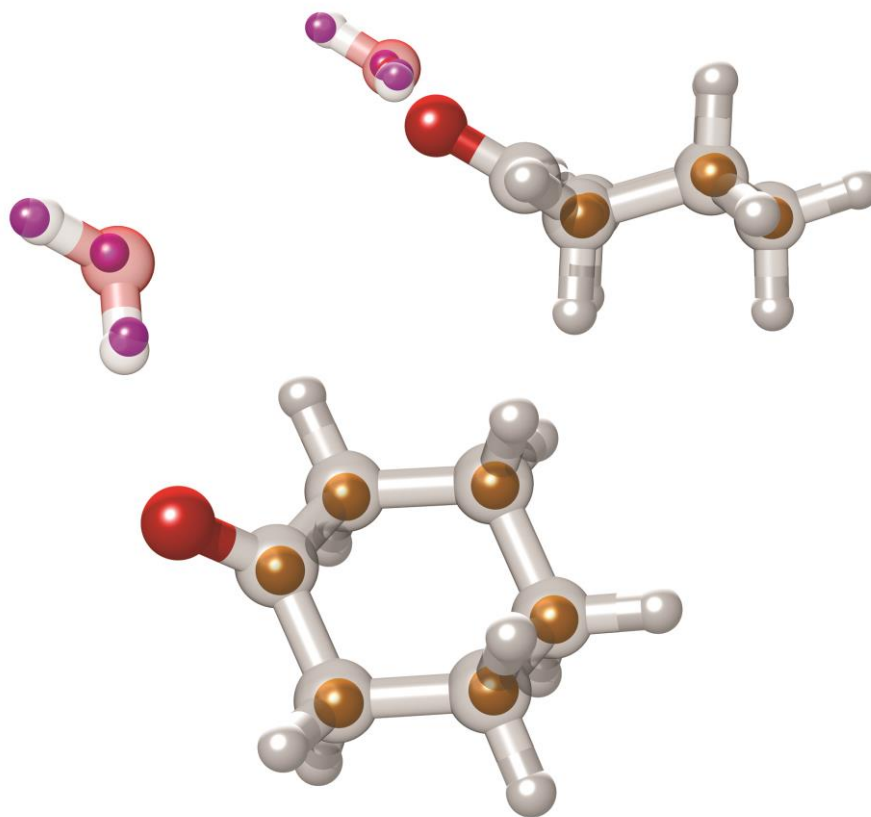


Figure 5.2. Side (top) and birds-eye (bottom) views of the B3LYP-D3/aVTZ structure (ball and stick model) overlaying the $r_m^{(1)}$ experimental geometry (colored spheres) of the *keto*-cyclohexanone-H₂O complex.

5.3.4 Intermolecular Interaction Analyses of Cyclohexanone-Water and Other Typical Ketone-Water Complexes

Bader's QTAIM^{43, 44} is a very powerful method for identifying and characterizing van der Waals and hydrogen bonding interactions in molecular complexes. Based on Bader's theory, the interaction between the atoms in a molecule can be identified by the BCPs, where the electron density gradient $\nabla\rho = 0$. To illustrate this in the context of cyclohexanone-water, we used the Multiwfn⁴⁵ program to identify the BCPs along the corresponding hydrogen bonding paths of five related ketone-water complexes using ab initio calculations at the B3LYP-D3/aVTZ level of theory. In Figure 5.3, the QTAIM results show that there is a bond path along the C=O \cdots H-OH hydrogen bond in each of the ketone-water complexes. Figure 5.3 also shows the isosurfaces of the reduced electron density gradient, $s = 0.5$ a.u., from NCI analyses⁵⁶ of the five ketone-water complexes.

Table 5.5. Relevant hydrogen bonding structural parameters for selected ketone-water complexes. Geometries used are the same as in Table 5.6. Values in square brackets are derived.

Ketone subunit	$r(\text{HOH}\cdots\text{O}=\text{C})$	$\angle(\text{HOH}\cdots\text{O}=\text{C})$	$r(\text{O}\cdots\text{H}-\text{C})$	Geometry used
Cyclohexanone	1.95(8)	169(4)	[2.64]	B3LYP-D3/aug-cc-pVTZ
Cyclopentanone	1.88	164.1	2.67	B3LYP-D3/aug-cc-pVTZ
Cyclobutanone ³²	1.95(2)	178(5)	[3.01]	r_0 geometry (C_s symmetric) ³²
Acetone	1.88	164.7	2.49	B3LYP /6-311++g(2d,p)
Formaldehyde ³⁰	2.012(29)	163.(9)	[2.68]	r_0 geometry (C_s symmetric) ³⁰

The relevant hydrogen bonding structural parameters for the selected ketone-water complexes are shown in Table 5.5, and the used geometries of these ketone-water complexes in this table are all close to their experimental structure. Secondary hydrogen bonds of the type (water) O \cdots H-C can be identified by their BCPs in Figure 5.2 for cyclohexanone-water (a),

cyclopentanone-water (b), and acetone-water (d) complexes, but are absent in the cyclobutanone-water (c) and formaldehyde-water (e) complexes.

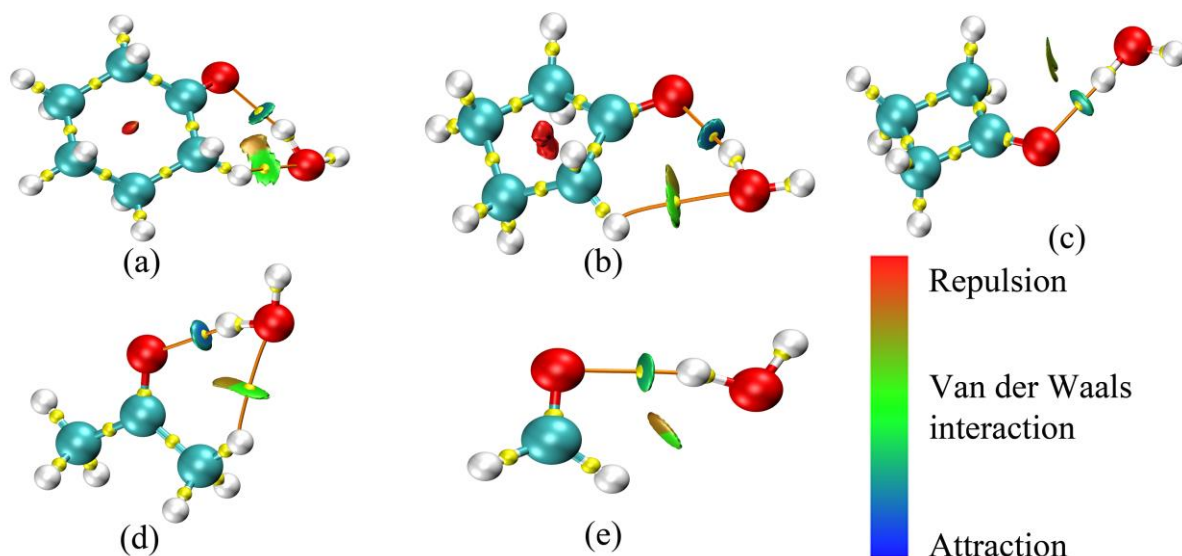


Figure 5.3. Results from QTAIM and NCI analyses for the five compared ketone-water complexes. The hydrogen bonding interactions are identified by the bond paths (orange splines) and corresponding bond critical points (yellow spheres). Also shown are the NCI isosurfaces at a fixed reduced density gradient, $s = 0.5$ a.u., colored by the values of $\text{sign}(\lambda_2)\rho$ [-0.04, 0.02] at each point in space, with colorations specified by the legend in the bottom right (red color denotes positive value, and blue color denotes negative value).

In the NCI plots in Figure 5.3, on the other hand, very weak secondary hydrogen-bonding interactions can be identified also in cyclobutanone-water and formaldehyde-water complexes. These qualitative differences in the secondary hydrogen-bonding interactions correlate with the corresponding hydrogen-bond lengths: the secondary bonding distances are about 3.01 Å in cyclobutanone-water and 2.68 Å in formaldehyde-water, significantly longer than in cyclohexanone-water (2.64 Å), cyclopentanone-water (2.67 Å), and acetone-water (2.49 Å). This implies that the secondary hydrogen bond in cyclohexanone is quite strong, and likely contributes to the stabilization of the keto \rightleftharpoons enol transition state (vide infra).

In addition, the binding energies of the five ketone-water isomers were calculated using symmetry adapted perturbation theory (SAPT),⁴⁷ including the BSSE correction. The results are listed in Table S5.18 of the Appendix III. As shown in Table 5.6, the binding energy in the

cyclohexanone-water complex is the largest among all five ketone-water complexes. Both SAPT and BSSE calculations suggest a slight increase in hydrogen-bond strength as a function of ring size, which is consistent with observations from vibrational and thermodynamic studies of cyclic oxygen-containing species, including ketones.⁵⁷⁻⁵⁹

Table 5.6. Results of SAPT(0)/jun-cc-pVDZ non-covalent interaction energy analyses for several ketone-water complexes.

Species	$\Delta E_{\text{elst/}}$ kJ mol ⁻¹	$\Delta E_{\text{exch/}}$ kJ mol ⁻¹	$\Delta E_{\text{ind/}}$ kJ mol ⁻¹	$\Delta E_{\text{disp/}}$ kJmol ⁻¹	$\Delta E_{\text{binding/}}$ kJ mol ⁻¹
Cyclohexanone	-50.6	45.2	-15.1	-10.9	-40.0
Cyclopentanone	-49.4	43.5	-14.6	-10.9	-31.4
Cyclobutanone	-38.5	31.4	-10.5	-8.8	-26.4
Acetone	-46.9	39.3	-13.0	-9.6	-30.1
Formaldehyde	-40.0	24.7	-7.9	-6.7	-21.3

5.3.5 Enol Form of Cyclohexanone-Water Complex

Previous studies have shown that intermolecular interactions can stabilize higher energy monomer conformers in molecular clusters. An example is the ternary 2, 2, 2-trifluoroethanol (TFE) cluster, which contains the unstable, *trans* conformer in its isolated form.²⁸ To see if a similar effect occurs with the enol form of cyclohexanone, we expended significant efforts to find evidence for its complex with water in the experimental spectra, but to no avail. Here, we describe our computational efforts to corroborate the experimental absence of the enol isomer. The enol form of cyclohexanone has been found to have an abundance ranging from 4.1×10^{-7} to 0.02% in the aqueous phase.²⁴⁻²⁷ Ignoring solution-dependent entropic changes, the calculated keto-enol energy difference of about 45 kJ mol⁻¹ implies a relative abundance of roughly 10^{-6} , which falls in line with the most recent experimental determinations. On the other hand, water can act both as a proton donor and as a proton acceptor, and a single water molecule may act as a bridge for proton relay in the keto-enol equilibrium when complexed with cyclohexanone. In fact, a recent study has shown that water can act as a proton donor to

the equatorial cyclohexanol ring in the cyclohexanol-water complex.⁶⁰ This may have significant effects on the kinetics of enol reactions.

To explore this further, we calculated the energies along the keto-enol tautomerism reaction pathway of the cyclohexanone monomer and the water assisted keto-enol tautomerism pathway in the cyclohexanone-water complex (see Figure 5.4). Using the most stable keto form as an example, the calculations show that the stability of the keto form increases relative to the enol form when cyclohexanone is complexed with water, but that the barrier between the keto and enol forms decreases significantly from ~ 340 kJ mol⁻¹ to 160 kJ mol⁻¹ in the monohydrate. Applying the Arrhenius equation, this implies a rate constant increase of $\sim 10^{33}$ at room temperature between the monohydrate and monomer. As such, complexation with water would speed up the kinetics of the keto-enol tautomerism in cyclohexanone strongly.

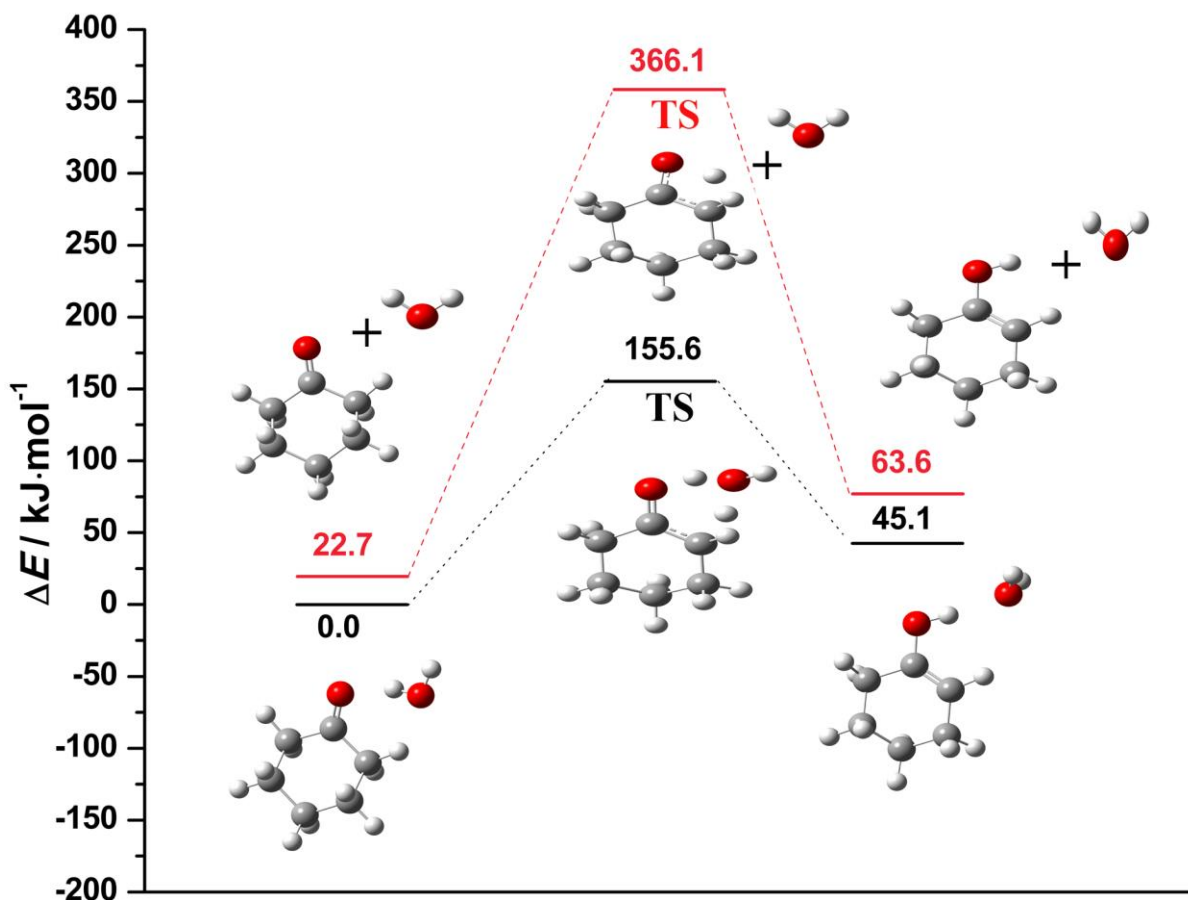


Figure 5.4. B3LYP-D3/aVTZ reaction coordinates of keto-enol tautomerization of the cyclohexanone monomer (red) and its most stable monohydrate (black).

To gain a better qualitative understanding of how hydrogen bonding between the ketone and water affects the kinetics of tautomerization, I have investigated how the total electron density of the cyclohexanone monomer changes upon complexation. As an example, Figure 5.5 shows the difference map of electron density between the cyclohexanone monomer and its monohydrate. The electron density increases in the carbonyl group region (especially the oxygen atom) upon complexation; correspondingly, the electron density decreases in the region of the donated proton in water, as would be expected in a canonical hydrogen bond. Interestingly, there is a decrease in electron density in the β hydrogen that forms the secondary (C)H \cdots OH₂ hydrogen bond. Unsurprisingly, these two electronic effects can explain the dramatic stabilization of the keto \rightleftharpoons enol transition state. In this conversion, keto-cyclohexanone must shuffle electron density in order to remove the β hydrogen and accept a proton from the water onto the carbonyl oxygen. Therefore, effective catalysis of this process would require a species to stabilize a more positive partial charge on the β hydrogen and a more negative partial charge on the carbonyl oxygen. Both conditions are satisfied by the two hydrogen bonding interactions with water.

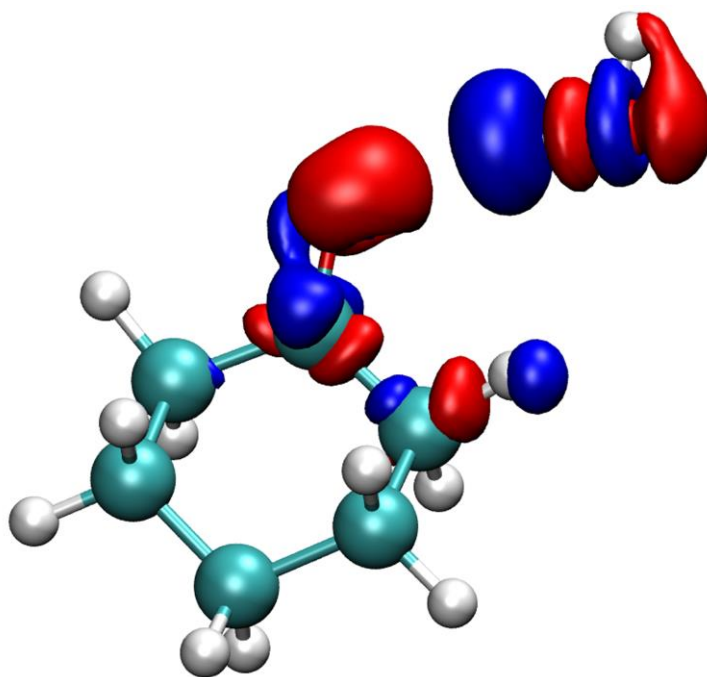


Figure 5.5. A difference map of electron density in the cyclohexanone-water complex after complexation. Blue regions specify relative depletion of electron density upon complexation, and red regions correspond to regions where electron density has increased.

I also performed theoretical calculations on keto-enol tautomerization of the cyclohexanone monomer in aqueous solution using the implicit polarizable continuum model (PCM) model and the combined implicit and explicit model with one water molecule added. The results also suggest that the water solvent provides no additional thermodynamic benefit to the enol form, regardless of whether the implicit model or combined implicit and explicit model is used. However, we found that application of implicit aqueous solvation using the PCM model leads to a reduction of the transition state energy from 343 kJ mol⁻¹ to 271 kJ mol⁻¹. With the addition of the single explicit water, the barrier does not change much upon application of PCM; the barrier is 163 kJ mol⁻¹ with PCM and 156 kJ mol⁻¹ without. This shows that even a single water molecule plays a significant role in lowering the barrier in keto-enol tautomerization in cyclohexanone, but that the bulk effects play a more diminished role.

In a future, more detailed, study, it may be pertinent to consider the effect of pH on the keto \rightleftharpoons enol equilibrium. Since experimental studies show that acidity plays a significant positive role on mass concentrations in SOAs,⁶¹ the atmospherically relevant equilibrium may not be between neutral keto and enol forms of cyclohexanone but rather the [keto-H]⁺ + ⁻OH \rightleftharpoons enol + H₂O equilibrium. Since the cyclohexanone pK_a has a low value of 16.7,⁶² concentrations of protonated ketones at atmospheric pH values are correspondingly low. However, the corrections to aerosol models by implementing enol-derived reactions are also consistent with low concentrations of these species.¹⁵⁻¹⁸ In addition, it may be interesting to consider stabilization of enol species in non-polar solvents, though some initial calculations using a PCM model for 1,4-dioxane suggest no significant change in the keto-enol relative stabilities.

With these observations in mind, it is not surprising that enols can play an important role in atmospheric contexts, especially for ketones with more stabilized enol forms than gas-phase cyclohexanone. Since H₂O is ubiquitous in atmospheric aerosols, hydration likely plays a significant role in oxidation reactions of ketones by providing a kinetic impetus for favorable reactivity for the enol species found in equilibrium.

5.4 Conclusions

Rotational spectra of the hydrogen-bonded complex between cyclohexanone and water were measured by FTMW spectroscopy and assigned with the aid of ab initio calculations. Cyclohexanone can undergo complicated keto-enol tautomeric and conformational changes,

but for the cyclohexanone-water complex only the chair conformer of the keto tautomer was observed. Theoretical results suggest that the relative abundances of seven other conformers and isomers of cyclohexanone-water are extremely low, and thus they are likely not detectable in our experiments. From the assigned rotational spectra of ten isotopologues of *keto*-cyclohexanone clustered with water, we have determined an experimental $r_m^{(1)}$ structure of cyclohexanone-water, which includes structural information about the hydrogen bonding.

Furthermore, we have investigated other typical ketone-water complexes systematically using QTAIM and symmetry adapted perturbation theory and find that electrostatic forces are dominant in all examples of ketone-water complexes, indicative of canonical hydrogen bonding. The QTAIM analyses suggest that the secondary hydrogen bonding effect is also a common characteristic in many of those ketone-water clusters, except for those where binding geometries prevent close contact between ketone C-H moieties and the water oxygen. Our results in this study improve our understanding of hydration on the kinetics of keto-enol tautomerism. However, the enol tautomer was not detected in this experiment, and the calculations also suggest that increasing the number of water molecules complexed with a keto species still may not improve the chances of observing the enol species in larger cyclohexanone-water clusters. The results show that a single water complexed with cyclohexanone mainly decreases the barrier of the keto-enol tautomerization compared with its monomer.

References

1. A. Metzger, B. Verheggen, J. Dommen, J. Duplissy, A. S. H. Prevot, E. Weingartner, I. Riipinen, M. Kulmala, D. V. Spracklen, K. S. Carslaw and U. Baltensperger, *Proc. Natl. Acad. Sci.*, 2010, **107**, 6646-6651.
2. R. Y. Zhang, *Science*, 2010, **328**, 1366-1367.
3. J. F. Hamilton, A. C. Lewis, J. C. Reynolds, L. J. Carpenter and A. Lubben, *Atmos. Chem. Phys.*, 2006, **6**, 4973-4984.
4. E. Grosjean, D. Grosjean, M. P. Fraser and G. R. Cass, *Environ. Sci. Technol.*, 1996, **30**, 2687-2703.
5. H. K. Wang, C. H. Huang, K. S. Chen and Y. P. Peng, *Aerosol Air Qual. Res.*, 2010, **10**, 559-570.
6. Y. L. Feng, S. Wen, Y. J. Chen, X. M. Wang, H. X. Lu, X. H. Bi, G. Y. Sheng and J. M. Fu, *Atmos. Environ.*, 2005, **39**, 1789-1800.
7. Y. L. Feng, S. Wen, X. M. Wang, G. Y. Sheng, Q. S. He, J. H. Tang and J. M. Fu, *Atmos. Environ.*, 2004, **38**, 103-112.
8. H. K. Wang, C. H. Huang, K. S. Chen, Y. P. Peng and C. H. Lai, *J. Hazard Mater.*, 2010, **179**, 1115-1121.
9. B. E. Olsson, M. Hallquist, E. Ljungström and J. Davidsson, *Int. J. Chem. Kinet.*, 1997, **29**, 195-201.
10. E. Martínez, A. Aranda, Y. Díaz-De-Mera, A. Rodríguez, D. Rodríguez and A. Notario, *J. Atmos. Chem.*, 2004, **48**, 283-299.
11. S. M. Aschmann and R. Atkinson, *Int. J. Chem. Kinet.*, 2013, **45**, 52-58.
12. S. M. Aschmann, J. Arey and R. Atkinson, *J. Phys. Chem. A*, 2011, **115**, 14452-14461.
13. D. Shemesh, S. A. Nizkorodov and R. B. Gerber, *J. Phys. Chem. A*, 2016, **120**, 7112-7120.
14. A. Chattopadhyay, K. Mondal, M. Samanta and T. Chakraborty, *Atmos. Environ.*, 2017, **157**, 125-134.
15. A. T. Archibald, M. R. McGillen, C. A. Taatjes, C. J. Percival and D. E. Shallcross, *Geophys. Res. Lett.*, 2007, **34**, L21801.
16. C. A. Taatjes, N. Hansen, A. McIlroy, J. A. Miller, J. P. Senosiain, S. J. Klippenstein, F. Qi, L. Sheng, Y. Zhang and T. A. Cool, *Science*, 2005, **308**, 1887-1889.
17. C. A. Taatjes, N. Hansen, J. A. Miller, T. A. Cool, J. Wang, P. R. Westmoreland, M. E. Law, T. Kasper and K. Kohse-Höinghaus, *J. Phys. Chem. A*, 2006, **110**, 3254-3260.
18. L. K. Huynh, H. R. Zhang, S. Zhang, E. Eddings, A. Sarofim, M. E. Law, P. R. Westmoreland and T. N. Truong, *J. Phys. Chem. A*, 2009, **113**, 3177-3185.
19. F. J. Devlin and P. J. Stephens, *J. Phys. Chem. A*, 1999, **103**, 527-538.
20. J. Dillen and H. J. Geise, *J. Mol. Struct.*, 1980, **69**, 137-144.
21. J. L. Alonso, *J. Mol. Struct.*, 1981, **73**, 63-69.
22. Y. Ohnishi and K. Kozima, *Bull. Chem. Soc. Jpn.*, 1968, **41**, 1323-1325.

23. R. Moradi, S. Jameh-Bozorghi, R. Kadivar, A. Mahdiani and H. Soleymanabadi, *APCBEE Procedia*, 2012, **3**, 70-74.
24. G. Schwarzenbach and C. Wittwer, *Helv. Chim. Acta*, 1947, **30**, 669.
25. R. Bell and P. Smith, *J. Chem. Soc. B*, 1966, 241-243.
26. J. E. Dubois, M. El-Alaoui and J. Toullec, *J. Am. Chem. Soc.*, 1981, **103**, 5393-5401.
27. A. J. Kresge, *Pure Appl. Chem.*, 1991, **63**, 213-221.
28. J. Thomas, N. A. Seifert, W. Jäger and Y. Xu, *Angew. Chem.*, 2017, **129**, 6386-6390.
29. N. A. Seifert, J. Thomas, W. Jäger and Y. Xu, *Phys. Chem. Chem. Phys.*, 2018, **20**, 27630-27637.
30. F. J. Lovas and C. Lugez, *J. Mol. Spectrosc.*, 1996, **179**, 320-323.
31. J. Gao, J. Thomas, Y. Xu and W. Jäger, Microwave spectra of the acetone-water complex, in preparation.
32. S. Melandri, A. Maris, B. M. Giuliano and W. Caminati, *J. Chem. Phys.*, 2005, **123**, 164304.
33. S. Ghosh, J. Thomas, W. Y. Huang, Y. J. Xu and W. Jäger, *J. Phys. Chem. Lett.*, 2015, **6**, 3126-3131.
34. G. B. Park and R. W. Field, *J. Chem. Phys.*, 2016, **144**, 200901-10.
35. E. G. Schnitzler, N. A. Seifert, S. Ghosh, J. Thomas, Y. J. Xu and W. Jäger, *Phys. Chem. Chem. Phys.*, 2017, **19**, 4440-4446.
36. E. G. Schnitzler, N. A. Seifert, I. Kusuma and W. Jäger, *J. Phys. Chem. A*, 2017, **121**, 8625-8631.
37. S. P. Dempster, O. Sukhorukov, Q. Y. Lei and W. Jäger, *J. Chem. Phys.*, 2012, **137**, 174303.
38. J. Thomas, J. Yiu, J. Rebling, W. Jäger and Y. Xu, *J. Phys. Chem. A*, 2013, **117**, 13249-13254.
39. Y. Xu, J. V. Wijngaarden and W. Jäger, *Int. Rev. Phys. Chem.*, 2005, **24**, 301-338.
40. Y. Xu and W. Jäger, *J. Chem. Phys.*, 1997, **106**, 7968-7980.
41. M. J. Frisch, G. W. Trucks, H. B. Schlegel, G. E. Scuseria, M. A. Robb, J. R. Cheeseman, G. Scalmani, V. Barone, B. Mennucci, G. A. Petersson, H. Nakatsuji, M. Caricato, X. Li, H. P. Hratchian, A. F. Izmaylov, J. Bloino, G. Zheng, J. L. Sonnenberg, M. Hada, M. Ehara, K. Toyota, R. Fukuda, J. Hasegawa, M. Ishida, T. Nakajima, Y. Honda, O. Kitao, H. Nakai, T. Vreven, J. A. Montgomery, Jr., J. E. Peralta, F. Ogliaro, M. Bearpark, J. J. Heyd, E. Brothers, K. N. Kudin, V. N. Staroverov, T. Keith, R. Kobayashi, J. Normand, K. Raghavachari, A. Rendell, J. C. Burant, S. S. Iyengar, J. Tomasi, M. Cossi, N. Rega, J. M. Millam, M. Klene, J. E. Knox, J. B. Cross, V. Bakken, C. Adamo, J. Jaramillo, R. Gomperts, R. E. Stratmann, O. Yazyev, A. J. Austin, R. Cammi, C. Pomelli, J. W. Ochterski, R. L. Martin, K. Morokuma, V. G. Zakrzewski, G. A. Voth, P. Salvador, J. J. Dannenberg, S. Dapprich, A. D. Daniels, O. Farkas, J. B. Foresman, J. V. Ortiz, J. Cioslowski, and D. J. Fox, *Gaussian 09, Revision D.01*, Gaussian, Inc., Wallingford CT, 2013.
42. L. Goerigk and S. Grimme, *J. Chem. Theory Comput.*, 2010, **7**, 291-309.
43. K. E. Laidig and R. F. Bader, *J. Chem. Phys.*, 1990, **93**, 7213-7224.
44. R. F. Bader, *Chem. Rev.*, 1991, **91**, 893-928.
45. T. Lu and F. Chen, *J. Comput. Chem.*, 2012, **33**, 580-592.

46. T. M. Parker, L. A. Burns, R. M. Parrish, A. G. Ryno and C. D. Sherrill, *J. Chem. Phys.*, 2014, **140**, 094106.
47. J. Turney, A. Simmonett, R. Parrish, E. Hohenstein, F. Evangelista, J. Fermann, B. Mintz, L. Burns, J. Wilke and M. Abrams, *Rev.: Comput. Mol. Sci.*, 2012, **2**, 556-565.
48. C. M. Western, *J. Quant. Spectrosc. Radiat. Transf.* 2017, **186**, 221-242.
49. Q. Gou, L. Spada, M. Vallejo-López, Z. Kisiel and W. Caminati, *Chem. Asian J.*, 2014, **9**, 1032-1038.
50. R. C. Dunbar, *J. Chem. Educ.*, 1982, **59**, 22-23.
51. G. D. Peckham and I. J. Mcnaught, *J. Chem. Educ.*, 1992, **69**, 554-558.
52. J. K. G. Watson, in *Vibrational Spectra and Structure*, ed. J. R. Durig, Elsevier, Amsterdam, 1977, vol. 6, pp. 1-89.
53. J. Kraitichman, *Am. J. Phys.*, 1953, **21**, 17-24.
54. J. K. Watson, A. Roytburg and W. Ulrich, *J. Mol. Spectrosc.*, 1999, **196**, 102-119.
55. Q. Gou, G. Feng, L. Evangelisti, D. Loru, J. L. Alonso, J. C. López and W. Caminati, *J. Phys. Chem. A*, 2013, **117**, 13531-13534.
56. E. R. Johnson, S. Keinan, P. Mori-Sanchez, J. Contreras-Garcia, A. J. Cohen and W. Yang, *J. Am. Chem. Soc.*, 2010, **132**, 6498-6506.
57. A. S. Murthy and C. Rao, *Appl. Spectrosc. Rev.*, 1968, **2**, 69-191.
58. M. Tamres and S. Searles Jr., *J. Am. Chem. Soc.*, 1959, **81**, 2100-2104.
59. E. J. Corey, *J. Am. Chem. Soc.*, 1953, **75**, 2301-2304.
60. M. Juanes, W. Li, L. Spada, L. Evangelisti, A. Lesarri and W. Caminati, *Phys. Chem. Chem. Phys.*, 2019, **21**, 3676-3682.
61. J. D. Surratt, M. Lewandowski, J. H. Offenberg, M. Jaoui, T. E. Kleindienst, E. O. Edney and J. H. Seinfeld, *Environ. Sci. Technol.*, 2007, **41**, 5363-5369.
62. E. P. Serjeant, B. Dempsey, *Ionisation constants of organic acids in aqueous solution; in IUPAC Chemical Data Series, No. 23*. Pergamon Press: Oxford, NY, 1979.

Chapter 6

Keto-Enol Tautomeric and Internal Rotation Dynamics Study of the Acetylacetone-Water Complex Investigated by Microwave Spectroscopy and Ab Initio Calculations

6. 1 Introduction

The acetylacetone monomer is a prototype molecule to study the process of keto-enol tautomerization, and many experimental¹⁻⁵ and theoretical studies⁶⁻⁸ on acetylacetone have been reported. Nevertheless, many questions regarding the detailed properties of its keto and enol tautomers remain. Firstly, the exact ratio of enol to keto tautomer is unclear. All the studies show that the enol tautomer is the more stable structure. NMR studies show that it is in the enol form 81% in the pure liquid¹ and 17% in aqueous solution.² Irving, R. J. et al. have derived the enol content to be 81.4% in the liquid phase and 93.3% in the gas phase, based on the experimental enthalpy of vaporization at 25 °C.³ A recent gas-phase electron diffraction (ED) study shows that the enol tautomer content is 100(3)% at 300(5) K and 64(5)% at 671(7) K.⁴ In a xenon matrix FT-IR study at 10 K, the abundance of the diketo form was derived to be ~10%.⁵ In a para-hydrogen matrix IR study, the diketo tautomer content was found to be 4.5%⁹ whereas the value is 1–1.5% in the neon matrix.¹⁰ In addition, the structure of the most stable enol tautomer is under controversy. Many techniques, including gas-phase vibrational spectroscopy,¹¹ gas-phase ED,^{4, 12} liquid-phase NMR,¹³ X-ray crystallography,¹⁴ and neutron crystallography¹⁵ all support a C_s symmetric structure, whether it is in the gas, liquid, or solid state. A recent microwave study, on the other hand, revealed that the enol tautomer has C_{2v} symmetry and that the two methyl groups are equivalent.¹⁶ However, the microwave work could not determine the low internal rotation barrier of the methyl internal rotation of the enol tautomer, and the diketo tautomer of acetylacetone could not be detected.

My previous study of water hydrogen bonded to acetone described in Chapter 4 indicates that water effectively lowers the height of the interconversion barrier of keto-enol tautomerization and stabilizes the less stable enol form of acetone. Similarly, when water is involved in acetylacetone, theoretical calculations showed that the interconversion barrier of

keto-enol tautomerization is lowered for the acetylacetone, and the thermal stability of the diketo tautomer increased when water is involved,⁷ indicating the abundance of the diketo tautomer would increase, then it would be possible to detect the diketo tautomer of acetylacetone. Moreover, the C_{2v} symmetry of the acetylacetone monomer will be broken when water complexes with acetylacetone, and the two methyl groups will become inequivalent so that each rotational transition will potentially split into a quintet (five components). This would make the rotational spectra complicated and interesting. If I could determine the internal rotation barrier of the water complex, it may help us to infer the internal rotation barrier in the monomer of the enol tautomer. Therefore, studying the hydrogen bonded acetylacetone-water complex is essential. Microwave spectroscopy is a powerful method to study hydrogen bonded clusters,¹⁷⁻²² and it can be used to determine the structure of a cluster precisely. The first goal is to use microwave spectra to identify the enol tautomer of the monohydrated acetylacetone-water complex and determine the internal rotation barrier of the methyl internal rotations. Next, I will try to capture the diketo tautomer of acetylacetone in hydrated clusters.

The microwave spectroscopic study of the acetylacetone-water complex was undertaken with the aid of high-level theoretical calculations. The keto-enol tautomers and conformational isomers of the acetylacetone monomer and water complexes are investigated first by ab initio calculations. After the spectra of the enol tautomer acetylacetone-water complex were measured and assigned, the properties of the structure and the hydrogen bonds were analyzed by noncovalent interaction (NCI) analyses qualitatively and by quantum theory of atoms in molecules (QTAIM) analyses quantitatively. The internal rotation dynamics of the methyl groups in the enol tautomer acetylacetone-water complex also is discussed in the present work. Last, I also tried to capture the diketo tautomer form of both the acetylacetone monomer and its monohydrate in the experiment.

6.2 Experimental and Computational Details

The microwave spectra of the acetylacetone-water complex were recorded initially using a broadband chirped pulse FTMW spectrometer; the design has been reported previously,^{23, 24} and its frequency uncertainty is ~25 kHz. All final frequencies were measured with a cavity based FTMW spectrometer in the region of 6–15 GHz, which has been described elsewhere in

detail^{25, 26}; its frequency uncertainty is ~2 kHz. The sample mixtures consisted of about 0.1% acetylacetone (97% purity, Fisher Scientific) and 0.2% water in helium or neon for the broadband and cavity instruments, respectively, at backing pressures of 2–5 atm.

To help assign the spectra of the acetylacetone-water complex, several ab initio calculations were performed using the Gaussian 09 package.²⁷ Second order Møller Plesset perturbation (MP2) theory, density functional theory (DFT) with B3LYP,²⁸ and M06-2X functionals²⁹ with the 6-311++G (2d, p) basis set³⁰ were implemented to obtain structural parameters, rotational constants, and dipole moment components, for initial spectroscopic searches. The calculation of vibrational frequencies was used to make sure that the optimized structure is a minimum-energy conformation by the absence of imaginary harmonic frequencies.

Transition frequencies were predicted from the calculated rotational constants using the PGOPHER program.³¹ Then, the measured transition frequencies were used to do a fit in the same program. Finally, the XIAM program was used to predict internal rotation splittings of transitions and fit the internal rotation splitting parameters.³²

6.3 Results and Discussion

6.3.1 Ab Initio Calculations of Keto-Enol Tautomeric and Conformational Changes of the Acetylacetone Monomer and the Monohydrated Complex

To predict rotational transition frequencies for the complex, I first calculated possible structures of the acetylacetone monomer. At the level of MP2/6-311++G (2d, p) theory, I found four tautomeric/conformational species of the acetylacetone monomer (two keto tautomers and two enol tautomers), as shown in Table 6.1, along with their corresponding relative stability, rotational constants, and dipole moment components. In a microwave experiment, the enol tautomer was found to have C_{2v} symmetry,¹⁶ even though it is calculated to be 0.25 kJ/mol higher energy than the C_s enol form. The energies of the two keto tautomers (one has C_2 symmetry, the other has C_s symmetry) are 10–28 kJ/mol higher. Assuming a Boltzmann distribution^{33, 34} at room temperature, the relative abundances of the higher energy species (i.e., the keto tautomers) are calculated to be in the range of 0.12%–1.54%. This infers that at even lower temperatures, the detection of the low abundance keto forms requires highly sensitive experimental techniques.

Table 6.1. Calculated rotational constants, dipole moment components, and relative energies of four tautomeric/conformational species of the acetylacetone monomer at the MP2/6-311++G(2d, p) level of theory.

monomer	Enol 1 (C_s)	Enol 2 (C_{2v})	Keto 1 (C_2)	Keto 2 (C_s)
A/MHz	5877.3	6032.2	4088.4	5250.4
B/MHz	1712.6	1750.8	1992.0	1655.2
C/MHz	1348.3	1380.1	1563.9	1288.0
$ \mu_a /\text{D}$	0.5	0.00	0.0	2.9
$ \mu_b /\text{D}$	3.7	0.00	0.0	1.1
$ \mu_c /\text{D}$	0.0	3.7	1.8	0.0
$V_3^{\text{CH}_3}/\text{kJ}\cdot\text{mol}^{-1}$	1.1/5.6 ^b	2.1	4.9	2.8/2.5 ^b
^a $\Delta E/\text{kJ}\cdot\text{mol}^{-1}$	0	0.3	10.3	27.9

^a Zero-point vibrational energy included.

^b The left methyl rotation barrier/the right methyl rotation barrier.

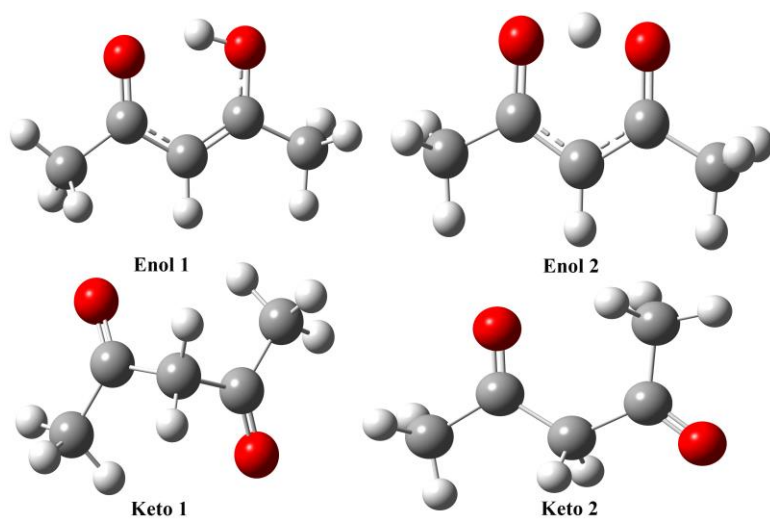


Figure 6.1. Structures of four tautomeric/conformational species of the acetylacetone monomer calculated at the MP2/6-311++G(2d, p) level of theory.

Table 6.2. Calculated rotational constants, dipole moment components, and relative energies of five acetylacetone monohydrates at the MP2/6-311++G(2d, p) level of theory.

Complex	Enol 1-H ₂ O	Enol 1-H ₂ O	Keto 1-H ₂ O	Keto 1-H ₂ O	Keto 2-H ₂ O
	I	II	I	II	I
<i>A</i> /MHz	4130.9	3958.2	1874.3	1908.4	2167.8
<i>B</i> /MHz	885.4	899.7	1689.1	1590.8	1565.4
<i>C</i> /MHz	736.0	760.5	973.1	1256.0	1079.4
$ \mu_a /D$	3.4	1.9	0.1	0.4	1.2
$ \mu_b /D$	1.9	2.0	0.8	5.2	0.6
$ \mu_c /D$	0.6	0.4	1.7	0.1	0.6
^a $V_3^{\text{CH}_3}/\text{kJ}\cdot\text{mol}^{-1}$	0.1		4.8		4.5
^b $V_3^{\text{CH}_3}/\text{kJ}\cdot\text{mol}^{-1}$	5.2		4.9		5.6
^c $\Delta E/\text{kJ}\cdot\text{mol}^{-1}$	0	3.7	6.5	17.7	4.8

^a Internal rotation barrier for the methyl group near the water.

^b Internal rotation barrier for the methyl group far from the water.

^c Zero-point vibrational energy included.

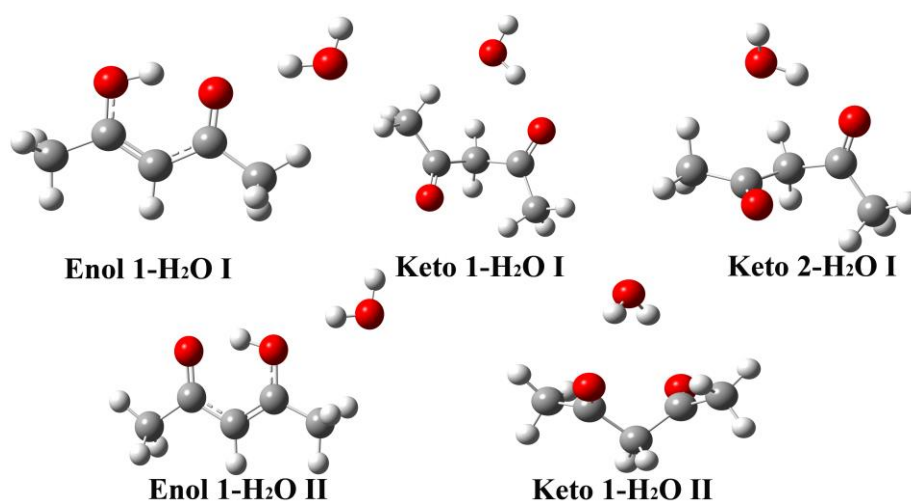


Figure 6.2. Structures of five acetylacetone monohydrates calculated at the MP2/6-311++G(2d, p) level of theory.

In the isolated environment of a molecular expansion, one way to regulate the abundance of the diketo forms or increase the reaction rate of the keto-enol tautomerism is by intermolecular interactions. Water can act both as a proton donor and as a proton acceptor and can act as a bridge for the proton transfer in acetylacetone, perhaps allowing the acetylacetone subunit easier access to the diketo tautomers. It was shown in a previous theoretical study of the acetylacetone monomer and its monohydrate that monohydrating will increase the thermal stability of the diketo form over the enol form, but that monohydrating also lowers the barrier between enol and keto form from 260–264 kJ/mol to 130–146 kJ/mol.⁷ According to the Arrhenius equation used to determine the rate of chemical reactions based on activation energy, I calculated that the ratio of the rate constant between the monohydrated complex and the monomer to be $\sim 10^{23}$. Monohydrating will therefore favor the kinetics of the keto-enol tautomerism.

Next, I calculated the effect of monohydrating on the stability of all the isomers of the acetylacetone monomer. Acetylacetone has four tautomeric/conformational species, given in Figure 6.1. When considering intermolecular interaction sites, I obtain two enol tautomer-water complexes (the C_s enol tautomer monomer with two different sites of water binding) and three diketo tautomer-water complexes at the MP2/6-311++G(2d, p) level of theory. The structures are shown in Figure 6.2, and their corresponding rotational constants, dipole moment components, and their relative energies are shown in Figure 6.2. The enol tautomer 1-water I complex is found to be far more stable than the other four acetylacetone-water conformational isomers. Based on these calculated relative energies, the diketo form is 4–18 kJ/mol higher in energy than the enol form, which means that the enol form will still have the highest abundance. Among the three diketo forms of the water complexes, only one isomer has an energy higher than 10 kJ/mol (Keto 1-H₂O II), and its relative abundance is 0.07%, while the other two isomers have energy less than 10 kJ/mol, and their relative abundances are 6.9% and 12.5%. This is higher than the abundances in the monomer (0.12%–1.54%), implying the monohydrating favors the diketo forms thermodynamically. There should therefore be a possibility for me to detect the diketo tautomer experimentally.

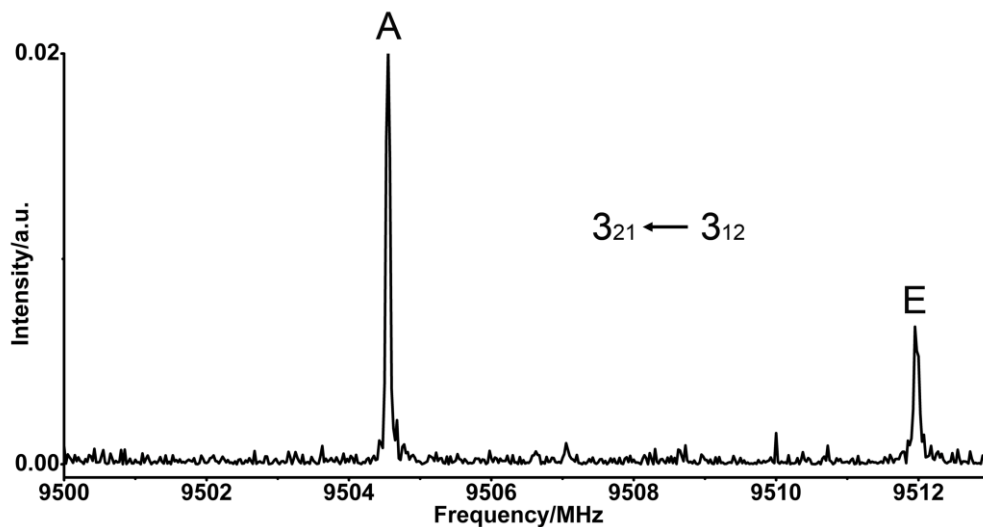


Figure 6.3. Spectrum of the $3_{21} \leftarrow 2_{12}$ rotational transition of acetylaceton-water measured with the chirped-pulse FTMW spectrometer.

6.3.2 Spectral Assignment of the Enol Tautomer Acetylaceton-Water Complex

To find the rotational transitions of the water complex, I relied on the known transitions of the acetylaceton monomer¹⁶ and the water dimer signal.³⁵ I started the search for transitions for the most stable enol tautomer of the acetylaceton-water complex using the rotational constants and dipole moments from the MP2 calculations, shown in Table 6.1. It is predicted that the μ_a dipole moment is much larger than others, therefore, I first did search scans for the stronger *a*-type transitions. I could assign 64 *a*-type transitions and observe that each transition is split into two components. As an example, the rotational spectrum of the $3_{21} \leftarrow 3_{12}$ transition is shown in Figure 6.3. Later, I could also measure eleven weaker *b*-type transitions. All the transition frequencies are listed in Table S6.1 in the Appendix IV. Because two fine structure components, rather than four or five, are observed in each transition, I treat the system as a one rotor system, in which the methyl rotor hydrogen bonded with water rotates almost freely, whereas the other methyl rotor has a moderate barrier. I will discuss the internal rotation dynamics of the acetylaceton-water complex in Section 6.3.4 in detail. The A species were fitted using the PGOPHER program, then both fine structure components were fitted using the XIAM program, and the results from the fit, including internal rotation parameters, are shown in Table 6.3.

Table 6.3. Experimental spectroscopic parameters for the acetylacetone-water complex.

Parameter	acetylacetone-water
A/MHz	4119.9929(43)
B/MHz	885.8760(8)
C/MHz	734.1100(6)
Δ_J/kHz	0.1100(39)
Δ_{JK}/kHz	1.099(29)
Δ_K/kHz	21.17(82)
δ_j/kHz	0.020(2)
δ_k/kHz	0.91(23)
$V_3/\text{kJ/mol}$	4.980(4)
^a ε/rad	0.0179
^b δ/rad	-0.089(44)
^c F_0/GHz	159.18
N	75
σ/kHz	6.0

^a ε is fixed, and it is the angle between the projection of the internal rotation axis onto the bc-plane and the b-principal inertial axis of the complex;

^b δ is the angle between internal rotation axis and a-axis of the complex.

^c F_0 is fixed, and it is the rotational constant of the methyl top ($F_0 = 505.379/I_a$ (in GHz); where I_a is the moment of inertia of the methyl top).

6.3.3 Structure and Hydrogen Bonding

Table 6.4 lists the bond lengths, bond angles, and complexation energies of the acetylacetone-water complex calculated MP2/6-311++G(2d, p) level of theory. Comparing the experimental and calculated rotational constants of the acetylacetone-water complex in Tables 6.1 and 6.2, it is found that the structure calculated using the MP2 method is very close to the experimental structure since the average deviation between the experimental and calculated rotational constants is only ~0.2%. In the structure shown in Figure 6.4, the distance between the carbonyl oxygen atom (O6) and the hydrogen atom (H18) in the water molecule is 1.93 Å (Table 6.4), which is shorter than that in the formaldehyde-water (2.01 Å),¹⁷ cyclobutanone-

water (1.95 Å)³⁶ and cyclohexanone-water (1.95 Å) complexes (Chapter 5), and longer than that in the acetone-water complex (1.88 Å) (Chapter 4).

Table 6.4. Calculated bond lengths, bond angles, and complexation energies of acetylacetonone-water complex using the MP2 method with the 6-311 ++ G (2d, p) basis set.

Acetylacetonone-water	MP2
$r(\text{C11}=\text{O12})/\text{Å}$	1.33
$r(\text{C12}-\text{H13})/\text{Å}$	1.00
$r(\text{O6}\cdots\text{H13})/\text{Å}$	1.62
$r(\text{C5}=\text{O6})/\text{Å}$	1.26
$r(\text{C5}=\text{O6}\cdots\text{H}-\text{O}(\text{w}))/\text{Å}$	1.93
$r(\text{C1}-\text{H4}\cdots\text{O}-\text{H}(\text{w}))/\text{Å}$	2.49
$\angle\text{C5}=\text{O6}\cdots\text{H18}(\text{w})/^\circ$	117.4
$\angle\text{O16}-\text{H18}\cdots\text{O6}(\text{C})/^\circ$	163.6
$\angle\text{O16}\cdots\text{H4}-\text{C}/^\circ$	137.4
$\angle\text{O11}-\text{H13}\cdots\text{O}=\text{C}/^\circ$	-3.58
^a $\Delta E_{\text{HB}}/\text{kcal mol}^{-1}$	2.4
^b $\Delta E/\text{kcal mol}^{-1}$	5.6

^a The regular intermolecular hydrogen bond energy for C=O...H(water) in the acetylacetonone-water complex, calculated by QTAIM analysis.

^b Basis set superposition error (BSSE) corrected complexation energy.

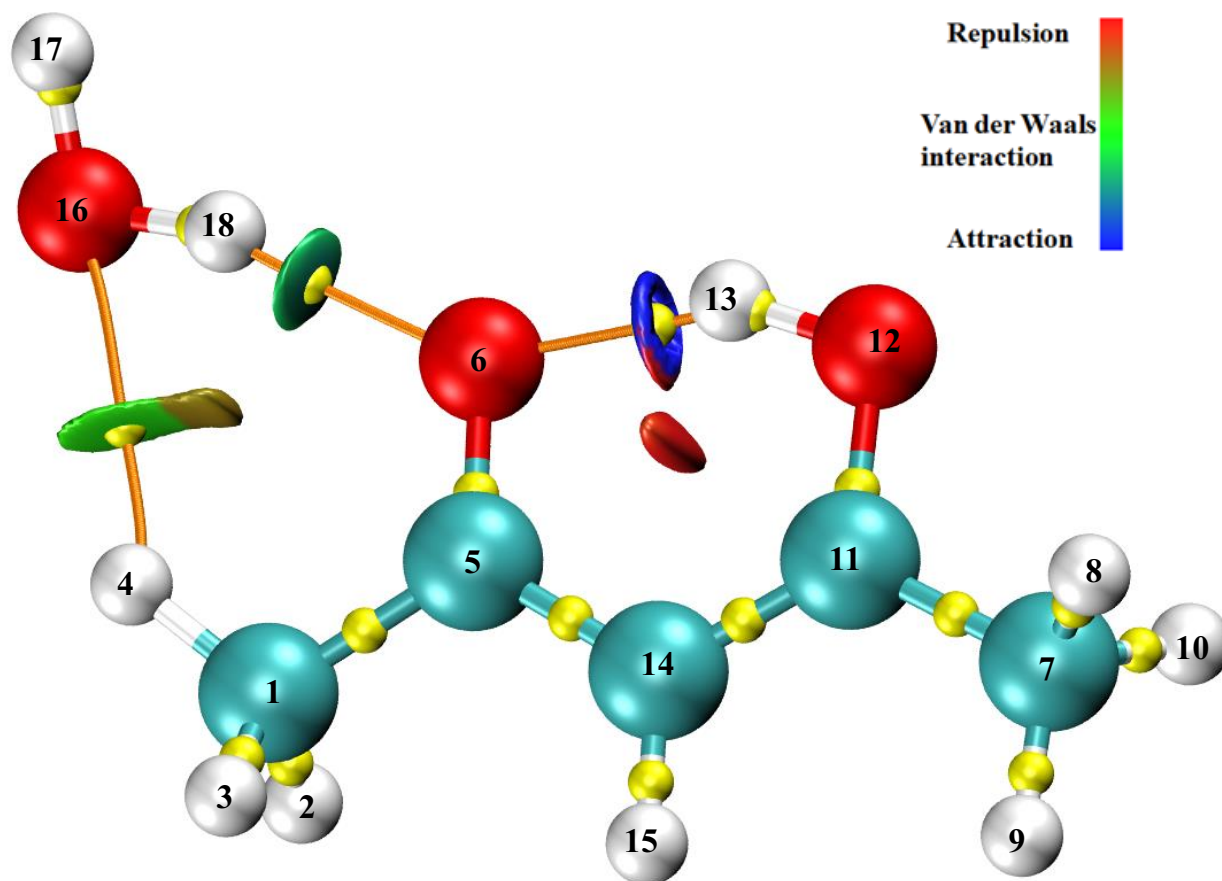


Figure 6.4. A plot resulting from a NCI analysis, including BCPs and the corresponding bond paths of the enol acetylacetonate-water complex. The orange lines are the bond paths for the weak bonds, and the yellow balls correspond to BCPs.

In all these ketone-water complexes, the $\text{C}=\text{O}\cdots\text{H}(\text{water})$ angles are smaller than 120° , which can be expected for an sp^2 lone pair.³⁶ All, acetone-water, formaldehyde-water, and acetylacetonate-water complexes form nonlinear hydrogen bonds. The $(\text{water})\text{O}16\text{-H}18\cdots\text{O}6(\text{C}5)$ angles in the structures of the acetone-water, formaldehyde-water, cyclohexanone-water, and acetylacetonate-water complexes are 165.3° , $163.(9)^\circ$, 165.7° , and 163.6° , respectively, while it is almost linear (178°) in the cyclobutanone-water complex. Moreover, it is found that a secondary hydrogen bond is formed in the acetone-water, formaldehyde-water, cyclohexanone-water, and acetylacetonate-water complexes, as indicated by the distances between the water oxygen atom and the H atom(C-H) of 2.56 \AA , 2.68 \AA , 2.64 \AA , and 2.49 \AA , respectively. However, such an interaction could not be seen in the cyclobutanone-water

complex, where the corresponding distance is 3.01 Å; typically, a secondary hydrogen bonding interaction needs a distance of 2.5–2.7 Å³⁶. As opposed to those four ketone-water complexes, acetylacetone has two C=O groups. When it forms a complex with water, both intramolecular and intermolecular hydrogen bondings can occur. To visualize them, I have used the NCI analysis.³⁷ Shown in Figure 6.4 is an NCI isosurface for the acetylacetone-water complex with reduced density gradient $s = 0.5$ a.u. A bluer color indicates a strong hydrogen bond, such as an interaction between the carbonyl oxygen (O6) and the hydrogen atom (H13) in the enol form of the other carbonyl group. A somewhat weaker hydrogen bond is between the carbonyl oxygen atom (O6) and the hydrogen (H18) in water, and it had some blue color surrounded by green. The much weaker hydrogen bond is the secondary hydrogen bond between hydrogen atom (H4) in the methyl group and the oxygen atom (O18) in the water molecule, and the color is all green. To quantitatively analyze the strength of those three hydrogen bonds, I integrate the domains enclosed by the reduced density gradient (RDG) isosurfaces in the NCI plot.³⁸⁻⁴⁰ The average value of electron density per contact region of the intramolecular hydrogen bonding (O6···H13), the intermolecular hydrogen bonding (O6···H18), and the secondary intermolecular hydrogen bonding (O16···H4) is 0.04419 a.u./ Bohr³, 0.02112 a.u./ Bohr³, and 0.00707 a.u./ Bohr³, respectively.

Figure 6.4 also displays the BCPs along with the corresponding bond paths (the orange lines) for the weak bonds, using the Multiwfn program.³⁹ There is one BCP which indicates the C=O-H···O=C hydrogen bond and two BCPs for the intermolecular hydrogen bonds between the acetylacetone monomer and the water molecule. These results are consistent with the ones shown in the NCI plot. To quantitatively describe these hydrogen bonds, I first used the counterpoise correction and basis set superposition error (BSSE) method to calculate a complexation energy between acetylacetone and water of 5.6 kcal/mol (see Table 6.4). I also calculated the hydrogen bond energy by using the empirical relationship $E_{\text{HB}} = 1.38(\Delta\nu_{\text{OH}} - 40)^{1/2}$, where the $\Delta\nu_{\text{OH}}$ is the redshift wavenumber of the OH stretching vibration.⁴¹ For the C=O···H(water) hydrogen bond, Čeponkus et al. have observed a redshift of -139 cm^{-1} of the OH stretching of the water molecule within the acetylacetone-water complex observed in an FTIR of the complex embedded in a solid argon matrix.⁴² Based on this, I can estimate that the corresponding hydrogen bond energy is 3.3 kcal/mol. Lastly, I applied the semi-empirical formula between the hydrogen bond energy and electron density (ρ_{BCP}) at the BCP to obtain

the hydrogen bonding energy, $E_{\text{HB}} \text{ (kcal/mol)} = -3.09 + 239 \rho_{\text{BCP}}$.⁴³ From the QTAIM analysis, the electron density (ρ_{BCP}) of $\text{C}=\text{O}\cdots\text{H}(\text{water})$ is 0.023 a.u., and the estimated hydrogen bond energy is 2.4 kcal/mol (shown in Table 6.4), which is a bit smaller than the above value derived from the band shift of the OH stretching vibration.

I could not observe splittings of the rotational lines due to the internal motions of the water moiety in the acetone-water, cyclohexanone-water, and acetylacetone-water complexes. Caminati and coworkers pointed out that such a splitting is related to the barrier height of the internal rotation of water and, therefore, to the strength of the hydrogen bond and to the motion pathway.³⁶

6.3.4 Internal Rotation Dynamics

To estimate the internal rotation barrier height of the methyl groups in the acetylacetone-water complex, the MP2 level of theory with the 6-311++G (2d, p) basis set was used, and a potential energy curve was generated by relaxed scanning the dihedral angles $\angle 1(\text{H3, C1, C5, O6})$ and $\angle 2(\text{H9, C7, C11, O12})$ in steps of 60° , as shown in Figure 6.5. The barrier was determined to be about 0.13 kJ/mol (hydrogen bonded methyl group) and 5.20 kJ/mol (the methyl group far away from water).

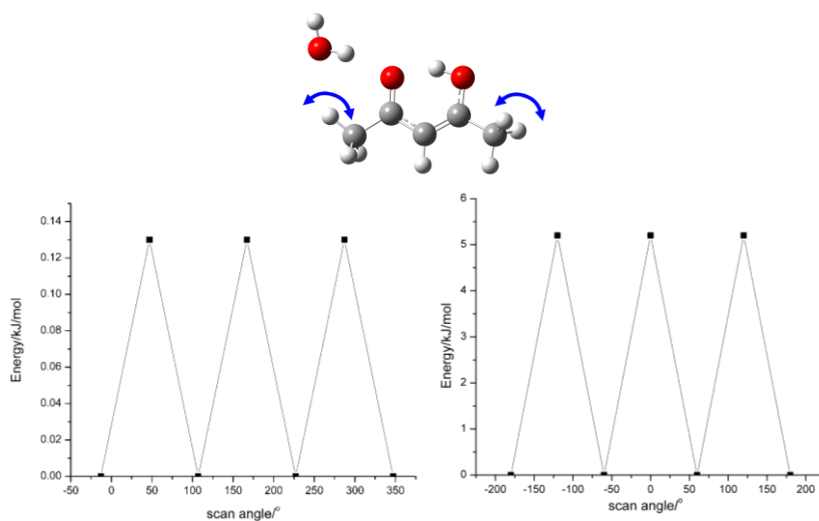


Figure 6.5. Calculated potential energies for two methyl internal rotations in the acetylacetone-water complex. The left bottom graph is for the internal rotation of methyl group hydrogen bonded with the water molecule; the right bottom graph is for the internal rotation of the methyl group far away from water.

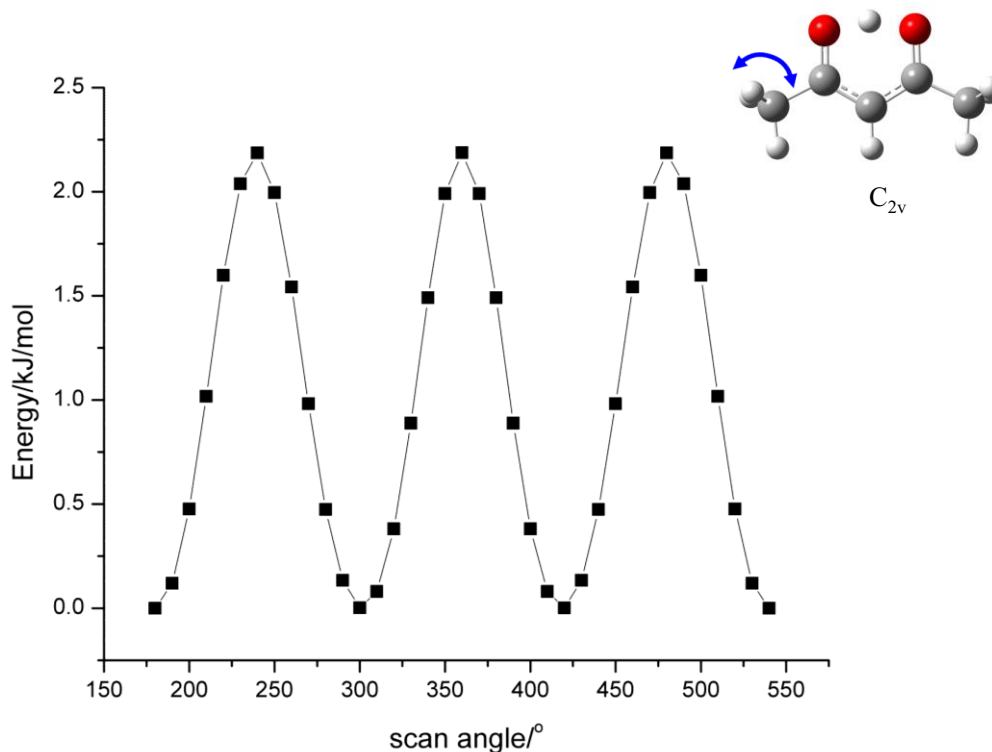


Figure 6.6. Calculated potential energies for two methyl internal rotations in the acetylacetonone monomer with C_{2v} symmetry.

The calculated barrier for the acetylacetonone monomer with C_{2v} symmetry at the same level of theory is 2.08 kJ/mol (shown in Figure 6.6). It seems that the barrier is not as low as I expected, and I probably could assign the spectrum completely (including the internal rotation splittings) starting with this barrier in the fit for this C_{2v} monomer; however, I tried but with no success. The possible reason is due to the center (enol form 2 in Table 6.1) proton transfer between the two carbonyl groups, whose wavefunction is then widely distributed, which may affect the internal rotation barrier significantly, as a result large splittings makes the spectral assignment difficult. When water is hydrogen bonded with acetylacetonone, the C_{2v} symmetry of the acetylacetonone monomer is broken and the center hydrogen between the two carbonyl groups moves to form a bond with one carbonyl group in an enolic form, i.e., it becomes a C_s symmetric structure. For comparison, I also calculated the methyl group internal rotation barriers for the C_s acetylacetonone monomer, and the two barriers are 1.12 and 5.59 kJ/mol (shown in Figure 6.7). I compared these two values with those in the acetylacetonone-water complex and found that the two internal rotation barriers in the complex become smaller than

those in the C_s monomer, so it is reasonable to use the calculated barriers in the complex as the starting point to do the assignment in the XIAM program.

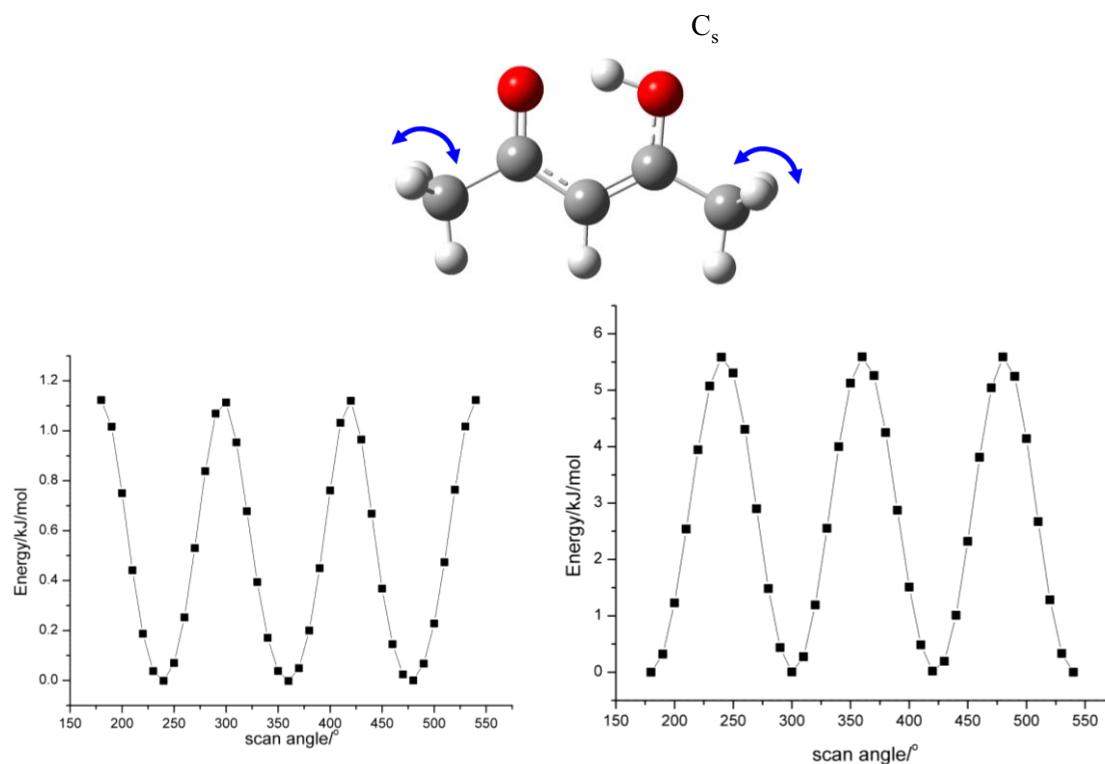


Figure 6.7. Calculated potential energies for two methyl internal rotations in the acetylacetonone monomer with C_s symmetry.

The internal rotation barrier height (V_3) of the methyl group far away from water is fitted experimentally to be 4.980(4) kJ/mol (Table 6.3) in the acetylacetonone-water complex, and the other methyl group is assumed to be a “free” rotor because its barrier is so low that a splitting of several GHz made the spectral assignment not possible. The calculated internal rotation barrier using the MP2 method is underestimated ~4% compared with the fitted barrier.

I tried to detect the three ^{13}C isotopologues of the acetylacetonone-water complex but was not successful. I also spent significant time searching for the diketo tautomer of the acetylacetonone monomer and its monohydrate but was also not successful. Although I captured only the enol form of the acetylacetonone-water complex using rotational spectra, it still gives us rich information about the hydrogen bonding of the enol and water interaction as well as the methyl rotation tunneling motion while both intra- and intermolecular hydrogen bondings are involved.

6. 4 Conclusions

Microwave spectra of the acetylacetonone-water complex were measured using both chirp-pulsed and cavity-based molecular beam Fourier-transform microwave spectrometers in the region from 5 to 14 GHz. Both *a*- and weaker *b*- type rotational transitions were observed in the acetylacetonone-water complex. The assignment of the rotational transitions was completed with the help of ab initio calculations. I only observed the most stable enol form of the acetylacetonone-water complex. A non-covalent interactions (NCI) analysis of the enolic acetylacetonone-water complex indicates that hydrogen bonding exists between the O(water) atom and an H atom of the methyl group of acetylacetonone, in addition to the more classical hydrogen bond between H(water) and an O atom of acetylacetonone, and that the strongest intramolecular hydrogen bond is between the carbonyl oxygen atom and the hydrogen atom in the other enolic carbonyl group. Furthermore, I analyzed the strength of the three hydrogen bonds quantitatively using the quantum theory of atoms in molecules (QTAIM) and compared the results derived from experimental ν_{OH} values. I was able to determine the barrier to internal rotation of the methyl group involved in hydrogen bonding from the splittings of the rotational transitions. Unfortunately, I failed in finding the diketo form of acetylacetonone in its hydrated form, even though it should have an abundance of 12.5%, based on theoretical calculations. The abundance of the monohydrate of a molecule is usually lower than that of the monomer in our experiments. So, possible reasons for not finding the diketo form is that the relative abundance of the diketo tautomer in the acetylacetonone monomer is very low (1.54%), the barrier from the enol tautomer to the diketo tautomer in the acetylacetonone monomer is quite high (~62 kcal/mol), and the interconversion of keto-enol tautomerization is not efficient when only one water is involved.

References

1. J. L. Burdett and M. T. Rogers, *J. Am. Chem. Soc.*, 1964, **86**, 2105-2109.
2. J. W. Bunting, J. P. Kanter, R. Nelander and Z. Wu, *Can. J. Chem.*, 1995, **73**, 1305-1311.
3. R. Irving and I. Wadso, *Acta Chem. Scand.*, 1970, **24(2)**, 589.
4. N. V. Belova, H. Oberhammer, N. H. Trang and G. V. Girichev, *J. Org. Chem.*, 2014, **79**, 5412-5419.
5. P. Roubin, T. Chiavassa, P. Verlaque, L. Pizzala and H. Bodot, *Chem. Phys. Lett.*, 1990, **175**, 655-659.
6. T. Ishida, F. Hirata and S. Kato, *J. Chem. Phys.*, 1999, **110**, 3938-3945.
7. G. Alagona and C. Ghio, *Int. J. Quantum Chem.*, 2008, **108**, 1840-1855.
8. T. Kaweetirawatt, T. Yamaguchi, T. Higashiyama, M. Sumimoto and K. Hori, *J. Phys. Org. Chem.*, 2012, **25**, 1097-1104.
9. R. R. Lozada-García, J. Ceponkus, M. Chevalier, W. Chin, J.-M. Mestdagh and C. Crépin, *Phys. Chem. Chem. Phys.*, 2012, **14**, 3450-3459.
10. A. Trivella, T. Wassermann, J. Mestdagh, C. M. Tanner, F. Marinelli, P. Roubin and S. Coussan, *Phys. Chem. Chem. Phys.*, 2010, **12**, 8300-8310.
11. S. Tayyari, T. Zeegers-Huyskens and J. Wood, *Spectrochim. Acta*, 1979, **35A**, 1289-1295.
12. R. Srinivasan, J. S. Feenstra, S. T. Park, S. Xu and A. H. Zewail, *J. Am. Chem. Soc.*, 2004, **126**, 2266-2267.
13. W. Egan, G. Gunnarsson, T. Bull and S. Forsen, *J. Am. Chem. Soc.*, 1977, **99**, 4568-4572.
14. R. Boese, M. Y. Antipin, D. Bläser and K. A. Lyssenko, *J. Phys. Chem. B*, 1998, **102**, 8654-8660.
15. M. Johnson, N. Jones, A. Geis, A. Horsewill and H. Trommsdorff, *J. Chem. Phys.*, 2002, **116**, 5694-5700.
16. W. Caminati and J.-U. Grabow, *J. Am. Chem. Soc.*, 2006, **128**, 854-857.
17. F. J. Lovas and C. Lugez, *J. Mol. Spectrosc.*, 1996, **179**, 320-323.
18. N. A. Seifert, J. Thomas, W. Jäger and Y. Xu, *Phys. Chem. Chem. Phys.*, 2018, **20**, 27630-27637.
19. W. Li, L. Evangelisti, Q. Gou, W. Caminati and R. Meyer, *Angew. Chem.*, 2019, **131**, 869-875.
20. M. Juanes, W. Li, L. Spada, L. Evangelisti, A. Lesarri and W. Caminati, *Phys. Chem. Chem. Phys.*, 2019, **21**, 3676-3682.
21. S. Ghosh, J. Thomas, W. Huang, Y. Xu and W. Jäger, *J. Phys. Chem. Lett.*, 2015, **6**, 3126-3131.
22. T. Lu, J. Zhang, J. Chen, Q. Gou, Z. Xia and G. Feng, *J. Chem. Phys.*, 2019, **150**, 064305.
23. S. P. Dempster, O. Sukhorukov, Q.-Y. Lei and W. Jäger, *J. Chem. Phys.*, 2012, **137**, 174303.
24. J. Thomas, J. Yiu, J. Rebling, W. Jäger and Y. Xu, *J. Phys. Chem. A*, 2013, **117**, 13249-13254.
25. Y. Xu and W. Jäger, *J. Chem. Phys.*, 1997, **106**, 7968-7980.
26. Y. Xu, J. V. Wijngaarden and W. Jäger, *Int. Rev. Phys. Chem.*, 2005, **24**, 301-338.
27. M. J. Frisch, G. W. Trucks, H. B. Schlegel, G. E. Scuseria, M. A. Robb, J. R. Cheeseman, G. Scalmani, V. Barone, B. Mennucci, G. A. Petersson, H. Nakatsuji, M. Caricato, X. Li, H. P. Hratchian, A. F. Izmaylov, J. Bloino, G. Zheng, J. L. Sonnenberg, M. Hada, M. Ehara, K. Toyota, R. Fukuda, J. Hasegawa, M. Ishida, T. Nakajima, Y. Honda, O. Kitao, H. Nakai, T. Vreven, J. A. Montgomery, Jr.,

- J. E. Peralta, F. Ogliaro, M. Bearpark, J. J. Heyd, E. Brothers, K. N. Kudin, V. N. Staroverov, T. Keith, R. Kobayashi, J. Normand, K. Raghavachari, A. Rendell, J. C. Burant, S. S. Iyengar, J. Tomasi, M. Cossi, N. Rega, J. M. Millam, M. Klene, J. E. Knox, J. B. Cross, V. Bakken, C. Adamo, J. Jaramillo, R. Gomperts, R. E. Stratmann, O. Yazyev, A. J. Austin, R. Cammi, C. Pomelli, J. W. Ochterski, R. L. Martin, K. Morokuma, V. G. Zakrzewski, G. A. Voth, P. Salvador, J. J. Dannenberg, S. Dapprich, A. D. Daniels, O. Farkas, J. B. Foresman, J. V. Ortiz, J. Cioslowski, and D. J. Fox, *Gaussian 09, Revision D.01*, Gaussian, Inc., Wallingford CT, 2013.
28. T. Yanai, D. P. Tew and N. C. Handy, *Chem. Phys. Lett.*, 2004, **393**, 51-57.
 29. E. R. Johnson, I. D. Mackie and G. A. DiLabio, *J. Phys. Org. Chem.*, 2009, **22**, 1127-1135.
 30. J. E. Del Bene, *J. Comput. Chem.*, 1985, **6**, 296-301.
 31. C. M. Western, *J. Quant. Spectrosc. Radiat. Transf.*, 2017, **186**, 221-242.
 32. H. Hartwig and H. Dreizler, *Z. Naturforsch. A*, 1996, **51**, 923-932.
 33. R. C. Dunbar, *J. Chem. Educ.*, 1982, **59**, 22-23.
 34. G. D. Peckham and I. J. Mcnaught, *J. Chem. Educ.*, 1992, **69**, 554-558.
 35. T. R. Dyke, K. M. Mack and J. S. Muentzer, *J. Chem. Phys.*, 1977, **66**, 498-510.
 36. S. Melandri, A. Maris, B. M. Giuliano and W. Caminati, *J. Chem. Phys.*, 2005, **123**, 164304.
 37. E. R. Johnson, S. Keinan, P. Mori-Sanchez, J. Contreras-Garcia, A. J. Cohen and W. Yang, *J. Am. Chem. Soc.*, 2010, **132**, 6498-6506.
 38. T. Lu and F. Chen, *J. Mol. Graph Model*, 2012, **38**, 314-323.
 39. T. Lu and F. Chen, *J. Comput. Chem.*, 2012, **33**, 580-592.
 40. P. De Silva and C. m. Corminboeuf, *J. Chem. Theory Comput.*, 2014, **10**, 3745-3756.
 41. A. Iogansen, *Spectrochim. Acta*, 1999, **55A**, 1585-1612.
 42. J. Čeponkus, R. Platakytė, V. Šablinskas and A. G. Quintanilla, *chemija*, 2018, **29(1)**, 1-16.
 43. T. Y. Nikolaienko, L. A. Bulavin and D. M. Hovorun, *Phys. Chem. Chem. Phys.*, 2012, **14**, 7441-7447.

Chapter 7

Rotational Spectra of the Benzoylacetone Monomer and Its Complex with Water

7.1 Introduction

Keto-enol tautomerization is of great importance as it is involved in the biochemical activity of amino acids, sugars, and nucleic acids.^{1,2} The equilibrium of this kind of tautomerization can be tuned by solvation. The solvent in solution can control the dynamics of a proton transfer by solute/solvent interactions, for example, hydrogen bonding. The study of hydrogen bonding and the connection to proton transfer processes attracts much attention, especially in inter-³ and intra-molecular⁴ proton-transfer dynamics.

The enol forms of β -diketones of the $R1-C(=O)-CH_2-C(=O)-R2$ type possess the intramolecular hydrogen bond of $(C)O-H\cdots O(C)$. One of the most studied β -diketones is acetylacetone (AcAc), where R1 and R2 are methyl groups. Many experimental techniques, including nuclear magnetic resonance (NMR),⁵⁻⁷ X-ray crystallography,⁸ gas-phase ED,⁹ gas-phase vibrational spectroscopy,¹⁰ and microwave spectroscopy,⁴ have been used to investigate its structure, mainly the enol tautomer. The microwave study revealed that the enol tautomer has C_{2v} symmetry and that the two methyl groups are equivalent,⁴ while studies with the other techniques determined that AcAc has C_s symmetry.^{8,9} In the microwave study, the internal rotation barrier of the methyl groups was found to be so low that the exact structure of AcAc could not be determined fully, and the keto form could not be detected. Our previous microwave spectroscopic study of the acetylacetone-water complex also showed that the abundance of the keto form is too low to be detected. The ratio of the abundances of keto form to the enol form depends on many factors, such as temperature, solvent, and phase.¹¹ The substituents R1 and R2 also could influence the keto-enol tautomerization equilibrium. If $R1 = CH_3$ and $R2 = C_6H_5$, we have benzoylacetone, which can form two enol, and several diketo tautomers.

Benzoylacetone has become the subject of many studies. One subject is to study the keto-enol tautomerization of benzoylacetone. Both NMR and near vacuum UV absorption spectra studies of benzoylacetone show that the enol tautomer is the dominant structure and is present as 77% in DMSO¹² and 100% in CCl₄.⁵ The spectrophotometric study of benzoylacetone in aqueous solution at room temperature indicates that the keto and enol tautomers coexist and that their abundances are similar (~58% of keto form).¹³ In a recent gas-phase electron diffraction study 100% enol tautomer at 331(5) K was detected.¹¹ The abundance ratio of keto to enol tautomers in benzoylacetone monomer is unclear. Another general consensus was to focus on the shape of the (C)O–H···O(C) potential function for the two isomers of the enol tautomer, i.e., whether it is a symmetric double well potential,^{14, 15} where the two enol forms are equally likely; or an asymmetric double well potential,^{16, 17} where the enolic proton is preferentially located near the C=O group connecting the phenyl group. Fourier transform microwave spectroscopy (FTMW) is an extremely sensitive tool that has been used for measuring fine structure changes of neutral molecules and clusters in the gas phase.^{18, 19} This technique may allow us to unravel these two questions.

The microwave spectra of the benzoylacetone monomer and its water complex were studied with the aid of high-level theoretical calculations. The keto-enol tautomers and conformers of the benzoylacetone monomer and water complexes were investigated first by ab initio calculations. After the spectra of the benzoylacetone monomer were assigned, the coupling of the proton transfer to the methyl internal rotation tunneling in the enol tautomer of the benzoylacetone monomer was investigated; we found that the methyl internal rotation tunneling barrier is very sensitive to the proton transfer in this molecule. Next, a deuterium isotopologue of benzoylacetone was studied to determine the position of the center hydrogen atom between the two carbonyl groups. Lastly, the spectra of the benzoylacetone-water complexes were assigned, and the properties of the structures and the hydrogen bonds of both the monomer and the complexes were analyzed by a noncovalent interaction (NCI) analysis.

7.2 Experimental and Computational Details

The microwave spectra of the benzoylacetone monomer were recorded using both a cavity-based molecular beam FTMW spectrometer^{20, 21} and a chirped-pulse FTMW spectrometer²² (2–6 GHz). The solid benzoylacetone sample was purchased from Aldrich and was used as

obtained. It was put in a stainless steel container that is mounted right behind the general valve pulsed nozzle. The nozzle was heated to 100 °C, and the container to 50–55 °C. The pressure of the Ne backing gas was held at 1–3 bar. The frequency uncertainty of the cavity-based molecular beam FTMW spectrometer is ~2 kHz.

The spectrum of the benzoylacetone-water complex was recorded using a broadband chirped pulse FTMW spectrometer in the range between 2 and 6 GHz. The design of the instruments has been reported previously,²² and its frequency uncertainty is ~15 kHz. Briefly, the solid sample is put into a small brass cylinder, which is mounted to the pulsed nozzle heated to 60 °C. The Ne backing gas (2 bar) was mixed with about 0.1% water. The resulting mixture of benzoylacetone and water with neon is expanded supersonically into the microwave interaction region, forming the benzoylacetone-water complex.

To help assign the spectra of the benzoylacetone monomer and the benzoylacetone-water complex, several ab initio calculations were performed using the Gaussian 09 package.²³ The dispersion-corrected B3LYP functional³⁰ was used for the DFT calculations with Becke–Johnson damping^{24, 25} (B3LYP-D3BJ) for initial spectroscopic searches. The basis set I used is aug-cc-pVTZ³¹. MP2/ cc-pVTZ was also used in the geometry optimization. Vibrational frequencies were calculated to make sure that the optimized structure is a minimum-energy conformation by the absence of imaginary harmonic frequencies.

Transition frequencies were predicted from the calculated rotational constants using the PGOPHER program.²⁶ Then, the observed and predicted frequencies were used in a fitting procedure using the same program. Finally, the XIAM program was used to predict the internal rotation splitting parameters,²⁷ and the PMIFST program was employed to predict rotational constants for the deuterium isotopologue of benzoylacetone.²⁸

7.3 Results and Discussion

7.3.1. Spectral Search and Assignment of the Benzoylacetone Monomer

7.3.1.1 Keto-Enol Tautomerization of the Benzoylacetone Monomer

The benzoylacetone monomer has two carbonyl groups (C=O), so that keto-enol tautomerization can occur in this molecule. I utilized two theoretical methods (B3LYP-D3BJ and MP2) to predict the structures (shown in Figure 7.1) of the benzoylacetone monomer. The

predicted rotational constants, dipole moment components, and their relative energies are shown in Table 7.1. The results show that each keto tautomer has two isomers and that each enol tautomer also has two isomers (see Figure 7.1). The keto tautomers are much more stable than the enol ones, by 22 and 51 kJ/mol, respectively, based on the B3LYP-D3BJ calculation results. As a result, there was little chance to capture the keto tautomer because its relative abundance is in the range of 1.16×10^{-7} – 0.014%, according to the Boltzmann distribution. I also used the MP2 method to calculate the two isomers of the keto tautomer and found that only one isomer exists in the keto tautomer; it has a relative energy of ~16 kJ/mol compared to the most stable enol tautomer. Its abundance is ~0.16%, so it is still not high enough to be detected with our instrument. Then, I focused on searching for the two isomers of the enol tautomer. The difference in the structures of the two isomers is the position of the hydrogen atom between the two carbonyl groups. The most stable isomer is the one where the hydrogen atom is hydrogen-bonded with the carbonyl group that connects to the methyl group, while the less stable structure has the hydrogen atom hydrogen-bonded with the carbonyl group that connects to the phenyl group. These two structures are very similar as their rotational constants are quite close and only differ by ~0.74 kJ/mol in energy in the B3LYP-D3BJ method. I also used the MP2 method to calculate the structures of the two isomers, rotational constants, dipole moments, and the relative energies, which are listed in Table 1. The calculated relative energy of the isomer II is ~0.62 kJ/mol, which is very close to the result using the B3LYP-D3BJ method. The two isomers of the enol tautomer should be detectable in our microwave experiment because the second isomer has an abundance of 43%, according to the Boltzmann distribution.

Table 7.1. Calculated rotational constants, dipole moment components, and relative energies of four tautomeric/conformational species of the benzoylacetone monomer at the B3LYP-D3BJ/aug-cc-pVTZ and MP2/cc-pVTZ levels of theory.

monomer	Enol 1	Enol 2	Keto 1	^b Keto 2
<i>A</i> /MHz	2651.3/2630.4	2639.7/2615.6	1824.7/1836.2	1715.4
<i>B</i> /MHz	474.3/475.0	476.7/477.0	615.7/607.0	630.2
<i>C</i> /MHz	404.7/407.1	406.0/408.9	498.2/493.0	515.4
$ \mu_a /\text{D}$	0.9/1.0	1.98/2.0	0.8/0.9	0.5
$ \mu_b /\text{D}$	3.0/3.3	2.84/3.2	0.1/0.1	3.5
$ \mu_c /\text{D}$	0.3/0.6	0.28/0.6	0.9/0.7	3.1
$V_3^{\text{CH}_3}/\text{kJ}\cdot\text{mol}^{-1}$	5.3 ^c	1.5 ^c		
^a $\Delta E/\text{kJ}\cdot\text{mol}^{-1}$	0/0	0.7/0.6	51.2/15.6	22.3

^a Zero-point vibrational energy included, B3LYP-D3BJ/MP2.

^b This structure can only be obtained at the B3LYP-D3BJ level.

^c The barrier is obtained at the B3LYP-D3BJ level.

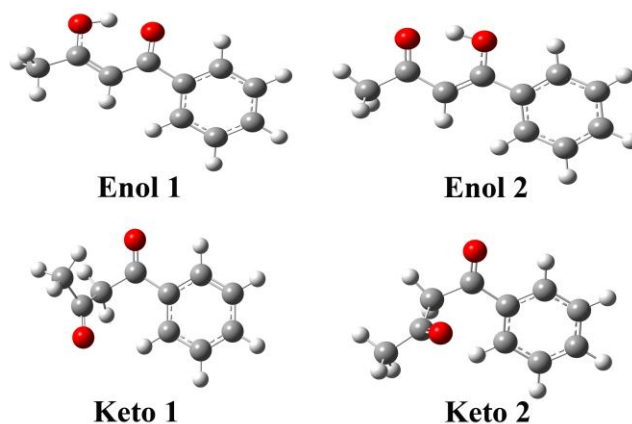


Figure 7.1. Structures of four tautomeric/conformational species of the benzoylacetone monomer at the B3LYP-D3BJ/aug-cc-pVTZ level of theory.

7.3.1.2 Proton Transfer Coupled Methyl Internal Rotation Tunneling in the Enol Tautomer of the Benzoylacetone Monomer

In the initial experiments, I located rotational transitions of the most stable enol tautomer for the benzoylacetone monomer. In the measurement, each rotational line is split into a doublet, and it was easy to assign the spectrum. The measured transition frequencies are given in Table S7.1 in the Appendix V, together with the quantum number assignments. The

frequencies were used in a fitting procedure, and the resulting spectroscopic constants are listed in Table 7.2. The fitted rotational constants are very close to the calculated rotational constants from the B3LYP-D3BJ method, and the deviation between experimental and calculated rotational constants is less than 1%. Next, I tried to assign the second component of the observed doublets to the second isomer, but without success. Later, I found that the observed splittings are due to a methyl internal rotation tunneling in the benzoylacetone monomer. One example of such internal rotation splitting can be found in Figure 7.2. The XIAM program was used to fit the methyl internal rotation splittings, and resulting parameters are shown in Table 7.2. The fitted barrier of the methyl internal rotation is 2.62(1) kJ/mol, which is far from the theoretical prediction of the barrier of 5.33 kJ/mol calculated at the B3LYP-D3BJ/aug-cc-pVTZ level of theory. Even more interestingly, the experimental rotational constants are close to the ones in both isomers of the enol tautomer, so it is hard to say whether the experimental structure observed is isomer one (Enol form I) or isomer two (Enol form II).

Table 7.2. Experimental spectroscopic parameters for the benzoylacetone monomer.

Parameter	benzoylacetone
A/MHz	2649.1787(18)
B/MHz	472.5502(2)
C/MHz	403.3169(2)
Δ_{JK}/kHz	0.081(24)
Δ_K/kHz	0.315(158)
$V_3/\text{kJ/mol}$	2.62(1)
ρ/rad	0.01246(2)
β/rad	0.1782(8)
${}^a\gamma/\text{rad}$	0.0907
${}^bF_0/\text{GHz}$	151.89
N	181
σ/kHz	28.8

^a γ is fixed.

^b F_0 is derived.

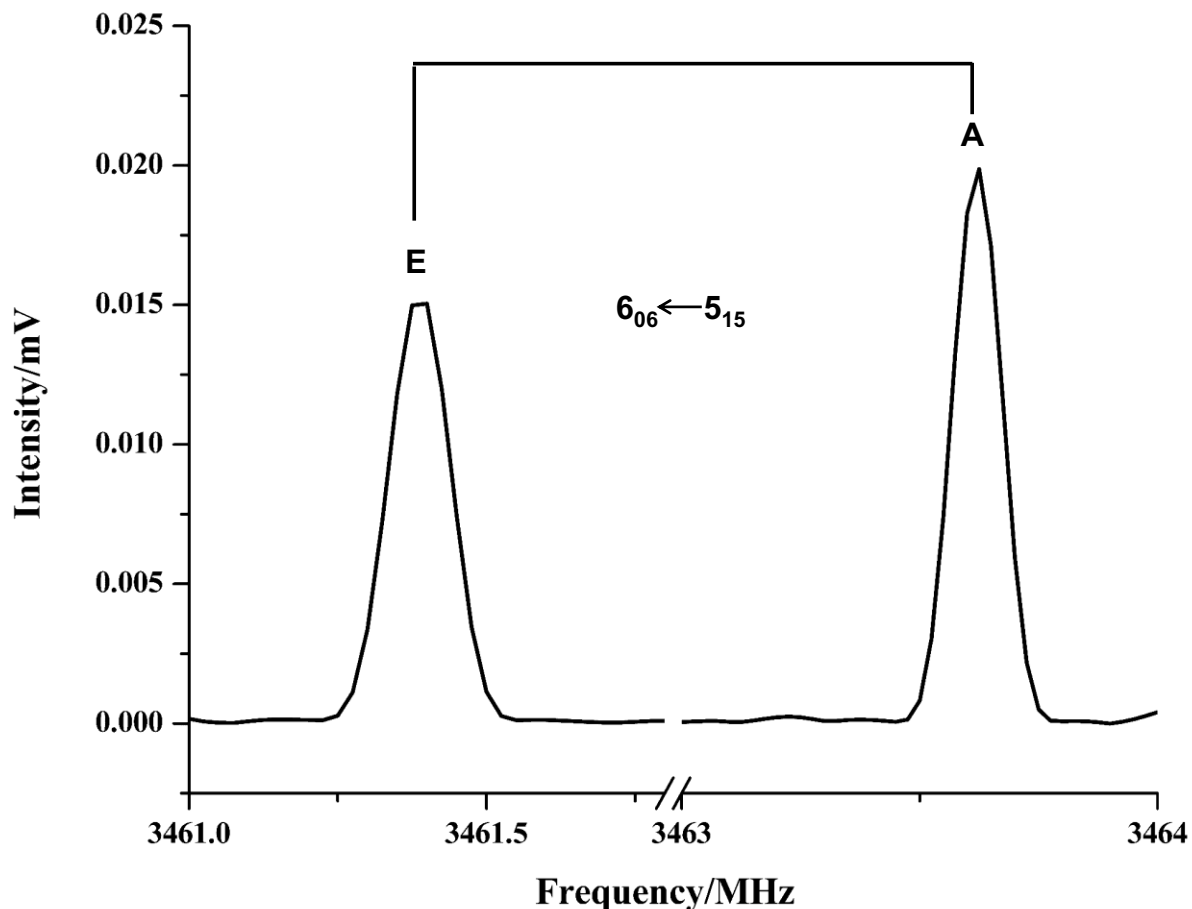


Figure 7.2. An example for the internal rotation splitting of rotational transitions of the benzoylacetone monomer, measured with a chirped-pulse FTMW spectrometer (2–6 GHz).

It is noticed that the fitted experimental barrier of the methyl group is just between the internal rotation barriers of the two isomers (1.54–5.33 kJ/mol). Therefore, the question is whether the experimental structure is perhaps an average of the two calculated isomers, i.e., if the hydrogen is near the midpoint between the two carbonyl groups or closer to the calculated position in the more stable isomer. To gain further insights, I calculated the reaction pathways of the proton transfer between these two carbonyl groups; the results are shown in Figure 7.3, and the barrier between the two isomers is ~ 9 kJ/mol, which means the zero-point energy level ($E_{\text{zpe}} \sim 18$ kJ/mol, the calculated vibration frequency $\nu_{\text{OH}} \sim 2900$ cm^{-1} in Enol 1) is above the barrier. Next, I calculated the internal rotation barrier of the transition state, i.e., when the hydrogen is near the midpoint between the two carbonyl groups. The calculated barrier is 2.4 kJ/mol, which is very close to our experimental value. This is indication that the hydrogen atom has significant probability to be between the two carbonyl groups in the benzoylacetone

monomer, even though it does not possess C_{2v} symmetry as the acetylacetonone monomer. In a previous microwave spectroscopic study, acetylacetonone was confirmed to have a structure with C_{2v} rather than C_s symmetry.⁴

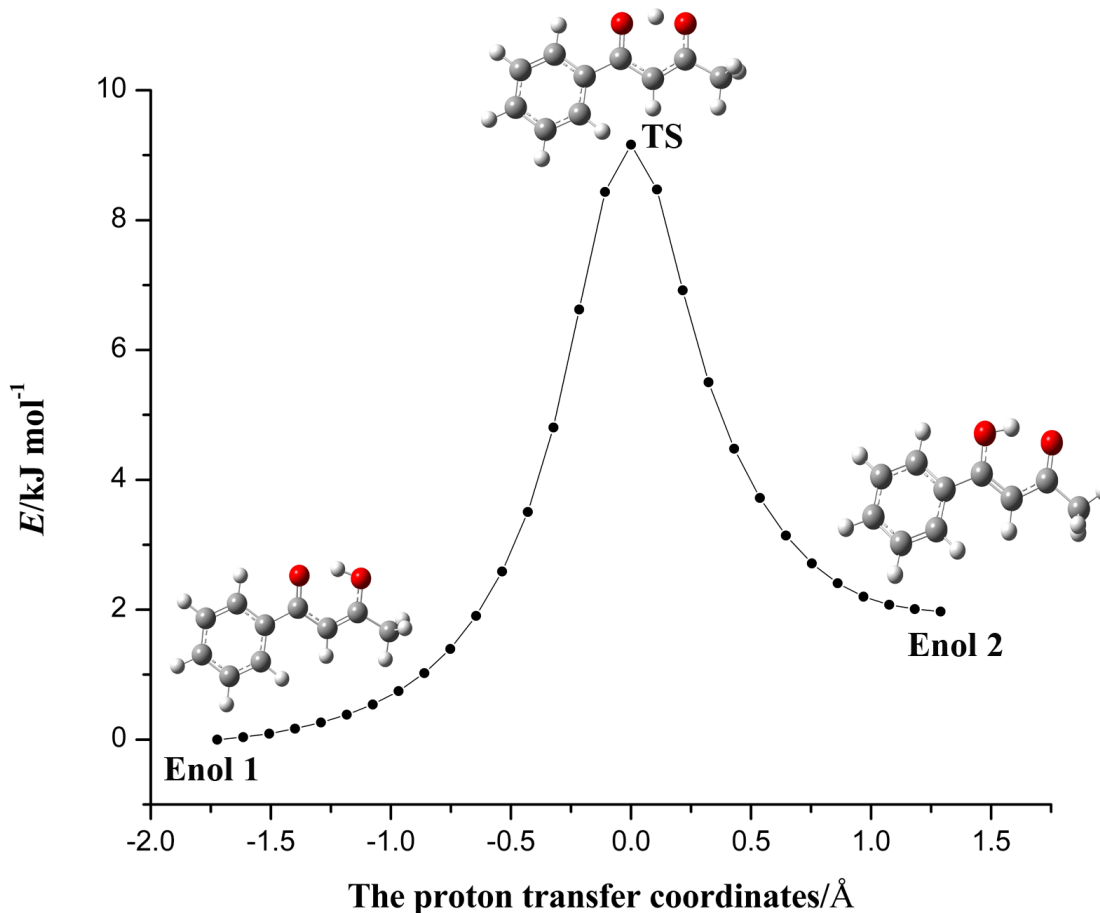


Figure 7.3. The proton transfer reaction path in the benzoylacetonone monomer.

To better determine the position of this hydrogen atom, it was replaced by deuterium, as shown in Figure S7.1 of the Appendix V, and I measured the corresponding rotational transitions (the measured rotational frequencies are listed in Table S7.2 in the Appendix V). I first fitted the A component using the PGOPHER programme. The AE internal rotation splitting is much smaller than that in the normal monomer of benzoylacetonone. One example of this internal rotation splitting is shown in Figure 7.4. The XIAM program was then used to fit the methyl internal rotation splitting. The fit results can be found in Table 7.3. The fitted barrier is 6.30(22) kJ/mol, which indicates that the experimental structure using of the deuterated form shifts to the Enol form I, and the hydrogen is no longer near the midpoint between the two

carbonyl groups. This can be explained by the fact that the zero-point energy (ZPE) for the deuterated form of benzoylacetone is estimated to be 12 kJ/mol based on the calculation in the normal benzoylacetone, which is still above the barrier (9 kJ/mol) of two enol isomers, but much lower than the 18 kJ/mol of the ZPE in normal benzoylacetone, and this increases the probability to detect the deuterated form closer to Enol form I. It is interesting that the methyl internal rotation barrier is very sensitive to the proton transfer between the two carbonyl groups in the benzoylacetone monomer.

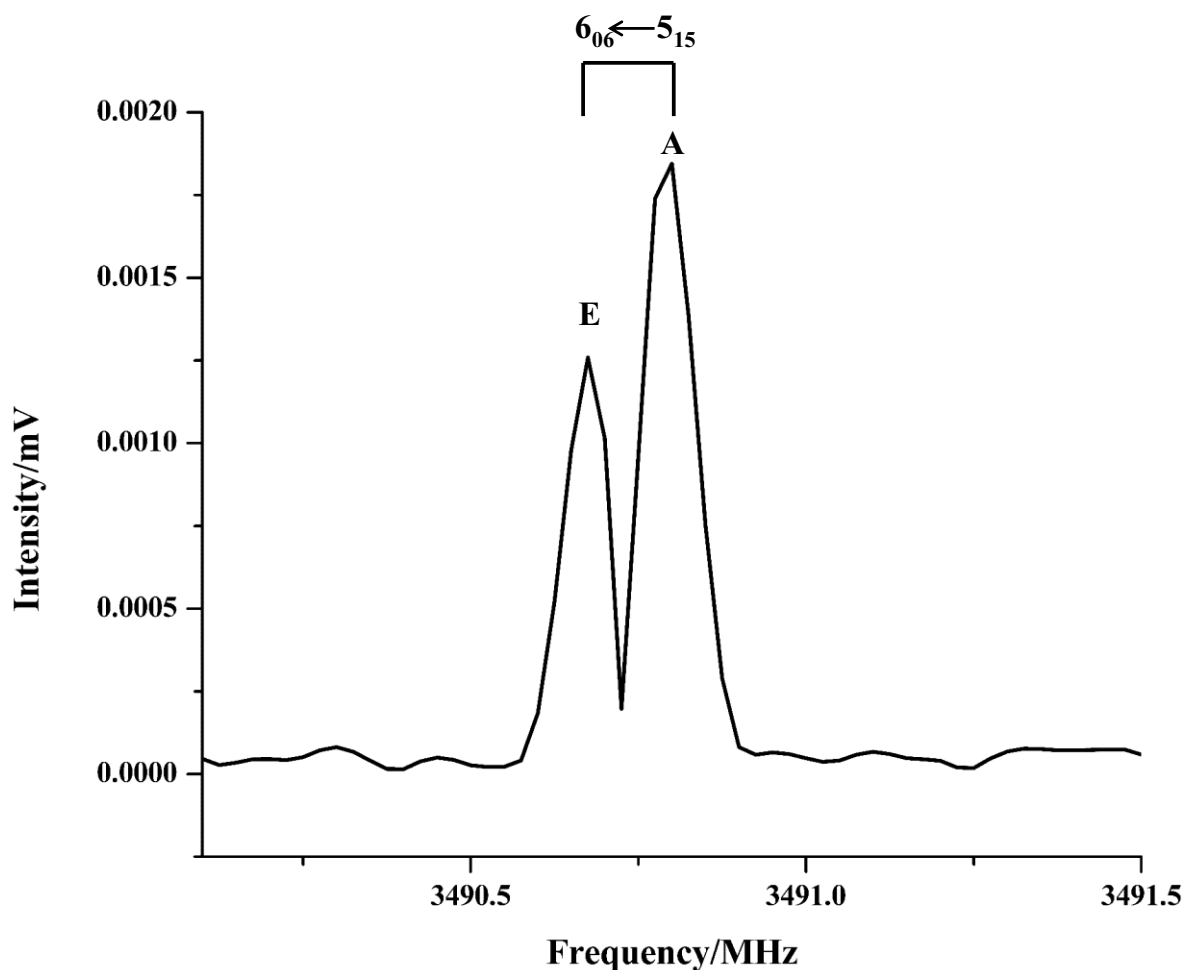


Figure 7.4. An example for internal rotation splitting in transitions of the deuterated benzoylacetone monomer (the central hydrogen is replaced by deuterium) measured using a chirped-pulse FTMW spectrometer (2—6 GHz).

Table 7.3. Experimental spectroscopic parameters for the deuterated benzoylacetone monomer (the central hydrogen atom is replaced by deuterium).

Parameter	benzoylacetone
A/MHz	2609.8378(20)
B/MHz	472.0362(49)
C/MHz	402.01279(48)
δ_j/kHz	0.002(1)
$V_3/\text{kJ/mol}$	6.30(21)
ε/rad	3.027
$^a \delta/\text{rad}$	1.042(97)
$^b F_0/\text{GHz}$	160.0569
N	78
σ/kHz	25.8

^a δ is fixed.

^b F_0 is fixed.

7.3.2. Spectral Search and Assignment of the Benzoylacetone-Water Complexes

In the theoretical calculations of the benzoylacetone monomer, four conformers were found. If one water molecule is attached into the benzoylacetone monomer, six isomers are calculated (see the structures in Figure 7.5), and their predicted rotational constants, dipole moments, and relative energies are listed in Table 7.4. For the enol tautomer, there are two stable isomers. Because the water molecule can be attached on both sides of the carbonyl group, two benzoylacetone-water complexes can be formed with each enol tautomer of benzoylacetone. Therefore, there are four enol tautomer-water complexes, whose relative energies are all below 10 kJ/mol. Two keto tautomer-water complexes, whose relative energies are too high (~20 kJ/mol) to be detected, were calculated.

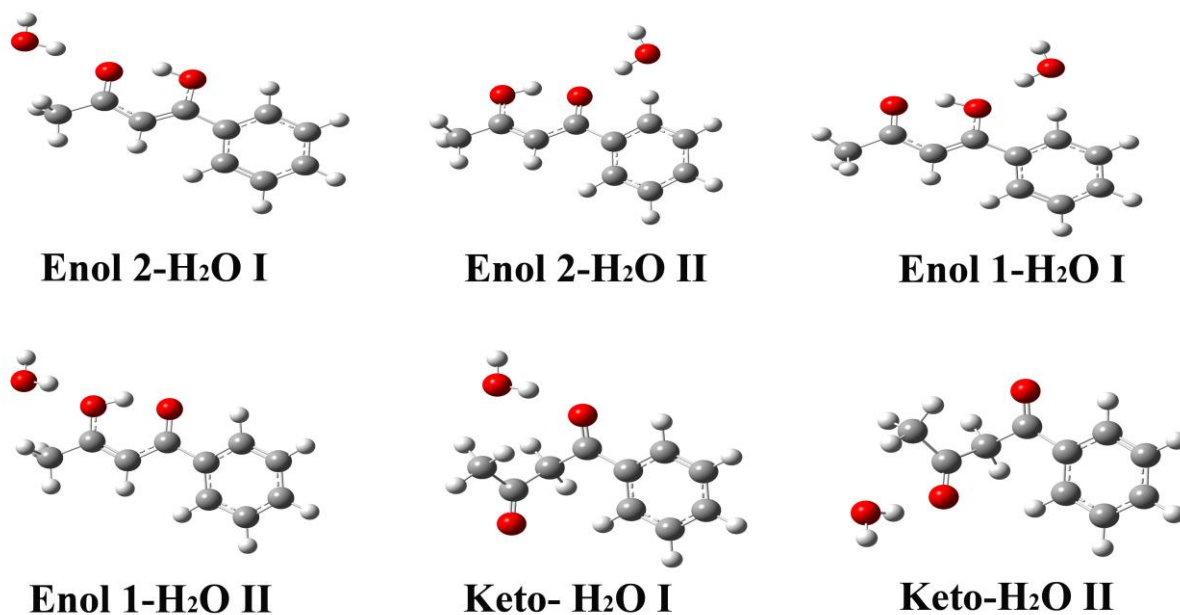


Figure 7.5. Structures of six benzoylacetone monohydrated complexes at the B3LYP-D3BJ/aug-cc-pvtz level of theory.

Table 7.4. Calculated spectroscopic constants and the relative energies of four tautomeric/conformational species of six benzoylacetone monohydrated complexes at the levels of B3LYP-D3BJ/aug-cc-pvtz theory.

Complex	Enol 2- H ₂ O I	Enol 2- H ₂ O II	Enol 1- H ₂ O I	Enol 1- H ₂ O II	Keto- H ₂ O I	Keto- H ₂ O II
<i>A</i> /MHz	2458.78	3958.21	1077.13	2371.03	1244.25	1185.75
<i>B</i> /MHz	305.80	899.71	470.86	305.34	487.83	430.80
<i>C</i> /MHz	273.24	760.46	332.23	274.40	378.13	352.17
$ \mu_a /D$	4.29	1.89	1.06	2.72	2.53	2.63
$ \mu_b /D$	1.32	1.97	3.96	1.56	1.44	0.80
$ \mu_c /D$	0.07	0.40	0.61	0.02	0.17	1.47
^a $\Delta E/kJ\cdot mol^{-1}$	0	7.5	1.3	4.5	17.01	23.18

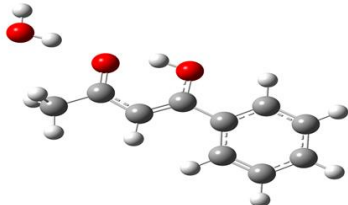
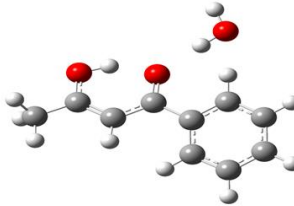
^a Zero-point vibrational energy included.

In the experiment, transitions of two water complexes were detected, Enol form 2-water I, the most stable structure, and Enol form 1-water I. The results from the fitting procedure are shown in Table 7.5. Notice that the structure of the benzoylacetone monomer is different in these two water complexes. In the most stable water complex (Enol form 2-water I), which

contains the less stable enol monomer, the hydrogen atom is hydrogen-bonded to the carbonyl group near the phenyl group. In the second most stable water complex (Enol form 1-water I), which contains the most stable benzoylacetone monomer, the water unit acts as hydrogen donor to the aldehyde group (H-C=O).

Table 7.5. Experimental spectroscopic parameters for the two isomers of the benzoylacetone-water complexes.

complex	Enol 2- H ₂ O I	Enol 1- H ₂ O I
<i>A</i> /MHz	2430.4725(22)	1048.11765(79)
<i>B</i> /MHz	303.19941(14)	469.08613(37)
<i>C</i> /MHz	270.63668(13)	328.72939(28)
Δ_J /kHz	0.0062(8)	
Δ_K /kHz	1.7(5)	
<i>N</i>	44	26
σ /kHz	3.9	11.8

From the assignment of the rotational transitions of the two enol tautomer-water complexes, it is found that the hydrogen bond favors the carbonyl group instead of the aldehyde group (C=O-H). Moreover, both isomers of the enol tautomer of benzoylacetone can be involved in forming the water complex. It is known that the water complex can be detected only if two monomer species (water + benzoylacetone) exist. If the two water complexes containing two isomers of the enol form of benzoylacetone are detected, two isomers of the enol form should coexist in the benzoylacetone monomer. This further confirms that the experimental structure of the benzoylacetone monomer is the average of the two isomers in the enol tautomer, i.e. the hydrogen atom should be near the midpoint of the two carbonyl groups in the benzoylacetone monomer.

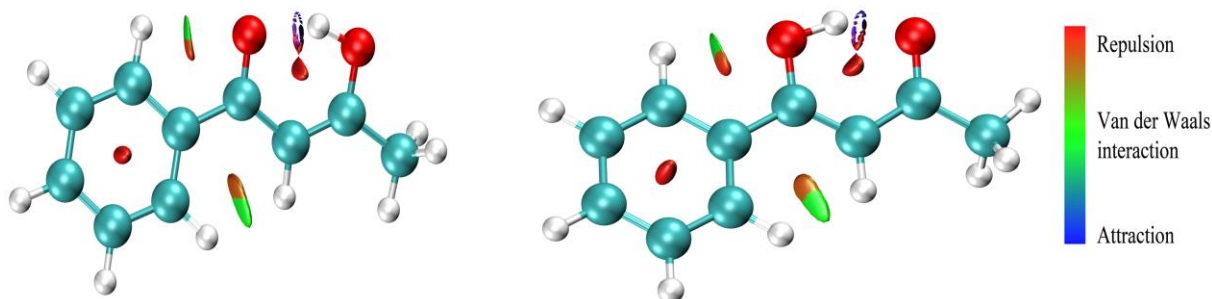


Figure 7.6. Results from NCI analyses of the benzoylacetone monomer; the isomer on the left side is Enol 1, and the isomer on the right side is Enol 2. Also shown are the NCI isosurfaces at a fixed reduced density gradient, $s = 0.54$ a.u., colored by the values of $\text{sign}(\lambda_2)\rho$ $[-0.04, 0.02]$ at each point in space, with colorations specified by the legend in the bottom right (red color denotes positive value, and blue color denotes negative value).

7.3.3. Hydrogen Bonding and Non-covalent Interaction Analysis

There is one proton between the two carbonyl groups in the benzoylacetone monomer, where the intramolecular hydrogen bond exists. Figure 7.6 shows the results from non-covalent interaction (NCI) analyses²⁹ of the two isomers of the enol tautomer of benzoylacetone monomer. As shown in Figure 7.6, there is a hydrogen bond between the C=O-H and the O=C, a van der Waals (vdW) interaction between the C=O and the adjacent phenyl H atom, and a weak interaction between the phenyl hydrogen atom and the H(C) in both isomers. When water is involved, the interaction becomes more complicated. Figure 7.7(a) shows the most stable conformer of the benzoylacetone-water complex. A hydrogen bond exists between the water H atom and the carbonyl oxygen atom in Enol form II, and a weak vdW interaction is between the water O atom and the hydrogen atom in the methyl group of benzoylacetone. In addition to the VdW interaction between the C=O and the adjacent phenyl H atom, there is a weak interaction between a phenyl hydrogen atom and the H(C) that is also seen in the benzoylacetone monomer. It seems that the strength of the intramolecular hydrogen bond between the C=O-H and the O=C does not change when water is involved in this conformer as one can observe that this intramolecular hydrogen bond exists in both the monomer and the complex. However, when water is hydrogen bonded on the other side of the benzoylacetone monomer, as shown in Figure 7.7 (d), this conformer (Enol form 2-water II) has an energy of 7.5 kJ/mol higher than the most stable conformer (Figure 7.7 (a)), and the intramolecular hydrogen bond between C=O-H and the O=C is weakened. One cannot observe any interaction

there in Figure 7.7 (d) as the hydrogen bond and the vdW interaction exist between the benzoylacetone monomer and the water molecule. Unfortunately, this conformer was not observed. A similar phenomenon can also be observed for isomer II of the enol tautomer of the benzoylacetone monomer and its water complex, as shown in Figure 7.7 (b) and (c). To conclude, when water is hydrogen bonded with the O=C group, the strength of the intramolecular hydrogen bond between the C=O-H and the O=C in the monomer after it is complexed with water will not change, whereas the strength of this intramolecular hydrogen bond will be weakened when water is hydrogen bonded with the H-O=C group.

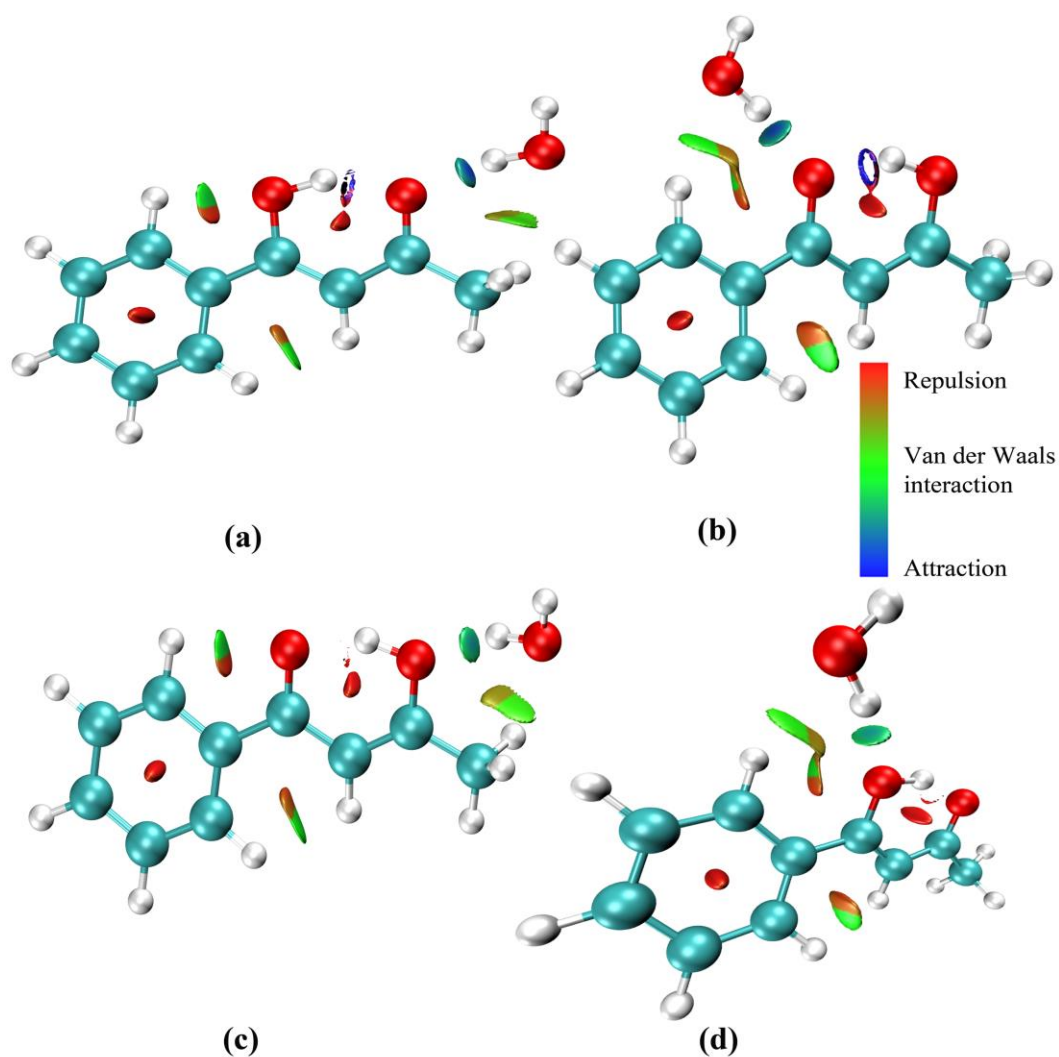


Figure 7.7. NCI analysis of the benzoylacetone-water complexes, (a) Enol 2-H₂O I complex (0 kJ/mol); (b) Enol 1-H₂O I complex (1.3 kJ/mol); (c) Enol 1-H₂O II complex (4.5 kJ/mol); (d) Enol 2-H₂O II complex (7.5 kJ/mol). Also shown are the NCI isosurfaces at a fixed reduced density gradient, $s = 0.54$ a.u., colored by the values of $\text{sign}(\lambda_2)\rho$ [-0.04, 0.02] at each point in space, with colorations specified by the legend in the bottom right (red color denotes positive value, and blue color denotes negative value).

7.4 Conclusions

Microwave spectra of the acetylacetone monomer and its monohydrate were measured using both chirp-pulsed and cavity-based molecular beam Fourier-transform microwave spectrometers in the region from 2 to 14 GHz. Both weaker *a*- and *b*- type rotational transitions were observed in the benzoylacetone monomer. Each rotational transition is split into a doublet due to the methyl internal rotation. The assignment of these rotational transitions was completed with the help of ab initio calculations. Keto-enol tautomerization exists in the benzoylacetone monomer. The enol tautomer is more stable, and two isomers were found in the calculations. The fitted rotational constants are quite close to the calculated ones for these two isomers, and it is difficult to decide whether the experimental structure is isomer I or isomer II. According to the fitted methyl internal rotation barrier of 2.62(1) kJ/mol, the experimental structure appears to be an average of these two isomers (Enol form I and Enol form II), i.e., the experimental structure will have significant probability for the H-atom to be found near the transition state of the proton transfer path, because the methyl internal rotation barriers in these two isomers are 5.3 kJ/mol and 1.5 kJ/mol, respectively. I also measured rotational transitions of the deuterated form of benzoylacetone monomer to better determine the position of the hydrogen atom between the two carbonyl groups. The internal rotation barrier in deuterated benzoylacetone is 6.30(21) kJ/mol, indicating that the experimental structure of the deuterated form is closer to Enol form I, surprisingly different from the experimental observation for the normal benzoylacetone monomer.

Two conformers of the enol benzoylacetone-water complex were observed, and these two complexes consist of two different enol isomers of the benzoylacetone monomer, which further confirms that the experimental structure in the benzoylacetone monomer is an average of the two isomers. NCI analyses show that when water is hydrogen bonded to the O=C group. The strength of the intramolecular hydrogen bond between the C=O-H and the O=C in the monomer after it is complexed with water does not change, whereas the strength of this intramolecular hydrogen bond will be weakened when water is hydrogen bonded with the H-O=C group.

References

1. E. P. Kündig, A. Enríquez García, T. Lomberget and G. Bernardinelli, *Angew. Chem. Int. Ed.*, 2006, **45**, 98-101.
2. W. Wang, H. W. Hellinga and L. S. Beese, *Proc. Natl. Acad. Sci.*, 2011, 108(43), 17644-17648.
3. Y. Matsuda, A. Yamada, K. i. Hanaue, N. Mikami and A. Fujii, *Angew. Chem.*, 2010, **122**, 5018-5021.
4. W. Caminati and J.-U. Grabow, *J. Am. Chem. Soc.*, 2006, **128**, 854-857.
5. J. L. Burdett and M. T. Rogers, *J. Am. Chem. Soc.*, 1964, **86**, 2105-2109.
6. R. M. Claramunt, C. López, M. D. Santa María, D. Sanz and J. Elguero, *Prog. Nucl. Magn. Reson. Spectrosc.*, 2006, **49**, 169-206.
7. X. Kong, A. Brinkmann, V. Terskikh, R. E. Wasylshen, G. M. Bernard, Z. Duan, Q. Wu and G. Wu, *J. Phys. Chem. B*, 2016, **120**, 11692-11704.
8. L. H. Thomas, A. J. Florence and C. C. Wilson, *New J. Chem.*, 2009, **33**, 2486-2490.
9. R. Srinivasan, J. S. Feenstra, S. T. Park, S. Xu and A. H. Zewail, *J. Am. Chem. Soc.*, 2004, **126**, 2266-2267.
10. R. R. Lozada-García, J. Ceponkus, W. Chin, M. Chevalier and C. Crépin, *Chem. Phys. Lett.*, 2011, **504**, 142-147.
11. N. V. Belova, G. V. Girichev, H. Oberhammer, T. N. Hoang and S. A. Shlykov, *J. Phys. Chem. A*, 2012, **116**, 3428-3435.
12. M. Bassetti, G. Cerichelli and B. Floris, *Tetrahedron*, 1988, **44**, 2997-3004.
13. J. W. Bunting, J. P. Kanter, R. Nelander and Z. Wu, *Can. J. Chem.*, 1995, **73**, 1305-1311.
14. E. V. Borisov, E. V. Skorodumov, V. M. Pachevskaya and P. E. Hansen, *Magn. Reson. Chem.*, 2005, **43**, 992-998.
15. P. Gilli, V. Bertolasi, L. Pretto, V. Ferretti and G. Gilli, *J. Am. Chem. Soc.*, 2004, **126**, 3845-3855.
16. H. Matsuzawa, T. Nakagaki and M. Iwahashi, *J. Oleo Sci.*, 2007, **56**, 653-658.
17. M. Gorodetsky, Z. Luz and Y. Mazur, *J. Am. Chem. Soc.*, 1967, **89**, 1183-1189.
18. S. Mata, V. Cortijo, W. Caminati, J. L. Alonso, M. E. Sanz, J. C. López and S. Blanco, *J. Phys. Chem. A*, 2010, **114**, 11393-11398.
19. J. Gao, N. A. Seifert, J. Thomas, Y. Xu and W. Jäger, *J. Mol. Spectrosc.*, 2016, **330**, 228-235.
20. Y. Xu, J. V. Wijngaarden and W. Jäger, *Int. Rev. Phys. Chem.*, 2005, **24**, 301-338.
21. Y. Xu and W. Jäger, *J. Chem. Phys.*, 1997, **106**, 7968-7980.
22. N. A. Seifert, J. Thomas, W. Jäger and Y. Xu, *Phys. Chem. Chem. Phys.*, 2018, **20**, 27630-27637.
23. G. G. Brown, B. C. Dian, K. O. Douglass, S. M. Geyer, S. T. Shipman and B. H. Pate, *Rev. Sci. Instrum.*, 2008, **79**, 053103.
24. S. Grimme, S. Ehrlich and L. Goerigk, *J. Comput. Chem.*, 2011, **32**, 1456-1465.
25. A. D. Becke and E. R. Johnson, *J. Chem. Phys.*, 2005, **123**, 154101.
26. C. M. Western, *J. Quant. Spectrosc. Radiat. Transf.*, 2017, **186**, 221-242.
27. H. Hartwig and H. Dreizler, *Z. Naturforsch.*, 1996, **51 A**, 923-932.

28. H. B. Thompson, *J. Chem. Phys.*, 1967, **47**, 3407-3410.
29. E. R. Johnson, S. Keinan, P. Mori-Sanchez, J. Contreras-Garcia, A. J. Cohen and W. Yang, *J. Am. Chem. Soc.*, 2010, **132**, 6498-6506.
30. T. Yanai, D. P. Tew and N. C. Handy, *Chem. Phys. Lett.*, 2004, **393**, 51-57.
31. R. A. Kendall, , T. H. Dunning Jr, and R. J. Harrison, *J. Chem. Phys.* 1992, **96(9)**, 6796-6806.

Chapter 8

Further Molecular Systems I Have Explored

The molecules I have studied and described in the previous chapters are either in their keto form or their enol form. None of the studies have captured both keto and enol tautomers simultaneously. In an effort to detect both keto- and enol-tautomers of the same molecule, I have done some exploratory studies of several other molecular systems. For some of these, I did both experiments and theoretical calculations, and for others just ab initio calculations. In this chapter, I will summarise those projects.

8.1 Theoretical Calculations of the Acetone-Formic Acid Complex

In Chapters 2 and 3, I have described my studies of the rotational spectra of acetone-Ne and acetone-water complexes and discussed the reasons why their enol abundances are so small that we did not detect them. In the traditional titration of the amount of the enol form, acid is added always into the solution to shift the equilibrium towards the enol tautomer^{1,2}. I wondered whether attaching an acid into the acetone molecule would increase the amount of the enol tautomer of the acetone. Therefore, I calculated the isomers of complexes in both the keto and enol tautomers of acetone with formic acid at the level of MP2/6-311++G(2d,p) theory. Figure 8.1 shows the calculated four isomers of the acetone-formic acid complex. Their calculated corresponding rotational constants and relative energies are shown in Table 8.1. The relative energy of the enol form of the acetone-formic acid complex is still very high (~56–89 kJ/mol) compared with the most stable keto form of the complex. There are two isomers of the enol form of the acetone-formic acid complex, one isomer is shown in Figure 8.1 (c), the H-O in the formic acid is pointing vertically towards the carbon-carbon double bond, and the OH group is twisted compared with the vinyl alcohol group in the enol tautomer of acetone. The other isomer of the acetone-formic acid complex is shown in Figure 8.1 (d), even the hydrogen bonds between acetone and formic acid are almost in a plane, its relative energy is even higher compared the isomer in Figure 8.1(c). In the acetone monomer and its monohydrate, the energy difference between the keto and enol tautomers is 41 kJ/mol and 40 kJ/mol, respectively. The

value of this difference is even larger in the acetone-formic acid complex (~56–89 kJ/mol). Therefore, there is little chance for us to detect the enol tautomer, even if it is complexed with formic acid.

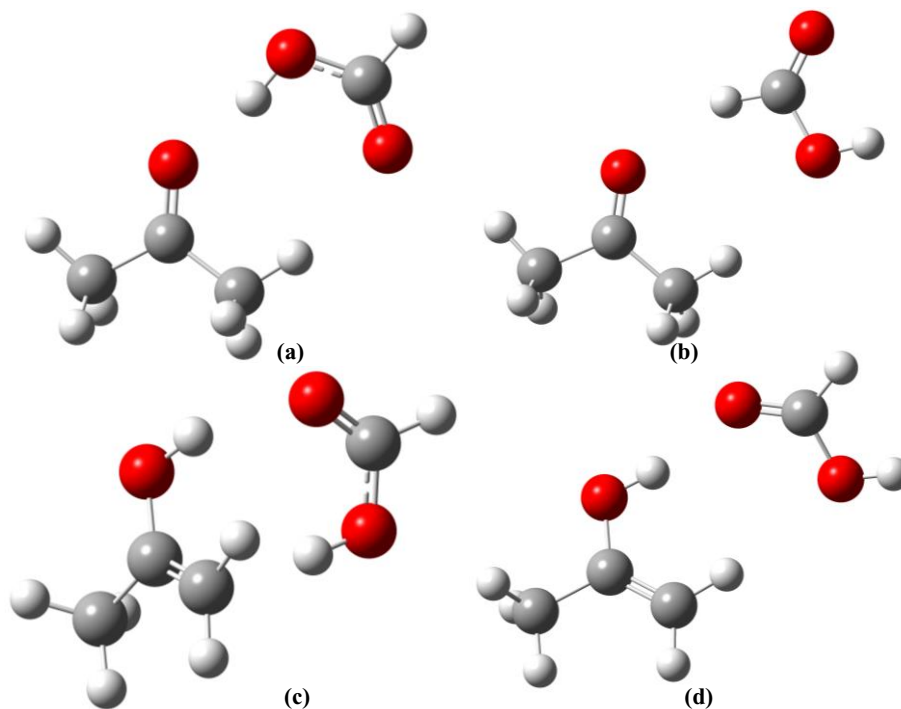


Figure 8.1. Structures of the acetone-formic acid complex.

Table 8.1. Calculated rotational constants, dipole moment components, and relative energies of four tautomeric/conformational species of the acetone-formic acid (FM) complex at the MP2/ 6-311++G(2d,p) level of theory.

complexes	Keto 1-FM	Keto 2-FM	Enol 1-FM	Enol 2-FM
A/MHz	5217.5	5791.5	4416.4	5630.3
B/MHz	1120.7	841.3	1394.3	985.6
C/MHz	943.6	741.8	1268.7	853.0
$ \mu_a /\text{D}$	3.3	4.2	0.1	5.4
$ \mu_b /\text{D}$	0.9	3.5	1.9	2.3
$ \mu_c /\text{D}$	0.4	0.1	0.4	0.7
$\Delta E/\text{kJ}\cdot\text{mol}^{-1}$	0	23.5	55.7	89.2

8.2 ^{14}N Nuclear Quadrupole Coupling in the 4-Hydroxypyrimidine Monomer and Its Water Complex

4-hydroxypyrimidine has a six-membered ring with the peptidic group ($-\text{C}=\text{O}-\text{N}-\text{H}$), which is of interest in biochemistry. The tautomeric equilibrium of the 4-hydroxypyrimidine monomer was studied by rotational spectroscopy by Caminati's group in 2007.³ They have assigned the rotational spectra of both its ketonic (4PO) and enolic forms (4HPcis). However, they did not assign the quadrupole coupling splittings due to the two nitrogen atoms in the 4-hydroxypyrimidine monomer. I am interested in whether the tautomeric equilibrium still exists when water is involved.

4-hydroxypyrimidine is a solid (Purchased from Alfa Aesar), with a melting point of 163 to 168 °C. I placed it into a stainless-steel container, and heated it to ~ 140 °C, with the nozzle temperature kept at ~ 155 °C. The setup is described in Chapter 7. I first measured the rotational spectrum of the 4-hydroxypyrimidine monomer in our cavity-based FTMW spectrometer based on the previous study,³ which listed the theoretical calculated quadrupole coupling constants. Next, I made the assignment of the quadrupole coupling splittings for both the keto and enol tautomers. The fitted rotational constants and the quadrupole coupling constants are listed in Table 8.2.

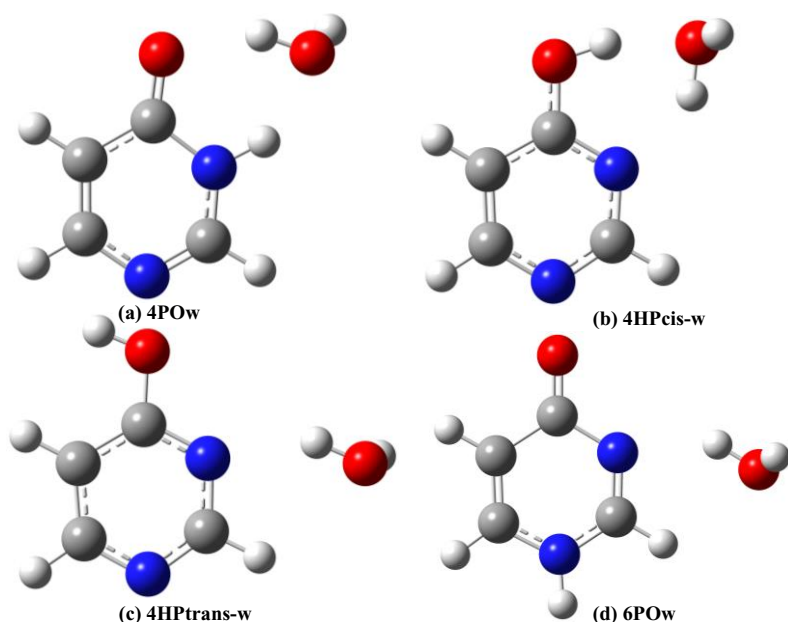


Figure 8.2. Structures of the 4-hydroxypyrimidine-water complex at the B3LYP/6-31G(d,p) level of theory.

Table 8.2. Experimental spectroscopic parameters for the keto and enol tautomers of 4-hydroxypyrimidine.

	4PO	4HPcis
A/MHz	5974.9639(129)	6173.40734(1014)
B/MHz	2807.11952(855)	2787.398259(275)
C/MHz	1910.10458(313)	1920.14083(376)
Δ_J/kHz	11.97(156)	11.28(197)
Δ_{JK}/kHz	-9.16(78)	15.45(28)
δ_j/kHz	-1.50(31)	-----
$^a \chi_{aa}(\text{N1})/\text{MHz}$	-4.160(11)	1.200(21)
$\chi_{bb-cc}(\text{N1})/\text{MHz}$	0.281(20)	-0.848(28)
$\chi_{aa}(\text{N2})/\text{MHz}$	1.562(23)	-0.747(20)
$\chi_{bb-cc}(\text{N2})/\text{MHz}$	3.858(30)	-0.260(30)
N	41	21
σ/kHz	9.0	9.9

^a Quadrupole coupling constants for nitrogen atom. Nitrogen N1 is at the bottom of the six membered ring as shown in Figure 8.2 (a) and (b).

To study the effect of water on the tautomeric equilibrium of 4-hydroxypyrimidine, I calculated the isomers of the 4-hydroxypyrimidine-water complex using different methods, including B3LYP, B3LYP-D3BJ, and MP2 methods. I used the first and third methods for the monomer calculations. Use of the B3LYP-D3BJ method is described in Chapters 5–7. The resulting structures of the isomers are shown in Figure 8.2, and their calculated corresponding rotational constants, dipole moment components, and relative energies are given in Table 8.3. The calculations indicate that the 4POw isomer (Figure 8.2(a)) is the most stable one. In this isomer, the hydrogen bonds with water (C=O...H-O(water)...H-N(C=O)) form a six-membered ring. The relative DFT energies of the enol tautomer, 4HPcis, with water (Figure 8.2(b)) are quite different from those obtained with the MP2 method. The relative energy of 4HPcis-w is 6.0 kJ/mol using the B3LYP method and 9.8 kJ/mol using the B3LYP-D3BJ

method, whereas the energy is 2.5 kJ/mol using the MP2 method. MP2 does not seem a good theoretical method to calculate such a molecular system with a six-membered ring, which has been mentioned in the rotational spectra study of the 4-hydroxypyrimidine monomer³ and also in the cyclohexanone-water complex study in Chapter 5. Based on the previous molecular systems I have studied, B3LYP-D3BJ is a reliable method to calculate both the rotational constants and relative energies.

Table 8.3. Calculated rotational constants, dipole moment components, and relative energies of four tautomeric/conformational species of the 4-hydroxypyrimidine monohydrated complexes at the B3LYP/6-31G(d,p), MP2/6-311++G(2d, p), and B3LYP-D3BJ/aug-cc-pVDZ levels of theory.

^a complexes	4POw	4HPcis-w	4HPtrans-w	6POw
<i>A</i> /MHz	4005.2	4187.3	2750.1	2805.3
<i>B</i> /MHz	1441.5	1428.1	1531.6	1515.2
<i>C</i> /MHz	1063.2	1068.3	986.9	986.7
$ \mu_a /D$	0.3	0.4	4.8	3.1
$ \mu_b /D$	0.9	0.0	2.5	6.3
$ \mu_c /D$	1.4	1.5	1.4	1.3
$\Delta E/kJ \cdot mol^{-1}$	0	6.0	57.3	63.6
^b complexes	4POw	4HPcis-w	4HPtrans-w	6POw
<i>A</i> /MHz	4036.4	4162.9	2850.1	4238.3
<i>B</i> /MHz	1427.7	1415.5	1479.1	1271.1
<i>C</i> /MHz	1056.1	1058.5	974.9	978.5
$ \mu_a /D$	0.2	0.4	4.5	6.7
$ \mu_b /D$	1.5	0.4	3.8	4.1
$ \mu_c /D$	1.1	1.4	0.8	0.6
$\Delta E/kJ \cdot mol^{-1}$	0	2.5	39.0	48.8
^c complexes	4POw	4HPcis-w	4HPtrans-w	6POw
<i>A</i> /MHz	4090.6	4168.3	2965.6	2863.4
<i>B</i> /MHz	1431.2	1436.2	1464.1	1510.5
<i>C</i> /MHz	1062.0	1070.6	981.3	988.8
$ \mu_a /D$	0.3	0.4	4.1	6.7
$ \mu_b /D$	1.0	0.1	4.2	4.1
$ \mu_c /D$	1.1	1.3	0.1	0.6
$\Delta E/kJ \cdot mol^{-1}$	0	9.8	45.8	50.0

^aCalculated at the B3LYP/6-31G(d,p) level of theory.

^bCalculated at the MP2/6-311++G(2d,p) level of theory.

^cCalculated at the DFT-D3BJ/aug-cc-pVDZ level of theory.

I have tried several times to search for the most stable isomer of the 4-hydroxypyrimidine-water complex using the cavity-based FTMW spectrometer; unfortunately, not successfully. I also tried it with our new chirped-pulse FTMW spectrometer in the range of 2–6 GHz but still could not get an assignment for the water complex. One possible reason is that the two nitrogen atoms in the 4-hydroxypyrimidine monomer cause quadrupole coupling splittings in the rotational transitions, which lower the intensity of the rotational transitions significantly.

8.3 Theoretical Calculations of the Dibenzoylmethane Monomer

The β -diketones are a type of molecule with two carbonyl groups ($R_1-C=O-CH_2-O=C-R_2$), which can undergo keto-enol tautomerization. In Chapters 6 and 7, I describe the rotational spectra of the acetylacetone-water complex ($R_1 = R_2 = CH_3$), the benzoylacetone monomer ($R_1 = C_6H_5$, $R_2 = CH_3$), and its monohydrate water complex. Dibenzoylmethane (DBM) is another molecule in the category of β -diketones where $R_1 = R_2 = C_6H_5$, so that no methyl internal rotation tunneling is expected, and the spectra will be simplified compared with the acetylacetone. I first calculated the rotational constants and relative energies of different conformational isomers of keto-enol tautomerization, as shown in Table 8.4. One enol form (enol form 2, Figure 8.3 (b)) and two keto forms were local minimum-energy conformations for the absence of imaginary harmonic frequencies.

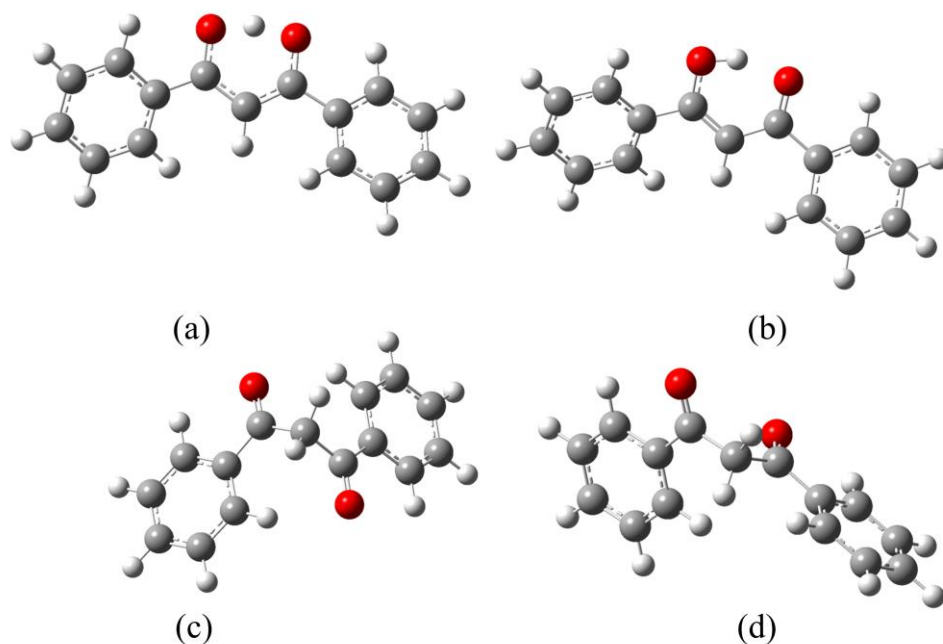


Figure 8.3. Structures of the dibenzoylmethane (DBM) monomer, (a) Enol 1; (b) Enol 2; (c) Keto 1; (d) Keto 2.

Table 8.4. Calculated rotational constants, dipole moment components, and relative energies of three tautomeric/conformational species and one special enol form (Enol 1) of the dibenzoylmethane (DBM) monomer at the MP2/cc-pVDZ level of theory.

monomer	^a Enol 1	Enol 2	Keto 1	Keto 2
<i>A</i> /MHz	1349.2	1292.9	1015.8	984.5
<i>B</i> /MHz	200.1	199.1	241.2	257.1
<i>C</i> /MHz	174.9	175.5	218.7	236.7
$ \mu_a /\text{D}$	0.0	0.5	2.8	0.0
$ \mu_b /\text{D}$	0.0	3.7	3.3	0.0
$ \mu_c /\text{D}$	3.8	0.1	3.1	0.5
$\Delta E/\text{kJ}\cdot\text{mol}^{-1}$	0	1.6	8.8	-0.8

^aThis enol 1 has one imaginary frequency with the proton in the middle of two C=O groups.

Based on previous studies of acetylacetone-water complex (Chapter 6) and benzoylacetone monomer and its monohydrate (Chapter 7), the detected structures of the β -diketones using microwave spectroscopy are all related to the transition state of the C_s enol form, i. e., the proton is in the middle of the two carbonyl groups. Therefore, I also calculated the enol form, in which the proton is in the center between the two carbonyl groups, and theoretical calculation suggests the two phenyl groups in this enol form of the DBM monomer are not in one plane. This enol form (enol form 1, Figure 8.3 (a)) has one imaginary frequency related to the vibration of the center proton back and forth between the two carbonyl groups. Figure 8.3 shows those four structures of the DBM monomer. The melting point of the DBM solid is 77–78 °C. I examined the molecule both in the cavity-based FTMW and chirped-pulse FTMW spectrometers in the range of 8–18 GHz, but could not get the signal of molecular rotational transitions.

8.4 Theoretical Calculations of the Ethyl Benzoylacetone Monomer

The structure of the ethyl benzoylacetone monomer is very similar to that of benzoylacetone, the only difference is that the methyl group in benzoylacetone is replaced by the $-O-CH_2-CH_3$ group. Figure 8.4 displays one enol tautomer and two keto tautomers in the ethyl benzoylacetone monomer that were obtained using calculations at the B3LYP-D3BJ/aug-cc-pVDZ level of theory. Their corresponding rotational constants and relative energies are listed in Table 8.5. The calculated results show that the enol tautomer is the most stable isomer, while the other two (keto) isomers have very high relative energies of 18.0–19.4 kJ/mol. This means that the relative abundance of the keto form is in the range of 0.04% to 0.07%, assuming room temperature and a Boltzmann distribution. Based on our previous studies, this is too small an abundance to be detectable.

Table 8.5. Calculated rotational constants, dipole moment components, and relative energies of three tautomeric/conformational species of the ethyl benzoylacetone monomer at the B3LYP-D3BJ/aug-cc-pVDZ level of theory.

monomer	Enol	Keto 1	Keto 2
A/MHz	2083.9	2268.3	1839.1
B/MHz	275.6	278.3	286.3
C/MHz	244.7	265.6	276.0
$ \mu_a /\text{D}$	0.1	2.0	2.2
$ \mu_b /\text{D}$	2.1	2.2	0.4
$ \mu_c /\text{D}$	0.2	2.1	3.0
$\Delta E/\text{kJ}\cdot\text{mol}^{-1}$	0	19.4	18.0

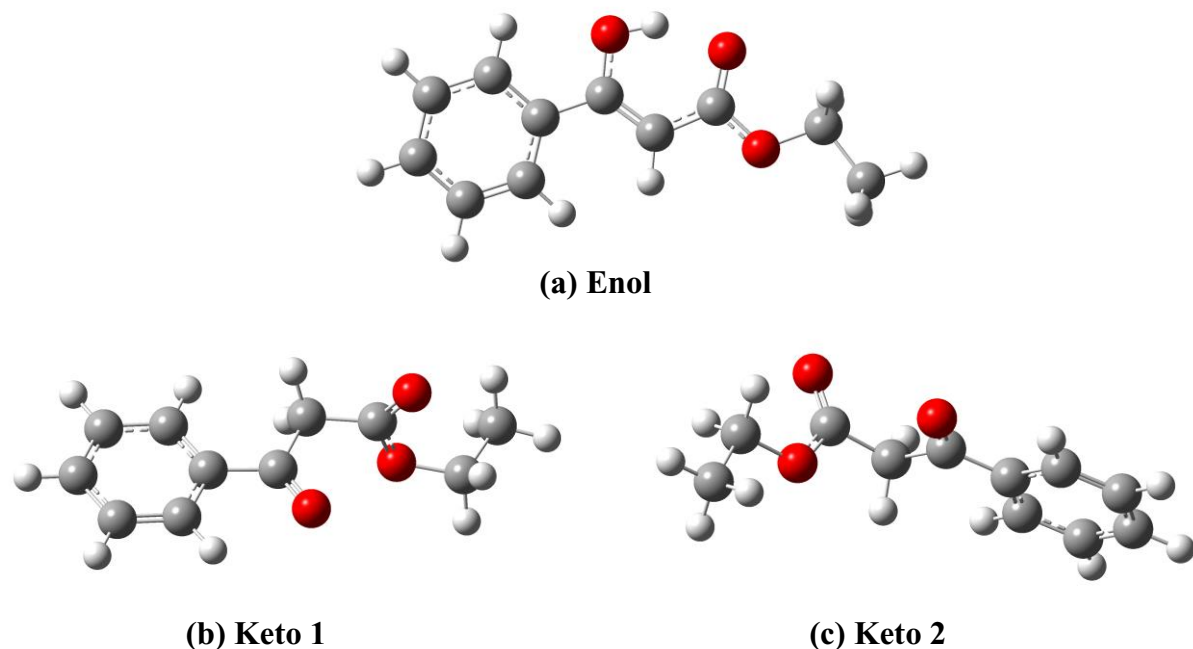


Figure 8.4. Structures of the ethyl benzoylacetone monomer.

8.5 Theoretical Calculations of the 2-Acetylcyclohexanone Monomer

The structure of the 2-acetylcyclohexanone monomer is very similar to that of acetylacetone. In the study of the rotational spectra of the acetylacetone monomer and its monohydrate, the MP2 method proved to be a good method to predict the rotational constants and the relative energies. Therefore, I only used the MP2 method to calculate the isomers of this 2-acetylcyclohexanone monomer. The predicted structures are shown in Figure 8.5. There are two enol tautomers (Figure 8.5 (a) and (b)) and one keto tautomer (Figure 8.5 (c)). Their corresponding rotational constants and relative energies are listed in Table 8.6. The enol form is the most stable isomer, and the keto tautomer has a higher relative energy of 11.4 kJ/mol than the most stable isomer. The relative abundance of the keto form is 1.0%, according to the Boltzmann distribution.

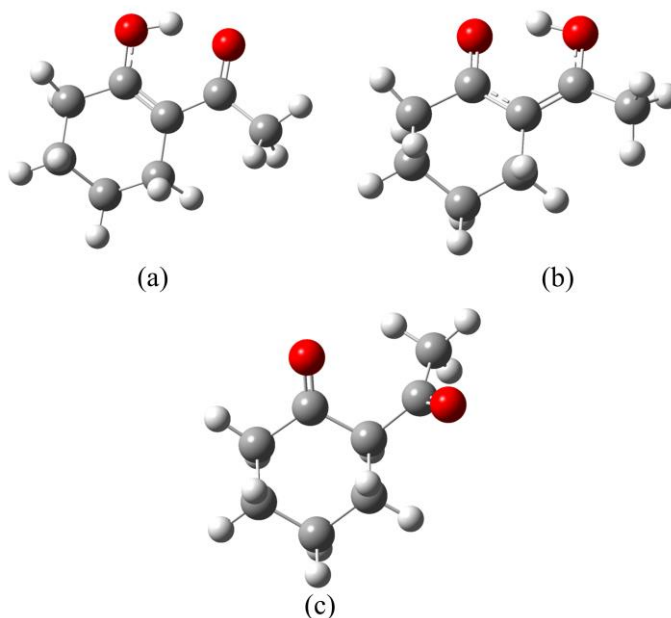


Figure 8.5. Structures of the 2-acetylcyclohexanone monomer.

Table 8.6. Calculated rotational constants, dipole moment components, and relative energies of three tautomeric/conformational species of the 2-acetylcyclohexanone monomer at the B3LYP-D3BJ/aug-cc-pVDZ level of theory.

monomer	Enol 1	Enol 2	Keto 1
A/MHz	2242.91	2131.65	2242.91
B/MHz	1039.60	1112.91	1039.60
C/MHz	818.21	759.26	818.21
$ \mu_a /\text{D}$	3.09	1.64	3.09
$ \mu_b /\text{D}$	0.34	3.77	0.34
$ \mu_c /\text{D}$	3.92	0.16	3.92
$\Delta E/\text{kJ}\cdot\text{mol}^{-1}$	0	6.5	11.4

8.6 Theoretical Calculations of the 1,3-Cyclohexanedione-Water Complex

The 1,3-cyclohexanedione monomer has been studied using microwave spectroscopy by Caminati's group.⁴ The structure of 1,3-cyclohexanedione is very similar to that of

cyclohexanone, except that 1,3-cyclohexanedione has two carbonyl groups in the hexane ring. In the monomer study of 1,3-cyclohexanedione, the chair-diketo and boat-diketo isomers have been detected. The enol tautomers of the monomer were not observed in the rotational spectroscopic study. I wondered whether we could observe both keto and enol tautomers when water is involved. The reason is that one enol tautomer has an energy of 7.7 kJ/mol higher than the most stable keto tautomer, based on theoretical calculations of the monomer. The relative abundance of the enol form would be 4.3%, according to a Boltzmann distribution. This abundance is the highest in all of the molecular monomers that I have studied.

I first calculated the rotational constants and relative energies of different conformational isomers of the complex using both the MP2 and DFT-D3BJ method. The calculated results are shown in Table 8.7. For the monomer, there is one diketo form (Figure 8.6 (a)), and there are two keto-enol forms, the cis-keto-enol tautomer (Figure 8.6 (b)), in which the aldehyde group (C=O-H) points towards to the C=O group, and for the trans-keto-enol tautomer (Figure 8.6 (c)), the aldehyde group (C=O-H) points away from the second C=O. Water can form hydrogen bonds at different sites of the C=O or C=O-H groups, and there are many possibilities to form different isomers of the 1,3-cyclohexanedione-water complex.

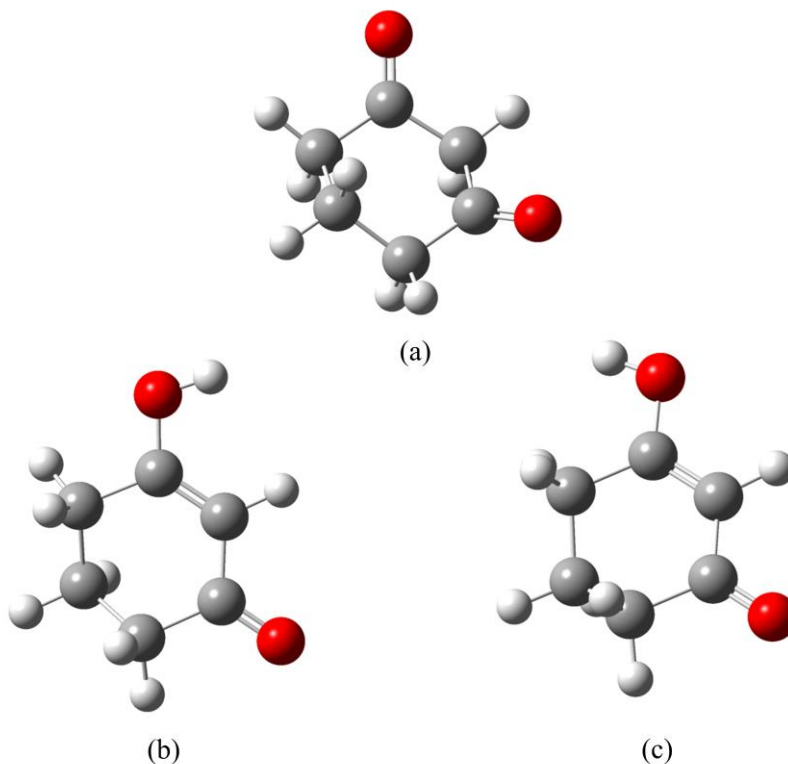


Figure 8.6. Structures of the 1,3-cyclohexanedione monomer.

Table 8.7. Calculated rotational constants, dipole moment components, and the relative energies of seven tautomeric/conformational species of the 1, 3-cyclohexanedione monohydrated complexes at the MP2/6-311++G(2d,p) and B3LYP-D3BJ/aug-cc-pVDZ levels of theory.

^a complex	Diketo 1	Diketo 2	<i>Cis</i> - ketoenol 1	<i>Cis</i> - ketoenol 2	<i>Trans</i> - ketoenol 1	<i>Trans</i> - ketoenol 2	<i>Trans</i> - ketoenol 3
<i>A</i> /MHz	2877.2	2133.5	2057.6	3301.3	2074.8	3301.8	3290.8
<i>B</i> /MHz	883.2	1077.6	1111.3	828.4	1079.9	829.9	800.1
<i>C</i> /MHz	739.5	759.0	739.4	676.5	728.2	677.6	659.1
$ \mu_a /D$	0.5	3.1	3.4	4.3	6.2	5.2	8.1
$ \mu_b /D$	1.7	3.3	0.1	0.0	0.6	2.5	3.0
$ \mu_c /D$	2.1	0.9	0.2	0.2	0.3	0.1	0.5
$\Delta E/kJ/mol$	0	2.3	-0.6	2.2	10.0	8.9	8.8
^b complex	Diketo 1	Diketo 2	<i>Cis</i> - ketoenol 1	<i>Cis</i> - ketoenol 2	<i>Trans</i> - ketoenol 1	<i>Trans</i> - ketoenol 2	<i>Trans</i> - ketoenol 3
<i>A</i> /MHz	2641.8	2137.5	3301.5	2057.2	2048.6	3296.5	2080.5
<i>B</i> /MHz	928.3	1082.1	826.2	1117.8	1093.6	828.3	1030.9
<i>C</i> /MHz	788.7	767.0	676.2	741.8	731.7	677.3	708.2
$ \mu_a /D$	0.1	3.2	4.1	3.4	6.5	5.0	0.8
$ \mu_b /D$	1.8	3.4	0.2	0.1	0.7	2.9	7.6
$ \mu_c /D$	2.9	1.2	0.2	0.8	0.7	0.1	1.2
$\Delta E/kJ/mol$	0	2.3	11.6	8.6	20.2	18.8	33.4

^aCalculated at the MP2/6-311++G (2d, p) level of theory.

^bCalculated at the B3LYP-D3BJ/aug-cc-pVDZ level of theory.

Figure 8.7 shows all seven structures of the 1, 3-cyclohexanedione-water complex calculated at B3LYP-D3BJ/aug-cc-pVDZ level of theory. The relative energies are quite different in some isomers when comparing the results from different theoretical methods. For

example, the energies of the keto-enol tautomer-water complexes are all above 8 kJ/mol, some even ~20 kJ/mol higher than that of the most stable isomer using the MP2 method. In contrast, all the isomers of the keto-enol tautomer-water complexes have energies of ~10 kJ/mol (most are below 10 kJ/mol) higher than that of the most stable isomer when using the B3LYP/D3BJ method. According to the monomer study⁴ and our previous studies described in Chapters 5–7, B3LYP-D3BJ is a reliable method to calculate the rotational constants. Therefore, I only analyzed the structures calculated by the B3LYP-D3BJ method. As shown in Table 8.7, one isomer of the keto-enol tautomer-water complexes is the most stable one (Figure 8.7 (c)), and the diketo tautomer-water (Figure 8.7 (a)) complex has an energy of ~0.6 kJ/mol higher than this isomer. This means that the diketo tautomer can convert into the ketoenol tautomer when one water molecule is involved, which increases our opportunity to detect the enol form in the 1, 3-cyclohexanedione-water complex experimentally.

We have performed experiments on the 1, 3-cyclohexanedione-water complex using the chirped-pulse FTMW spectrometer in the range of 2–6 GHz. The analysis of the spectra is ongoing.

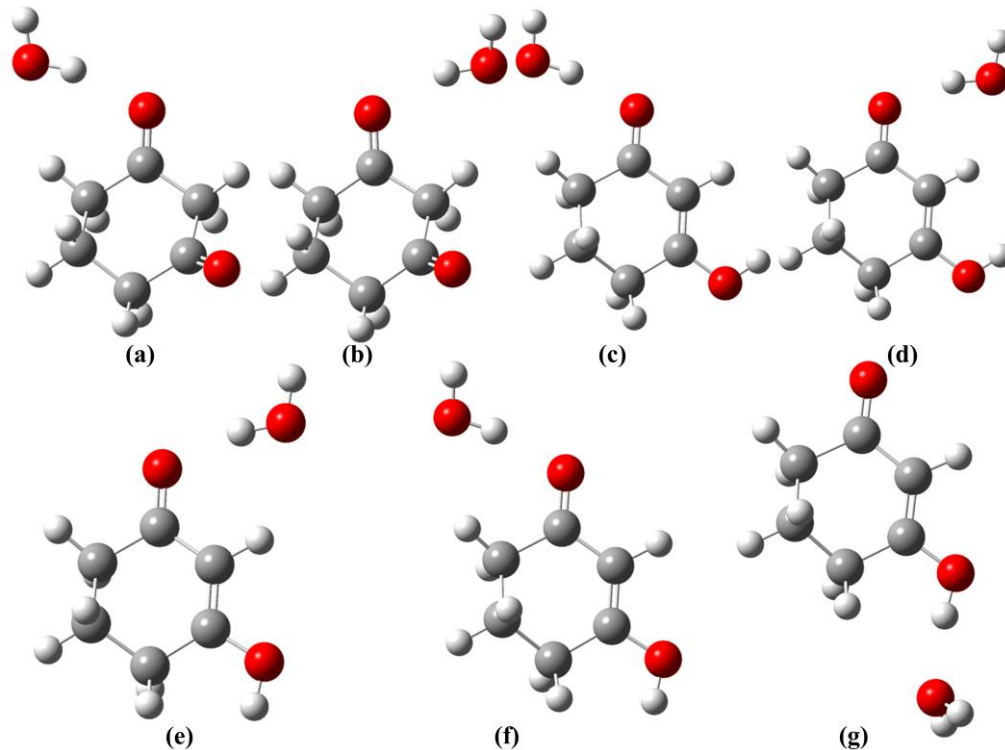


Figure 8.7. Structures of the 1,3-cyclohexanedione–water complexes: (a) Diketo 1; (b) Diketo 2; (c) *Cis*-ketoenol 1; (d) *Cis*-ketoenol 2; (e) *Trans*-ketoenol 1; (f) *Trans*-ketoenol 2; (g) *Trans*-ketoenol 3.

References

1. Y. Chiang, A. Kresge and N. Schepp, *J. Am. Chem. Soc.*, 1989, **111**, 3977-3980.
2. Y. Chiang, A. J. Kresge, Y. S. Tang and J. Wirz, *J. Am. Chem. Soc.*, 1984, **106**, 460-462.
3. R. Sanchez, B. M. Giuliano, S. Melandri, L. B. Favero and W. Caminati, *J. Am. Chem. Soc.*, 2007, **129**, 6287-6290.
4. C. Calabrese, A. Maris, L. Evangelisti, L. B. Favero, S. Melandri and W. Caminati, *J. Phys. Chem. A*, 2013, **117**, 13712-13718.

Chapter 9

Conclusions

In this thesis, I have investigated several prototype molecules that can undergo keto-enol tautomerization and the catalytic role of H₂O molecules on the tautomerism of neutral molecules using chirped-pulse and cavity-based Fourier transform microwave spectroscopy. The significant results of my thesis, which provide a deeper understanding of the catalytic role of a single water molecule on keto-enol tautomerism both experimentally and theoretically, and of the influence of microsolvation on the keto-enol tautomerization equilibrium of neutral molecules, are summarized as follows.

In Chapters 3 and 4, I explored how water affects the keto-enol tautomerization of acetone using microwave spectroscopy. In order to assign the rotational spectrum of the acetone-water complex, I first investigated the microwave spectrum of the acetone-Ne van der Waals complex in Chapter 3. In this study, the rotational spectrum was found to be complicated by splittings arising from the internal rotation of two high-barrier methyl rotors. The spectrum was fully assigned with the help of ab initio calculations and by constructing closed frequency loops. The two methyl groups were found to be equivalent, as evidenced by the splitting of each transition into four components. High-level [CCSD(T)] ab initio calculations suggest that the Ne atom lies directly above the plane formed by the carbonyl group and the two carbon-carbon bonds in the equilibrium configuration. In Chapter 4, I describe the assignment of rotational transitions observed for the keto tautomer of the acetone-water complex and the acetone-D₂O complex. I found that increased stabilization of the carbonyl group makes the internal rotation barrier lower when forming an acetone-water complex compared with the acetone monomer when rotating the “free” methyl group (i.e. not the hydrogen bonded methyl group). The electronic populations shift more from the C₉=O₁₀ moiety in the acetone-water complex than in the acetone monomer when the methyl group rotates, leading to a lower barrier height in the acetone-water complex. Furthermore, the larger stabilization of both the C=O and the rotating methyl group makes the rotational barrier of the hydrogen bonded methyl group even lower compared to the “free” methyl group. Unfortunately, I did not succeed in finding

the enol form of acetone in its hydrated form because its abundance is so low (0.0003%) that I could not detect it.

In Chapter 5, I explored the keto-enol tautomeric and conformational changes of the cyclohexanone monomer and its monohydrate by Fourier-transform microwave spectroscopy and ab initio calculations. I determined structures and relative energies of four keto tautomer-water complexes and four enol tautomer-water complexes using ab initio calculations. The experimental and theoretical results suggest that the chair conformer of the keto tautomer is the most stable structure. I measured and assigned the rotational spectra of ten isotopologues, where four of them have been obtained from different isotopic species of water (H_2O , D_2O , DOH , and HOD) (D in DOH or HOD is hydrogen bonded with the $\text{C}=\text{O}$ group) and the remaining six are singly substituted ^{13}C species of cyclohexanone, observed in their natural abundances. The heavy atom structure of cyclohexanone-water was determined directly using this isotopic information, revealing that both canonical and secondary hydrogen bonding exist using QTAIM analyses. The results in this study improve our understanding of hydration on the kinetics of keto-enol tautomerism. Cyclohexanone complexed with a single water molecule mainly decreases the barrier of the keto-enol tautomerization compared with its monomer. However, the enol tautomer was not detected in the experiments, and my calculations also suggest that increasing the number of water molecules complexed with a keto species may still not improve our chances of observing the enol species in larger cyclohexanone-water clusters.

In Chapter 6, I studied the process of keto-enol tautomerization of the acetylacetone-water complex; acetylacetone is the prototype molecule of this tautomerization. Aided by ab initio calculations, two enol tautomer-water complexes and three keto tautomer-water complexes were obtained. In the experiment, I observed only the enol form of the acetylacetone-water complex. The barrier to internal rotation of the methyl group involved in hydrogen bonding in the complex was determined from the double splittings of the rotational transitions. I did not observe the diketo form of acetylacetone.

In Chapter 7, I investigated the rotational spectra of the benzoylacetone monomer and its monohydrate. The calculated results show that each keto tautomer has two isomers and each enol tautomer also has two isomers in the benzoylacetone monomer. The experimental and theoretical results suggest that the two enol tautomers are more stable than the others. The fitted methyl internal rotation barrier of the benzoylacetone monomer indicates that the

monomer structure is a weighted average of these two enol tautomers, i.e., the proton is in the middle position of the two carbonyl groups. In the deuterated form of the benzoylacetone monomer shows that benzoylacetone falls into enol form I, which also is the most stable isomer of the enol tautomer as its internal rotation splittings are much smaller than that in the normal benzoylacetone monomer. These results suggest that the proton transfer motion between the two carbonyl groups in the benzoylacetone monomer is coupled with the internal rotation of the methyl group. Furthermore, two conformers of the benzoylacetone-water complex were detected using the chirped-pulse Fourier-transform microwave spectrometer. The structures of these two conformers suggest that both isomers of the enol tautomer of benzoylacetone exist in its complexes with water. As water is not just hydrogen bonded with different sites of one enol tautomer, each conformer contains different enol tautomers; this further confirms that two enol tautomers should coexist in its monomer.

In Chapter 8, I summarized some projects I have attempted by experiment or theoretical calculations. In the rotational spectroscopic study of the acetone-water complex, I did not detect the enol form of acetone, even one water molecule could lower the barrier between keto and enol form, but the abundance of the enol acetone in its water complex is still quite low. I also have performed theoretical calculation on the acetone-formic acid complex; however, the enol form of acetone in this complex has a very high energy (~ 56 kJ/mol) compared with its keto form, therefore, it also is difficult for us to detect the enol form. In the microwave spectra study of acetylacetone and its water complex, the enol form of acetylacetone is detected; the abundance of the diketo form is $\sim 1.74\%$, too low to detect it. Then, I tried some molecules with a similar structure to acetylacetone (also called β -diketones), including dibenzoylmethane, ethyl benzoylacetone, and 2-acetylcyclohexaneone using theoretical calculations, but the relative energy of the diketo form in all of them is very high compared with the most stable enol form. I measured the rotational spectra of the 4-hydroxypyrimidine monomer and its water complex, and I detected both the keto and enol tautomers for the monomer but could not detect the signal of the 4-hydroxypyrimidine-water complex. One of the possible reasons is that there are two nitrogen atoms in the 4-hydroxypyrimidine monomer, which would result in complicated quadrupole coupling splittings in the rotational spectrum of the water complex. As a result, the intensity of the rotational transitions would be weakened significantly. Lastly, I have calculated the possible conformers and tautomers of the 1, 3-cyclohexanedione-water

complex. It is interesting to notice that the enol form of the 1, 3-cyclohexanedione-water complex becomes more stable than the keto form, whereas the keto form is more stable than the enol form in the monomer of 1, 3-cyclohexanedione. This means that water plays not only an important catalytic role in the keto-enol tautomerization equilibrium, but that it also shifts the equilibrium to the enol form. We have performed the experiment on the 1, 3-cyclohexanedione-water complex using the chirped-pulse FTMW spectrometer in the range of 2–6 GHz. The analysis of the spectra is ongoing.

From all the projects studied in this thesis, we conclude that: firstly, in almost all the molecules I studied, a single water molecule can lower the barrier of the keto-enol tautomerism significantly and plays thus an important role in catalyzing the keto-enol tautomerism. Secondly, a secondary hydrogen bond is crucial because it not only stabilizes the keto \rightleftharpoons enol transition state, but also it can also stabilize the “transition state” during methyl group rotation, thus lowering the methyl internal rotation barrier (in acetone-water, for example). Lastly, studying the internal rotation splitting is vital when determining the exact molecular structure, for example, in the benzoylacetone case, analysis of internal rotation tunneling splittings of the methyl group in the molecule helped us to identify the experimental structure by considering the coupling between methyl internal rotation and proton transfer motion.

In this thesis, I only studied how a single water molecule affects the keto-enol tautomerization. However, one water molecule is still not enough to shift the equilibrium sufficiently to the less stable form to allow spectroscopic detection in most of the systems I have studied. Since the barrier of the keto-enol tautomerization is still too high to let the more stable form interconvert into the less stable form for some molecules, future work, on one hand, can be focused on applying external excitation sources (for example, laser) to help the less stable form to cross the barrier. On the other hand, future focus can be centered on determining how the keto-enol equilibrium shifts when more water molecules are added to our target molecules to form larger clusters. The energy difference will be smaller in larger water clusters between keto and enol tautomers in most cases.

Bibliography

- I. Lukovits, J. Fodor, Á. Gömöry, K. István, G. Keresztury and L. Kótai, *SAR QSAR Environ. Res.*, 2006, **17**, 323-335.
- C. Dugave and L. Demange, *Chem. Rev.*, 2003, **103**, 2475-2532.
- C. S. Cucinotta, A. Ruini, A. Catellani and A. Stirling, *ChemPhysChem*, 2006, **7**, 1229-1234.
- E. P. Kündig, A. Enríquez García, T. Lomberget and G. Bernardinelli, *Angew. Chem. Int. Ed.*, 2006, **45**, 98-101.
- W. Wang, H. W. Hellinga and L. S. Beese, *Proc. Natl. Acad. Sci.*, 2011, **108**, 17644-17648.
- O. K. Abou-Zied, R. Jimenez and F. E. Romesberg, *J. Am. Chem. Soc.*, 2001, **123**, 4613-4614.
- J. D. Watson and F. H. Crick, *Nature*, 1953, **171**, 964-967.
- H. Grebneva, *J. Mol. Struct.*, 2003, **645**, 133-143.
- J. McConnell, B. Sharma and R. Marsh, *Nature*, 1964, **203**, 399.
- T. Steiner and G. Koellner, *Chem. Commun.*, 1997, **13**, 1207-1208.
- M. Kubicki, *Acta Crystallogr., Sect. B: Struct. Sci.*, 2004, **60**, 191-196.
- Z. H. Wu, J. P. Ma, X. W. Wu, R. Q. Huang and Y. B. Dong, *Acta Crystallogr., Sect. C: Cryst. Struct. Commun.*, 2009, **65**, 0128-0130.
- H. Brandstetter, F. Grams, D. Glitz, A. Lang, R. Huber, W. Bode, H.-W. Krell and R. A. Engh, *J. Biol. Chem.*, 2001, **276**, 17405-17412.
- K. Senthilkumar and P. Kolandaivel, *J. Comput. Aided Mol. Des.*, 2002, **16**, 263-272.
- A. R. Katritzky, C. D. Hall, B. E.-D. M. El-Gendy and B. Draghici, *J. Comput. Aided Mol. Des.*, 2010, **24**, 475-484.
- Y. C. Martin, *J. Comput. Aided Mol. Des.*, 2009, **23**, 693.
- P. Pospisil, P. Ballmer, L. Scapozza and G. Folkers, *J. Recept. Signal Transduct.*, 2003, **23**, 361-371.
- X. Yan, P. Day, T. Hollis, A. F. Monzingo, E. Schelp, J. D. Robertus, G. Milne and S. Wang, *Proteins: Struct., Funct., Bioinf.*, 1998, **31**, 33-41.
- L. Gorb and J. Leszczynski, *J. Am. Chem. Soc.*, 1998, **120**, 5024-5032.
- D. Ivanova, V. Deneva, D. Nedeltcheva, F. S. Kamounah, G. Gergov, P. E. Hansen, S. Kawauchi and L. Antonov, *RSC Adv.*, 2015, **5**, 31852-31860.
- J. Šponer, J. Leszczynski and P. Hobza, *J. Phys. Chem.*, 1996, **100**, 1965-1974.
- A. L. Lehninger, D. L. Nelson, M. M. Cox, *Lehninger Principles of Biochemistry*, Worth Publishers, New York, 2000.
- W. Stumm, J. J. Morgan, *Aquatic Chemistry, Chemical Equilibria and Rates in Natural Waters*, 3rd ed. Wiley, New York, 1996.
- P. M. Wiggins, *Microbiol. Rev.*, 1990, **54**, 432-449.
- Y. Matsuda, A. Yamada, K. i. Hanaue, N. Mikami and A. Fujii, *Angew. Chem.*, 2010, **122**, 5018-5021.

- M. W. Wong, K. B. Wiberg and M. J. Frisch, *J. Am. Chem. Soc.*, 1992, **114**, 1645-1652.
- G. Alagona, C. Ghio and P. I. Nagy, *Phys. Chem. Chem. Phys.*, 2010, **12**, 10173-10188.
- M. Kabeláč, and P. Hobza, *Phys. Chem. Chem. Phys.*, 2007, **9**, 903–917.
- P. I. Nagy, *Biochem. Pharmacol.*, 2013, **S4**, 2167-0501.
- S. Mata, V. Cortijo, W. Caminati, J. L. Alonso, M. E. Sanz, J. C. López and S. Blanco, *J. Phys. Chem. A*, 2010, **114**, 11393-11398.
- Y. Chiang, A. Kresge and N. Schepp, *J. Am. Chem. Soc.*, 1989, **111**, 3977-3980.
- J. L. Burdett and M. T. Rogers, *J. Am. Chem. Soc.*, 1964, **86**, 2105-2109.
- T. J. Zielinski and A. Grushow, *J. Chem. Educ.*, 2002, **79**, 707.
- J. W. Bunting, J. P. Kanter, R. Nelander and Z. Wu, *Can. J. Chem.*, 1995, **73**, 1305-1311.
- A. Andreassen and S. Bauer, *J. Mol. Struct.*, 1972, **12**, 381-403.
- K. Iijima, A. Ohnogi and S. Shibata, *J. Mol. Struct.*, 1987, **156**, 111-118.
- S. A. Broadbent, L. A. Burns, C. Chatterjee and P. H. Vaccaro, *Chem. Phys. Lett.*, 2007, **434**, 31-37.
- M. A. Rios and J. Rodríguez, *J. Mol. Struct. THEOCHEM*, 1990, **204**, 137-144.
- J. Dannenberg and R. Rios, *J. Phys. Chem.*, 1994, **98**, 6714-6718.
- W. Caminati and J.-U. Grabow, *J. Am. Chem. Soc.*, 2006, **128**, 854-857.
- N. V. Belova, H. Oberhammer, N. H. Trang and G. V. Girichev, *J. Org. Chem.*, 2014, **79**, 5412-5419.
- V. Feyer, K. C. Prince, M. Coreno, S. Melandri, A. Maris, L. Evangelisti, W. Caminati, B. M. Giuliano, H. G. Kjaergaard and V. Carravetta, *J. Phys. Chem. Lett.*, 2018, **9**, 521-526.
- P. F. Bernath, in *Spectra of Atoms and Molecules*, ed. D. G. Truuhlar, Oxford University Press, New York, 1995, ch. 6, pp.159-194.
- W. Gordy, R. L. Cook, *Microwave Molecular Spectra*, John Wiley & Sons, New York, 1984.
- J. C. McGurk and W. H. Flygare, *J. Chem. Phys.*, 1973, **59**, 5742-5743.
- T. G. Schmalz, W. H. Flygare, *Laser and Coherence Spectroscopy*, ed. J. I. Steinfeld, Plenum, New York, 1978, pp. 125-196.
- H. Dreizler, *Mol. Phys.*, 1986, **59**, 1-28.
- Blum, K., *Density matrix theory and applications*, Springer Science & Business Media, Berlin Heidelberg, 2012.
- Von Neumann, J., *Wahrscheinlichkeitstheoretischer aufbau der quantenmechanik*. Nachrichten von der Gesellschaft der Wissenschaften zu Göttingen, Mathematisch-Physikalische Klasse, 1927, pp.245-272.
- Y. Wu and X. X. Yang, *Phys. Rev. Lett.*, 2007, **98**, 013601.
- Allen, L. and Eberly, J.H., *Optical resonance and two-level atoms*. Courier Corporation, 2012.
- Arecchi, F. and Bonifacio, R., *Theory of optical maser amplifiers*. IEEE Journal of Quantum Electronics, vol. 1, 1965, pp.169-178.
- K. B. McAfee, R. H. Hughes and E. B. Wilson, *Rev. Sci. Instrum.*, 1949, **20**, 821-826.
- R. H. Hughes and E. B. Wilson, *Phys. Rev.*, 1947, **71**, 562-563.
- N. L. Owen, *J. Mol. Struct.*, 1970, **6**, 37-47.

- T. J. Balle, E. J. Campbell, M. R. Keenan and W. H. Flygare, *J. Chem. Phys.*, 1979, **71**, 2723-2724.
- T. J. Balle, E. J. Campbell, M. R. Keenan and W. H. Flygare, *J. Chem. Phys.*, 1980, **72**, 922-932.
- T. J. Balle and W. H. Flygare, *Rev. Sci. Instrum.*, 1981, **52**, 33-45.
- Y. Hirahara, Y. Ohshima and Y. Endo, *J. Chem. Phys.*, 1994, **101**, 7342-7349.
- Y. Ohshima and Y. Endo, *J. Mol. Spectrosc.*, 1992, **153**, 627-634.
- K. Seki, Y. Sumiyoshi and Y. Endo, *J. Chem. Phys.*, 2002, **117**, 9750-9757.
- Y. Ohshima and Y. Endo, *Chem. Phys. Lett.*, 1996, **256**, 635-640.
- M. Becucci and S. Melandri, *Chem. Rev.*, 2016, **116**, 5014-5037.
- W. Li, L. Evangelisti, Q. Gou, W. Caminati and R. Meyer, *Angew. Chem.*, 2019, **131**, 869-875.
- L. Spada, I. Uriarte, W. Li, L. Evangelisti, E. J. Cocinero and W. Caminati, *Phys. Chem. Chem. Phys.*, 2019.
- J. U. Grabow and W. Stahl, *Z. Naturforsch.*, 1990, **45A**, 1043-1044.
- J. U. Grabow, W. Stahl and H. Dreizler, *Rev. Sci. Instrum.*, 1996, **67**, 4072-4084.
- E. Arunan, S. Dev and P. K. Mandal, *Appl. Spectrosc. Rev.*, 2004, **39**, 131-181.
- Y. Xu and W. Jäger, *J. Chem. Phys.*, 1997, **106**, 7968-7980.
- G. G. Brown, B. C. Dian, K. O. Douglass, S. M. Geyer, S. T. Shipman and B. H. Pate, *Rev. Sci. Instrum.*, 2008, **79**, 053103.
- S. P. Dempster, O. Sukhorukov, Q. Y. Lei and W. Jäger, *J. Chem. Phys.*, 2012, **137**, 174303-174308.
- J. C. Slater, *Phys. Rev.*, 1952, **87**, 807-835.
- C. Møller and M. S. Plesset, *Phys. Rev.*, 1934, **46**, 0618-0622.
- U. Fano, *Phys. Rev.*, 1961, **124**, 1866.
- K. L. Bak, P. Jorgensen, J. Olsen, T. Helgaker and J. Gauss, *Chem. Phys. Lett.*, 2000, **317**, 116-122.
- W. Kohn and L. J. Sham, *Phys. Rev.*, 1965, **140**, 1133.
- A. D. Becke, *J. Chem. Phys.*, 1993, **98**, 5648-5652.
- K. Kim and K. D. Jordan, *J. Phys. Chem.*, 1994, **98**, 10089-10094.
- P. Stephens, F. Devlin, C. Chabalowski and M. J. Frisch, *J. Phys. Chem.*, 1994, **98**, 11623-11627.
- J. P. Perdew, M. Ernzerhof and K. Burke, *J. Chem. Phys.*, 1996, **105**, 9982-9985.
- E. G. Hohenstein, S. T. Chill and C. D. Sherrill, *J. Chem. Theory Comput.*, 2008, **4**, 1996-2000.
- S. Grimme, J. Antony, S. Ehrlich and H. Krieg, *J. Chem. Phys.*, 2010, **132**, 154104.
- S. Grimme, S. Ehrlich and L. Goerigk, *J. Comput. Chem.*, 2011, **32**, 1456-1465.
- R. Krishnan, J. S. Binkley, R. Seeger and J. A. Pople, *J. Chem. Phys.*, 1980, **72**, 650-654.
- H. B. Thompson, *J. Chem. Phys.*, 1967, **47**, 3407-3410.
- C. M. Western, *J. Quant. Spectrosc. Radiat. Transf.*, 2017, **186**, 221-242.
- H. Hartwig and H. Dreizler, *Z. Naturforsch.*, 1996, **51A**, 923-932.
- Z. Kisiel, *J. Mol. Spectrosc.*, 2003, **218**, 58-67.
- R. F. Bader, *Chem. Rev.*, 1991, **91**, 893-928.
- K. B. Wiberg and P. R. Rablen, *J. Comput. Chem.*, 1993, **14**, 1504-1518.

- T. Lu and F. Chen, *J. Comput. Chem.*, 2012, **33**, 580-592.
- W. Humphrey, A. Dalke and K. Schulten, *J. Mol. Graph.*, 1996, **14**, 33-38.
- E. R. Johnson, S. Keinan, P. Mori-Sanchez, J. Contreras-Garcia, A. J. Cohen and W. Yang, *J. Am. Chem. Soc.*, 2010, **132**, 6498-6506.
- T. L. Weatherly and D. Williams, *J. Chem. Phys.*, 1952, **20**, 755-755.
- J. Swalen and C. Costain, *J. Chem. Phys.*, 1959, **31**, 1562-1574.
- P. Groner, S. Albert, E. Herbst, F. C. De Lucia, F. J. Lovas, B. J. Drouin and J. C. Pearson, *Astrophys. J. Suppl. Ser.*, 2002, **142**, 145-151.
- J. M. Vacherand, B. P. Vaneijck, J. Burie and J. Demaison, *J. Mol. Spectrosc.*, 1986, **118**, 355-362.
- R. Nelson and L. Pierce, *J. Mol. Spectrosc.*, 1965, **18**, 344-352.
- R. Peter and H. Dreizler, *Z. Naturforsch.*, 1965, **20 A**, 301-312.
- F. J. Lovas and P. Groner, *J. Mol. Spectrosc.*, 2006, **236**, 173-177.
- F. Combes, M. Gerin, A. Wootten, G. Wlodarczak, F. Clausset and P. J. Encrenaz, *Astron. Astrophys.*, 1987, **180**, L13-L16.
- L. E. Snyder, F. J. Lovas, D. M. Mehringer, N. Y. Miao, Y. J. Kuan, J. M. Hollis and P. R. Jewell, *Astrophys. J.*, 2002, **578**, 245-255.
- S. A. Peebles, R. A. Peebles, Y. Tatamitani and Y. Kawashima, *J. Phys. Chem. A*, 2006, **110**, 7080-7085.
- D. J. Frohman, E. S. Contreras, R. S. Firestone, S. E. Novick and W. Klemperer, *J. Chem. Phys.*, 2010, **133**, 244303-244307.
- Q. Wen and W. Jaeger, *Phys. Chem. Chem. Phys.*, 2008, **10**, 2496-2501.
- C. C. Lin and J. D. Swalen, *Rev. Mod. Phys.*, 1959, **31**, 841-892.
- Y. Q. Liu and W. Jager, *J. Chem. Phys.*, 2003, **119**, 8449-8463.
- S. Melandri, P. G. Favero, W. Caminati and B. Velino, *J. Chem. Phys.*, 2005, **122**, 134310-134317.
- R. D. Suenram, F. J. Lovas, G. T. Fraser, J. Z. Gillies, C. W. Gillies and M. Onda, *J. Mol. Spectrosc.*, 1989, **137**, 127-137.
- G. T. Fraser, F. J. Lovas and R. D. Suenram, *J. Mol. Spectrosc.*, 1994, **167**, 231-235.
- X. Q. Tan, L. H. Sun and R. L. Kuczkowski, *J. Mol. Spectrosc.*, 1995, **171**, 248-264.
- J. Rottstegge, H. Hartwig and H. Dreizler, *J. Mol. Spectrosc.*, 1999, **195**, 1-10.
- B. Velino, S. Melandri, P. G. Favero, A. Dell'Erba and W. Caminati, *Chem. Phys. Lett.*, 2000, **316**, 75-80.
- L. Kang, A. R. Keimowitz, M. R. Munrow and S. E. Novick, *J. Mol. Spectrosc.*, 2002, **213**, 122-129.
- R. F. Bader, *Atoms in molecules*, Wiley Online Library, 1990.
- J. Thomas, J. Yiu, J. Rebling, W. Jaeger and Y. Xu, *J. Phys. Chem. A*, 2013, **117**, 13249-13254.
- Y. J. Xu, J. Van Wijngaarden and W. Jager, *Int. Rev. Phys. Chem.*, 2005, **24**, 301-338.
- Y. J. Xu and W. Jager, *J. Chem. Phys.*, 1997, **106**, 7968-7980.

- M. J. Frisch, G. W. Trucks, H. B. Schlegel, G. E. Scuseria, M. A. Robb, J. R. Cheeseman, G. Scalmani, V. Barone, B. Mennucci, G. A. Petersson, H. Nakatsuji, M. Caricato, X. Li, H. P. Hratchian, A. F. Izmaylov, J. Bloino, G. Zheng, J. L. Sonnenberg, M. Hada, M. Ehara, K. Toyota, R. Fukuda, J. Hasegawa, M. Ishida, T. Nakajima, Y. Honda, O. Kitao, H. Nakai, T. Vreven, J. A. Montgomery, Jr., J. E. Peralta, F. Ogliaro, M. Bearpark, J. J. Heyd, E. Brothers, K. N. Kudin, V. N. Staroverov, T. Keith, R. Kobayashi, J. Normand, K. Raghavachari, A. Rendell, J. C. Burant, S. S. Iyengar, J. Tomasi, M. Cossi, N. Rega, J. M. Millam, M. Klene, J. E. Knox, J. B. Cross, V. Bakken, C. Adamo, J. Jaramillo, R. Gomperts, R. E. Stratmann, O. Yazyev, A. J. Austin, R. Cammi, C. Pomelli, J. W. Ochterski, R. L. Martin, K. Morokuma, V. G. Zakrzewski, G. A. Voth, P. Salvador, J. J. Dannenberg, S. Dapprich, A. D. Daniels, O. Farkas, J. B. Foresman, J. V. Ortiz, J. Cioslowski, and D. J. Fox, *Gaussian 09, Revision D.01*, Gaussian, Inc., Wallingford CT, 2013.
- E. R. Johnson, I. D. Mackie and G. A. DiLabio, *J. Phys. Org. Chem.*, 2009, **22**, 1127-1135.
- L. Goerigk and S. Grimme, *J. Chem. Theory Comput.*, 2011, **7**, 291-309.
- S. Grimme and M. Steinmetz, *Phys. Chem. Chem. Phys.*, 2013, **15**, 16031-16042.
- N. Hansen, H. Mäder and T. Bruhn, *Molec. Phys.*, 1999, **97**, 587-595.
- J. O. Richardson, C. Perez, S. Lobsiger, A. A. Reid, B. Temelso, G. C. Shields, Z. Kisiel, D. J. Wales, B. H. Pate and S. C. Althorpe, *Science*, 2016, **351**, 1310-1313.
- J. S. Crichton and S. Bell, *J. Mol. Spectrosc.*, 1986, **118**, 383-396.
- C. E. Dykstra and D. J. Malik, *J. Chem. Phys.*, 1987, **87**, 2806-2811.
- J. Kraitchman, *Am. J. Phys.*, 1953, **21**, 17-24.
- R. D. Suenram, G. T. Fraser, F. J. Lovas, C. W. Gillies and J. Zozom, *J. Chem. Phys.*, 1988, **89**, 6141-6146.
- L. N. Hadley and D. M. Dennison, *Phys. Rev.*, 1946, **70**, 780-781.
- E. P. Kundig, A. E. Garcia, T. Lomberget and G. Bernardinelli, *Angew. Chem., Int. Ed.*, 2006, **45**, 98-101.
- W. N. Wang, H. W. Hellinga and L. S. Beese, *Proc. Natl. Acad. Sci.*, 2011, **108**, 17644-17648.
- H. F. Judson, *The Eighth Day of Creation*, Simon & Schuster, New York, 1979.
- M. D. Topal and J. R. Fresco, *Nature*, 1976, **263**, 285-289.
- B. Boekfa, P. Pantu, M. Probst and J. Limtrakul, *J. Phys. Chem. C*, 2010, **114**, 15061-15067.
- C. S. Cucinotta, A. Ruini, A. Catellani and A. Stirling, *Chemphyschem*, 2006, **7**, 1229-1234.
- E. Tapuhi and W. P. Jencks, *J. Am. Chem. Soc.*, 1982, **104**, 5758-5765.
- T. Lu, J. Zhang, J. Chen, Q. Gou, Z. Xia and G. Feng, *J. Chem. Phys.*, 2019, **150**, 064305.
- S. Melandri, A. Maris, B. M. Giuliano and W. Caminati, *J. Chem. Phys.*, 2005, **123**, 164304.
- N. A. Seifert, J. Thomas, W. Jäger and Y. Xu, *Phys. Chem. Chem. Phys.*, 2018, **20**, 27630-27637.
- P. A. Stockman, G. A. Blake, F. J. Lovas and R. D. Suenram, *J. Chem. Phys.*, 1997, **107**, 3782-3790.
- J. Thomas and Y. Xu, *J. Chem. Phys.*, 2014, **140**, 234307/1-5.
- E. G. Schnitzler and W. Jäger, *Phys. Chem. Chem. Phys.*, 2014, **16**, 2305-2314.

- S. Ghosh, J. Thomas, W. Huang, Y. Xu and W. Jäger, *J. Phys. Chem. Lett.*, 2015, **6**, 3126-3131.
- J. E. Del Bene, *J. Comput. Chem.*, 1985, **6**, 296-301.
- T. Yanai, D. P. Tew and N. C. Handy, *Chem. Phys. Lett.*, 2004, **393**, 51-57.
- J. Gao, N. A. Seifert, J. Thomas, Y. J. Xu and W. Jäger, *J. Mol. Spectrosc.*, 2016, **330**, 228-235.
- R. F. W. Bader, *Atoms in Molecules: A Quantum Theory*, Oxford University Press, New York, 1990.
- R. F. W. Bader, *Chem. Rev.*, 1991, **91**, 893-928.
- E. Espinosa, E. Molins and C. Lecomte, *Chem. Phys. Lett.*, 1998, **285**, 170-173.
- I. Mata, I. Alkorta, E. Espinosa and E. Molins, *Chem. Phys. Lett.*, 2011, **507**, 185-189.
- E. G. Schnitzler, M. R. Poopari, Y. J. Xu and W. Jäger, *Phys. Chem. Chem. Phys.*, 2015, **17**, 21942-21949.
- G.R. Desiraju and T. Steiner, *The weak hydrogen bond: in structural chemistry and biology*, Oxford University Press Inc., New York, 2001.
- A. V. Iogansen, *Spectrochim. Acta*, 1999, **55A**, 1585-1612.
- X. K. Zhang, E. G. Lewars, R. E. March and J. M. Parnis, *J. Phys. Chem.*, 1993, **97**, 4320-4325.
- T. Y. Nikolaienko, L. A. Bulavin and D. M. Hovorun, *Phys. Chem. Chem. Phys.*, 2012, **14**, 7441-7447.
- A. Metzger, B. Verheggen, J. Dommen, J. Duplissy, A. S. H. Prevot, E. Weingartner, I. Riipinen, M. Kulmala, D. V. Spracklen, K. S. Carslaw and U. Baltensperger, *Proc. Natl. Acad. Sci.*, 2010, **107**, 6646-6651.
- R. Y. Zhang, *Science*, 2010, **328**, 1366-1367.
- J. F. Hamilton, A. C. Lewis, J. C. Reynolds, L. J. Carpenter and A. Lubben, *Atmos. Chem. Phys.*, 2006, **6**, 4973-4984.
- E. Grosjean, D. Grosjean, M. P. Fraser and G. R. Cass, *Environ. Sci. Technol.*, 1996, **30**, 2687-2703.
- H. K. Wang, C. H. Huang, K. S. Chen and Y. P. Peng, *Aerosol Air Qual. Res.*, 2010, **10**, 559-570.
- Y. L. Feng, S. Wen, Y. J. Chen, X. M. Wang, H. X. Lu, X. H. Bi, G. Y. Sheng and J. M. Fu, *Atmos. Environ.*, 2005, **39**, 1789-1800.
- Y. L. Feng, S. Wen, X. M. Wang, G. Y. Sheng, Q. S. He, J. H. Tang and J. M. Fu, *Atmos. Environ.*, 2004, **38**, 103-112.
- H. K. Wang, C. H. Huang, K. S. Chen, Y. P. Peng and C. H. Lai, *J. Hazard Mater.*, 2010, **179**, 1115-1121.
- B. E. Olsson, M. Hallquist, E. Ljungström and J. Davidsson, *Int. J. Chem. Kinet.*, 1997, **29**, 195-201.
- E. Martínez, A. Aranda, Y. Díaz-De-Mera, A. Rodríguez, D. Rodríguez and A. Notario, *J. Atmos. Chem.*, 2004, **48**, 283-299.
- S. M. Aschmann and R. Atkinson, *Int. J. Chem. Kinet.*, 2013, **45**, 52-58.
- S. M. Aschmann, J. Arey and R. Atkinson, *J. Phys. Chem. A*, 2011, **115**, 14452-14461.

- D. Shemesh, S. A. Nizkorodov and R. B. Gerber, *J. Phys. Chem. A*, 2016, **120**, 7112-7120.
- A. Chattopadhyay, K. Mondal, M. Samanta and T. Chakraborty, *Atmos. Environ.*, 2017, **157**, 125-134.
- A. T. Archibald, M. R. McGillen, C. A. Taatjes, C. J. Percival and D. E. Shallcross, *Geophys. Res. Lett.*, 2007, **34**, L21801.
- C. A. Taatjes, N. Hansen, A. McIlroy, J. A. Miller, J. P. Senosiain, S. J. Klippenstein, F. Qi, L. Sheng, Y. Zhang and T. A. Cool, *Science*, 2005, **308**, 1887-1889.
- C. A. Taatjes, N. Hansen, J. A. Miller, T. A. Cool, J. Wang, P. R. Westmoreland, M. E. Law, T. Kasper and K. Kohse-Höinghaus, *J. Phys. Chem. A*, 2006, **110**, 3254-3260.
- L. K. Huynh, H. R. Zhang, S. Zhang, E. Eddings, A. Sarofim, M. E. Law, P. R. Westmoreland and T. N. Truong, *J. Phys. Chem. A*, 2009, **113**, 3177-3185.
- F. J. Devlin and P. J. Stephens, *J. Phys. Chem. A*, 1999, **103**, 527-538.
- J. Dillen and H. J. Geise, *J. Mol. Struct.*, 1980, **69**, 137-144.
- J. L. Alonso, *J. Mol. Struct.*, 1981, **73**, 63-69.
- Y. Ohnishi and K. Kozima, *Bull. Chem. Soc. Jpn.*, 1968, **41**, 1323-1325.
- R. Moradi, S. Jameh-Bozorgh, R. Kadivar, A. Mahdiani and H. Soleymanabadi, *APCBEE Procedia*, 2012, **3**, 70-74.
- G. Schwarzenbach and C. Wittwer, *Helv. Chim. Acta*, 1947, **30**, 669.
- R. Bell and P. Smith, *J. Chem. Soc. B*, 1966, 241-243.
- J. E. Dubois, M. El-Alaoui and J. Toullec, *J. Am. Chem. Soc.*, 1981, **103**, 5393-5401.
- A. J. Kresge, *Pure Appl. Chem.*, 1991, **63**, 213-221.
- J. Thomas, N. A. Seifert, W. Jäger and Y. Xu, *Angew. Chem.*, 2017, **129**, 6386-6390.
- F. J. Lovas and C. Lugez, *J. Mol. Spectrosc.*, 1996, **179**, 320-323.
- G. B. Park and R. W. Field, *J. Chem. Phys.*, 2016, **144**, 200901-10.
- E. G. Schnitzler, N. A. Seifert, S. Ghosh, J. Thomas, Y. J. Xu and W. Jäger, *Phys. Chem. Chem. Phys.*, 2017, **19**, 4440-4446.
- E. G. Schnitzler, N. A. Seifert, I. Kusuma and W. Jäger, *J. Phys. Chem. A*, 2017, **121**, 8625-8631.
- Y. Xu, J. V. Wijngaarden and W. Jäger, *Int. Rev. Phys. Chem.*, 2005, **24**, 301-338.
- K. E. Laidig and R. F. Bader, *J. Chem. Phys.*, 1990, **93**, 7213-7224.
- T. M. Parker, L. A. Burns, R. M. Parrish, A. G. Ryno and C. D. Sherrill, *J. Chem. Phys.*, 2014, **140**, 094106.
- J. Turney, A. Simmonett, R. Parrish, E. Hohenstein, F. Evangelista, J. Fermann, B. Mintz, L. Burns, J. Wilke and M. Abrams, *Rev.: Comput. Mol. Sci.*, 2012, **2**, 556-565.
- Q. Gou, L. Spada, M. Vallejo-López, Z. Kisiel and W. Caminati, *Chem. Asian J.*, 2014, **9**, 1032-1038.
- R. C. Dunbar, *J. Chem. Educ.*, 1982, **59**, 22-23.
- G. D. Peckham and I. J. Mcnaught, *J. Chem. Educ.*, 1992, **69**, 554-558.

- J. K. G. Watson, in *Vibrational Spectra and Structure*, ed. J. R. Durig, Elsevier, Amsterdam, 1977, vol. 6, pp. 1–89.
- J. K. Watson, A. Roytburg and W. Ulrich, *J. Mol. Spectrosc.*, 1999, **196**, 102-119.
- Q. Gou, G. Feng, L. Evangelisti, D. Loru, J. L. Alonso, J. C. López and W. Caminati, *J. Phys. Chem. A*, 2013, **117**, 13531-13534.
- A. S. Murthy and C. Rao, *Appl. Spectrosc. Rev.*, 1968, **2**, 69-191.
- M. Tamres and S. Searles Jr., *J. Am. Chem. Soc.*, 1959, **81**, 2100-2104.
- E. J. Corey, *J. Am. Chem. Soc.*, 1953, **75**, 2301-2304.
- M. Juanes, W. Li, L. Spada, L. Evangelisti, A. Lesarri and W. Caminati, *Phys. Chem. Chem. Phys.*, 2019, **21**, 3676-3682.
- J. D. Surratt, M. Lewandowski, J. H. Offenberg, M. Jaoui, T. E. Kleindienst, E. O. Edney and J. H. Seinfeld, *Environ. Sci. Technol.*, 2007, **41**, 5363-5369.
- E. P. Serjeant, B. Dempsey, *Ionisation constants of organic acids in aqueous solution; in IUPAC Chemical Data Series, No. 23*. Pergamon Press, Oxford, NY, 1979.
- R. Irving and I. Wadso, *Acta Chem. Scand.*, 1970, **24(2)**, 589.
- P. Roubin, T. Chiavassa, P. Verlaque, L. Pizzala and H. Bodot, *Chem. Phys. Lett.*, 1990, **175**, 655-659.
- T. Ishida, F. Hirata and S. Kato, *J. Chem. Phys.*, 1999, **110**, 3938-3945.
- G. Alagona and C. Ghio, *Int. J. Quantum Chem.*, 2008, **108**, 1840-1855.
- T. Kaweetirawatt, T. Yamaguchi, T. Higashiyama, M. Sumimoto and K. Hori, *J. Phys. Org. Chem.*, 2012, **25**, 1097-1104.
- R. R. Lozada-García, J. Ceponkus, M. Chevalier, W. Chin, J.-M. Mestdagh and C. Crépin, *Phys. Chem. Chem. Phys.*, 2012, **14**, 3450-3459.
- A. Trivella, T. Wassermann, J. Mestdagh, C. M. Tanner, F. Marinelli, P. Roubin and S. Coussan, *Phys. Chem. Chem. Phys.*, 2010, **12**, 8300-8310.
- S. Tayyari, T. Zeegers-Huyskens and J. Wood, *Spectrochim. Acta*, 1979, **35A**, 1289-1295.
- R. Srinivasan, J. S. Feenstra, S. T. Park, S. Xu and A. H. Zewail, *J. Am. Chem. Soc.*, 2004, **126**, 2266-2267.
- W. Egan, G. Gunnarsson, T. Bull and S. Forsen, *J. Am. Chem. Soc.*, 1977, **99**, 4568-4572.
- R. Boese, M. Y. Antipin, D. Bläser and K. A. Lyssenko, *J. Phys. Chem. B*, 1998, **102**, 8654-8660.
- M. Johnson, N. Jones, A. Geis, A. Horsewill and H. Trommsdorff, *J. Chem. Phys.*, 2002, **116**, 5694-5700.
- T. R. Dyke, K. M. Mack and J. S. Muentner, *J. Chem. Phys.*, 1977, **66**, 498-510.
- T. Lu and F. Chen, *J. Mol. Graph Model*, 2012, **38**, 314-323.
- P. De Silva and C. m. Corminboeuf, *J. Chem. Theory Comput.*, 2014, **10**, 3745-3756.
- A. Iogansen, *Spectrochim. Acta*, 1999, **55A**, 1585-1612.
- J. Čeponkus, R. Platakytė, V. Šablinskas and A. G. Quintanilla, *chemija*, 2018, **29(1)**, 1-16.

- R. M. Claramunt, C. López, M. D. Santa María, D. Sanz and J. Elguero, *Prog. Nucl. Magn. Reson. Spectrosc.*, 2006, **49**, 169-206.
- X. Kong, A. Brinkmann, V. Terskikh, R. E. Wasylshen, G. M. Bernard, Z. Duan, Q. Wu and G. Wu, *J. Phys. Chem. B*, 2016, **120**, 11692-11704.
- L. H. Thomas, A. J. Florence and C. C. Wilson, *New J. Chem.*, 2009, **33**, 2486-2490.
- R. R. Lozada-Garcia, J. Ceponkus, W. Chin, M. Chevalier and C. Crépin, *Chem. Phys. Lett.*, 2011, **504**, 142-147.
- N. V. Belova, G. V. Girichev, H. Oberhammer, T. N. Hoang and S. A. Shlykov, *J. Phys. Chem. A*, 2012, **116**, 3428-3435.
- M. Bassetti, G. Cerichelli and B. Floris, *Tetrahedron*, 1988, **44**, 2997-3004.
- E. V. Borisov, E. V. Skorodumov, V. M. Pachevskaya and P. E. Hansen, *Magn. Reson. Chem.*, 2005, **43**, 992-998.
- P. Gilli, V. Bertolasi, L. Pretto, V. Ferretti and G. Gilli, *J. Am. Chem. Soc.*, 2004, **126**, 3845-3855.
- H. Matsuzawa, T. Nakagaki and M. Iwahashi, *J. Oleo Sci.*, 2007, **56**, 653-658.
- M. Gorodetsky, Z. Luz and Y. Mazur, *J. Am. Chem. Soc.*, 1967, **89**, 1183-1189.
- W. Caminati and J.-U. Grabow, in *Frontiers of molecular spectroscopy*, Elsevier, 2009, ch. 15, pp. 455-552.
- A. D. Becke and E. R. Johnson, *J. Chem. Phys.*, 2005, **123**, 154101.
- Y. Chiang, A. J. Kresge, Y. S. Tang and J. Wirz, *J. Am. Chem. Soc.*, 1984, **106**, 460-462.
- R. Sanchez, B. M. Giuliano, S. Melandri, L. B. Favero and W. Caminati, *J. Am. Chem. Soc.*, 2007, **129**, 6287-6290.
- C. Calabrese, A. Maris, L. Evangelisti, L. B. Favero, S. Melandri and W. Caminati, *J. Phys. Chem. A*, 2013, **117**, 13712-13718.

Appendix I. Supplementary Material for Chapter 3

Structure and internal rotation dynamics of the acetone-neon complex studied by microwave spectroscopy

Contents:

Table S3.1. Measured transition frequencies of acetone- ²⁰ Ne.....	158
Table S3.2. Measured transition frequencies of acetone- ²² Ne.....	159
Table S3.3. Integrated electronic atomic charges of acetone-Ne.....	160
Figure S3.1. Survey spectrum of acetone-Ne.....	161

Table S3.1. Measured transition frequencies (in MHz) and assigned quantum numbers of the acetone-²⁰Ne complex.

J'	K _a '	K _c '	J''	K _a ''	K _c ''	AA	^a o-c	EE	o-c	AE	o-c	EA	o-c
1	1	0	0	0	0	7344.7531	-0.0035	7344.5544	-0.0088	7344.1802	-0.0109	7344.5544	0.0034
2	0	2	1	0	1	9006.9073	0.0019	9004.4131	-0.0002	9002.6997	-0.0133	9001.1270	-0.0087
2	1	1	1	0	1	11954.7986	0.0113	11954.0038	0.0019	11951.1540	-0.0143	11955.2638	0.0035
2	1	2	1	1	1	8900.7647	-0.0084	8899.8598	0.0088	8899.8598	-0.0206	8897.9877	0.0076
2	2	1	1	1	1	17418.5757	0.0221	17408.9513	0.0281	17398.0024	-0.0364	17416.9695	-0.0020
2	0	2	1	1	0	6167.6085	0.0087	6164.0317	0.0103	6161.8717	-0.0124	6159.0049	-0.0021
2	1	1	1	1	0	9115.4998	0.0181	9113.6237	0.0137	9110.3279	-0.0116	9113.1392	0.0077
2	2	0	1	1	0	17314.2364	0.0020	17322.1658	-0.0089	17331.5513	0.0538	17312.2903	-0.0043
2	2	0	2	1	2	8520.8818	0.0290	8529.9291	-0.0187	8539.6118	0.0251	8522.0591	-0.0050
2	2	1	2	1	1	8195.6641	-0.0163	8187.6943	0.0052	8179.6878	-0.0420	8196.0912	-0.0132
3	0	3	2	0	2	13500.3809	0.0025	13496.7985	0.0055	13494.0239	-0.0128	13492.3977	0.0033
3	0	3	2	1	1	10552.4896	-0.0069	10547.2078	0.0034	10545.5696	-0.0117	10538.2656	-0.0064
3	1	2	2	0	2	16616.8386	0.0084	16615.7988	-0.0049	16610.5714	0.0262	16618.9896	0.0012
3	1	3	2	1	2	13347.0864	-0.0390	13345.6009	-0.0176	13345.2233	0.0090	13342.9973	-0.0113
3	1	2	2	1	1	13668.8473	-0.0010	13666.2080	-0.0071	13662.0640	-0.0258	13664.8553	-0.0086
3	2	2	3	1	2	8028.3229	-0.0328	8024.4152	0.0270	8019.1504	0.0257	8028.0645	-0.0094
3	2	1	3	1	3	8687.6639	0.0362	8691.9760	-0.0297	8698.2689	-0.0461	8688.0990	-0.0113
4	0	4	3	0	3	17981.9519	-0.0112	17977.4266	0.0040	17973.3839	0.0258	17972.4439	0.0047
4	0	4	3	1	2	14865.4942	-0.0171	14858.4263	0.0144	14856.8434	-0.0062	14845.8427	-0.0025
4	2	2	4	1	4	8925.2101	-0.0997	8925.2101	0.0591	-----	-----	-----	-----
4	3	2	4	2	2	13875.3175	0.0000	-----	-----	-----	-----	-----	-----

^a observed-calculated

Table S3.2. Measured transition frequencies (in MHz) and assigned quantum numbers of the acetone- ^{22}Ne complex.

J'	K_a'	K_c'	J''	K_a''	K_c''	AA	o-c	E_iE	o-c	AE	o-c	EA	o-c
1	1	0	0	0	0	7224.2187	-0.0033	7224.0588	-0.0073	7223.8420	-0.0064	7224.0588	0.0854
2	0	2	1	0	1	8551.2076	-0.0020	8548.9987	0.0021	8547.4761	-0.0081	8546.0800	-0.0078
2	1	1	1	0	1	11595.5936	-0.0060	11594.8584	-0.0072	11592.3635	-0.0097	11595.8787	-0.0075
2	2	1	1	1	1	17296.0574	0.0049	17286.4902	0.0278	17275.9386	-0.0345	17294.5635	-0.0035
2	0	2	1	1	0	5604.2224	0.0068	5601.0369	0.0109	5599.0006	-0.0051	5596.6757	0.0036
2	1	1	1	1	0	8648.6091	0.0035	8646.8992	0.0042	8643.8880	-0.0068	8646.4744	0.0040
2	2	0	1	1	0	17201.7146	-0.0063	17209.7208	-0.0199	17218.8053	0.0313	17199.9536	0.0015
2	2	0	2	1	2	8843.2360	0.0116	8852.3009	-0.0134	8861.8584	0.0414	8844.1964	-0.0019
3	0	3	2	0	2	12818.7005	-0.0054	12815.5075	0.0025	12813.0758	-0.0079	12811.5318	-0.0052
3	0	3	2	1	1	9774.3135	-0.0025	9769.6480	0.0120	9768.1912	-0.0035	9761.7393	0.0007
3	1	2	2	0	2	16013.6145	0.0028	16012.6424	-0.0005	16007.9400	0.0029	16015.4000	0.0068
3	1	3	2	1	2	12679.3308	-0.0057	12677.9837	-0.0047	12677.6097	0.0123	12675.6925	0.0078
3	1	2	2	1	1	12969.2285	0.0067	12966.7827	0.0088	12963.0526	0.0046	12965.6013	0.0065
3	2	2	3	1	2	8399.6654	0.0063	8395.0251	0.0291	8389.1594	0.0123	8399.3722	-0.0114
3	2	1	3	1	3	8991.6250	0.0174	8996.5695	-0.0294	9003.4188	-0.0052	8991.9104	0.0075
4	0	4	3	0	3	17076.5116	-0.0107	17072.4527	0.0061	17068.9252	-0.0050	17067.8411	0.0038
4	0	4	3	1	2	13881.6166	-0.0190	13875.3157	0.0069	13874.0694	-0.0074	13863.9762	-0.0049
4	2	3	4	1	3	8199.4025	-0.0116	-----	-----	-----	-----	-----	-----
3	3	1	3	2	1	14483.9214	0.0000	-----	-----	-----	-----	-----	-----
2	2	1	2	1	1	8550.7070	-0.0161	8542.5804	0.0120	8534.4764	-0.0453	8551.0896	-0.0120

Table S3.3. Integrated electronic atomic charges for acetone and acetone-Ne at the MP2/6-311++g(2d,p) level of theory.

	Acetone	Acetone-Ne
N(C1)/a.u.	0.020577	0.021134
N(H2)/a.u.	0.036883	0.036799
N(H3)/a.u.	0.009190	0.011922
N(H4)/a.u.	0.010282	0.007952
N(C5)/a.u.	0.020587	0.020909
N(H6)/a.u.	0.010269	0.009012
N(H7)/a.u.	0.036903	0.037419
N(H8)/a.u.	0.009173	0.011200
N(C9)/a.u.	1.133401	1.131977
N(O10)/a.u.	-1.287264	-1.286340
N(Ne)/a.u.	-----	-0.001985

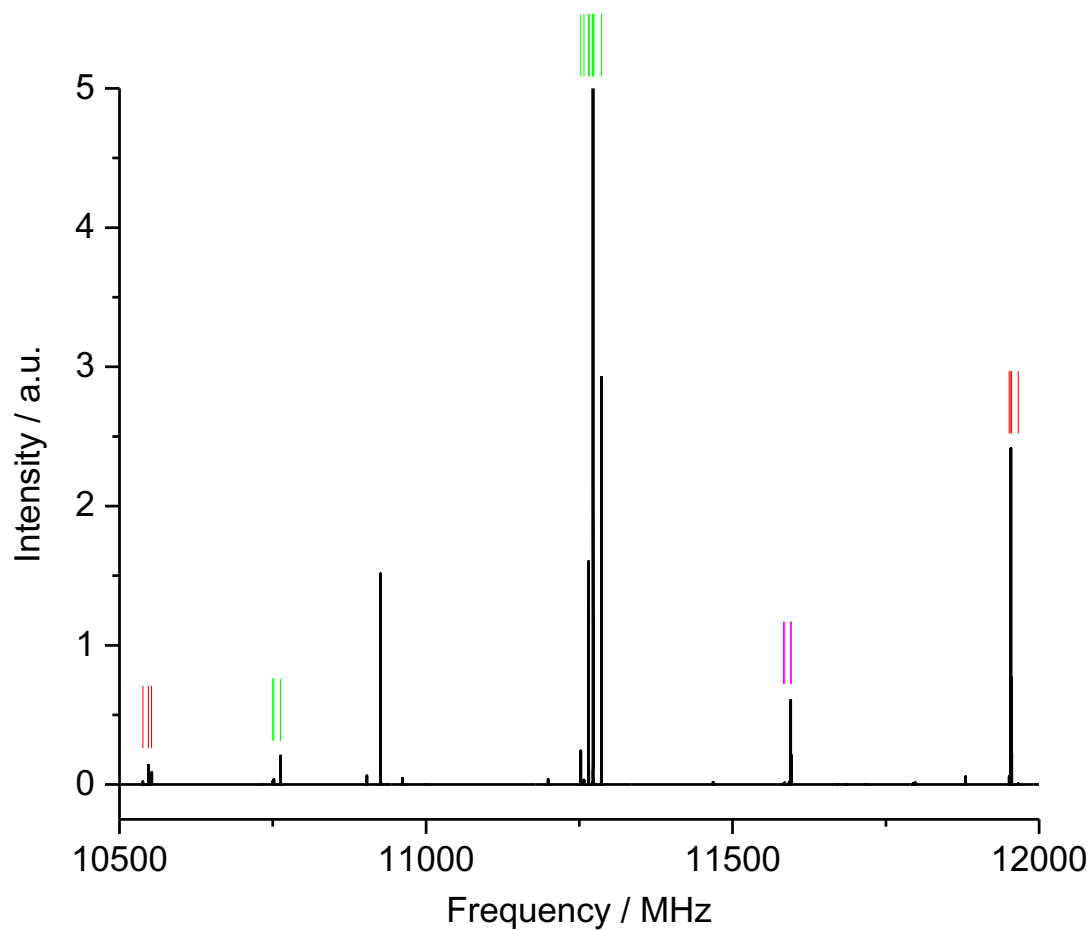


Figure S3.1. Assigned survey spectrum of acetone-water: the red lines indicate transitions of acetone- ^{20}Ne , green lines identify acetone monomer transitions, and the pink ones belong to the acetone- ^{22}Ne complex.

Appendix II. Supplementary Material for Chapter 4

Non-Equivalent Methyl Internal Rotations in Acetone- Water Complex Studied by Microwave Spectroscopy and ab initio Calculations

Contents:

Table S4.1. Measured transition frequencies of acetone-water complex.....163

Table S4.2. Measured transition frequencies of acetone- D₂O complex.....164

Table S4.1. Measured and assigned transition frequencies (MHz) of the acetone-water complex.

J'	Ka'	Kc'	J''	Ka''	Kc''	AA	^a o-c	E:E	o-c	EE _j	o-c	AE	o-c	EA	o-c
1	1	0	1	0	1	7384.4588	-0.0121	7392.3794	0.0352					7484.1132	0.0601
2	1	2	1	1	1	7531.7137	0.0099	7536.4695	0.0072	7577.0601	-0.1354	7554.0162	0.0488	7599.3164	0.0221
2	1	1	2	0	2	7771.1215	-0.0028	7772.5506	0.0066	7781.6047	-0.0817	7763.7199	0.0207	7801.7074	0.0060
2	0	2	1	0	1	7889.6031	0.0027	7886.8066	0.0049	7889.4416	0.0139	7886.8427	0.0078	7886.4280	0.0076
2	1	1	1	1	0	8276.2703	0.0164	8266.9974	-0.0042	8230.7097	0.1648	8249.1216	-0.0352	8204.0448	-0.0239
3	1	2	3	0	3	8377.8200	0.0005	8376.7710	0.0077	8374.1598	-0.0284	8362.5082	0.0192	8383.7138	0.0041
4	1	3	4	0	4	9235.2857	0.0010	9231.6990	0.0149	9225.9659	-0.0012	9215.1587	0.0065	9229.5893	-0.0097
4	0	4	3	1	3	9520.1567	0.0173	9514.5763	0.0017	9552.5343	-0.0585	9538.1531	0.0245	9555.7391	0.0088
5	1	4	5	0	5	10381.0850	0.0041	10373.8151	-0.0055	10369.2073	0.0216	10356.3710	-0.0045	10367.4705	-0.0278
1	1	1	0	0	0	10964.2186	-0.0082	10952.7925	0.0020	10871.2314	0.2898	10906.2956	-0.0751	10824.1304	-0.0413
3	1	3	2	1	2	11288.6076	-0.0050	11288.1661	0.0013	11302.7225	-0.0491	11293.2047	0.0226	11310.7411	0.0193
3	0	3	2	0	2	11798.3544	0.0000	11794.5009	0.0044	11798.0279	0.0131	11793.9056	0.0063	11794.4179	0.0049
3	2	2	2	2	1	11855.6082	-0.0052	11875.9616	0.0276	11882.9851	0.0094	11878.1556	-0.0297	11880.1007	0.0606
3	2	1	2	2	0	11913.1935	-0.0043	11885.6568	0.1334	11885.6568	0.0145	11882.9874	-0.0306	11881.2431	-0.0400
5	0	5	4	1	4	13961.9165	0.0083	13953.4239	-0.0081	13987.6690	-0.0301	13974.3136	0.0089	13984.1068	-0.0093
3	1	2	2	1	1	12405.0548	0.0052	12398.9313	-0.0003	12390.5929	0.0763	12393.1937	-0.0091	12375.8986	-0.0089
2	1	2	1	0	1	14543.8808	-0.0111	14538.6929	0.0076	14496.3248	0.1419	14509.6959	-0.0300	14473.0513	-0.0059
4	1	4	3	1	3	15035.2632	-0.0108	15033.3004	-0.0040	15040.9680	-0.0045	15035.2632	0.0139	15042.6787	0.0077
4	0	4	3	0	3	15664.6895	0.0004	15660.1243	-0.0023	15664.1027	0.0123	15659.7914	0.0027	15659.2740	0.0049
4	2	3	3	2	2	15796.0426	-0.0073			15854.4218	-0.0135	15842.8633	-0.0141	15853.4401	0.0721
4	2	2	3	2	1	15939.0497	-0.0159			15880.5630	0.0352	15881.9968	0.0259	15871.6007	-0.0665
4	1	3	3	1	2	16522.1526	-0.0017	16515.0419	-0.0055	16515.9086	0.0393	16512.4453	-0.0066	16505.1546	-0.0038
3	1	3	2	0	2	17942.8777	-0.0264	17940.0519	0.0035	17909.5600	0.0476	17915.9400	-0.0146	17897.3603	0.0017

^aobserved-calculated.

Table S4.2. Measured and assigned transition frequencies (MHz) of the acetone-D₂O complex.

J'	K _a '	K _c '	J''	K _a ''	K _c ''	AA	^a o-c	E _i E	o-c	EE _j	o-c	AE	o-c	EA	o-c
2	1	2	1	1	1	7141.2989	-0.0297	7146.6073	-0.0175	7188.0202	-0.1021	7164.6473	0.0700	7210.0742	0.0004
2	1	1	2	0	2	7718.8074	-0.0018	7720.6962	0.0104			7712.9855	0.0535	7753.3976	-0.0103
2	0	2	1	0	1	7466.7435	0.0168	7464.0536	0.0073	7466.5866	0.0249	7464.0960	0.0054	7463.6817	0.0124
2	1	1	1	1	0	7815.7286	0.0210	7806.0819	-0.0908			7787.9159	0.0366	7742.6599	0.0231
3	1	2	3	0	3	8264.2303	0.0005	8263.6694	0.0048	8262.1020	-0.0485	8250.2011	0.0110	8272.8586	-0.0250
4	1	3	4	0	4	9031.5217	0.0228	9028.6541	0.0153	9023.2989	0.0121	9012.7364	0.0291	9028.1399	-0.0193
1	1	1	0	0	0	10771.9305	-0.0031	10759.8668	-0.0059			10713.0328	-0.0357	10628.2007	-0.0152
4	0	4	3	1	3	8597.9957	0.0173	8592.6921	-0.0115	8630.8917	-0.0560	8616.0847	0.0048	8635.1367	0.0193
1	1	0	1	0	1	7369.8089	-0.0195	7378.5789	0.0195						
3	1	3	2	1	2	10704.6483	0.0046	10704.4157	0.0025	10719.6115	-0.0601	10709.7026	0.0173	10728.2893	0.0238
3	0	3	2	0	2	11170.5222	0.0152	11166.7869	0.0061	11170.2300	0.0324	11166.2176	0.0129	11166.7318	-0.0046
3	2	2	2	2	1	11217.5301	0.0462			11240.1071	-0.0298	11235.7803	-0.0613		
3	1	2	2	1	1	11715.9474	0.0199	11709.7512	-0.0084	11703.9918	-0.0027			11685.6761	-0.0044
2	1	2	1	0	1	14173.9712	0.0086	14168.6133	0.0132			14139.6912	-0.0117	14100.5729	-0.0070
4	1	4	3	1	3	14259.5048	0.0163	14257.6825	-0.0013	14267.7247	0.0067	14259.7698	0.0163	14265.5937	-0.0129
4	0	4	3	0	3	14839.3598	0.0088	14834.8927	0.0029	14838.8527	0.0271	14834.6444	0.0033	14834.1033	0.0145
4	2	3	3	2	2	14947.2588	-0.0111	14976.1376	0.0487	14997.0151	-0.0050	14987.4998	-0.0488	14995.2042	0.0480
4	1	3	3	1	2	15606.6252	0.0051	15599.8390	-0.0250	15600.0207	0.0588	15597.1428	-0.0154	15589.3410	-0.0234
3	1	3	2	0	2	17411.8758	-0.0038	17408.9482	-0.0188	17385.2996	0.0020			17365.1777	0.0016
5	1	5	4	1	4	17803.6617	-0.0003	17801.0021	-0.0152	17801.9254	-0.0017	17805.8917	-0.0085	17806.5667	-0.0005
5	1	4	5	0	5	10052.1176	-0.0075	10045.9996	-0.0477	10041.0160	-0.0195	10028.9682	-0.0284	10041.0160	0.0722
5	0	5	4	1	4	12801.8390	-0.0060	12793.5267	-0.0077	12827.8625	-0.0180	12814.2548	-0.0093	12824.8598	0.0169

^aobserved-calculated

Appendix III. Supplementary Material for Chapter 5

A Microwave Spectroscopic and ab-initio Study of Keto-enol Tautomerism and Isomerism in the Cyclohexanone-Water Complex

Contents:

1. Table S5.1-S5.13 Cartesian coordinates for the predicted structures in Table 1...166-178
2. Table S5.14 Measured and assigned transition frequencies (MHz) of cyclohexanone-water complex and its ^{13}C isotopologues.....179-180
3. Table S5.15 Measured and assigned transition frequencies (MHz) of cyclohexanone-water complex and its deuterium isotopologues.....181
4. Table S5.16 Spectroscopic parameters of cyclohexanone-water complex and its ^{13}C and deuterium isotopologues.....182
5. Table S5.17 Cartesian coordinates for the fitted $r_m^{(1)}$ geometry of cyclohexanone-water complex.....183
6. Table S5.18 BSSE corrected interaction energy analysis for a selection of ketone-water complexes at the MP2/6-311++g (2d, p) level of theory.....184

Table S5.1. Cartesian coordinates for the predicted structure of Keto chair in Table 5.1 at the B3LYP-D3/aVTZ level of theory.

Atom	X	Y	Z
C1	-1.080	0.000	-0.095
O2	-2.215	0.000	0.326
C3	-0.315	-1.279	-0.372
H4	-0.192	-1.358	-1.457
H5	-0.915	-2.124	-0.040
C6	1.075	-1.260	0.287
H7	1.627	-2.155	-0.001
H8	0.954	-1.301	1.373
C9	1.855	0.000	-0.086
H10	2.054	0.000	-1.162
H11	2.826	0.000	0.412
C12	1.075	1.260	0.287
H13	1.627	2.155	-0.001
H14	0.954	1.301	1.373
C15	-0.315	1.279	-0.372
H16	-0.915	2.124	-0.040
H17	-0.192	1.358	-1.457

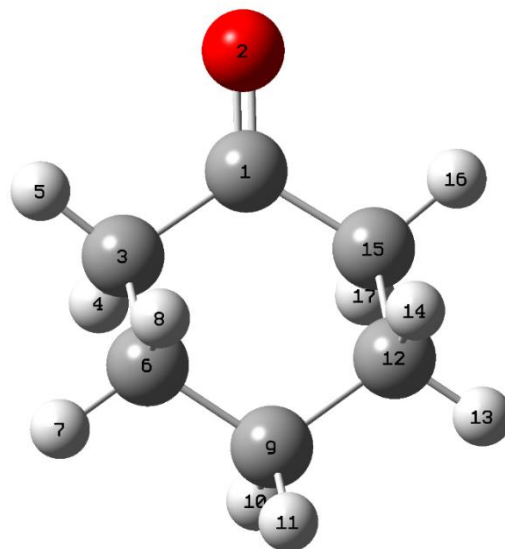


Table S5.2. Cartesian coordinates for the predicted structure of Keto boat in Table 5.1 at the B3LYP-D3/aVTZ level of theory.

Atom	X	Y	Z
C1	-1.068	1.230	-0.364
C2	-1.923	0.000	0.000
C3	-1.068	-1.230	0.364
C4	0.282	-1.229	-0.355
C5	1.099	0.000	0.000
C6	0.282	1.229	0.355
H7	-2.577	-0.239	-0.839
H8	-2.577	0.239	0.839
H9	-0.883	-0.243	1.440
H10	-1.611	-2.147	0.140
H11	0.877	-2.114	-0.134
H12	0.131	-1.212	-1.440
H13	0.131	1.212	1.440
H14	0.877	2.114	0.134
H15	-0.883	1.243	-1.440
H16	-1.611	2.147	-0.140
O17	2.309	0.000	0.000

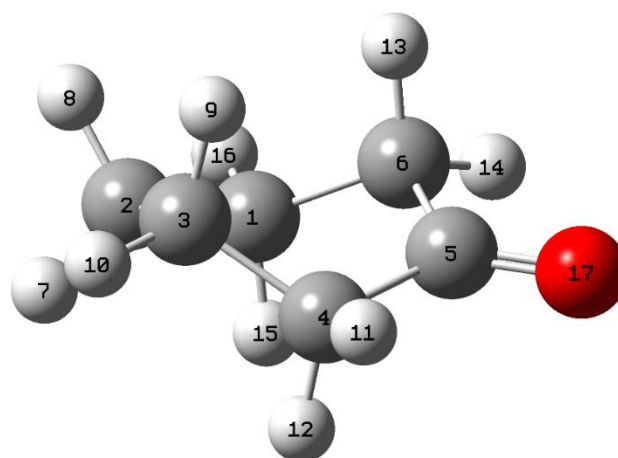


Table S5.3. Cartesian coordinates for the predicted structure of Keto skew in Table 5.1 at the B3LYP-D3/aVTZ level of theory.

Atom	X	Y	Z
C1	-1.711	-0.017	-0.524
C2	-1.077	1.330	-0.120
C3	1.070	-0.023	0.047
C4	0.315	-1.344	0.091
C5	-1.187	-1.168	0.335
H6	-0.967	1.961	-1.001
H7	-1.739	1.864	0.563
H8	-1.380	-0.962	1.391
H9	-1.472	-0.236	-1.568
H10	0.783	-1.960	0.864
H11	0.501	-1.850	-0.858
H12	-1.712	-2.095	0.102
H13	-2.798	0.050	-0.464
C14	0.301	1.170	0.564
H15	0.148	0.994	1.634
H16	0.912	2.064	0.463
O17	2.205	0.050	-0.367

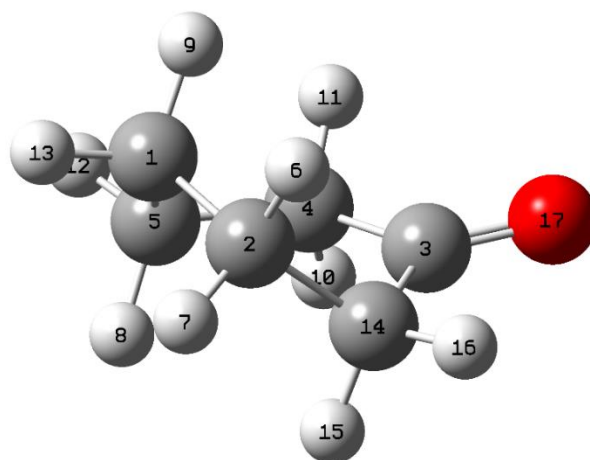


Table S5.4. Cartesian coordinates for the predicted structure of Enol 1(cis) in Table 5.1 at the B3LYP-D3/aVTZ level of theory.

Atom	X	Y	Z
C1	-0.965	0.075	-0.006
C2	-0.325	-1.275	-0.077
H3	-0.447	-1.668	-1.092
H4	-0.875	-1.955	0.576
C5	1.154	-1.224	0.305
H6	1.642	-2.157	0.024
H7	1.241	-1.134	1.392
C8	1.844	-0.030	-0.351
H9	1.748	-0.116	-1.437
H10	2.912	-0.032	-0.124
C11	1.211	1.284	0.108
H12	1.551	2.102	-0.531
H13	1.565	1.530	1.116
C14	-0.291	1.220	0.092
H15	-0.838	2.155	0.165
O16	-2.335	-0.012	-0.056
H17	-2.712	0.874	-0.053

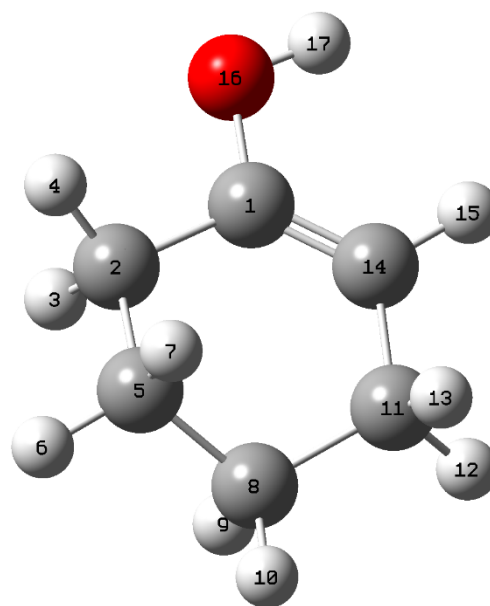


Table S5.5. Cartesian coordinates for the predicted structure of Enol 2(trans) in Table 5.1 at the B3LYP-D3/aVTZ level of theory.

Atom	X	Y	Z
C1	0.966	0.077	0.001
C2	0.323	-1.275	0.073
H3	0.447	-1.677	1.085
H4	0.855	-1.960	-0.596
C5	-1.159	-1.226	-0.303
H6	-1.645	-2.160	-0.018
H7	-1.249	-1.138	-1.388
C8	-1.844	-0.031	0.355
H9	-1.743	-0.116	1.441
H10	-2.912	-0.034	0.133
C11	-1.210	1.280	-0.108
H12	-1.547	2.100	0.531
H13	-1.569	1.526	-1.115
C14	0.291	1.219	-0.099
H15	0.849	2.144	-0.168
O16	2.342	0.100	0.064
H17	2.678	-0.799	0.038

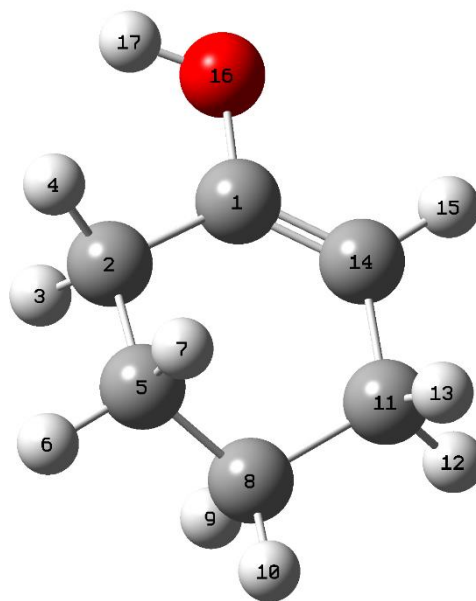


Table S5.6. Cartesian coordinates for the predicted structure of Keto chair-H₂O in Table 5.1 at the B3LYP-D3/aVTZ level of theory.

Atom	X	Y	Z
C1	0.258	-0.649	0.240
C2	0.216	0.811	0.625
C3	-0.877	1.559	-0.158
C4	-2.232	0.862	-0.043
C5	-2.145	-0.591	-0.508
C6	-1.070	-1.369	0.270
O7	1.284	-1.215	-0.089
H8	-1.376	-1.446	1.318
H9	-0.933	-2.377	-0.116
H10	-3.107	-1.092	-0.395
H11	-1.901	-0.617	-1.573
H12	-2.570	0.892	0.997
H13	-2.979	1.398	-0.631
H14	-0.938	2.586	0.203
H15	-0.584	1.614	-1.209
H16	1.197	1.256	0.481
H17	-0.022	0.855	1.694
O18	3.487	0.555	-0.234
H19	4.314	0.155	-0.512
H20	2.835	-0.169	-0.213

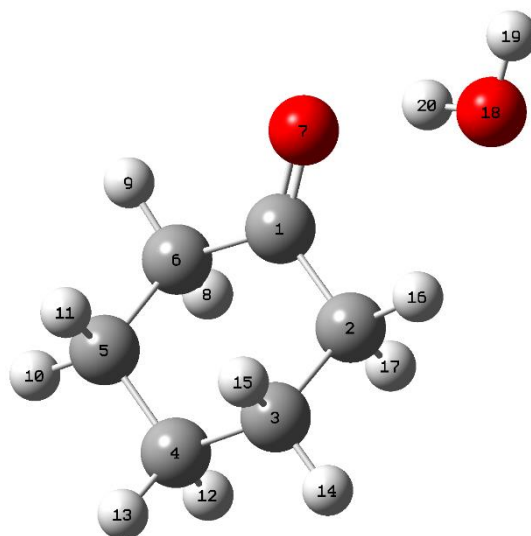


Table S5.7. Cartesian coordinates for the predicted structure of Keto boat-H₂O in Table 5.1 at the B3LYP-D3/aVTZ level of theory.

Atom	X	Y	Z
C1	-1.052	1.470	-0.433
C2	-2.348	0.803	0.068
C3	-2.134	-0.665	0.486
C4	-1.000	-1.329	-0.298
C5	0.311	-0.609	-0.079
C6	0.200	0.870	0.209
H7	-3.103	0.859	-0.715
H8	-2.746	1.359	0.918
H9	-1.890	-0.714	1.549
H10	-3.056	-1.232	0.361
H11	-0.868	-2.379	-0.043
H12	-1.211	-1.287	-1.373
H13	0.153	0.974	1.299
H14	1.116	1.366	-0.106
H15	-0.972	1.352	-1.516
H16	-1.083	2.544	-0.249
O17	1.377	-1.192	-0.129
O18	3.541	0.601	0.157
H19	4.400	0.229	-0.062
H20	2.905	-0.129	0.059

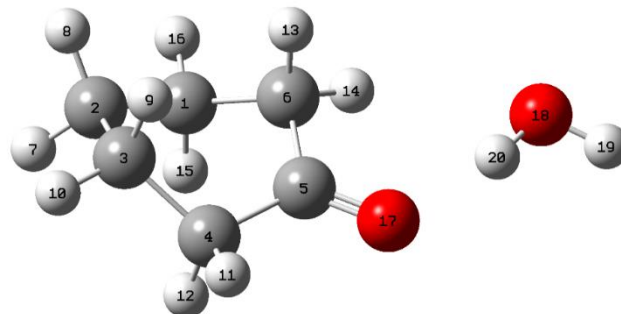


Table S5.8. Cartesian coordinates for the predicted structure of Keto skew-H₂O I in Table 5.1 at the B3LYP-D3/aVTZ level of theory.

Atom	X	Y	Z
C1	-1.953	-0.874	-0.664
C2	-2.147	0.648	-0.505
C3	0.267	0.625	0.267
C4	0.260	-0.872	0.494
C5	-1.151	-1.465	0.495
H6	-2.137	1.124	-1.485
H7	-3.124	0.858	-0.068
H8	-1.654	-1.254	1.442
H9	-1.411	-1.080	-1.590
H10	0.785	-1.061	1.434
H11	0.879	-1.323	-0.282
H12	-1.093	-2.550	0.412
H13	-2.921	-1.365	-0.757
C14	-1.069	1.306	0.387
H15	-0.957	2.367	0.178
H16	-1.367	1.204	1.435
O17	1.289	1.236	0.013
O18	3.432	-0.568	-0.358
H19	4.242	-0.166	-0.681
H20	2.804	0.166	-0.236

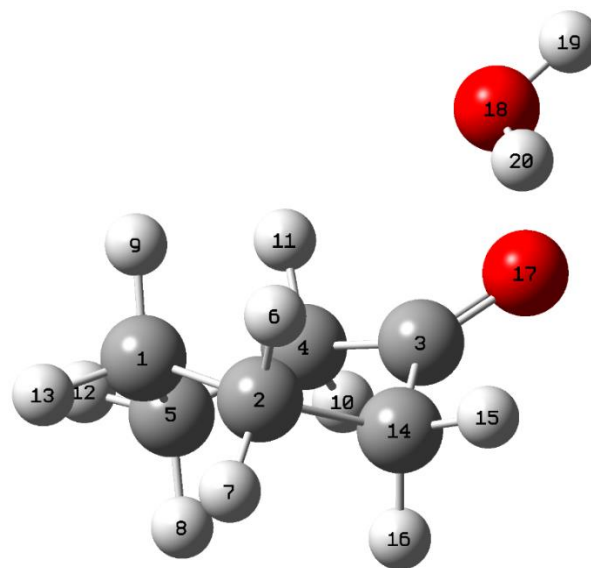


Table S5.9. Cartesian coordinates for the predicted structure of Keto skew-H₂O II in Table 5.1 at the B3LYP-D3/aVTZ level of theory.

Atom	X	Y	Z
C1	-2.057	0.831	-0.575
C2	-0.832	1.611	-0.053
C3	0.244	-0.675	0.118
C4	-1.089	-1.391	0.025
C5	-2.285	-0.455	0.218
H6	-0.331	2.109	-0.883
H7	-1.152	2.396	0.631
H8	-2.417	-0.220	1.278
H9	-1.901	0.561	-1.622
H10	-1.077	-2.196	0.764
H11	-1.124	-1.876	-0.952
H12	-3.200	-0.952	-0.103
H13	-2.942	1.465	-0.549
C14	0.191	0.718	0.685
H15	1.184	1.159	0.693
H16	-0.129	0.602	1.726
O17	1.273	-1.215	-0.239
O18	3.474	0.544	-0.101
H19	2.823	-0.174	-0.188
H20	4.315	0.171	-0.378

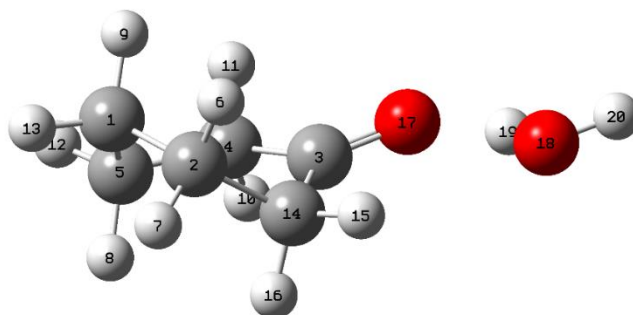


Table S5.10. Cartesian coordinates for the predicted structure of (cis)Enol I-H₂O I in Table 5.1 at the B3LYP-D3/aVTZ level of theory.

Atom	X	Y	Z
C1	0.223	0.563	-0.314
C2	0.124	-0.918	-0.487
H3	0.686	-1.404	0.315
H4	0.626	-1.195	-1.417
C5	-1.332	-1.385	-0.495
H6	-1.372	-2.469	-0.378
H7	-1.780	-1.153	-1.465
C8	-2.134	-0.692	0.604
H9	-1.681	-0.919	1.573
H10	-3.155	-1.073	0.632
C11	-2.145	0.823	0.396
H12	-2.518	1.319	1.296
H13	-2.852	1.083	-0.399
C14	-0.777	1.353	0.060
H15	-0.614	2.423	0.137
O16	1.497	1.026	-0.591
H17	1.539	1.974	-0.419
O18	3.537	-0.550	0.741
H19	4.185	-0.858	0.102
H20	2.913	-0.009	0.233

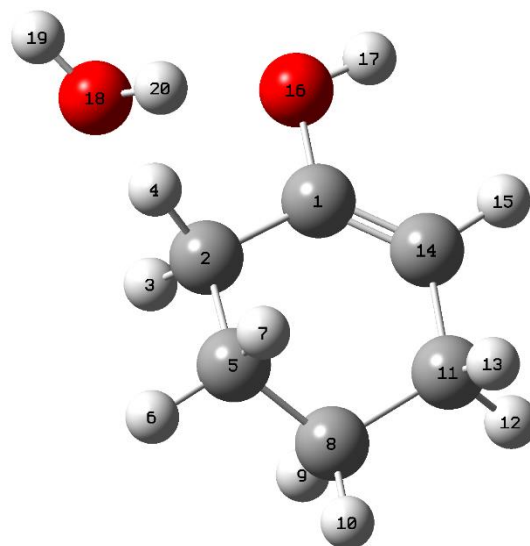


Table S5.11. Cartesian coordinates for the predicted structure of (cis)Enol I-H₂O II in Table 5.1 at the B3LYP-D3/aVTZ level of theory.

Atom	X	Y	Z
C1	0.237	-0.463	0.004
C2	-0.936	-1.392	0.083
H3	-0.998	-1.793	1.100
H4	-0.742	-2.248	-0.565
C5	-2.244	-0.699	-0.300
H6	-3.093	-1.324	-0.017
H7	-2.284	-0.583	-1.387
C8	-2.340	0.677	0.351
H9	-2.288	0.561	1.438
H10	-3.301	1.143	0.126
C11	-1.194	1.577	-0.114
H12	-1.141	2.465	0.521
H13	-1.410	1.950	-1.123
C14	0.130	0.862	-0.099
H15	1.031	1.460	-0.176
O16	1.423	-1.142	0.051
H17	2.168	-0.518	0.031
O18	3.765	0.498	-0.002
H19	4.274	0.434	0.811
H20	4.366	0.238	-0.707

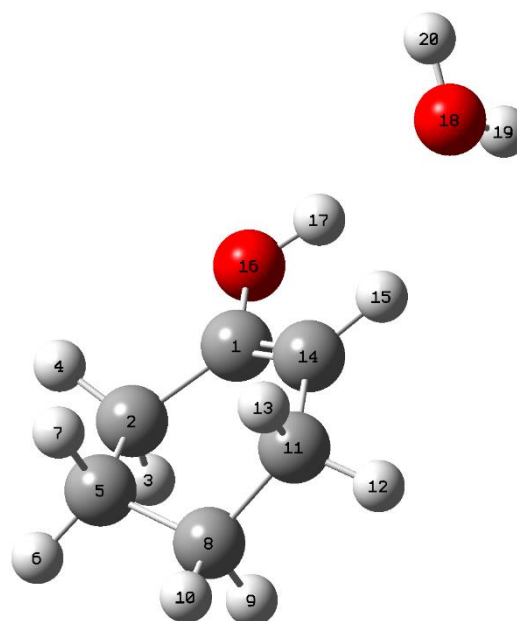


Table S5.12. Cartesian coordinates for the predicted structure of (trans)Enol II-H₂O I in Table 5.1 at the B3LYP-D3/aVTZ level of theory.

Atom	X	Y	Z
C1	-0.237	-0.459	-0.044
C2	0.939	-1.386	-0.051
H3	1.051	-1.819	-1.051
H4	0.744	-2.223	0.627
C5	2.226	-0.668	0.365
H6	3.090	-1.290	0.127
H7	2.222	-0.528	1.449
C8	2.331	0.693	-0.316
H9	2.328	0.552	-1.401
H10	3.275	1.175	-0.061
C11	1.156	1.591	0.076
H12	1.115	2.460	-0.584
H13	1.320	1.995	1.082
C14	-0.157	0.863	0.028
H15	-1.072	1.442	0.040
O16	-1.481	-1.065	-0.133
H17	-1.382	-2.020	-0.143
O18	-3.890	0.553	-0.025
H19	-3.121	-0.033	-0.062
H20	-4.151	0.567	0.899

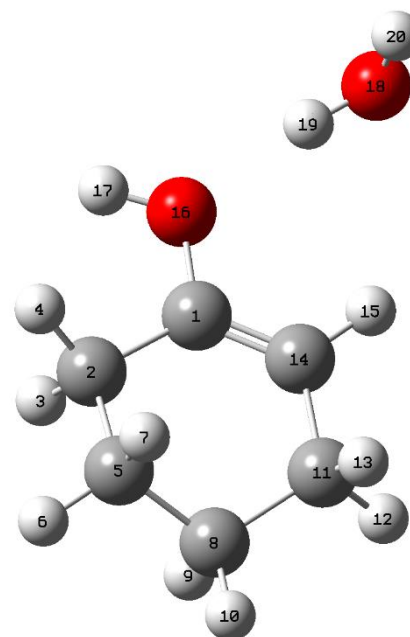


Table S5.13. Cartesian coordinates for the predicted structure of (cis)Enol II-H₂O II in Table 5.1 at the B3LYP-D3/aVTZ level of theory.

Atom	X	Y	Z
C1	-0.179	-0.605	0.003
C2	-0.165	0.896	0.065
H3	-0.446	1.212	1.076
H4	-0.940	1.290	-0.597
C5	1.199	1.475	-0.312
H6	1.244	2.530	-0.035
H7	1.321	1.425	-1.397
C8	2.326	0.688	0.353
H9	2.196	0.728	1.438
H10	3.293	1.142	0.130
C11	2.307	-0.771	-0.103
H12	2.961	-1.366	0.538
H13	2.737	-0.844	-1.110
C14	0.920	-1.350	-0.089
H15	0.808	-2.426	-0.149
O16	-1.410	-1.202	0.067
H17	-2.116	-0.538	0.044
O18	-3.715	0.486	-0.014
H19	-4.200	0.446	0.815
H20	-4.309	0.125	-0.680

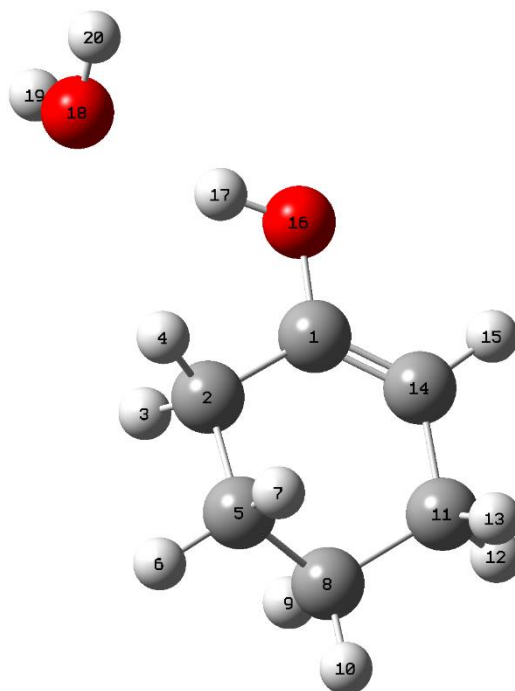


Table S5.14. Measured and assigned transition frequencies (MHz) of cyclohexanone-water complex and its ^{13}C isotopologues.

J'	K_a'	K_c'	J''	K_a''	K_c''	Parent species	o-c^a	$^{13}\text{C1}$	o-c	$^{13}\text{C2}$	o-c	$^{13}\text{C3}$	o-c
4	1	4	3	1	3	7653.4669	-0.0014	7648.4162	0.0004	7616.9535	-0.0023	7582.5818	-0.0002
4	0	4	3	0	3	7966.8746	-0.0001	7961.7640	-0.0004	7930.1009	-0.0026	7892.0374	-0.0004
4	2	3	3	2	2	8105.8421	0.0015	8101.9076	0.0004			8026.0685	-0.0004
4	3	1	3	3	0	8151.5101	0.0059						
4	3	2	3	3	1	8147.3348	-0.0092						
4	2	2	3	2	1	8256.6417	0.0012	8253.9858	-0.0011	8229.0496	0.0035	8171.4966	0.0006
4	1	3	3	1	2	8519.7005	0.0002	8516.5409	0.0004	8490.1650	-0.0043	8432.4521	0.0001
5	1	5	4	1	4	9541.9745	-0.0001	9535.4694	0.0008	9495.6188	-0.0002	9454.2051	0.0011
5	0	5	4	0	4	9857.5866	0.0002	9850.4869	-0.0006	9808.9700	-0.0023	9767.2686	-0.0009
5	2	4	4	2	3	10112.7261	0.0023	10107.6361	-0.0012	10071.5926	-0.0098	10013.7249	0.0011
5	3	3	4	3	2	10194.0923	0.0030						
5	3	2	4	3	1	10208.5433	-0.0015						
5	2	3	4	2	2	10401.8661	-0.0011	10399.0891	0.0004	10369.3599	-0.0066	10292.9389	-0.0017
5	1	4	4	1	3	10615.4494	0.0020	10611.1653	0.0003	10577.2781	-0.0002	10507.7230	0.0009
6	1	6	5	1	5	11417.2271	-0.0025	11409.1916	0.0006	11360.7386	0.0046	11312.9647	0.0003
6	0	6	5	0	5	11702.4169	-0.0011	11693.2252	-0.0004	11641.5896	-0.0003	11597.5194	-0.0005
6	2	5	5	2	4	12106.7479	0.0024	12100.3976	0.0009	12056.4676	-0.0048	11988.9800	-0.0002
3	1	2	2	0	2	9028.3536	0.0007	9017.0353	0.0001				
2	2	0	1	1	0	10810.3779	-0.0006						
2	2	1	1	1	1	11012.4566	0.0003						
4	1	3	3	0	3	11521.3266	-0.0007						
6	2	4	5	2	3	12579.4457	-0.0035	12576.5300	-0.0000	12541.9568	0.0020	12446.3464	0.0001
6	1	5	5	1	4	12684.6070	0.0008	12678.9231	-0.0003	12636.7553	0.0056	12557.4922	0.0002
7	1	7	6	1	6	13279.3988	0.0001	13269.7679	-0.0002				
7	0	7	6	0	6	13513.9845	0.0011	13502.8208	-0.0001				

^a observed - calculated

Table S5.14. (continued)

J'	Ka'	Kc'	J''	Ka''	Kc''	¹³ C4	o-c ^a	¹³ C5	o-c	¹³ C6	o-c
4	1	4	3	1	3	7574.5005	-0.0001	7617.1697	-0.0011	7644.9030	0.0014
4	0	4	3	0	3	7884.8118	0.0019	7930.9659	-0.0003	7957.1899	0.0000
4	2	3	3	2	2	8020.2680	-0.0022	8076.7644	0.0003	8097.3671	-0.0026
4	3	1	3	3	0						
4	3	2	3	3	1						
4	2	2	3	2	1	8167.2506	0.0016	8235.0237	-0.0001	8249.4938	-0.0015
4	1	3	3	1	2	8428.5224	0.0003	8495.8662	0.0005	8510.9652	-0.0004
5	1	5	4	1	4	9443.8626	-0.0009	9495.4873	0.0032	9531.0759	0.0015
5	0	5	4	0	4	9757.3152	-0.0003	9808.5389	-0.0021	9844.8003	0.0010
5	2	4	4	2	3	10006.2699	0.0008	10075.3792	0.0006	10101.9580	0.0010
5	3	3	4	3	2						
5	3	2	4	3	1						
5	2	3	4	2	2	10288.3390	0.0000	10377.9834	-0.0015	10393.4354	-0.0002
5	1	4	4	1	3	10502.4178	-0.0018	10583.7110	0.0009	10604.1693	0.0005
6	1	6	5	1	5	11300.2564	0.0002	11360.0767	0.0013	11403.9288	0.0042
6	0	6	5	0	5	11584.6077	-0.0001	11639.5866	-0.0027	11686.5223	-0.0071
6	2	5	5	2	4	11979.7365	0.0003	12060.4897	0.0007	12093.5701	0.0012
3	1	2	2	0	2						
2	2	0	1	1	0						
2	2	1	1	1	1						
4	1	3	3	0	3						
6	2	4	5	2	3	12441.4757	-0.0003	12553.2338	-0.0016	12569.6020	-0.0001
6	1	5	5	1	4	12550.4986	0.0007	12643.3443	0.0019	12670.4755	0.0004
7	1	7	6	1	6						
7	0	7	6	0	6						

^a observed – calculated

Table S5.15. Measured and assigned transition frequencies (MHz) of cyclohexanone-water complex and its deuterium isotopologues.

J'	Ka'	Kc'	J''	Ka''	Kc''	D ₂ O	o-c ^a	DOH(D1)	o-c	HOD(D2)	o-c
4	1	4	3	1	3	7296.6310	-0.0002	7402.5886	-0.0012	7538.3193	0.0013
4	0	4	3	0	3	7591.5310	-0.0004	7702.8872	-0.0005	7846.2262	0.0002
4	2	3	3	2	2	7703.4802	-0.0069	7822.5315	0.0014	7975.8315	-0.0025
4	2	2	3	2	1			7952.2881	0.0019	8116.4520	-0.0005
4	1	3	3	1	2	8079.5313	0.0020	8209.4646	0.0012	8377.5305	0.0016
5	1	5	4	1	4	9100.5082	0.0015	9231.6430	0.0005	9399.6161	0.0004
5	0	5	4	0	4	9406.1798	0.0008	9540.2448	-0.0005	9712.8163	-0.0020
5	2	4	4	2	3	9613.6802	0.0019	9761.3717	-0.0015	9951.5784	0.0018
5	2	3	4	2	2	9848.3957	-0.0007	10011.6262	-0.0039	10221.9882	-0.0016
5	1	4	4	1	3	10072.5027	0.0020	10232.8715	0.0014	10440.2929	0.0010
6	1	6	5	1	5	10893.2658	0.0009	11048.9561	-0.0002	11248.3846	0.0012
6	0	6	5	0	5	11179.9637	-0.0017	11335.1898	-0.0008	11535.0647	-0.0027
6	2	5	5	2	4	11513.5416	0.0057	11689.1650	0.0031	11915.3410	0.0027
3	1	2	2	0	2	8704.2522	0.0001	8795.1668	-0.0000	8927.9227	0.0003
2	2	0	1	1	0	10747.3514	-0.0030	10752.7578	-0.0001	10803.2995	-0.0001
2	2	1	1	1	1	10931.4029	0.0028				
6	2	4	5	2	3	11901.9789	-0.0029	12101.8222	-0.0019	12359.3091	-0.0023
6	1	5	5	1	4	12044.8057	-0.0010	12233.9507	0.0012	12478.5632	0.0013
7	1	7	6	1	6	12764.7708	-0.0016				

^a observed – calculated

Table S5.16. Spectroscopic parameters of cyclohexanone-water complex and its ^{13}C and deuterium isotopologues.

Rotational constant	$^{13}\text{C-C1}$	$^{13}\text{C-C2}$	$^{13}\text{C-C3}$	$^{13}\text{C-C4}$	$^{13}\text{C-C5}$	$^{13}\text{C-C6}$
A/MHz	3285.9316(25)	3255.551(71)	3283.8142(59)	3280.540(25)	3244.814(11)	3273.634(11)
B/MHz	1123.32189(21)	1120.4620(13)	1111.45482(28)	1111.27360(47)	1121.60512(58)	1122.4991(10)
C/MHz	905.21272(13)	901.0346(11)	897.98257(25)	896.74560(38)	900.77576(32)	904.90316(78)
$\Delta_{\text{k}}/\text{kHz}$	17.23(17)	21(18)	24.87234771	18.0(67)	24.87234771	17.4(73)
$\Delta_{\text{jk}}/\text{kHz}$	-7.7041(16)	-7.63(13)	-7.474(23)	-7.62(4)	-7.467(49)	-7.601(69)
$\Delta_{\text{j}}/\text{kHz}$	1.0469(16)	1.038(12)	1.0182(15)	1.0294(42)	1.0483(33)	1.042(7)
$\delta_{\text{j}}/\text{kHz}$	0.1704(13)	0.17(1)	0.161(2)	0.1700(35)	0.1715(42)	0.1583(73)
N	18	14	15	15	15	15
σ/kHz	0.57	3.0	0.72	1.0	1.5	2.5

Rotational constant	$^{\text{a}}\text{DOH(D1)}$	$^{\text{b}}\text{HOD(D2)}$	D_2O
A/MHz	3287.2880(41)	3298.6954(42)	3289.7280(63)
B/MHz	1080.39298(61)	1103.76562(61)	1062.38808(90)
C/MHz	877.82359(50)	893.01318(50)	865.90822(54)
$\Delta_{\text{k}}/\text{kHz}$	25.5(9)	25.61(91)	19.3(13)
$\Delta_{\text{jk}}/\text{kHz}$	-7.290(45)	-7.089(46)	-6.706(71)
$\Delta_{\text{j}}/\text{kHz}$	0.9803(35)	0.970(35)	0.9099(58)
$\delta_{\text{j}}/\text{kHz}$	0.1500(45)	0.01564(45)	0.1402(52)
N	17	17	18
σ/kHz	1.6	1.6	2.7

^a D1 is the free proton of water.

^b D2 is the proton of water hydrogen bonded with cyclohexanone carbonyl oxygen.

Table S5.17. Cartesian coordinates for the fitted $r_m^{(1)}$ geometry of cyclohexanone-water complex.

Atom	X	Y	Z
C1	0.202	0.648	-0.263
C2	0.170	-0.792	-0.667
C3	-0.912	-1.561	0.162
C4	-2.259	-0.860	0.044
C5	-2.174	0.574	0.551
C6	-1.105	1.372	-0.267
O7	1.341	1.237	0.084
H8	-0.952	2.379	0.120
H9	-1.440	1.450	-1.309
H10	1.167	-1.214	-0.540
H11	-0.093	-0.843	-1.731
H12	-1.920	0.565	1.617
H13	-3.140	1.074	0.459
H14	-0.628	-1.621	1.219
H15	-0.979	-2.590	-0.197
H16	-3.000	-1.419	0.621
H17	-2.601	-0.858	-0.998
H18	2.889	0.070	0.298
O19	3.615	-0.577	0.242
H20	4.409	-0.102	0.502

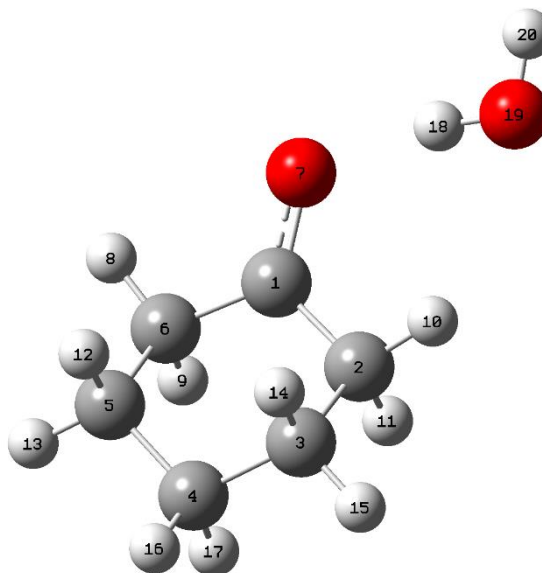


Table S5.18. BSSE corrected interaction energy analysis for a selection of ketone-water complexes at the MP2/6-311++g(2d,p) level of theory.

Species	Cyclohexanone	Cyclopentanone	Cyclobutanone	Acetone	Formaldehyde
$\Delta E_{\text{binding}}(\text{kcal mol}^{-1})$	-5.60	-5.35	-4.52	-5.43	-3.75

Appendix IV. Supplementary Material for Chapter 6

Keto-Enol Tautomeric and Internal Rotation Dynamics Study of the Acetylacetone-Water Complex Probed by Microwave Spectroscopy and *ab initio* Calculations

Contents:

1. Table S6.1. Measured transition frequencies (MHz) and assigned quantum numbers of the acetylacetone-water complex.....186

Table S6.1. Measured transition frequencies (MHz) and assigned quantum numbers of the acetylacetonone-water complex.

J'	K _a '	K _c '	J''	K _a ''	K _c ''	AA	^a o-c	AE	o-c
3	0	3	2	0	2	4839.1189	-0.0069	4839.1189	-0.0109
4	1	4	3	1	3	6166.3057	0.0021	6166.3328	-0.0027
2	1	2	1	0	1	6322.5864	0.0040	-----	-----
4	0	4	3	0	3	6428.1390	0.0087	6428.1155	-0.0079
4	2	3	3	2	2	6475.8286	0.0036	-----	-----
4	2	2	3	2	1	6527.6137	0.0087	-----	-----
4	1	3	3	1	2	6772.6421	0.0047	6772.5969	-0.0048
6	0	6	5	1	5	7226.3079	0.0022	7226.7075	0.0004
5	1	5	4	1	4	7698.8248	0.0015	7698.8377	0.0005
3	1	3	2	0	2	7716.9409	-0.0163	7716.4381	-0.0062
5	0	5	4	0	4	7997.3864	0.0025	7997.3674	-0.0040
5	2	4	4	2	3	8088.2491	0.0023	8090.2995	0.0004
5	3	3	4	3	2	8116.5601	0.0057	8117.6956	-0.0039
5	3	2	4	3	1	8118.9090	0.0060	8117.7552	-0.0055
5	2	3	4	2	2	8190.7258	0.0031	8188.6685	-0.0096
5	1	4	4	1	3	8455.2263	0.0015	8455.2010	-0.0029
4	1	4	3	0	3	9044.1189	0.0060	9043.6505	-0.0065
7	0	7	6	1	6	9066.3777	0.0018	9066.7416	-0.0005
6	1	6	5	1	5	9225.8900	0.0015	9225.8900	-0.0033
4	2	2	4	1	3	9259.5269	0.0036	14856.8434	-0.0062
3	2	1	3	1	2	9504.5504	-0.0007	9511.9595	-0.0049
6	0	6	5	0	5	9543.7294	0.0020	9543.7044	-0.0021
6	2	5	5	2	4	9696.3301	0.0035	9697.1369	-0.0037
6	2	4	5	2	3	9872.3547	0.0051	9871.5402	-0.0080
6	1	5	5	1	4	10130.1364	0.0032	10130.1125	-0.0040
5	1	5	4	0	4	10314.8139	0.0080	10134.3641	-0.0066
7	1	7	6	1	6	10746.9652	0.0080	10746.9485	-0.0075
7	0	7	6	0	6	11065.9614	0.0028	11065.9252	-0.0030
7	2	6	6	2	5	11299.2275	0.0052	11299.5785	-0.0056
6	1	6	5	0	5	11543.3172	0.0071	11542.8857	-0.0070
7	2	5	6	2	4	11572.7832	0.0061	11572.4270	-0.0058
8	1	8	7	1	7	12261.7456	0.0067	12261.7255	-0.0073
8	0	8	7	0	7	12565.3564	0.0150	12565.2884	-0.0129
8	1	7	7	1	6	13447.9332	0.0053	13447.9018	-0.0041
9	1	9	8	1	8	13770.2011	0.0086	13770.1742	-0.0079
8	1	8	7	0	7	13942.3281	0.0079	13941.9377	-0.0091
9	0	9	8	0	8	14045.4980	0.0049	14045.4395	-0.0049
9	2	8	8	2	7	14486.2565	0.0040	14486.3348	-0.0059
3	2	2	2	1	1	14562.7665	0.0020	11795.1767	-----

^a observed-calculated

Appendix V. Supplementary Material for Chapter 7

Rotational Spectra of Benzoylacetone Monomer and Its Monohydrated Complex

Contents:

1. Table S7.1. Measured transition frequencies (MHz) and assigned quantum numbers of the benzylacetone monomer.....180-190
2. Table S7.2. Measured transition frequencies (MHz) and assigned quantum numbers of deuterium benzoylacetone monomer.....190-191
3. Table S7.3. Measured transition frequencies (MHz) and assigned quantum numbers of benzoylacetone-water I complex.....191-192
4. Table S7.4. Measured transition frequencies (MHz) and assigned quantum numbers of the benzoylacetone-water II complex.....192-193
5. Figure S7.1. The structure of the deuterium form of the benzoylacetone monomer.193

Table S7.1. Measured transition frequencies (MHz) and assigned quantum numbers of the benzylacetone monomer.

J'	Ka'	Kc'	J''	Ka''	Kc''	AA	^a o-c	AE	o-c
5	2	3	6	1	6	2182.6210	-0.0087	2247.7662	0.0662
1	1	0	1	0	1	2246.5310	0.0019	2268.1144	0.0029
2	1	1	2	0	2	2317.4060	-0.0022	2326.0361	-0.0111
3	1	2	3	0	3	2426.7570	-0.0002	2430.8600	-0.0197
5	0	5	4	1	4	2461.4340	0.0166	2464.8019	0.0123
4	1	3	4	0	4	2578.1440	-0.0003	2580.3624	-0.0324
5	1	4	5	0	5	2776.1640	0.0041	2777.4248	-0.0399
6	1	5	6	0	6	3026.1780	0.0033	3026.8491	-0.0506
1	1	1	0	0	0	3053.1660	0.0015	3029.6260	-0.0103
13	4	9	14	3	12	3128.9120	0.0266	3352.7816	-0.0325
1	1	1	0	0	0	3053.1660	0.0015	3029.6260	-0.0103
7	1	6	7	0	7	3333.9460	0.0066	3334.1853	-0.0402
4	1	4	3	1	3	3361.8850	0.0187	3363.7037	-0.0244
6	0	6	5	1	5	3461.3910	0.0244	3463.6191	0.0131
4	0	4	3	0	3	3487.3720	0.0220	3487.1277	-0.0152
3	2	1	4	1	4	3490.6940	-0.0287	3577.6845	0.0339
4	2	3	3	2	2	3502.3090	0.0211	3509.6103	-0.0192
4	3	2	3	3	1	3506.7430	0.0123	3506.7430	0.0455
4	3	1	3	3	0	3506.9010	0.0272	3506.5980	-0.0542
4	2	2	3	2	1	3518.5150	0.0221	3510.8843	-0.0211
4	1	3	3	1	2	3638.7550	0.0179	3636.6320	-0.0260
8	1	7	8	0	8	3705.0180	0.0073	3704.8527	-0.0430
7	3	5	8	2	6	3796.6010	-0.0221	3635.7014	0.0002
2	2	1	3	1	2	3801.2830	-0.0208	3703.4288	0.0160
2	1	2	1	0	1	3859.8100	0.0105	3849.2853	-0.0169
10	1	9	9	2	8	3890.4500	0.0184	3907.6805	-0.0491
12	4	8	13	3	11	4010.9070	0.0177		
9	1	8	9	0	9	4144.0570	0.0136	4143.4908	-0.0264
5	1	5	4	1	4	4199.4650	0.0223	4200.2964	-0.0321
2	2	0	3	1	3	4218.4100	-0.0168	4310.5373	0.0306
5	0	5	4	0	4	4347.2140	0.0201	4346.9376	-0.0236
5	2	4	4	2	3	4375.8480	0.0202	4388.4246	-0.0287
5	4	1	4	4	0	4383.0850	0.0390	4382.8158	-0.0460
5	4	2	4	4	1	4383.0850	0.0413	4382.9063	-0.0001
5	3	2	4	3	1	4385.3070	0.0275	4384.8371	0.0075
5	2	3	4	2	2	4408.1020	0.0263	4395.1173	-0.0248
7	0	7	6	1	6	4469.1470	0.0257	4470.6735	0.0152
5	1	4	4	1	3	4545.2280	0.0185	4543.9944	-0.0367
3	1	3	2	0	2	4632.4440	0.0150	4626.5552	-0.0308

10	1	9	10	0	10	4654.0620	0.0083	4653.0738	-0.0138
6	3	4	7	2	5	4770.1530	-0.0235	4595.9170	0.0412
11	4	8	12	3	9	4779.3850	0.0007		
6	3	3	7	2	6	4972.8690	-0.0290	5137.7877	0.0605
6	1	6	5	1	5	5035.2440	0.0250	5035.6272	-0.0425
11	1	10	10	2	9	5085.3610	0.0006		
6	0	6	5	0	5	5199.4093	0.0175	5199.1150	-0.0300
11	1	10	11	0	11	5235.8130	0.0127	5234.3636	-0.0012
6	2	5	5	2	4	5248.0410	0.0258	5264.2697	-0.0209
6	3	4	5	3	3	5263.6430	0.0324	5264.1173	-0.0299
6	3	3	5	3	2	5264.9740	0.0302	5263.9890	-0.0334
6	2	4	5	2	3	5303.9710	0.0251	5287.2644	-0.0350
4	1	4	3	0	3	5373.1412	0.0147	5369.2656	-0.0489
6	1	5	5	1	4	5449.4320	0.0254	5448.5486	-0.0314
8	0	8	7	1	7	5477.6570	0.0227	5478.7178	0.0234
11	2	9	11	1	10	5544.7210	0.0229	5549.3842	-0.0371
12	2	10	12	1	11	5566.7090	0.0275	5569.6519	-0.0478
10	2	8	10	1	9	5575.4730	0.0188	5582.8826	-0.0284
13	2	11	13	1	12	5649.1970	0.0183	5651.0286	-0.0601
9	2	7	9	1	8	5650.0790	0.0167	5661.9847	-0.0073
5	3	3	6	2	4	5713.3320	-0.0303		
8	2	6	8	1	7	5758.5950	0.0113	5777.8238	0.0013
10	4	6	11	3	9	5785.4360	-0.0147		
5	3	2	6	2	5	5826.5030	-0.0343		
7	1	7	6	1	6	5868.9803	0.0231	5869.1330	-0.0505
12	1	11	12	0	12	5887.4260	0.0074	5885.4955	0.0010
7	2	5	7	1	6	5890.3200	0.0088	5920.9363	0.0116
6	2	4	6	1	5	6034.2546	0.0014	6080.1745	0.0112
7	0	7	6	0	6	6042.9956	0.0219	6042.6807	-0.0412
5	1	5	4	0	4	6085.2390	0.0198	6082.4319	-0.0683
5	2	3	5	1	4	6179.7122	-0.0018	6241.4483	0.0045
4	2	2	4	1	3	6316.8346	-0.0132	6390.3449	0.0120
3	2	1	3	1	2	6437.0860	-0.0059	6516.0900	0.0045
9	0	9	8	1	8	6480.2112	0.0185	6480.9340	0.0260
2	2	0	2	1	1	6533.4378	-0.0097	6611.0517	0.0062
8	1	8	7	1	7	6700.5091	0.0292	6700.5091	-0.0690
6	1	6	5	0	5	6773.2653	0.0211		
3	2	2	3	1	3	6844.4658	0.0005	6759.4710	-0.0057
8	0	8	7	0	7	6877.4913	0.0210	6877.1677	-0.0520
4	2	3	4	1	4	6984.8855	-0.0014	6905.3777	-0.0003
8	2	7	7	2	6	6987.2973	0.0280	6998.7453	-0.0501
8	3	6	7	3	5	7023.7397	0.0369	7026.4469	-0.0399
8	3	5	7	3	4	7029.7044	0.0361	7026.3190	-0.0470

8	2	6	7	2	5	7116.8404	0.0264	7104.7337	-0.0541
5	2	4	5	1	5	7161.2705	-0.0015	7093.5142	0.0114
8	1	7	7	1	6	7248.5649	0.0233	7247.8443	-0.0456
6	2	5	6	1	6	7374.0697	0.0015	7322.1440	0.0203
7	1	7	6	0	6	7442.8345	0.0249	0.0000	
10	0	10	9	1	9	7471.0227	0.0169	7471.4929	0.0352
9	1	9	8	1	8	7529.6983	0.0249	7529.6983	0.0047
7	2	6	7	1	7	7623.7016	0.0075	7587.1109	0.0349
9	0	9	8	0	8	7703.0599	0.0216	7702.7279	-0.0637
9	2	8	8	2	7	7853.8468	0.0291	7861.1541	-0.0620
8	2	7	8	1	8	7910.4968	0.0133	7885.3443	0.0511
8	1	8	7	0	7	8100.3411	0.0253		
9	1	9	8	0	8	8752.5478	0.0288		
10	1	10	9	0	9	9405.9904	0.0203		

^a observed-calculated.

Table S7.2. Measured transition frequencies (MHz) and assigned quantum numbers of deuterium benzoylacetone monomer.

J'	Ka'	Kc'	J''	Ka''	Kc''	AA	o-c	AE	o-c
1	1	1	0	0	0	3011.8272	-0.0307	3011.8272	-0.0129
7	1	6	7	0	7	3310.9506	0.0071	3310.9506	0.0339
4	0	4	3	0	3	3479.2241	0.0022	3479.2241	0.0059
6	0	6	5	1	5	3490.7943	0.0312	3490.6754	-0.0869
4	2	3	3	2	2	3494.7583	0.0050		
4	2	2	3	2	1	3511.5956	-0.0038		
4	1	3	3	1	2	3632.5929	0.0019	3632.5929	0.0082
8	1	7	8	0	8	3688.2089	-0.0120	3688.2089	0.0209
2	1	2	1	0	1	3815.8649	-0.0190	3815.8649	-0.0061
7	3	4	8	2	7	3954.7767	-0.0224		
10	1	9	9	2	8	4003.0546	-0.0054	4003.0546	-0.0055
2	2	0	3	1	3	4109.1344	-0.0310		
9	1	8	9	0	9	4134.6299	-0.0263	4134.6299	0.0140
5	1	5	4	1	4	4187.9752	-0.0010	4187.9752	0.0012
5	0	5	4	0	4	4336.5667	-0.0024	4336.5667	0.0019
5	2	4	4	2	3	4366.3259	-0.0029	4366.3259	-0.0429
5	3	2	4	3	1	4376.1684	0.0001		
5	2	3	4	2	2	4399.8410	-0.0016		
7	0	7	6	1	6	4495.9830	0.0011	4495.9830	0.0042
3	1	3	2	0	2	4585.6536	0.0926	4585.5325	-0.0173

10	1	9	10	0	10	4653.0704	-0.0033	4653.0704	0.0454
6	3	3	7	2	6	4792.4891	-0.0186		
6	1	6	5	1	5	5021.3069	0.0001	5021.3069	0.0027
6	0	6	5	0	5	5185.9972	0.0025	5185.9972	0.0073
11	1	10	10	2	9	5197.2076	-0.0308	5197.2076	-0.0249
6	2	5	5	2	4	5236.4955	-0.0027	5236.4955	-0.0137
11	1	10	11	0	11	5243.8419	-0.0405	5243.8419	0.0176
6	4	2	5	4	1	5249.8498	-0.0085	5249.8498	0.0040
6	3	4	5	3	3	5252.6973	-0.0021	5253.2470	0.0645
6	3	3	5	3	2	5254.1343	0.0089		
6	2	4	5	2	3	5294.5953	0.0007	5294.5953	0.0249
4	1	4	3	0	3	5323.0186	-0.0278	5323.0186	-0.0180
6	1	5	5	1	4	5439.8118	-0.0116	5439.8118	-0.0028
11	2	9	11	1	10	5446.2497	-0.0103	5446.2497	0.0130
10	2	8	10	1	9	5469.2442	-0.0017	5469.2442	0.0186
12	2	10	12	1	11	5477.9283	-0.0061	5477.9283	0.0211
8	0	8	7	1	7	5501.1691	-0.0133	5501.1691	-0.0083
13	2	11	13	1	12	5572.0690	0.0201	5572.0690	0.0524
5	3	2	6	2	5	5643.3330	-0.0336		
7	2	5	7	1	6	5771.5613	0.0017	5771.5613	0.0144
7	1	7	6	1	6	5852.5670	0.0367	5852.5670	0.0398
12	1	11	12	0	12	5904.7395	0.0030		
6	2	4	6	1	5	5914.2660	-0.0142	5914.2660	-0.0078
5	1	5	4	0	4	6031.7784	-0.0223	6031.7784	-0.0140

Table S7.3. Measured transition frequencies (MHz) and assigned quantum numbers of benzoylacetone-water I complex.

J'	Ka'	Kc'	J''	Ka''	Kc''	measured	o-c
4	1	4	3	1	3	2229.4712	-0.0120
4	0	4	3	0	3	2291.6426	0.0067
4	2	3	3	2	2	2295.0454	-0.0088
4	1	3	3	1	2	2359.7235	0.0052
5	1	5	4	1	4	2786.1731	-0.0019
5	0	5	4	0	4	2861.7752	0.0029
5	2	4	4	2	3	2868.3535	0.0006
5	2	3	4	2	2	2875.7553	-0.0026
5	1	4	4	1	3	2948.9343	0.0011
6	1	6	5	1	5	3342.4291	0.0007
6	0	6	5	0	5	3430.0796	-0.0003
6	2	5	5	2	4	3441.3405	-0.0014

6	1	5	5	1	4	3537.6557	-0.0012
7	1	7	6	1	6	3898.1643	-0.0056
7	0	7	6	0	6	3996.2241	-0.0016
7	2	6	6	2	5	4013.9628	0.0035
7	2	5	6	2	4	4034.5788	0.0030
7	1	6	6	1	5	4125.7750	-0.0014
10	0	10	9	1	9	4174.5481	0.0038
4	1	4	3	0	3	4276.9721	0.0003
3	2	1	4	1	4	4300.9248	-0.0027
14	1	13	14	0	14	4306.4894	0.0001
8	1	8	7	1	7	4453.3318	-0.0014
8	0	8	7	0	7	4559.9137	0.0030
8	2	7	7	2	6	4586.1457	0.0021
8	2	6	7	2	5	4616.9021	-0.0017
8	1	7	7	1	6	4713.1786	0.0081
5	1	5	4	0	4	4771.5103	-0.0006
11	0	11	10	1	10	4846.9147	-0.0034
9	1	9	8	1	8	5007.8595	-0.0010
9	0	9	8	0	8	5120.8869	0.0007
9	2	8	8	2	7	5157.8330	-0.0008
9	2	7	8	2	6	5201.4462	0.0044
6	1	6	5	0	5	5252.1676	0.0006
9	1	8	8	1	7	5299.7037	-0.0045
10	1	10	9	1	9	5561.7036	0.0003
10	0	10	9	0	9	5678.9757	0.0031
7	1	7	6	0	6	5720.2571	0.0001
10	2	9	9	2	8	5728.9683	-0.0008
10	2	8	10	1	9	5734.8491	0.0048
10	2	8	9	2	7	5788.2989	-0.0067
9	2	7	9	1	8	5831.7809	-0.0056
10	1	9	9	1	8	5885.2498	0.0019
8	2	6	8	1	7	5930.0564	0.0035

Table S7.4. Measured transition frequencies (MHz) and assigned quantum numbers of the benzoylacetone-water II complex.

J'	Ka'	Kc'	J''	Ka''	Kc''	measured	o-c
3	1	3	2	0	2	2630.9953	-0.0267
4	0	4	3	1	3	2669.5677	-0.0001
4	1	4	3	0	3	3195.7115	-0.0092
5	1	5	4	0	4	3762.2713	0.0078
6	0	6	5	1	5	4178.5664	-0.0077

6	1	6	5	0	5	4351.8327	0.0038
7	0	7	6	1	6	4878.0392	-0.0041
7	1	7	6	0	6	4967.1334	0.0119
8	1	8	7	0	7	5601.2817	0.0034
5	0	5	4	1	4	3446.5545	-0.0242
8	0	8	7	1	7	5557.5454	-0.0008
5	2	4	4	1	3	5235.2941	0.0140
3	2	1	2	1	2	4660.8207	0.0091
6	1	5	6	0	6	2831.9984	0.0034
4	2	3	4	0	4	2885.8463	-0.0135
5	2	4	5	1	5	3062.6617	0.0140
4	2	3	3	2	2	3173.5965	-0.0046
2	2	1	1	1	0	3473.0568	-0.0256
8	4	4	8	3	5	3918.8020	0.0066
3	2	2	2	1	1	4130.5473	0.0062
7	4	3	7	3	4	4166.1612	-0.0144
4	4	0	4	3	1	4494.2896	0.0087
6	2	4	6	1	6	4645.0124	-0.0099
8	2	6	7	3	5	4787.5571	0.0072
3	3	0	2	2	0	5632.3736	0.0109
6	2	5	5	1	4	5706.0603	0.0017

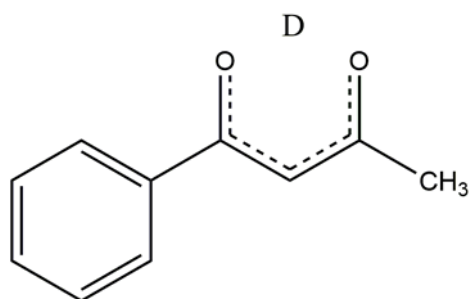


Figure S7.1. The structure of the deuterium form of the benzoylacetone monomer.